Mechanism of Corrosion by Naphthenic Acids and Organosulfur Compounds at High

Temperatures

A dissertation presented to

the faculty of

the Russ College of Engineering and Technology of Ohio University

In partial fulfillment

of the requirements for the degree

Doctor of Philosophy

Peng Jin

December 2013

This dissertation titled

Mechanism of Corrosion by Naphthenic Acids and Organosulfur Compounds at High

Temperatures

by

PENG JIN

has been approved for

the Department of Chemical and Biomolecular Engineering

and the Russ College of Engineering and Technology by

Srdjan Nesic

Russ Professor of Chemical and Biomolecular Engineering

Dennis Irwin

Dean, Russ College of Engineering and Technology

ABSTRACT

JIN, PENG, Ph.D., December 2013, Chemical Engineering

Mechanism of Corrosion by Naphthenic Acids and Organosulfur Compounds at High

Temperatures

Director of Dissertation: Srdjan Nesic

Due to the law of supply and demand, the last decade has witnessed a

skyrocketing in the price of light sweet crude oil. Therefore, refineries are increasingly

interested in "opportunity crudes", characterized by their discounted price and relative

ease of procurement. However, the attractive economics of opportunity crudes come with

the disadvantage of high acid/organosulfur compound content, which could lead to

corrosion and even failure of facilities in refineries. However, it is generally accepted that

organosulfur compounds may form protective iron sulfide layers on the metal surface and

decrease the corrosion rate. Therefore, it is necessary to investigate the corrosive property

of crudes at high temperatures, the mechanism of corrosion by acids (naphthenic acids) in

the presence of organosulfur compounds, and methods to mitigate its corrosive effect.

In 2004, an industrial project was initiated at the Institute for Corrosion and

Multiphase Technology to investigate the corrosion by naphthenic acids and organosulfur

compounds. In this project, for each experiment there were two experimentation phases:

pretreatment and challenge. In the first pretreatment phase, a stirred autoclave was filled

with a real crude oil fraction or model oil of different acidity and organosulfur compound

concentration. Then, the stirred autoclave was heated to high temperatures to examine the

corrosivity of the oil to different materials (specimens made from CS and 5% Cr

containing steel were used). During the pretreatment, corrosion product layers were formed on the metal surface.

In the second challenge phase, the steel specimens pretreated in the first phase were inserted into a rotating cylinder autoclave, called High Velocity Rig (HVR). The HVR was fed with a high-temperature oil solution of naphthenic acids to attack the iron sulfide layers. Based on the difference of specimen weight loss between the two steps, the net corrosion rate could be calculated and the protectiveness of corrosion product layer against naphthenic acid corrosion could be assessed.

Routinely, the layers generated in pretreatment and challenge phases were investigated with SEM/EDS (Scanning Electron Microscopy/Energy Dispersive Spectroscopy). Selectively, some thin layers formed in the first or second phase were analyzed with FIB-TEM (Focused Ion Beam - Transmission Electron Microscopy).

FIB-TEM analysis revealed that there was an iron oxide layer beneath the iron sulfide layer. Experimental results showed that the iron oxide layer was closely related to the layer protectiveness against naphthenic acid corrosion and its formation was due to the presence of naphthenic acids in the fluid.

Finally, a new mechanism of naphthenic acid/organosulfur compound corrosion was proposed based on properties of crudes, results of corrosion experimentation, and microscopic analysis of developed surface layers.

ACKNOWLEDGMENTS

At last, I should not forget my family members and my beloved Weiwei Wang. It was their priceless support and encouragement that made me strong and optimistic in confronting the challenges.

TABLE OF CONTENTS

LIST OF TABLES

LIST OF FIGURES

CHAPTER 1: INTRODUCTION

Since 1859, when the first oil well was drilled in Pennsylvania, USA[1], petroleum, or crude oil, has been changing the world. In the first several decades since the establishment of the petroleum industry, the dark fluid emerging from underground reservoirs was refined to produce kerosene to light lamps around the world. After the introduction of electric light bulbs, invented by Thomas Alva Edison, crude oil became less important. However, the development of the internal combustion engine powered by gasoline, another product of crude oil refining, initiated a new era of petroleum and revolutionized the lives of people. Today, petroleum is the "blood" of modern industry and manifests itself as the most important natural resource influencing every corner of the world.

High-temperature corrosion due to aggressive components in crude oil has long been known to be an important issue in refineries.[2] In particular, naphthenic acids and organosulfur compounds in crude oil are corrosive at high temperatures. In recent years, the increasing price of crude oil has stimulated refineries to look for "opportunity crudes", which are characterized by their ease of procurement and lower price relative to light sweet crudes. However, they have disadvantages related to their processing due to their higher content of corrosive naphthenic acids and/or organosulfur compounds.

The presence of naphthenic acids and organosulfur compounds may lead to two opposite effects. On the one hand, both may be corrosive and degrading to the steel infrastructure in refineries. On the other hand, under certain conditions, organosulfur compounds form a protective iron sulfide layer on the metal surface which may protect

the steel and deter corrosion. However, the protective properties of developed iron sulfide

layers formed in different crudes cannot be predicted reliably.

In the first phase of naphthenic acid/organosulfur corrosion research within the

Institute for Corrosion and Multiphase Technology (ICMT), properties of iron sulfide

layers formed on the surface of steel specimens, including its porosity, thickness, and

protectiveness against naphthenic acid corrosion, were extensively investigated.[3] An iron

sulfide layer was formed in, and derived from, various crude factions with different

acidic and sulfur content/speciation. Each iron sulfide layer was challenged with a

naphthenic acid solution to examine its protectiveness. Moreover, the morphology of

each layer was analyzed with SEM (Scanning Electron Microscopy) at the layer of

microns. It was found that the iron sulfide layer morphology, including its thickness and

porosity, could not be related to the layer's protectiveness against naphthenic acid

corrosion. Additionally, the prediction of corrosion rates was inaccurate based only on

the concentration of naphthenic acids and organosulfur compounds.

The next stage of this project focused on the factors involved in the corrosion by

naphthenic acids and organosulfur compounds and on the layer morphology,

characterized at the nanometer level. Following the same pretreatment-challenge

experimentation procedures, three phases of experiments and analysis were conducted.

Initially, corrosion in model compounds which imitated the real crude fractions

was investigated. Commercial dialkyl sulfide and naphthenic acids were utilized to

substitute the sulfur and acidic content of real crudes when their hydrocarbon component

was replaced by inert mineral model oil. By deliberately varying the concentration of

corrosive species, the corrosion by sulfur compounds and naphthenic acids and the effect on the properties of corrosion product layer could be investigated.

Secondly, it was suspected that other chemical components in the crude, such as asphaltenes, might affect the corrosion by crude oil at high temperatures. A series of crude oil fractions with different concentrations of asphaltenes were selected to pretreat steel specimens. Following the pretreatment, naphthenic acid solution was used to challenge the pretreated specimens. Evaluation of the possible correlation between the asphaltene concentration and the corrosion rate was expected to reveal the possible effect of asphaltene.

Thirdly, examination of the layer at the nanometer level was possible with advanced TEM (Transmission Electron Microscopy) analysis; SEM analysis was insufficient to reveal morphological details at sufficiently high resolution. Information from TEM analysis proved helpful to explain the corrosive behavior of fluids.

Finally, a corrosion model was constructed based on the aforementioned experimental results and analysis. This model factored in the effects of the concentration of naphthenic acids and organosulfur compounds, the temperature, and the formation of layers.

CHAPTER 2: LITERATURE REVIEW

2.1 Naphthenic Acid Structure

In the petroleum industry, naphthenic acids refer to a particular type of carboxylic acids in the crude oil. In 1956, Derungs defined naphthenic acids as saturated carboxylic acids with a five-member ring.[2] However, subsequent research revealed that the side chains connecting the carboxylic group are not necessarily saturated and could be aromatic and polycyclic.[4]

The carboxylic group in the naphthenic acids can react with or corrode iron, especially at elevated temperatures. To measure the corrosiveness of the crude, the TAN or the total acidic number is used. TAN is defined as the amount of KOH (in mg) needed to neutralize the acidity in one gram of crude oil. There are two ASTM standards to measure TAN: ASTM D974[5] and ASTM D664.[6] ASTM D974 measures the acid content using chemical titration indicated by the color of the solution while ASTM D664 employs a potentiometric titration. It should be noted that these two methods may give different results.

As Dzidic, *et al*., noted, the general chemical formula for naphthenic acids is $C_nH_{2n+z}O_2$, where z is zero or a negative even integer and relates to the number of rings in the molecule.[7] Figure 1 illustrates some typical structures of naphthenic acids with increasing number of rings (from 0 to 3).[7] Despite these various structures, naphthenic acids share some common characteristics. Usually, the α position of the carboxylic group is CH_2. The number of carbons (n) is in the range of 10 to 30.
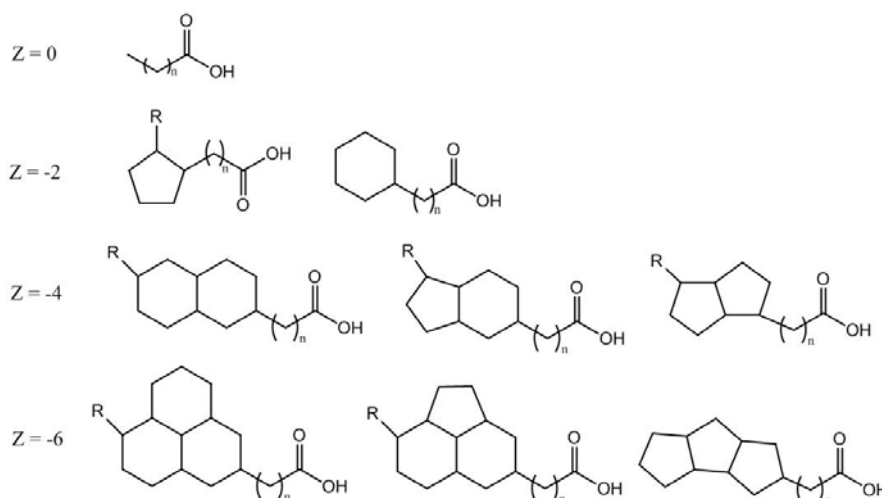
Figure 1. Typical structures of naphthenic acids (based on Dzidic, I.; Somerville A.C.; Raia J.C.; Hart H.V.; Determination of Naphthenic Acids in California Crudes And Refinery Wastewaters by Fluoride Ion Chemical Ionization Mass Spectrometry. *Anal Chem.,* **1988**, *60*(13), 1318–1323.).

Recent development of high resolution mass spectrometry provided the unique opportunity to find the exact mass of molecules and their differentiation based upon the presence of heteroatoms including sulfur, nitrogen, and oxygen. For instance, Qian, *et al.*, discovered more than 3000 acids in a heavy crude oil from South America analyzed by ESI-MS.[8]

2.2 Organosulfur Compound Structure
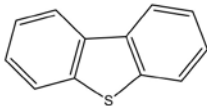
Organosulfur compounds, along with other forms of sulfur including elemental sulfur and dissolved hydrogen sulfide, can have complex structures and may account for 10% of crude oil by weight. Investigation on the structures of organosulfur compounds in crude oils started more than 40 years ago.[9] Among more than 10,000 organosulfur compounds found in the crude, there are four types of structures: mercaptans, sulfides, disulfides, and thiophenes.[10]

The general structure of mercaptans is R-SH, where R is an alkyl group. Mercaptans are the most reactive organosulfur compounds, followed by sulfides (R_1-S-R_2) and disulfides (R_1-S-S-R_2). Thiophenes have one or more resonant five-member rings in their molecular structures and are relatively stable.[10] Some typical structures of organosulfur compounds are shown in Table 1.[10, 61]

Table 1.

Typical Structures of Organosulfur Compounds

Name	Structure
n-Cetyl mercaptan	$CH_3(CH_2)_{15}SH$
n-Decyl sulfide	$CH_3(CH_2)_9S(CH_2)_9CH_3$
Di-*n*-octyl disulfide	$CH_3(CH_2)_7S-S(CH_2)_7CH_3$
Dibenzothiophene	

However, determining organosulfur compound structures in complex mixtures, such as in crudes, is difficult, tedious and costly. Consequently, as a first step, refineries measure the total sulfur content in crudes. There are several methods to measure the total sulfur, in elemental form and otherwise, in crudes. For example, the ASTM D5623 standard test method detects and measures the total sulfur with gas chromatography.[11] In this method, oil samples are analyzed in a gas chromatography equipped with a detector for sulfur-containing compounds. By calibration with standard samples, the concentration

of volatile sulfur-containing compounds in the crude can be calculated. Without additional separation or purification, ASTM D4294 is commonly used to rapidly measure the total amount of sulfur in the oil (2 to 4 min) utilizing energy-dispersive X-ray fluorescence spectrometry.[12] Moreover, aliphatic sulfides, including mercaptans, sulfides, disulfides, can form complexes with iodine and be detected with UV.[13]

As stated in preceding paragraphs, mercaptans, sulfides, and disulfides are reactive/corrosive while thiophenes are not. Crude oils are complex mixtures and the distribution of reactive/corrosive organosulfur compounds varies among different crudes. Therefore, the total amount of sulfur is not particularly helpful in the prediction of sulfidation of steels in refineries. Consequently, the industry is more interested in measuring the total amount of corrosive or active organosulfur compounds in the crude oil.

There are several standard and proprietary methods to measure the corrosive or active organosulfur compounds. ASTM D1275 provides a method to measure the corrosive sulfur.[14] By observing the color change of a copper strip, the amount of corrosive sulfur can be qualitatively measured. US Patent 5,744,702 proposed a method to measure the "total reactive sulfur".[15] In the method, crude samples were analyzed in the 70 ev electron ionization (EI) mass spectrometry. Ionized and energized reactive organosulfur compounds, including mercaptans, sulfides, and disulfides, could undergo intramolecular rearrangements and generate characteristic fragment ions including SH^+, $H_2S_2^+$, CH_3S^+, etc. By measuring the signal intensity of characteristic ions and calibration against a standard sample, the total amount of reactive sulfur could be calculated.

2.3 Factors in Corrosion by Naphthenic Acids and Organosulfur Compounds

Proposed is that naphthenic acids, in the presence of H_2S derived from organosulfur compounds, can be involved in the following sequence of reactions related to the corrosion of steel:[7]

$$Fe + 2RCOOH \rightarrow Fe(RCOO)_2 + H_2 \qquad\qquad \text{Reaction 1}$$
$$Fe + H_2S \rightarrow FeS + H_2 \qquad\qquad \text{Reaction 2}$$
$$Fe(RCOO)_2 + H_2S \rightarrow FeS + 2RCOOH \qquad\qquad \text{Reaction 3}$$
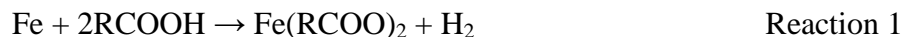
The corrosion of iron by naphthenic acids is described by Reaction 1. The product of this reaction is $Fe(RCOO)_2$ and is known as iron naphthenates, which are soluble in the crude and cannot directly affect the corrosion rate. On the other hand, sulfide compounds would decompose at high temperatures and release H_2S (the mechanism of sulfide compound decomposition will be discussed later).[16] According to Reaction 2, H_2S will corrode steel forming FeS (iron sulfide) which will not dissolve in the crude and may lay a protective layer on the metal surface. Reaction 3 indicates that iron sulfide can precipitate in the crude when iron naphthenates react with hydrogen sulfide. This reaction also releases naphthenic acids back to the fluid. In this project, it was found that Reaction 4 (reverse of Reaction 3) was possible and a solution of high naphthenic acid content (TAN 18) was used to dissolve residual sulfur compounds (such as FeS and organosulfur compounds) in the equipment.

$$FeS + 2RCOOH \rightarrow Fe(RCOO)_2 + H_2S \qquad\qquad \text{Reaction 4}$$
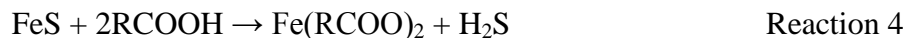
Given the many compounds that are involved and the complex mechanisms, the corrosion related to naphthenic acids is affected by multiple factors. In the following paragraphs, these factors are identified through a review of the available literature.

2.3.1 Effect of Molecular Structure

As a group of organic compounds, the reactivity of naphthenic acids should be influenced by the overall molecular structure. As early as 1956, Derungs proposed that low-molecular-weight naphthenic acids would be more active or corrosive.[2] Turnbull, *et al.*, investigated the effect of carbon numbers of single-ring model acids on the corrosion of naphthenic acids.[17] It was found that corrosion rates increased with carbon numbers from six to nine and decreased from ten to fourteen. It was postulated that a larger number of -CH_2- groups in the molecule would lead to higher adsorbability, but a large branch group would show an effect of steric hindrance.

A few years ago Messer, *et al.*, proposed a new theory on naphthenic acid corrosion based on over 50 years experience of processing Athabasca crudes.[18, 19] The TAN of crude was in the range from 3 to 4, but no evidence of naphthenic acid corrosion was found. It was postulated that naphthenic acids in the Athabasca crude belonged to β (good) type, which was characterized by low corrosivity, high molecular weight, high boiling point, etc, and could not fit the classical naphthenic acid corrosion model. However, they admitted that properties of high molecular weight naphthenic acids should be investigated in detail to validate their model.

Corrosion by the organosulfur compounds is also closely related to their molecular structure. Among the four types of organosulfur compounds, mercaptans,

sulfides, and disulfides are reactive and could decompose to release H_2S at high temperatures while thiophenes are relatively stable and perceived to be noncorrosive.[16] It was estimated that two thirds of total organosulfur compounds in the crude were thiophenic.[20]

Dettman, *et al*., investigated the thermal decomposition of different types of organosulfur compounds and their influence on naphthenic acid corrosion.[21] It was found that the corrosion was enhanced if the sulfide compound generated a low-level H_2S, forming little in the way of corrosion products. On the contrary, the corrosion was inhibited in the presence of organosulfur compounds that generated high-concentrations of H_2S, which might be due to the formation of a protective iron sulfide layer on the steel surface.

2.3.2 Effect of Temperature

Temperature is an important factor determining the rate of chemical reactions, including the corrosion of iron. First, it is claimed that naphthenic acid corrosion was not a significant concern below 220°C.[2] Moreover, Gutzeit found that naphthenic acid corrosion followed the Arrhenius equation and the calculated activation energy was 69 kJ/mol.[22] However, Turnbull, *et al.*, reported the activation energy as 31.8 kJ/mol for cyclohexylcarboxylic acid and 23.8 kJ/mol for a mixture of acids.[17] This effect was thought to be due to different structures of naphthenic acids in their experiments.

It was also reported that there was an upper limit of temperature on naphthenic acid corrosion. Derungs observed that naphthenic acids could not corrode steel above 400°C.[2] Gutzeit showed that the increase of corrosion rate was not significant when the

temperature was over 385°C.[22] Given that naphthenic acids were stable at least below 380°C, this phenomenon may be due to the evaporation and pyrolytic decomposition of naphthenic acids at elevated temperatures.[23]

For practical purposes, the rate of steel sulfidation could be estimated by the so called modified McConomy curves.[24] Assuming the total sulfur content is 0.6 wt%, these curves predict that corrosion rates increase with temperature in a parabolic fashion over time. Carbon steel is least resistant against sulfidation and the steel benefits from increasing the amount of chromium as an alloying element. The 18/8 stainless steel corresponds to an alloy that contains 18% Cr and 8% Ni, which is an ideal material in the presence of organosulfur compounds. The corrosion rate multiplier is used to calibrate the corrosion when the total sulfur content is different from 0.6 wt%.

Although modified McConomy curves are widely applied in material selection, they fail to take into account the activities of organosulfur compounds in the crude. As stated in the preceding section, thiophenes are non-corrosive and the sulfidation rates would be much lower if thiophenes in the crudes comprise a significant proportion of the total sulfur content. On the other hand, a higher proportion of active organosulfur compounds in the total sulfur would increase the corrosion rate. As far back as the 1963, mercaptans were found to be more corrosive than expected.[25] Jong, *et al.*, investigated the corrosion by four types of active mercaptans (thiols) at elevated temperatures.[26] It was found that corrosion by the mercaptans was much more severe than predicted by modified McConomy curves.

2.3.3 Effect of Velocity

Flow velocity and associated turbulence enhance the transport of corrosive components towards the metal surface and result in more severe corrosion. Another related flow factor is the wall shear stress which may be able to remove the protective surface layer. In the field, it was noticed that corrosion rates were higher in the locations of maximum turbulence, such as furnaces and bends of the transfer lines.[22] However, the enhanced naphthenic acid corrosion in the liquid phase was difficult to replicate in the laboratory. Gutzeit found that velocity was not a major concern for carbon steel up to 4 m/s.[22] Slavcheva, *et al.*, also reported that flow velocity could not affect the general corrosion of 5Cr and 9Cr steel, but pitting corrosion was more severe at high velocities.[28] It was claimed that enhancement of corrosion was due to synergy of wall shear stress and multi-phase flow.[28, 29] Wang, *et al.*, also noticed that flow rate was not a significant factor up to 7 m/s in a rotating kettle.[30] In fact, the effect of liquid fluid was negligible if the velocity was lower than 30 m/s.[31]

In other studies, it was shown that flow of fluid or wall stress could accelerate naphthenic acid corrosion.[27] Velocity increased the corrosion rate of specimens exposed to the condensate of naphthenic acid vapor.[22] Impingement experiments provided a unique way to investigate corrosion under high velocity/shear stress conditions. Wu, *et al.*, found that corrosion rates of carbon steel were significantly enhanced at the flow rate of 49 m/s.[32] It was also observed that the flow resulted in more severe corrosion at higher temperatures. Qu, *et al.*, also found a critical flow rate for naphthenic acid corrosion.[33]

Velocity was also found to be an important factor in corrosion by organosulfur compounds. High velocity flow may remove iron sulfide layer formed during corrosion and accelerate the corrosion of steel. The API standard recommends the velocity of should be less than 60 m/s.[34] Impingement experiments were also helpful to explore the effect of velocity. Kane and Cayard found that sulfidation was accelerated at high velocity conditions.[27]

2.3.4 Interaction between Naphthenic Acids and Organosulfur Compounds

In addition to the complexities of naphthenic acids and organosulfur compounds, their interaction could lead to more complicated corrosion phenomena and contradictory roles of sulfur compounds. It was argued that an insoluble iron sulfide layer formed during corrosion by sulfur compounds might deter corrosion. For instance, polysulfides were patented for their properties to form protective films and inhibit corrosion.[35] Slavcheva, *et al.*, found that 0.1% of H_2S could inhibit corrosion by over 50% in stagnant experimentation.[36] On the other hand, Piehl claimed that high levels of H_2S were detrimental to corrosion mitigation.[37]

Yépez employed iron powder experimentation to investigate the interaction between sulfur compounds and naphthenic acids.[38] By measuring the concentration of dissolved iron in the solution, it was found that generated H_2S showed an inhibition effect at a high concentration ($> 7.5\%$). It was also observed that disulfide showed a stronger inhibition effect than mercaptan, while thiophene did not affect the iron concentration. Despite these interesting results, it should be noted that the iron powder was more

reactive than the bulk steel. Consequently, iron powder experimentation did not give a measure of the absolute corrosion rate.

Impingement experimentation also reveals complicated interactions between sulfur compounds and naphthenic acids. Kane and Cayard found that low levels of H_2S load (0.2 psia) in the naphthenic acid solution could inhibit the corrosion while an excessive amount of H_2S (0.45 psia) would enhance the impingement attack.[27] It was also observed that the inhibitive effect of organosulfur compounds was closely related to the ability to decompose to H_2S. Qu, *et al.*, found that the presence of 1% total sulfur (in the form of dimethyl disulphide) in the high-TAN solution would accelerate the erosion-corrosion.[33] However, the erosion-corrosion of steel was found to relate to the mechanical properties of steel, *e.g.,* hardness, which made the corrosion of steel more complicated.

Experimentation in stagnant conditions eliminates the effect of flow/velocity and other related factors and reveals the interaction between naphthenic acids and sulfur compounds. Qu, *et al.*, investigated the corrosivity of a series of solutions containing 1% total sulfur (in the form of dimethyl disulfide) and various amounts of naphthenic acids in a static environment at 270°C.[39] It was found that there were threshold TAN values for the corrosion of carbon steel and 5Cr steel. For carbon steel, the increase of the corrosion rate due to the presence of the sulfur compound was not significantly until a TAN of 6 mg KOH/g. For 5Cr steel, the addition of sulfur compound decreased the corrosion rate when the TAN was less than 16 mg KOH/g. It was postulated that sulfur corrosion and naphthenic acid corrosion could be inhibited within the threshold values, but the inhibitive effect diminished for large TAN values.

Huang, *et al.*, studied the concurrent corrosion of carbon steel (Q235) and stainless steel (316) by naphthenic acids and dimethyl disulfide at 280°C.[40] According to Figure 2, the presence of naphthenic acid would inhibit the corrosivity of a low-sulfur solution while the corrosion was accelerated for a high-sulfur solution. It seemed that the inhibition of corrosion could be achieved within a range of total sulfur contents.
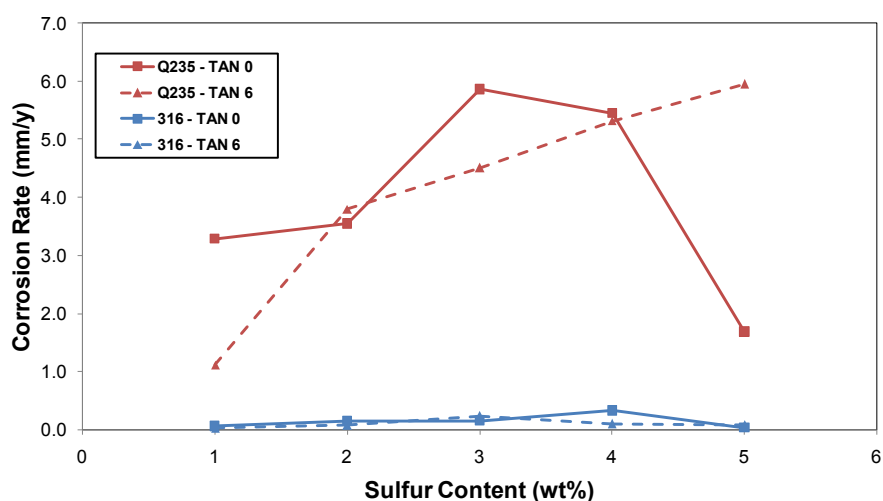
Figure 2. Interaction between naphthenic acid and sulfur content for different metallurgies. This plot was prepared based on the data of Table 2 & 4 in Huang, B. S.; Yin, W. F.; Sang, D. H.; & Jiang, Z. Y.; Synergy Effect of Naphthenic Acid Corrosion and Sulfur Corrosion in Crude Oil Distillation Unit. *Appl. Surf. Sci.,* **2012**, *259*, 664-670.

Kanukuntla, *et al.*, spiked organosulfur-containing base stock oil with commercial naphthenic acids and investigated the corrosion in the static autoclave and Flow Through Mini-Autoclave (FTMA).[41] For experiments with a solution of low organosulfur content (0.15% to 0.38%), it was found that the naphthenic acid corrosion was inhibited before a threshold value of TAN was achieved. Moreover, the higher content of organosulfur in the solution would lead to a growing threshold TAN value.

Given that the iron sulfide layer was supposed to be protective, presulfidated specimens were challenged by naphthenic acid solution to examine the protectiveness.[3] However, the morphology or thickness of iron sulfide layer was found to be unrelated to its protectiveness against naphthenic acid corrosion.

On the other hand, the inhibition of naphthenic acid corrosion could be achieved in the presence of acidic components. For instance, it was claimed that pretreating steel with certain aromatic acids could inhibit naphthenic acid corrosion effectively.[42] Other organic acids[43, 44, 45] and metal naphthenates[46] could serve to inhibit corrosion or decrease the corrosivity of crude. However, the mechanism of inhibition is still vague.

CHAPTER 3: RESEARCH OBJECTIVES

3.1 Global Objective

As shown by the literature review, the mechanism of corrosion by naphthenic acids and organosulfur compounds is not well understood. These two corrosive components interact with each other and lead to complex corrosion phenomena. Moreover, properties of corrosion product layer left on the metal surface cannot be reliably predicted.

Therefore, the global project objective is to clarify the interaction between organosulfur corrosion and naphthenic acid corrosion; investigate the effect of protective corrosion product layers and propose a corrosion model which takes into account the effect of sulfur compounds and naphthenic acids. To be more specific, the goals are as follows:

1) Investigation of the structure and chemical composition of the corrosion product layer formed in different conditions (TAN, S%, and temperature).

2) Correlate the layer chemistry with its protectiveness against naphthenic acid corrosion.

3) Model the mechanism of corrosion.

3.2 Milestones

The characteristics of the corrosion product layer formed on the metal surface were expected to give clues as to the mechanism of corrosion. Therefore, experimental and analytical work focused on the generation and characterization of layers. To this end, the following milestones have been set out and completed:

1) Pretreatment of steel specimens with model dialkylsulfide and naphthenic acids. In the stirred autoclave filled with model dialkylsulfide and/or naphthenic acids, steel specimens were pretreated to form the corrosion product layer on the surface. The specimens were analyzed using weight loss and SEM/EDS.

2) Pretreatment of steel specimens with crude oil fractions. Following the same procedure as in Milestone 1, real crude oil fractions were used to generate the surface layer.

3) Challenge experiments with model naphthenic acids. In order to investigate the layer protectiveness against naphthenic acid corrosion, pretreated steel specimens were transferred into the High Velocity Rig (HVR). The HVR was filled with a solution of naphthenic acids in the mineral model oil and was used to examine the protection conferred by the layer. The specimens were analyzed using weight loss and SEM/EDS.

4) TEM (Transmission Electron Microscopy) analysis on the selected layer formed on the metal surface. As an advanced analytical technique, TEM allowed observation of fine layer structure at the nanometer level. Comparisons between protective layers and unprotective layers provided valuable information on the corrosion mechanism.

5) Modeling the mechanism of corrosion. Based on the experimental data and analytical results, a model was developed to simulate the corrosion process.

CHAPTER 4: EQUIPMENT AND EXPERIMENT PROCEDURES

4.1 Equipment

4.1.1 Stirred Autoclave

As shown in Figure 3, stirred autoclaves were used in the first step of the experimental procedure to assess the corrosivity of real crudes and model compounds. They were also used to generate surface layers for further experimentation in the second step described below. Steel specimens were exposed to various oils at high temperatures in this so called "pretreatment" step. Vent lines fed nitrogen to the stirred autoclave to remove any residual oxygen before the experiments. During experiments, the stirred autoclave was sealed and its impeller rotated (~500 rpm) to eliminate any temperature gradients inside. After the experiment, the stirred autoclave was cooled to room temperature and the vent line opened to release any autogenous gas.
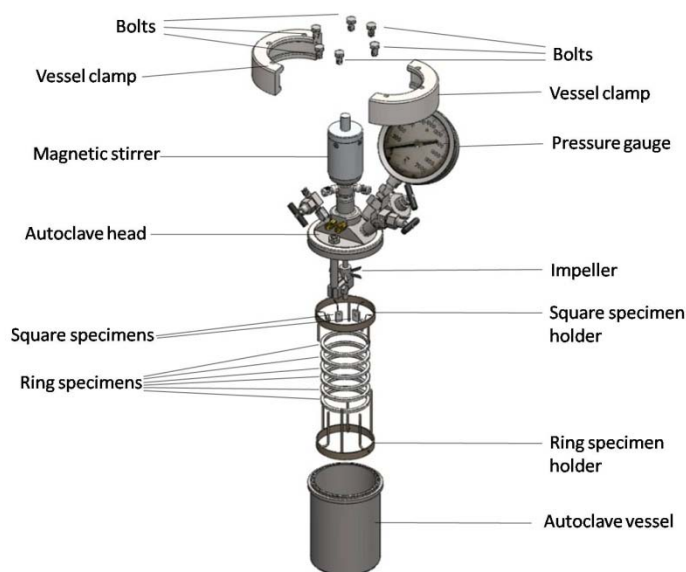
Figure 3. Stirred autoclave for generating the corrosion product layer in crude fractions and model compounds (reproduced from ICMT image library).

4.1.2 High Velocity Rig (HVR)

As shown in Figure 4, a flow-through rotating cylinder autoclave called the High Velocity Rig (or HVR) was used in the second step of the experimental procedure. Specimens pretreated in the stirred autoclave (as described in the previous paragraph) were transferred to the HVR for the so called "challenge" step where they were exposed to the mineral model oil containing various amounts of model naphthenic acids. The HVR was designed to create a high flow velocity and associated turbulence and shear stress. The core of the HVR system is the reactor, or autoclave with a rotating cylinder setup that enables flow through of a solution of mineral model oil with naphthenic acids (Figure 5).
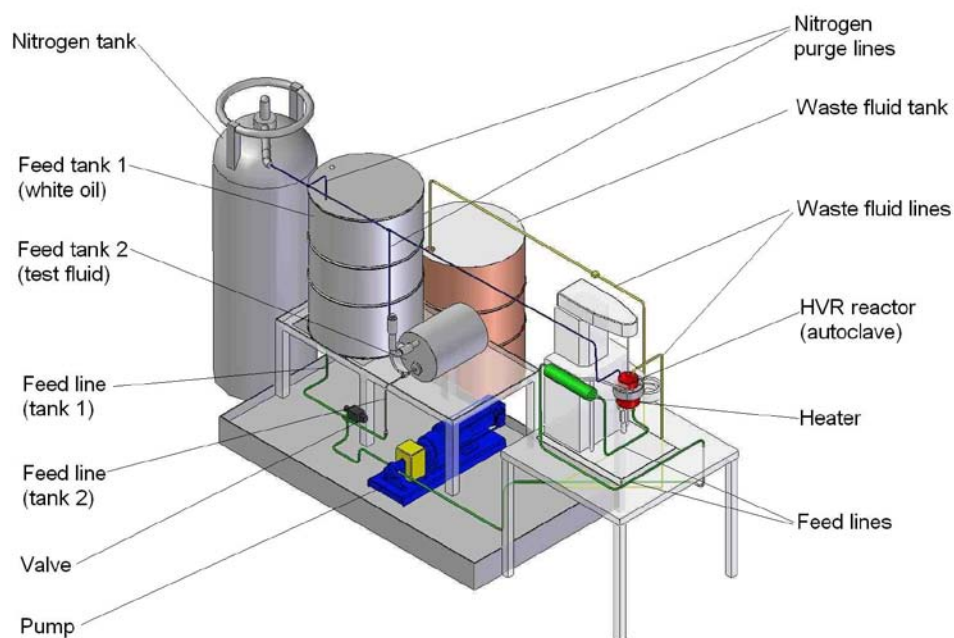
Figure 4. High Velocity Rig (HVR) for examining the layer protectiveness against naphthenic acid corrosion (reproduced from ICMT image library).
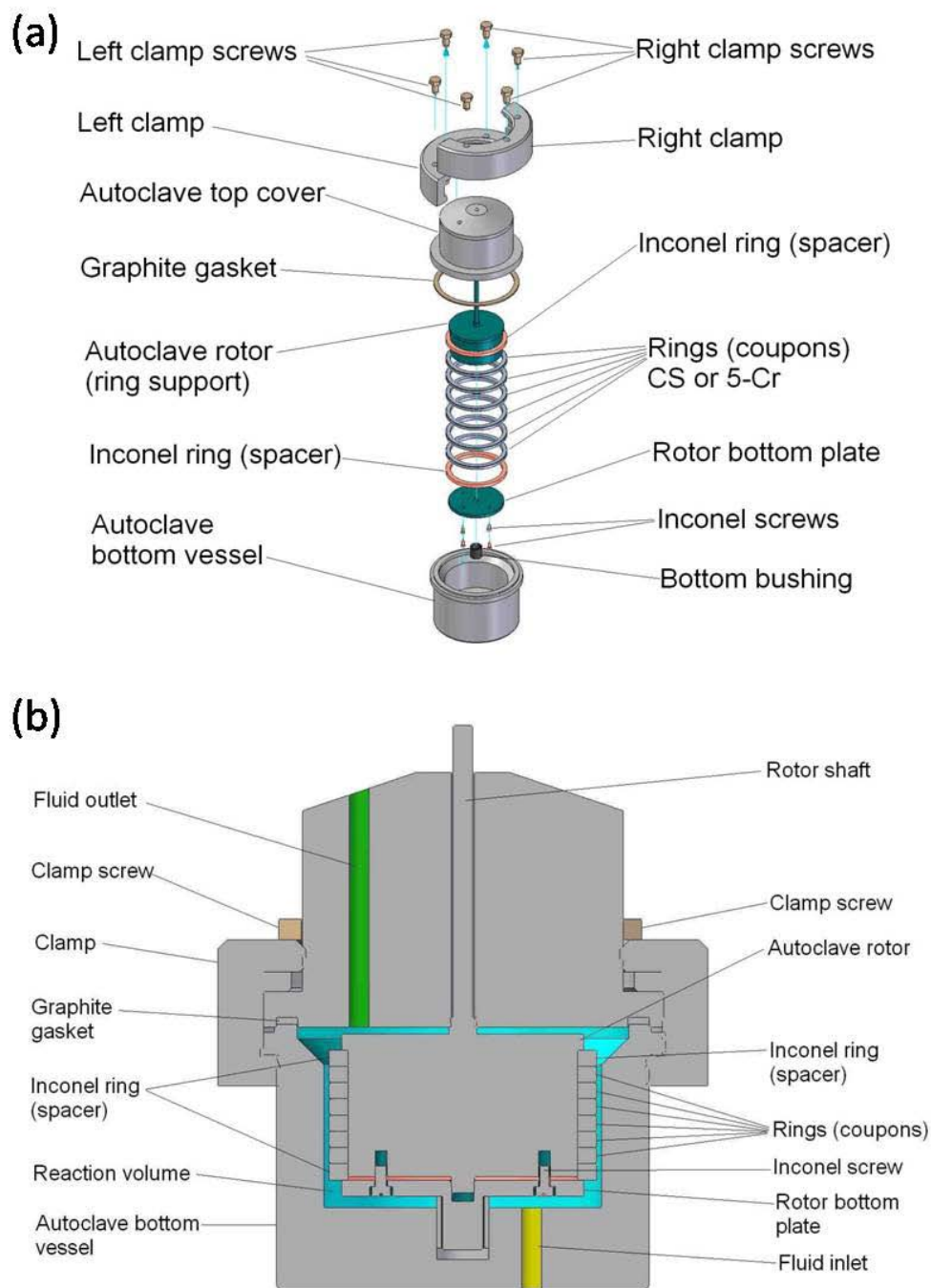
Figure 5. Scheme of HVR reactor. (a) Exploded view; (b) Cross-section view (reproduced from ICMT image library).

4.1.3 Analytical Equipment

Generally, layers formed in the stirred autoclave or HVR were examined with a JEOL JSM-6390 SEM located in ICMT. Prior to analysis, any possible carbonaceous deposits was rinsed away with toluene and acetone during sample cleaning, and dried. With the maximum magnification of 300,000x, the layer morphology (both top view and cross section) could be examined in detail. More importantly, a Genesis EDAX attached to the SEM permits EDS (Energy Dispersive Spectroscopy) analysis (both locally and over large areas) on samples and provides valuable information on the layer chemical composition.

Furthermore, some layers were selected to be analyzed with a FEI Helios 600 for FIB (Focused Ion Beam) and FEI Tecnai F20XT for TEM (Transmission Electron Microscopy) located at the Ohio State University. The technique of FIB-TEM is suitable to analyze layers that are too thin to be visible with the SEM. The FIB-TEM could show the fine structure of layer cross-section. The EDS function is available on the TEM equipment as well.

4.2 Experimentation Materials

4.2.1 Steel Specimens

To simulate the corrosion of the materials used in the field, two of the most commonly utilized steels in refineries were selected for experimentation, i.e., A106 carbon steel (CS) and A182-F5 chrome steel (5Cr steel). There were two geometries of experiment specimens. One was in the shape of rings with an inner diameter 70.43 mm, an outer diameter 81.76 mm, and a thickness 5 mm – used in the pretreatment-challenge

experimental protocol. The other specimen type was square with a central hole with

dimensions of 19.12 mm $\times$ 12.72 mm $\times$ 3.20 mm. The central hole located on the largest

surface had a diameter of 3.26 mm (Figure 6). These were used primarily for weight loss

and analytical purposes.
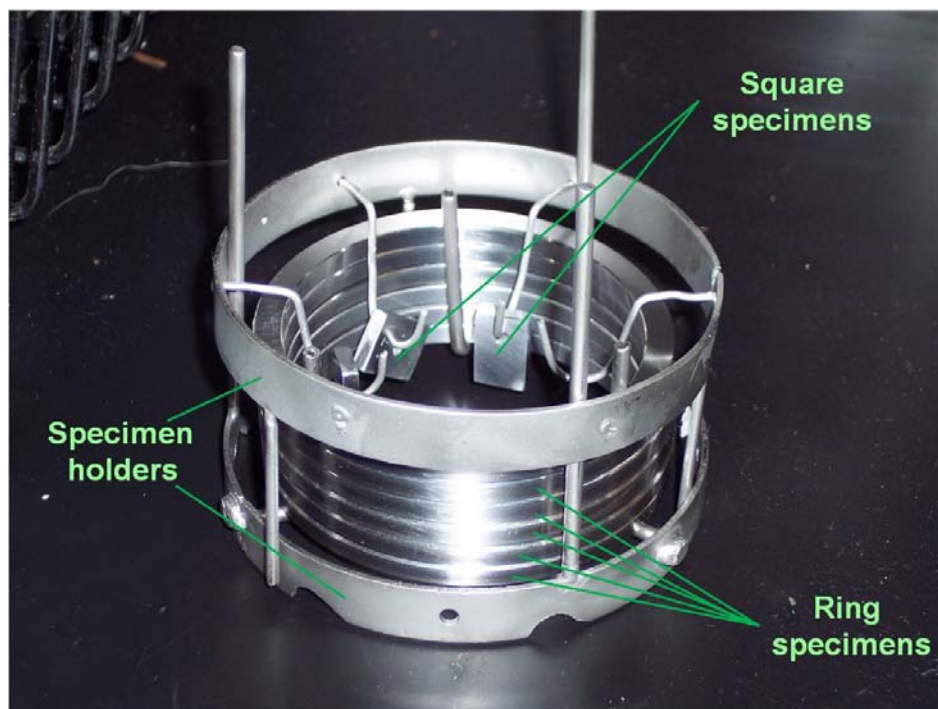
Figure 6. Ring and square specimens in the experimentation (reproduced from ICMT image library).

4.2.2 Mineral Model Oil

An inert mineral model oil was used to flush the HVR and as the solvent to

prepare model solutions. This is an inert naphthenic oil with outstanding resistance

against oxidation and pyrolysis. Table 2 shows selected physical and chemical properties

for the oil.

Table 2.[1]

Selected Physical and Chemical Properties of the Mineral Model Oil

Parameter	Description
Appearance	Clear Liquid
Color	Colorless
Odor	Odorless
Density (at 16°C, kg/m^3)	876
Flash Point (°C)	254
Average Molecular Weight	530
Initial Boling Point (°C)	388

4.2.3 Chemicals Used for Layer Removal

After corrosion experimentation, the layer formed on the metal surface was removed chemically by a Clarke solution. According to ASTM G 1-90, the Clarke solution was prepared by dissolving stannous chloride (5 g, $SnCl_2,\cdot2H_2O$, 99.99%, Fluka), and antimony (III) oxide (5 g, Sb_2O_3, 99.999%, Sigma-Aldrich) in hydrochloric acid (84 mL, HCl 12.1 N, analytical purity, Fisher).

4.3 Experiment Procedures

4.3.1 Specimen Preparation

Steel specimens had to be polished before experimentation to ensure repeatability and reliability of results. Each specimen was polished with 400 and 600-grit silicon-

---

[1] CITGO Tufflo Process Oil Product Information

carbide papers (SiC) in succession. Isopropanol was used to flush specimens during polishing to prevent oxidation and overheating. After polishing, specimens were wiped with a paper towel, rinsed with toluene and acetone, and dried with nitrogen flow. Weights of fresh clean specimens were taken on an analytical scale with accuracy up to 0.1 mg.

4.3.2 Pretreatment Experiment

Layers were generated in the stirred autoclave filled with experimentation fluid (real crude fractions or model compounds: mineral model oil containing a dialkylsulfide and a blend of model naphthenic acids). In a typical experiment, specimens (CS and 5Cr steel) were mounted in the one-liter stirred autoclave filled with 0.7 liter of fluid. After the stirred autoclave was sealed, nitrogen was purged through the system to remove oxygen. Then, the gas valve was closed and the temperature was raised to 316°C or 343°C, the impeller rotation was started, and the experiment began. During the experiment, the stirred autoclave was pressurized by the autogenous gas released by experimentation fluid. At the end of the experiment the electrical heating was turned off, the impeller was stopped and the stirred autoclave was cooled to room temperature. Specimens were removed, rinsed with toluene and acetone, gently rubbed with a soft plastic brush, treated with "Clarke" solution, and reweighed. Based on the weight difference of specimens before and after the experiment, the corrosion rate was calculated.

Generally, the corrosion product layer formed on the metal surface during the pretreatment experiment was examined under SEM to analyze its surface morphology

and cross section profile. At the same time, EDS analysis was conducted to investigate the chemical composition. For some layers of particular interest, FIB-TEM analysis was done.

4.3.3 Challenge Experiment

After experimentation in the stirred autoclave, specimens were taken out without any cleaning to preserve the layer integrity on the metal surface. These pretreated specimens were then installed in the HVR to examine the protectiveness of layer. In a typical challenge experiment, there was a flow through the HVR using a solution of commercial naphthenic acids in mineral model oil (at TAN 3.5 and a temperature of 343°C). During the experiment, the speed of the rotating cylinder was set to 2000 rpm (translating to a peripheral velocity of 8.56 m/s, Reynolds number of 1771 and wall shear stress of 74 Pa). The back-pressure of 150 psig was applied to suppress gas breakout and the flow through rate of the oil containing fresh naphthenic acid was set to 7.5 cm^3/min. A comparison of the stirred autoclave and the HVR is shown in Table 3.

Table 3.

Comparison between Stirred Autoclave and HVR

Stirred Autoclave	HVR
Stagnant Liquid	Replenishing Fluid
No Effect of Flow	Effect of Flow
Autogenous Pressure	Fixed Pressure
Vapor and Liquid Phases	Liquid Phase

After the challenge experiment, specimens were treated identically to those recovered in the pretreatment experiment. Based on the weight loss difference between the pretreatment and the challenge experiments, the net weight loss in the challenge and its corresponding corrosion rate could be calculated and the layer protectiveness could be assessed. Then the possible correlation between the layer properties and the TAN or organosulfur content of crudes could be examined.

4.3.4 Calculation of Corrosion Rate

Corrosion rates of specimens were calculated based on their weight loss during the experiment. For a single experiment conducted in the stirred autoclave, the corrosion rate was calculated using Equation (1).

$$CR = \frac{(IW - FW)}{\rho_{steel} \times A_s \times t} \times 10 \times 24 \times 365 \tag{1}$$

where:

CR – Corrosion rate, mm/y

IW – Initial weight of fresh polished steel specimen, g

FW – Final weight of steel specimen after treatment with a Clarke solution, g

ρ_{steel} – Density of steel specimen, g/cm^3

A_s – Area of steel specimen exposed to corrosive fluid, cm^2

t – Duration of experimentation in the stirred autoclave, h

In a pretreatment-challenge experiment, fresh polished specimens were pretreated in the stirred autoclave followed by challenging in the HVR. While the corrosion rate in the pretreatment step was calculated according to Equation (1), the challenge corrosion was assessed in the following equation.

$$CR = \frac{(IW - FW - WL_{Pretreatment})}{\rho_{steel} \times A_s \times t} \times 10 \times 24 \times 365 \qquad (2)$$

where:

CR – Corrosion rate, mm/y

IW – Initial weight of fresh polished steel specimen, g

FW – Final weight of steel specimen after treatment with Clarke solution, g

$WL_{Pretreatment}$ – Weight loss of specimen in the pretreatment phase, g

ρ_{steel} – Density of steel specimen, g/cm^3

A_s – Area of steel specimen exposed to corrosive fluid, cm^2

t – Duration of experimentation in the HVR, h

For each metallurgy (CS or 5Cr steel), three ring specimens were used in the experiment and the corrosion rate of each specimen was calculated according to Equation (1) or (2). In the figures showing experiment results in this dissertation, the data points represent the average corrosion rate of these specimens while the error bar shows the maximum or the minimum measured value in a single experiment.

CHAPTER 5: EXPERIMENTAL RESULTS: PURE TAN EXPERIMENTS IN THE HVR

5.1 Introduction

Pure TAN experiments refer to the experiments in which fresh polished specimens were installed in the HVR and were challenged by the solution of naphthenic acids dissolved in the mineral model oil. Experimental conditions in the pure TAN experiment were the same as the conditions in a typical challenge experiment described in the preceding chapter except that specimens were not pretreated in the stirred autoclave. Since there was no protective layer, the corrosion rates obtained in this experiment were expected to be the upper limit for a given TAN value. In this way, results from pure TAN experiments could serve as the reference for comparing of the protectiveness of the layer formed in the stirred autoclave.

5.2 Results and Discussion

In the HVR, the naphthenic acid solution (TAN 3.5) flowed through at 343°C for 24 hours. To ensure the reliability of the experiment results, three repeated experiments were conducted, as shown in Figure 7. The repeatability of the results is acceptable, particularly between the 2nd and 3rd experiment, with the 1st experiment being about 25% higher.

Pure TAN 3.5 corrosion rates for CS vary from between 8 mm/y to 10 mm/y, while 5Cr steel seems to be more resistant against pure naphthenic acid attack (the corrosion rate is around 1 mm/y to 2 mm/y). However, the presence of 5% chromium in the steel was not expected to produce such a significant effect, according to industrial

experience. Actually, the rationale for using a 5Cr steel in the field was to help resist

corrosion by sulfur compounds rather than naphthenic acids. Nevertheless these results

were clearly showing a beneficial effect of Cr in the case of pure naphthenic acid attack.

The reasons for this behavior were actually discovered in the present study and will be

discussed below.
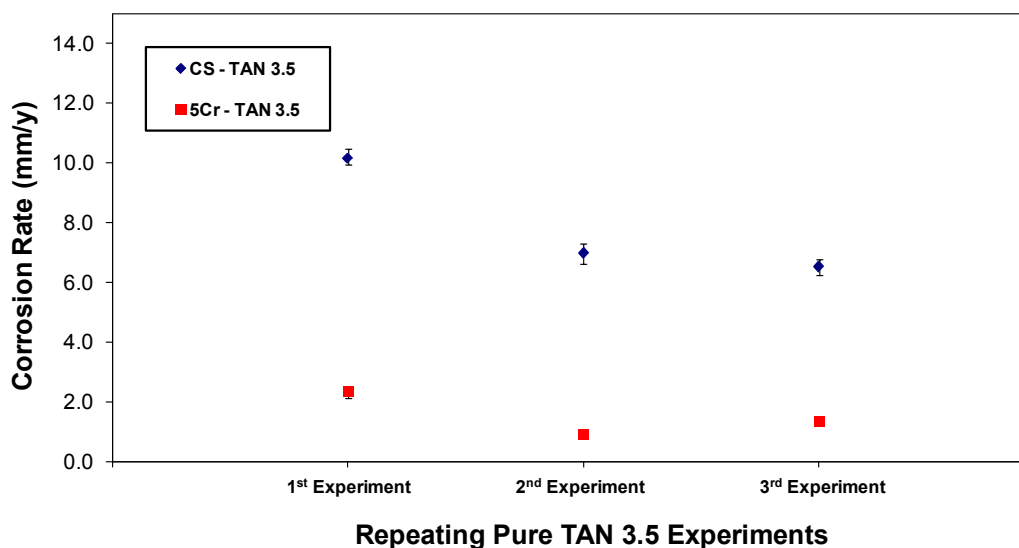
Figure 7. Results of repeating pure TAN 3.5 experiments for CS and 5Cr steel in the
HVR. The time of exposure was 24 hours, the temperature was 343°C, and the peripheral
velocity was 8.56 m/s.

SEM analysis should provide a hint as to the nature of this corrosive behavior.

Shown in Figure 8, EDS analysis indicates that the surface of the CS specimens is

partially covered by a layer comprised of iron and sulfur. It might not be surprising to

find sulfur on the metal surface because there are trace amounts of organosulfur in the

naphthenic acids.
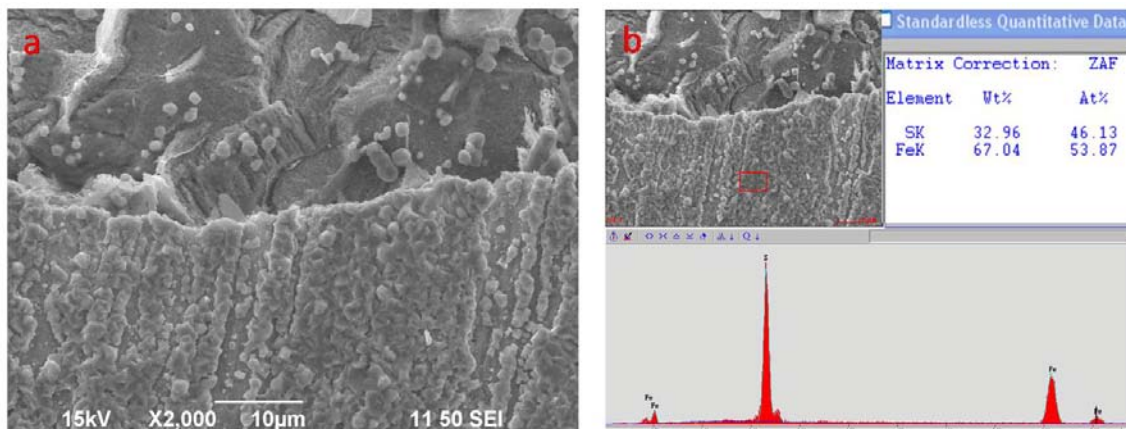
Figure 8. Surface of CS specimen after pure TAN 3.5 experiment. (a) Surface SEM image; (b) EDS analysis on the surface. For corrosion rates see Figure 7. SEM and EDS analysis of the cross section is given in Figure 9.

SEM images of the layer cross-section of the CS steel sample (Figure 9) reveal that the surface layer is detached from the metal, which explains the high corrosion rate. Cross-section EDS analysis confirms that the layer is composed of primarily iron and sulfur (probably iron sulfide), which is consistent with the surface EDS analysis.
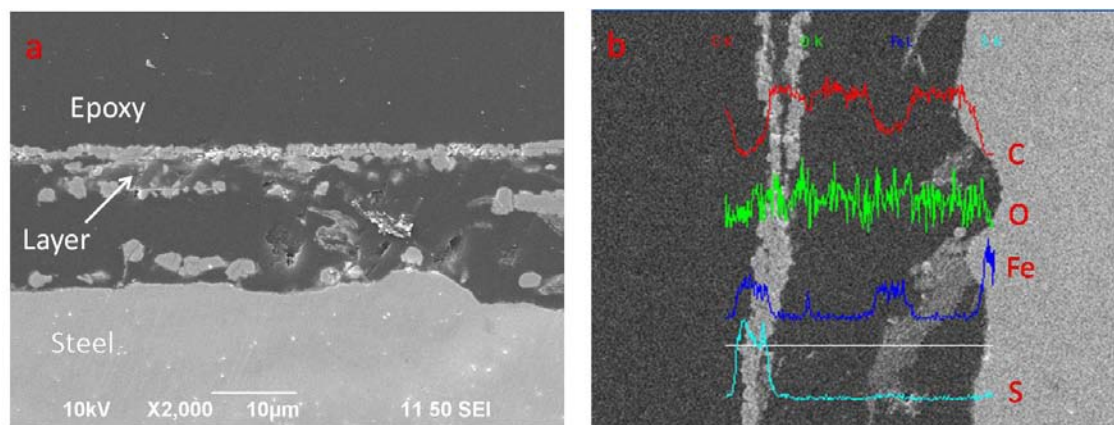
Figure 9. Cross-section analysis of CS specimen after pure TAN 3.5 experiment. (a) Cross-section SEM image; (b) Corresponding EDS analysis along the white line on the bottom. For corrosion rates see Figure 7. SEM and EDS analysis of the surface is given in Figure 8.

The surface of the 5Cr steel after the pure TAN 3.5 experiment is different from that of CS (Figure 10). The steel is fully covered by the surface layer which was found to consist of iron and sulfur by EDS analysis. Chromium was found at a concentration consistent with that in the 5Cr steel.
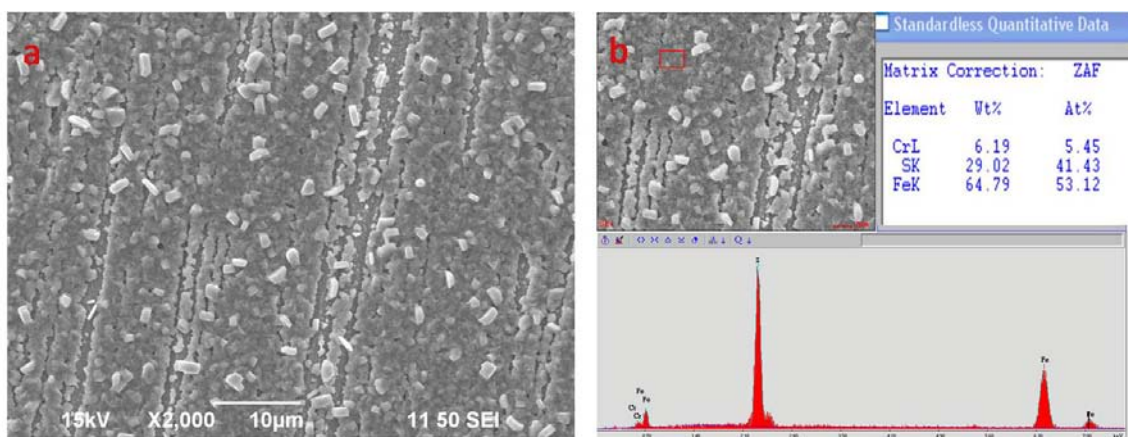
Figure 10. Surface of 5Cr steel specimen after pure TAN 3.5 experiment. (a) Surface SEM image; (b) EDS analysis on the surface. For corrosion rates see Figure 7. SEM and EDS analysis of the cross section is given in Figure 11.

Figure 11 shows the corresponding SEM image of the layer cross-section, which is different from the layer that forms on CS. The layer formed on 5Cr steel is thinner (< 0.5 µm) and attaches to metal surface. Compared with the CS, the EDS analysis on 5Cr steel reveals peaks of oxygen and chromium; this is consistent with formation of an oxide layer beneath the iron sulfide layer. The surface layer structure might be related to the lower corrosion rate for 5Cr steel. However, magnification limitations in the SEM image do not allow for a more detailed examination of the layer.
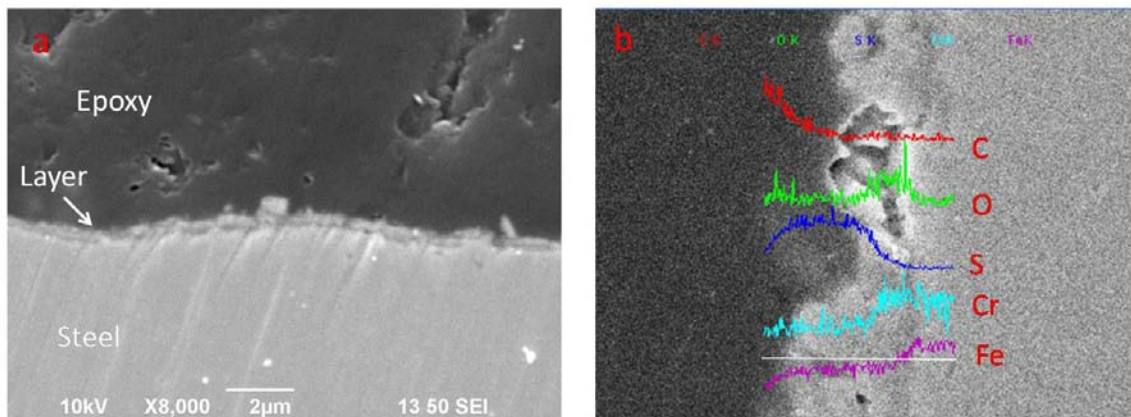
Figure 11. Cross-section analysis of 5Cr steel specimen after pure TAN 3.5 experiment. (a) Cross-section SEM image; (b) Corresponding EDS analysis along the white line on the bottom. For corrosion rates see Figure 7. SEM and EDS analysis of the surface is given in Figure 10.

5.3 Summary

The pure TAN 3.5 corrosion rate for CS measured in the HVR was in the range of 8 – 10 mm/y while the corrosion rate for 5Cr was only 1 – 2 mm/y. It was found that the presence of chromium was helpful to resist pure naphthenic acid corrosion, contradicting some of the anecdotal field experience.

SEM analysis (surface and cross-section) indicated that a thin detached unprotective iron sulfide layer formed on both metal surfaces (CS and 5Cr), which was not expected in the pure TAN experiment. It was postulated that a trace concentration of sulfur compounds in the naphthenic acid could account for the formation of thin iron sulfide layer.

However, the layer morphology on CS and 5Cr specimens was quite different, as shown by SEM images. The layer on 5Cr adhered to the metal surface. The EDS analysis along the layer cross-section suggested the presence of an oxide layer. Both the layer

adherence and presence of oxygen in the layer were suspected to contribute to the low corrosion rate.

CHAPTER 6: EFFECT OF PRETREATMENT DURATION AND

TEMPERATURE

6.1 Introduction

As discussed in previous chapters, the temperature was a vital factor related to corrosion by crude oil factions. Consequently, it could be reasonably expected that temperature would affect the layer protectiveness.

Experiment duration was another factor in forming a surface layer. For short experiment duration, the bare steel was exposed to the crude and the corrosion rate was at a maximum. As the duration became longer, a layer formed and the corrosion rate decreased. However, the layer delaminated from the metal surface as it was being formed. A stable layer generation and corrosion rate should be achieved if the experiment duration was sufficiently long and a balance between layer formation and layer delimitation was achieved.

How exactly the pretreatment duration affected the challenge corrosion rate was an open question. Therefore, it was necessary to find the optimum experimentation condition which would be applied in various experiments.

6.2 Results and Discussion

6.2.1 Effect of Pretreatment Duration

Given limited time and facilities, Fraction G and F were selected to investigate the effect of pretreatment temperature and duration. Fraction G and F were distilled from the same crude oil. Fraction G, labeled as 650+, was distilled at 650°F (343°C) in the atmospheric distilling unit. To extract more fractions and minimize decomposition,

residues from atmospheric distillation were fed into a vacuum distilling unit where a

vacuum was applied on the top of the tower to lower the boiling point of fractions.

Fraction F, or vacuum gas oil (VGO), was generated in this step.

As shown in Table 4, Fractions G and F were used to pretreat steel specimens in

the stirred autoclave. The temperature was fixed at 316°C and the pretreatment duration

varied from 24 hours to 96 hours. The possible effect of pretreatment duration could be

examined.

Table 4.

Experiment Matrix - Effect of Duration on the Pretreatment Corrosion Rate

Feed	TAN (mg KOH / g oil)	Sulfur Content (wt%)	Temperature (°C)	Duration (hour)
G (650+)	3	5.19	316	24
G (650+)	3	5.19	316	48
G (650+)	3	5.19	316	96
F (VGO)	4.6	3.65	316	24
F (VGO)	4.6	3.65	316	48
F (VGO)	4.6	3.65	316	96

Figure 12 shows the corrosion rates of steel specimens pretreated in Fraction G

for 24 hours to 96 hours. Given that the corrosion rate was calculated from the specimen

weight loss at the end of each experiment, data points in this figure indicate the average

corrosion rates for corresponding pretreatment durations. For shorter term pretreatment,

CS is slightly less resistant against corrosion than 5Cr steel. However, their corrosion

rates become stabilized and converge in a 96-hour experiment. This suggests that the

pretreatment duration of 24 hours is long enough to replicate long-term corrosion rate.
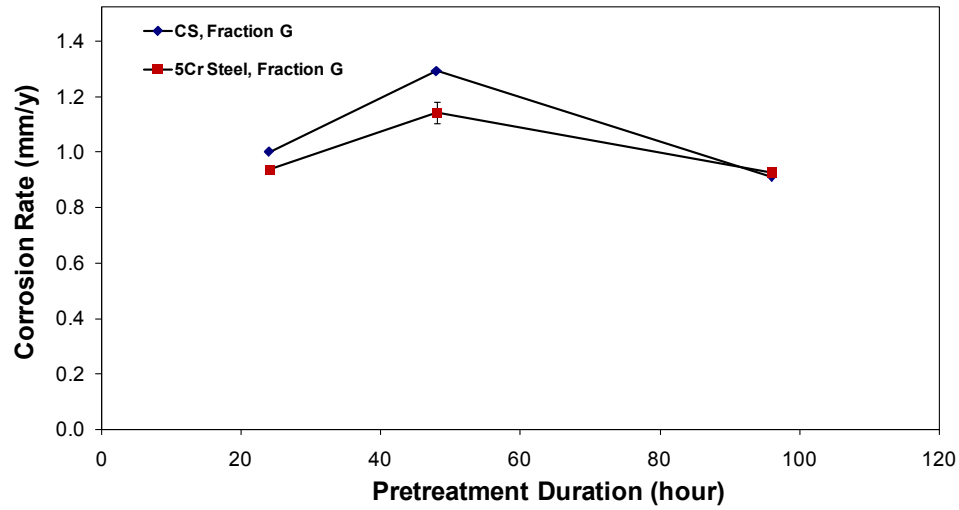
Figure 12. Pretreatment corrosion rates for CS and 5Cr steel specimens pretreated with Fraction G in the stirred autoclave. The pretreatment duration varied from 24 hours to 96 hours and the temperature was 316°C.

The evolution of corrosion rates for Fraction F is different from Fraction G (Figure 13). 5Cr steel exhibits stable corrosion rates in all experiments. On the contrary, CS shows more variance in corrosion rates. The average corrosion rate for the 96 hour pretreatment is the highest.
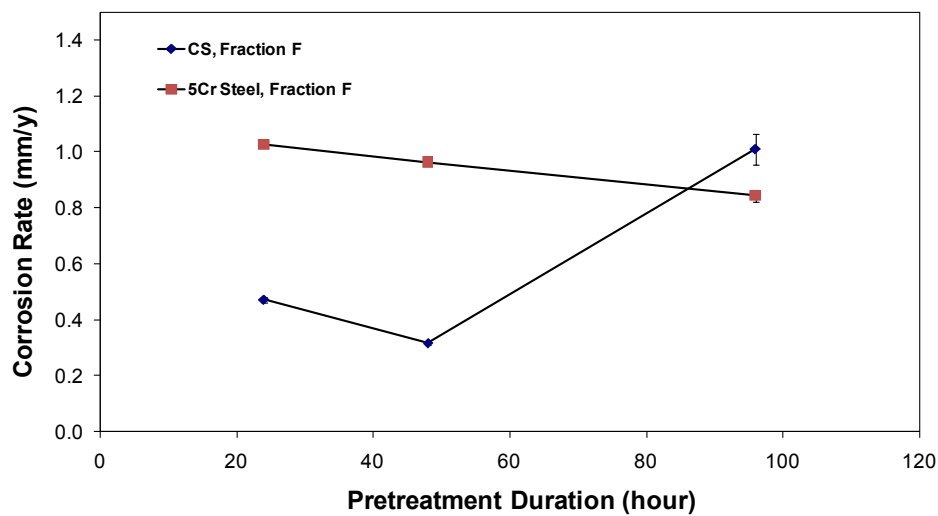
Figure 13. Pretreatment corrosion rates for CS and 5Cr steel specimens pretreated with Fraction F in the stirred autoclave. The pretreatment duration varied from 24 hours to 96 hours and the temperature was 316°C.

Another question arose as to whether the pretreatment duration could affect the property of layer, i.e., layer protectiveness against naphthenic acid corrosion. To this end, an experiment matrix was designed as shown in Table 5. In the pretreatment-challenge experiment, steel specimens were pretreated with Fraction G or F at 316 °C for 24 or 48 hours, followed by the challenge by naphthenic acid solution (TAN 3.5) in HVR. The challenge condition was identical to the condition of the pure TAN experiment.

Table 5.

Pretreatment-Challenge Experiment Matrix - Effect of Pretreatment Duration on Layer Protectiveness

Pretreatment			Challenge			
Feed	Temperature (°C)	Duration (hour)	Feed	TAN (mg KOH / g oil)	Temperature (°C)	Duration (hour)
G (650+)	316	24	Mineral Model Oil + Naphthenic Acids	3.5	343	24
G (650+)	316	48	Mineral Model Oil + Naphthenic Acids	3.5	343	24
F (VGO)	316	24	Mineral Model Oil + Naphthenic Acids	3.5	343	24
F (VGO)	316	48	Mineral Model Oil + Naphthenic Acids	3.5	343	24

The effect of pretreatment duration could be seen in Figure 14. For both CS and 5Cr steel, it seems that the layer formed in a 24-hour pretreatment is more protective. 5Cr steel performs better in HVR challenge. However, neither pretreatment duration could promote a layer that could resist naphthenic acid attack in HVR.
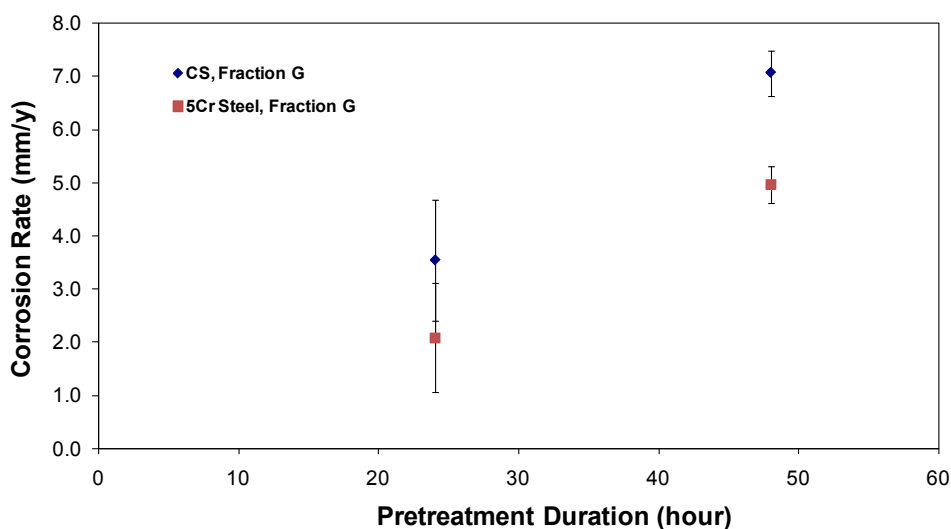
Figure 14. Challenge corrosion rates for CS and 5Cr steel specimens pretreated with Fraction G. For the pretreatment in the stirred autoclave, the pretreatment duration varied from 24 hours to 48 hours and the temperature was 316°C. For the challenge in the HVR, the time of exposure was 24 hours, the temperature was 343°C, and the peripheral velocity was 8.56 m/s.

Pretreatment in Fraction F shows a similar trend as Fraction G (Figure 15). Longer pretreatment does not improve the protectiveness of layer.
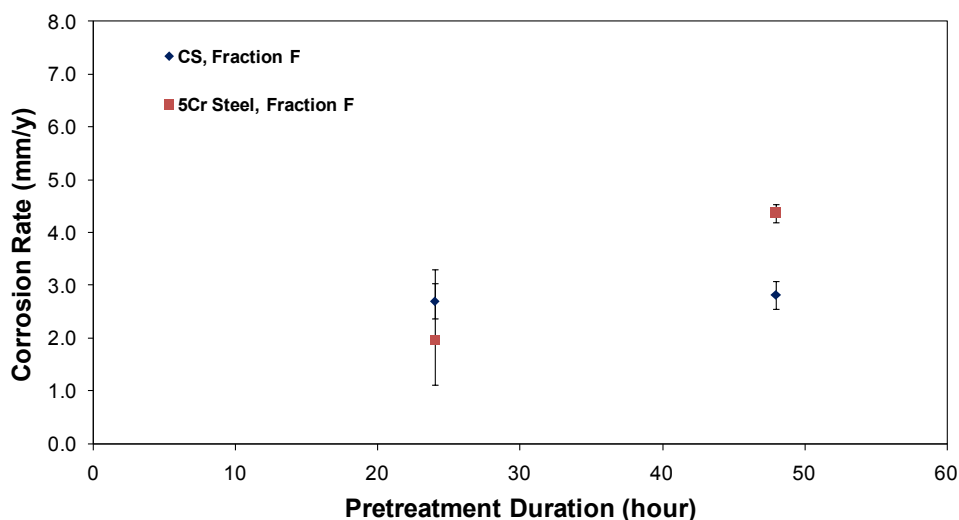
Figure 15. Challenge corrosion rates for CS and 5Cr steel specimens pretreated with Fraction F. For the pretreatment in the stirred autoclave, the pretreatment duration varied from 24 hours to 48 hours and the temperature was 316°C. For the challenge in the HVR, the time of exposure was 24 hours, the temperature was 343°C, and the peripheral velocity was 8.56 m/s.

6.2.2 Effect of Pretreatment Temperature

Experimental data presented in the previous section indicated that pretreatment for 24 hours was sufficient to explore the layer properties. However, there was another important factor to be investigated before applying experimentation procedures to other crudes, *i.e.*, pretreatment temperature. The next goal of experimentation was to find a favorable pretreatment temperature to form the protective layer.

Four representative fluids were selected in the following experiments (Table 6). Yellow oil was a refined mineral oil without acidic content distilled to remove aromatic content with the total sulfur content of 0.25%. Before experimentation, yellow oil was mixed with naphthenic acids to boost its TAN to 0.1. Fraction B was a high-sulfur vacuum gas oil. To be consistent with the previous experimentation, Fractions G and F

were retained as experiment fluids. The pretreatment temperature was changed from

316°C to 343°C (For Fraction B, the lower pretreatment temperature was 302°C, which

was close to 316°C).

Table 6.

Experiment Matrix - Effect of Temperature on Pretreatment Corrosion Rate

Feed	TAN (mg KOH / g oil)	Total Sulfur Content (wt%)	Temperature (°C)	Duration (hour)
Yellow Oil	0.1	0.25	316	24
B (VGO)	< 0.1	1.92	302	24
G (650+)	3	5.19	316	24
F (VGO)	4.6	3.65	316	24
Yellow Oil	0.1	0.25	343	24
B (VGO)	< 0.1	1.92	343	24
G (650+)	3	5.19	343	24
F (VGO)	4.6	3.65	343	24

Figure 16 and Figure 17 show the pretreatment corrosion rates for CS and 5Cr

steel at different temperatures. For both types of steel, a higher temperature results in a

twofold or threefold increase in corrosion rates. Moreover, it seems that total sulfur

content is the predominant factor determining the crude corrosivity – fractions with

higher sulfur content shows higher corrosion rates regardless of their different TAN

values. For each fraction, 5Cr steel and CS specimens give comparable corrosion rates,

indicating that 5% of chromium in the steel is insufficient to affect the corrosion rate.
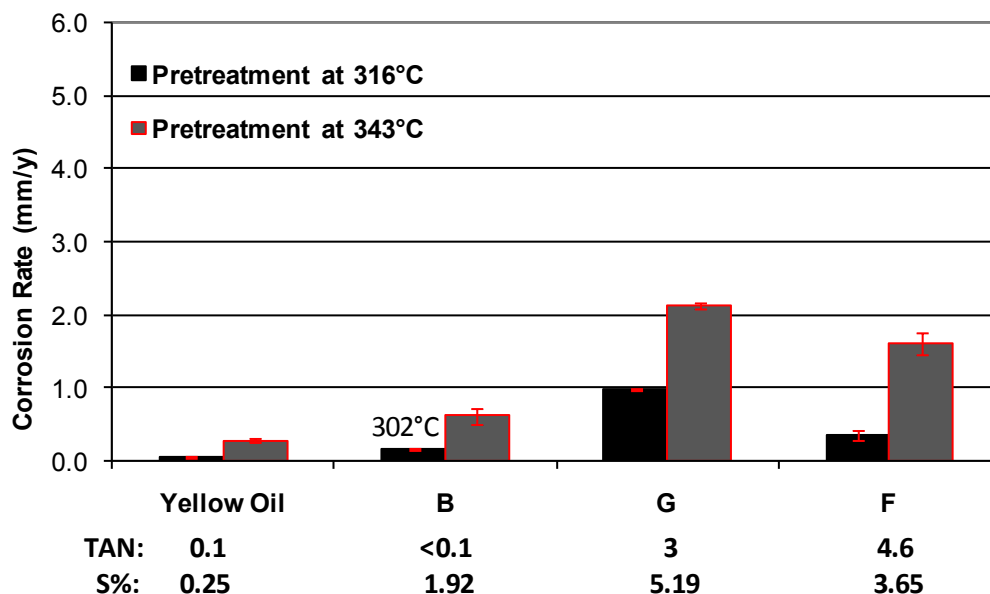
Figure 16. Pretreatment corrosion rates for CS pretreated with different fluids in the stirred autoclave. The pretreatment duration was 24 hours and the temperature was 316°C or 343°C.
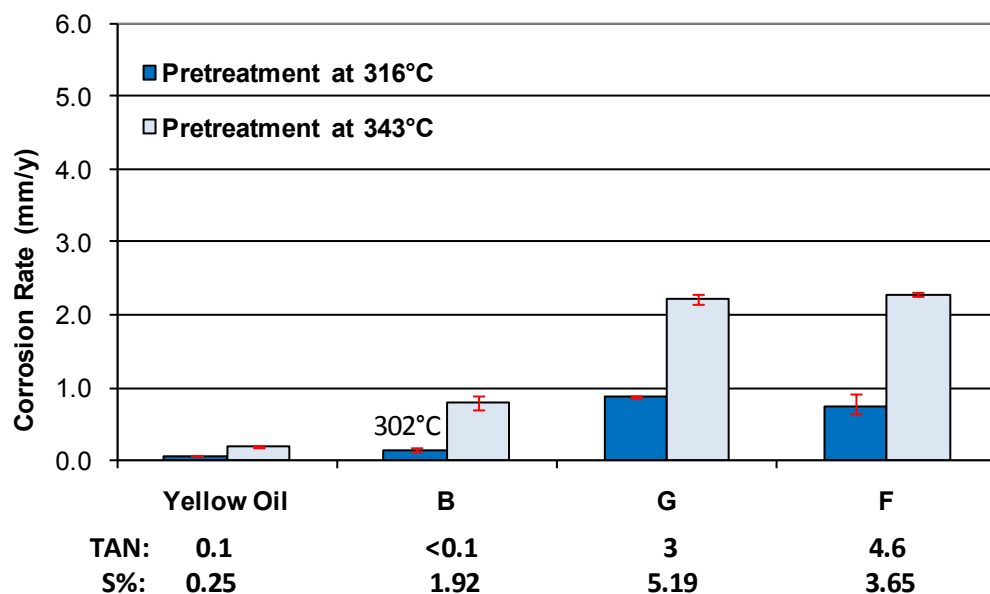
Figure 17. Pretreatment corrosion rates for 5Cr steel with different fluids in the stirred autoclave. The pretreatment duration was 24 hours and the temperature was 316°C or 343°C.

The next step was to examine the effect of pretreatment temperature on the layer protectiveness. As shown in Table 7 steel specimens pretreated with various fluids at 316 or 343°C were challenged by naphthenic acid solution (TAN 3.5) in the HVR. The results of the challenge are shown in the following figures (Figure 18 and Figure 19).

Table 7.

Pretreatment-Challenge Experiment Matrix - Effect of Pretreatment Temperature on Layer Protectiveness

Pretreatment			Challenge			
Feed	Temperature (°C)	Duration (hour)	Feed	TAN (mg KOH / g oil)	Temperature (°C)	Duration (hour)
Yellow Oil	316	24	Mineral Model Oil + Naphthenic Acids	3.5	343	24
B (VGO)	302	24	Mineral Model Oil + Naphthenic Acids	3.5	343	24
G (650+)	316	24	Mineral Model Oil + Naphthenic Acids	3.5	343	24
F (VGO)	316	24	Mineral Model Oil + Naphthenic Acids	3.5	343	24
Yellow Oil	316	24	Mineral Model Oil + Naphthenic Acids	3.5	343	24
B (VGO)	302	24	Mineral Model Oil + Naphthenic Acids	3.5	343	24
G (650+)	316	24	Mineral Model Oil + Naphthenic Acids	3.5	343	24
F (VGO)	316	24	Mineral Model Oil + Naphthenic Acids	3.5	343	24

Figure 18 does not give affirmative evidence relating to the effect of pretreatment temperature. However, it is clear that the layer formed at either pretreatment temperature is nonprotective and all the challenge corrosion rates are higher than 1 mm/y. For yellow oil and Fraction B, a higher pretreatment temperature helps to increase the layer protectiveness. But this effect is negligible for Fraction G. For Fraction F, the lower pretreatment temperature promotes formation of a more protective layer.
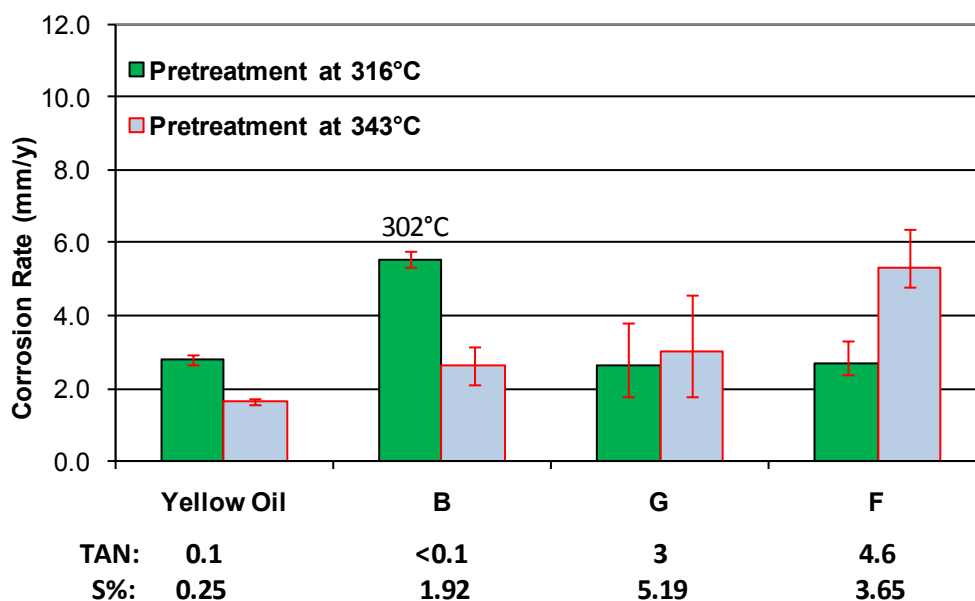
Figure 18. Challenge corrosion rates for CS specimens pretreated with different fluids. For the pretreatment in the stirred autoclave, the pretreatment duration was 24 hours and the temperature was 316°C or 343°C. For the challenge in the HVR, the time of exposure was 24 hours, the temperature was 343°C, and the peripheral velocity was 8.56 m/s.

The effect of the pretreatment temperature is more consistent when challenging the 5Cr steel specimens (Figure 19). For all four fluids, a lower pretreatment temperature facilitates the formation of more protective layers. For Fractions G and F, the contrast between challenge corrosion rates with different pretreatment temperatures strongly

suggests that lower pretreatment temperature is preferable. Particularly, the layer formed

in Fraction B at 302°C is most protective. This suggests that lower pretreatment

temperature (316°C) should be used form protective layers.
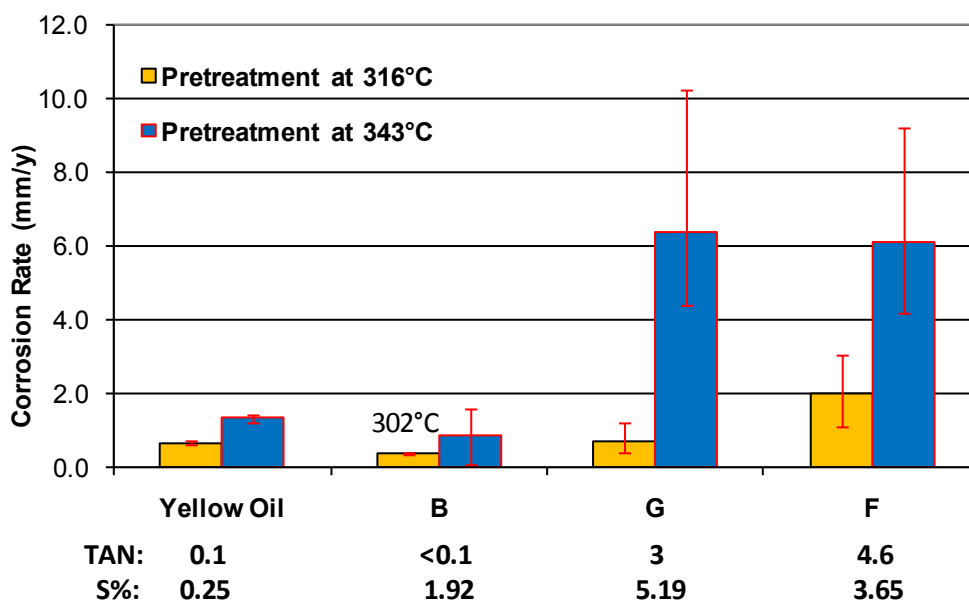
Figure 19. Challenge corrosion rates for 5Cr steel specimens pretreated with different fluids. For the pretreatment in the stirred autoclave, the pretreatment duration was 24 hours and the temperature was 316°C or 343°C. For the challenge in the HVR, the time of exposure was 24 hours, the temperature was 343°C, and the peripheral velocity was 8.56 m/s.

6.3 Summary

Regarding the pretreatment duration, experimental data suggested that

experimentation for 24 hours was long enough to explore the corrosion by crude oil

fractions. Moreover, the corrosion rates for CS and 5Cr steel were comparable as they

were converging to long-term corrosion rates. The presence of 5% chromium could not

help to resist corrosion by crudes, which was consistent with field experience.

In view of layer protectiveness, shorter pretreatment duration (24 hours) was still favorable. Longer pretreatment could not make the layer more resistant against naphthenic acid corrosion. Moreover, challenges on the specimens pretreated for 24 hours indicated that 5Cr steel might perform better than CS in the HVR.

Figure 20 summarizes the pretreatment corrosion rates for CS and 5Cr steel at 316°C and 343°C. Generally, both types of steel are nearly equally corroded for each fluid at each temperature. Corrosion rates double or triple with the increase of pretreatment temperature.
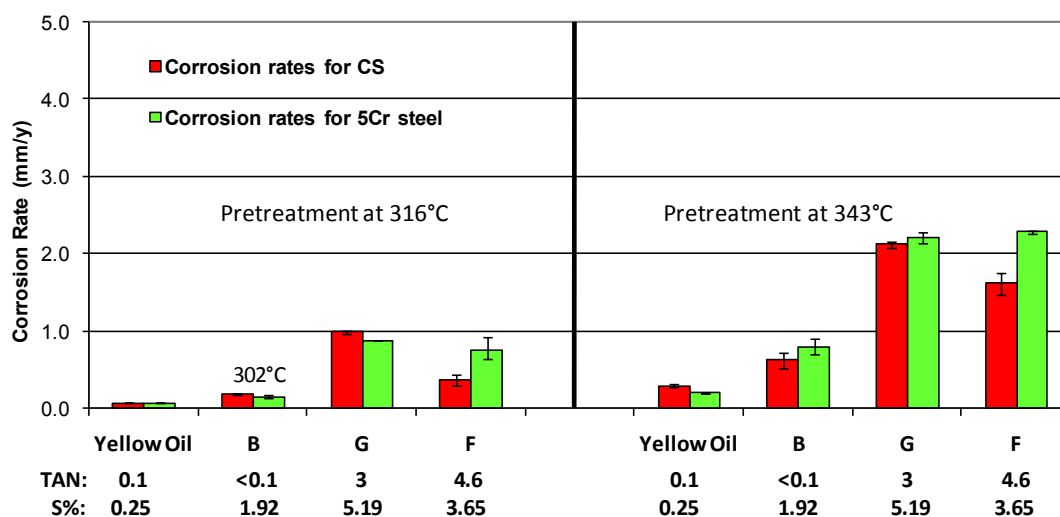
Figure 20. Pretreatment corrosion rates for CS and 5Cr steel specimens pretreated with different fluids in the stirred autoclave. The pretreatment duration was 24 hours and the temperature was 316°C or 343°C.

When challenged with naphthenic acid solution in the HVR, layers formed on CS and 5Cr steel show significant differences, especially in the case of pretreatment at 316°C

(Figure 21). It seems that pretreatment at higher temperature (343°C) tends to narrow the difference between the challenge performance of CS and 5Cr steel.
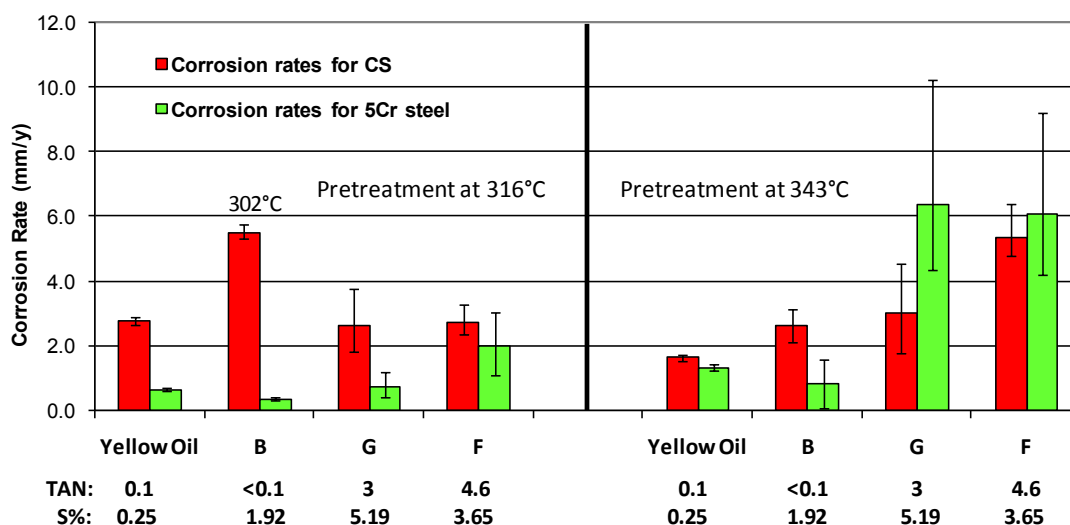
Figure 21. Challenge corrosion rates for CS and 5Cr steel pretreated with different fluids. For the pretreatment in the stirred autoclave, the pretreatment duration was 24 hours and the temperature was 316°C or 343°C. For the challenge in the HVR, the time of exposure was 24 hours, the temperature was 343°C, and the peripheral velocity was 8.56 m/s.

To increase the experimentation efficiency, facilitate a protective layer formation, and to explore the role of chromium in the steel, it was determined that the experimentation conditions should be as follows: 1) Pretreatment in the stirred autoclave at 316°C for 24 hours; and 2) Challenge in the HVR with naphthenic acid solution of TAN 3.5 at 343°C for 24 hours.

CHAPTER 7: CORROSION BY MODEL COMPOUNDS

7.1 Introduction

Due to their complex chemical compositions and physical properties, real crude oil fractions constitute a major challenge for corrosion prediction. The corrosion behavior of crude fractions shown in the preceding chapter clearly illustrated the difficulties in TAN or sulfur content correlation with crude corrosivity or layer protectiveness. Therefore, it appeared to be more feasible to investigate the corrosion processes by using model compounds that could mimic the main characteristics of corrosive species in crude oils and then apply these results to real crudes.

To this end, several model compounds were blended to replicate the real crude oil. Mineral model oil was selected to replace the hydrocarbon fraction due to its inert chemical properties, high boiling point, and ability to dissolve other components. Properties of the mineral model oil were shown in Chapter 4.

Another concern was to replicate the natural organosulfur compounds as described in Chapter 1. Given their complexity, it would be unrealistic to extract all natural organosulfur compounds and mix them in the mineral model oil. As organosulfur compound corrosion was determined by its activity, one active and representative organosulfur compound was chosen.

DDS (n-dodecyl sulfide) is an active organosulfur compound and its selected properties are shown in Table 8. After purchase, the commercial product of DDS was re-crystallized to achieve the purity of over 99%. DDS could dissolve in the mineral model oil, decompose to H_2S at high temperatures, and corrode the steel. For instance, Dettman,

et.al., investigated the corrosion by DDS and other sulfur compounds and their thermolysis at different temperatures.[21] It was found that DDS could undergo decomposition and release H_2S with a yield of 50%, which was higher than for most other organosulfur compounds. This suggested that the activity of DDS was high enough to substitute for natural sulfur compounds in crudes.

A commercial mixture of naphthenic acids was used to mimic the acidic component in crudes. With all necessary ingredients available, three mineral model solutions were prepared to investigate the role of naphthenic acid and organosulfur compounds in the corrosion of steel:

1) Naphthenic Acid (NAP) only (TAN = 1.75, S% = 0)

2) DDS only (TAN = 0, S% = 0.25%)

3) DDS + NAP (TAN = 1.75, S% = 0.25%)

Values of TAN and total sulfur content for Solution 3 were selected to be identical to values for crude Fraction A. Solution 1 and 2 contains no organosulfur compound or naphthenic acid, respectively, to examine their individual effects. All of the three solutions were used to pretreat steel specimens in typical pretreatment-challenge experiments, as described in the previous chapters.

Table 8.[2]

Selected Physical and Chemical Properties of DDS (n-Dodecyl Sulfide)

Parameter	Description
Chemical Name	n-Dodecyl Sulfide
CAS Number	2469-45-6
Chemical Formula	$CH_3(CH_2)_{11}S(CH_2)_{11}CH_3$
Molecular Weight	370
Physical State	White Powder
Melting Point (°C)	36-43
Boiling Point (°C at 4 mmHg)	260-263

7.2 Results and Discussion

7.2.1 Corrosion Rates and Discussion

In the first step, steel specimens were pretreated by the three solutions at 316°C or 343°C for 24 hours. Figure 22 shows the corrosion rates of CS specimens pretreated in the three solutions. Note that the pretreatment of steel specimens in the solution of NAP was conducted at 316°C only. For the other two solutions, increasing temperature resulted in more severe corrosion, which was consistent with the findings for real crude fractions.

---

[2] Fisher Scientific Product Information
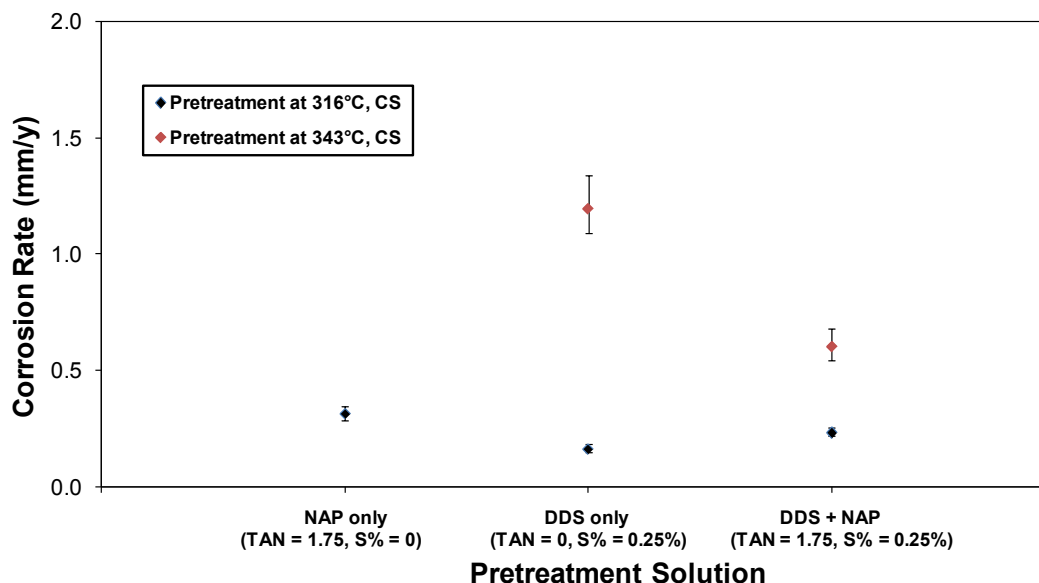
Figure 22. Pretreatment corrosion rates for CS specimens pretreated with three solutions in the stirred autoclave. The pretreatment duration was 24 hours and the temperature was 316°C or 343°C.

Figure 22 also reveals interesting effects of corrosive components. At 316°C, the corrosion rate for the "DDS + NAP" solution is close to the corrosion rates for the other solutions. This suggests that adding corrosive species to the solution of "DDS + NAP" or "DDS only" did not enhance the solution corrosivity. This phenomenon was also observed at 343°C. In actuality, adding naphthenic acids into the solution of "DDS only" would decrease the corrosion rate. This is consistent with the practical conduct of refineries where mixing acidic crude with high-sulfur-content crude was done to mitigate damage to facilities.[20] It was postulated that the presence of both naphthenic acid and organosulfur compounds could prompt the formation of protective layer and deter the corrosion by the same fluid.

The profile of pretreatment corrosion rates for 5Cr steel is similar as that for CS (Figure 23). Generally, 5 percent of chromium in the steel cannot decrease the corrosion rate. Moreover, the "DDS + NAP" solution seems to be equally corrosive when compared with other solutions. At both temperatures, the presence of naphthenic acid is not a major concern regarding the pretreatment corrosion rates.
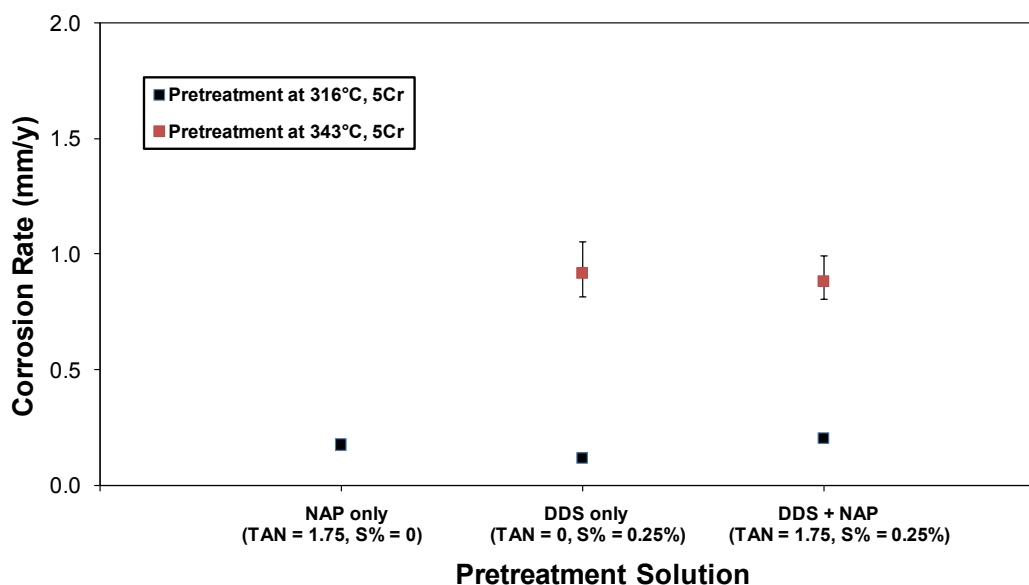
Figure 23. Pretreatment corrosion rates for 5Cr steel specimens pretreated with three solutions in the stirred autoclave. The pretreatment duration was 24 hours and the temperature was 316°C or 343°C.

The next step was to move the pretreated specimens into the HVR and to challenge the layer with the naphthenic acid solution (TAN 3.5) at 343°C for 24 hours. As shown in Figure 24, the performance of layers generated in the three solutions is quite different. For the "NAP only" solution, the challenge corrosion rate is about 8 mm/y, quite close to the pure TAN 3.5 corrosion rate of CS. It is not surprising since the

traditional theory claims that corrosion by naphthenic acid cannot leave any corrosion

product on the metal surface, let alone any protective layer. For the "DDS only" solution,

the layer formed at 343°C is more protective. However, the most protective layer among

all experiments was generated in the "DDS + NAP" solution at 316°C and its challenge

corrosion is only one fourth of the pure TAN 3.5 corrosion rate. The trend is consistent

with the observation for real crude fractions, i.e., the layer formed at lower temperature

was more protective and the presence of naphthenic acid was necessary to promote a

protective layer.
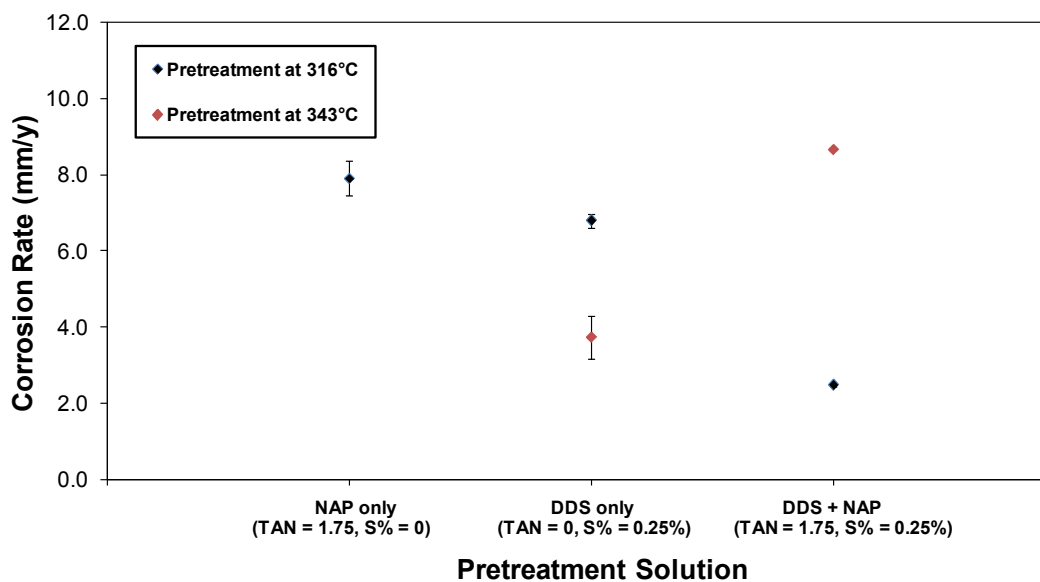
Figure 24. Challenge corrosion rates for CS specimens pretreated with three solutions. For the pretreatment in the stirred autoclave, the pretreatment duration was 24 hours and the temperature was 316°C or 343°C. For the challenge in the HVR, the time of exposure was 24 hours, the temperature was 343°C, and the peripheral velocity was 8.56 m/s.

Similar to the results for real crude fractions, 5Cr steel shows a different profile of

challenge corrosion compared to that of CS despite the fact that their pretreatment

corrosion rates are close (Figure 25). The most striking finding is that specimens

pretreated in the "NAP only" solution at 316°C gives a near zero challenge corrosion

rate, which contradicts the traditional theory on naphthenic acid corrosion. This

experiment was repeated four times. But surprisingly, the challenge corrosion rate was

confirmed each time. It seems that there is "something" protecting the steel from attack

by naphthenic acids. Microscopy analysis on the metal surface should help understand

what it is.
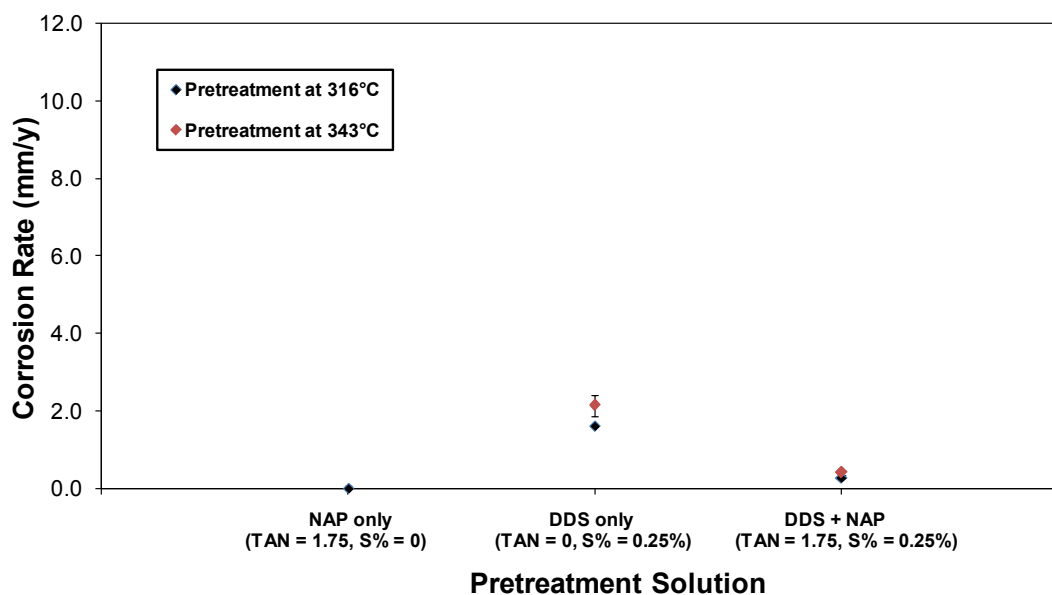
Figure 25. Challenge corrosion rates for 5Cr steel specimens pretreated with three
solutions. For the pretreatment in the stirred autoclave, the pretreatment duration was 24
hours and the temperature was 316°C or 343°C. For the challenge in the HVR, the time
of exposure was 24 hours, the temperature was 343°C, and the peripheral velocity was
8.56 m/s.

Conversely, 5Cr steel specimens pretreated in the "DDS only" solution could not

form any protective layer at either pretreatment temperatures and the challenge corrosion

rates are of the same order of magnitude as pure TAN 3.5 corrosion rate (~1.2 mm/y). However, the layer became protective when naphthenic acids were added into the pretreatment solution, as shown by the challenge corrosion rates for the "DDS + NAP" solution. Again, the acidic component was found to be a crucial factor in the formation of protective layer.

7.2.2 Surface Analytical Results and Discussion

7.2.2.1 Specimens Pretreated at 316°C

Experimental data for model compounds clearly indicates the important role of naphthenic acids. Surface microscopy analysis on specimens after corrosion experimentation should give clues as to what sort of surface layer forms during the experiments. SEM analysis was conducted on the pretreated specimens to examine the surface layer. In addition to the surface morphology, cross-sections of specimens were polished to view the layer structure. In conjunction with SEM imaging, EDS (energy dispersive X-ray spectrometry) provided valuable information on the elemental composition of layer.

Figure 26 shows the results of SEM/EDS analysis on the CS specimens pretreated in three solutions at 316°C. For the "NAP only" solution, the surface SEM image suggests that no layer was formed as the polishing marks are still visible. The corresponding EDS analysis confirms that iron is the major element on the surface while the trace amount of sulfur and oxygen could be explained by residual sulfur in the stirred autoclave and oxidation of specimens after cleaning, respectively.
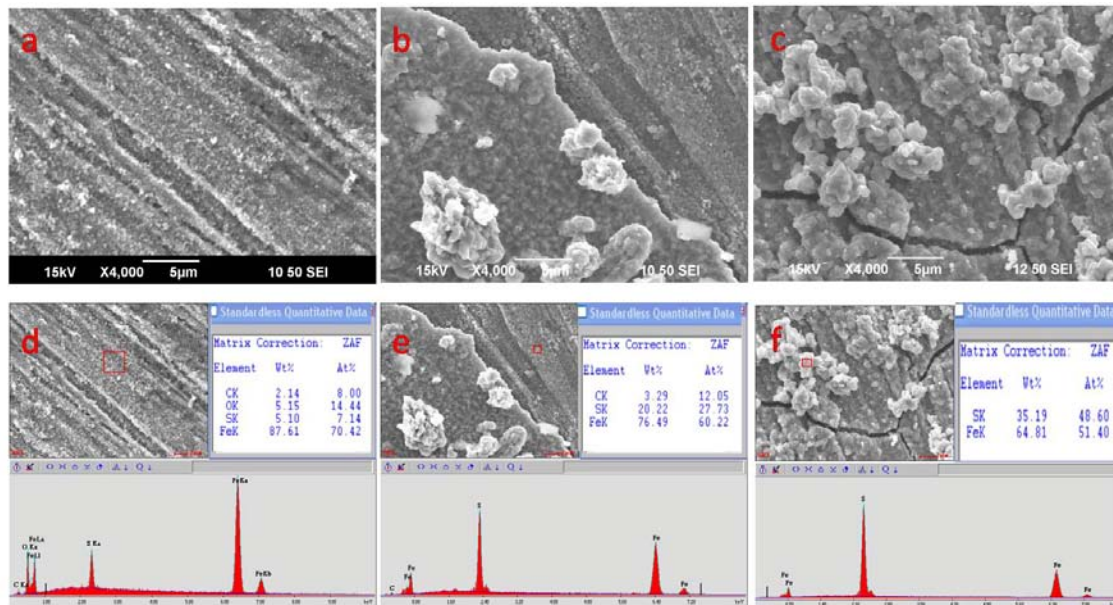
Figure 26. SEM images of CS specimens pretreated at 316°C with (a) the "NAP only" solution, (b) the "DDS only" solution, and (c) the "DDS + NAP" solution. Images (d), (e), and (f) show corresponding EDS analysis on the surface. For corrosion rates see Figure 22. SEM and EDS analysis of the cross section is given in Figure 27.

When the DDS was added to the solutions ("DDS only" and "DDS + NAP"), a layer was formed on the metal surface and EDS analysis suggests it is iron sulfide. According to Figure 24, the layer shown in Figure 27 (c) is more protective, which might be related to superior layer integrity.

Cross-section SEM images of the layers in Figure 26 reveals more information on the layer morphology and chemical composition (Figure 27). There seems to be something left on the steel pretreated in the "NAP only" solution, but the resolution is not high enough to determine the details. Successive layers were formed in "DDS only" solution and the "DDS + NAP" solution and the total layer thickness is close for both solutions. Cross-section EDS analysis confirms the formation of iron sulfide on the metal

surface. The peak of oxygen is interesting and deserves more detailed investigation given

that SEM analysis is not precise enough to reveal the fine structure of the layer.
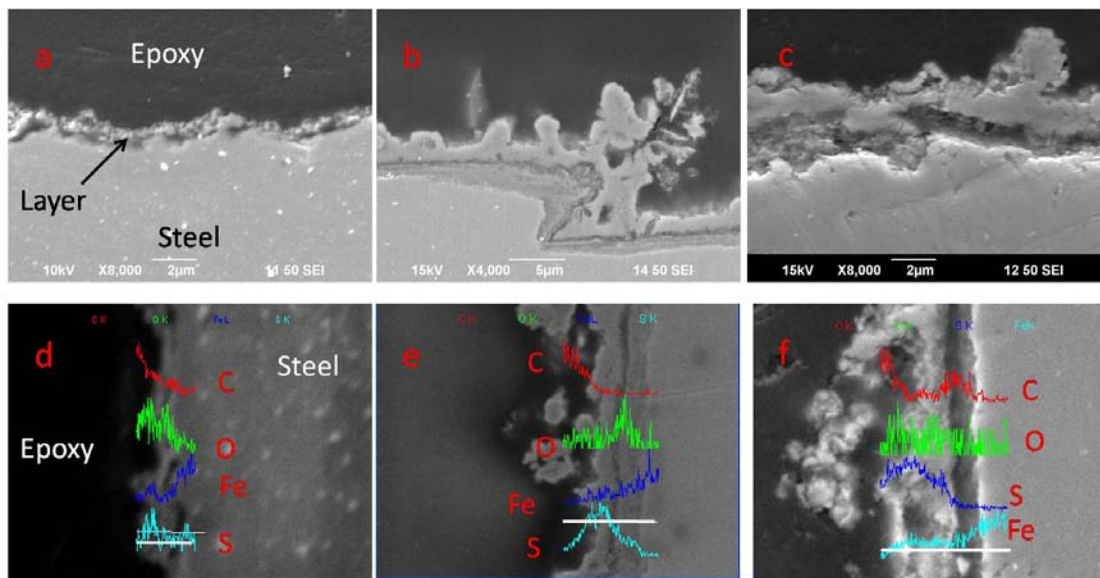
Figure 27. Cross-section SEM images of CS specimens pretreated at 316°C with (a) the "NAP only" solution, (b) the "DDS only" solution, and (c) the "DDS + NAP" solution. Images (d), (e), and (f) show corresponding EDS analysis along the white line on the bottom. For corrosion rates see Figure 22. SEM and EDS analysis of the surface is given in Figure 26.

The surface of 5Cr steel looks similar to the corresponding CS surface (Figure

28). The "NAP only" solution seems to leave nothing on the metal surface, which is

confirmed by EDS analysis. However, the challenge experimentation indicated that the

specimen of Figure 28 (a) was most resilient in the harsh condition while the CS

specimen pretreated with the "NAP only" solution failed completely. Surface SEM/EDS

analysis is not helpful to explain this difference in behavior. Multiple layers were formed

in the "DDS only" solution and chromium was found in the inner layer. With the

presence of naphthenic acids, the integrity of layer is superior as shown by Figure 28 (c)

and the corresponding challenge corrosion rate is low. For both Figure 28 (b) and (c),

about 5 percentage of chromium was found in the inner layer.
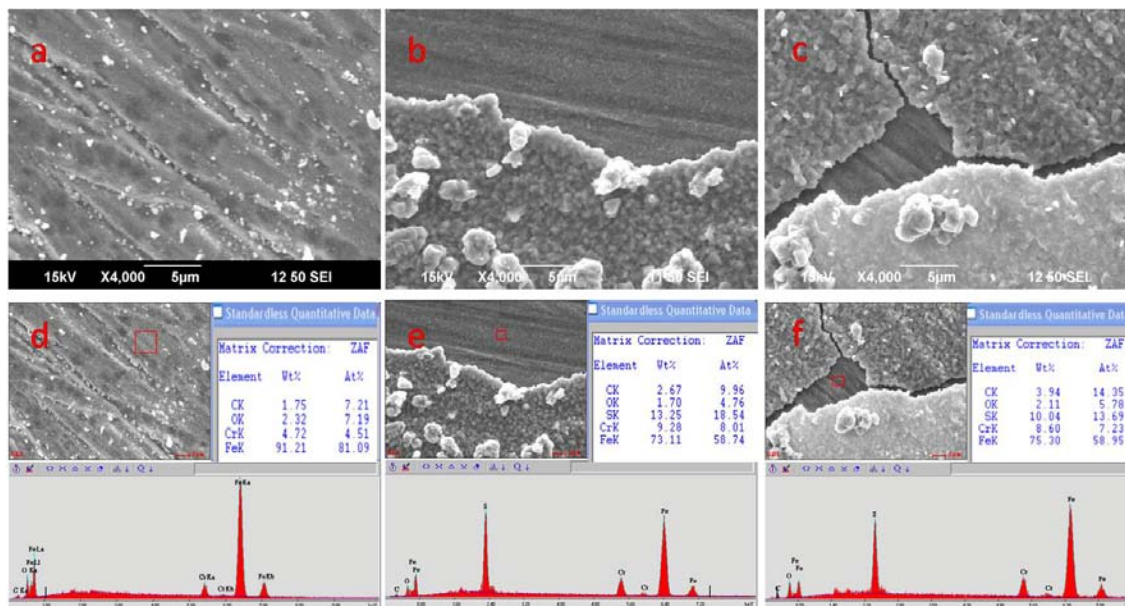
Figure 28. SEM images of 5Cr steel specimens pretreated at 316°C with (a) the "NAP only" solution, (b) the "DDS only" solution, and (c) the "DDS + NAP" solution. Images (d), (e), and (f) show corresponding EDS analysis on the surface. For corrosion rates see Figure 23. SEM and EDS analysis of the cross section is given in Figure 29.

Layer cross-section analysis for 5Cr steel reveals consistent information with the

surface analysis (Figure 29). No obvious layer could be seen in Figure 29 (a). Figure 29

(b) shows the delaminated layer formed in the "DDS only" solution and the gap is filled

with epoxy. When naphthenic acid was added into the solution, the layer became thicker

with some materials filled between the outer iron sulfide layer and the bare metal surface.

The resolution of the image is not high enough to reveal a detailed layer morphology or

profile of chemical composition.
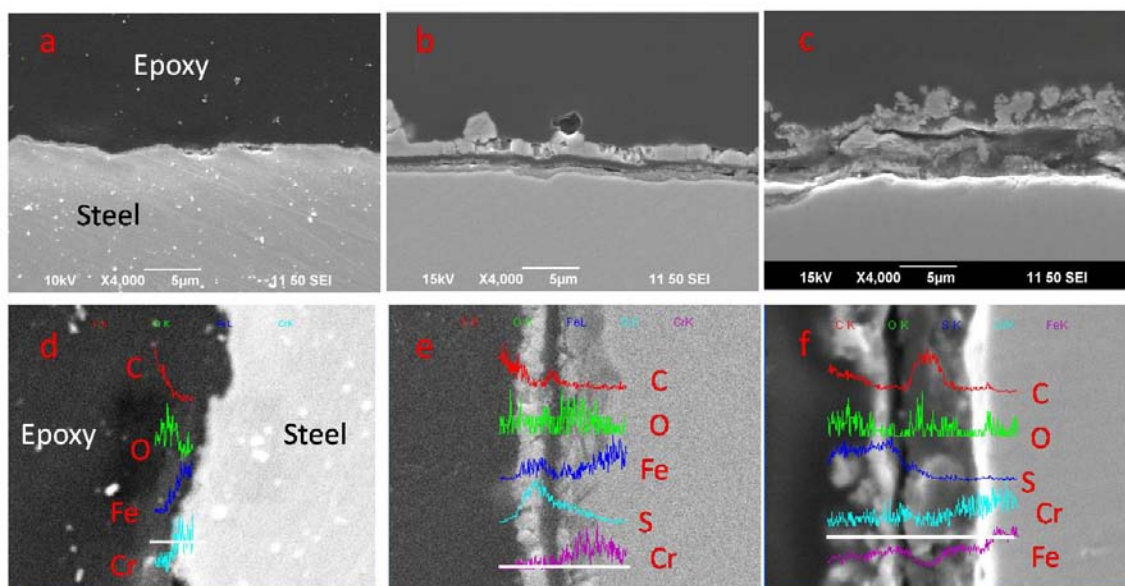
Figure 29. Cross-section SEM images of 5Cr specimens pretreated at 316°C with (a) the "NAP only" solution, (b) the "DDS only" solution, and (c) the "DDS + NAP" solution. Images (d), (e), and (f) show corresponding EDS analysis along the white line on the bottom. For corrosion rates see Figure 23. SEM and EDS analysis of the surface is given in Figure 28.

The layer formed on CS specimens changed after the challenge (Figure 30). For the "NAP only" solution, both the challenge corrosion rate and the iron sulfide layer formed after challenge are similar to the finding in the pure TAN 3.5 experiment. The trace amount of sulfur content in the naphthenic acid should account for the iron sulfide layer and the collapse of the layer indicates that naphthenic acid could diffuse though the layer and corrode the metal below. After the challenge, the specimen pretreated with the "DDS only" solution was covered by flakes of iron sulfide and the layer morphology was preserved compared with Figure 26. The layer formed in the "DDS + NAP" solution was still intact after challenge, which might explain the lower challenge corrosion rate.
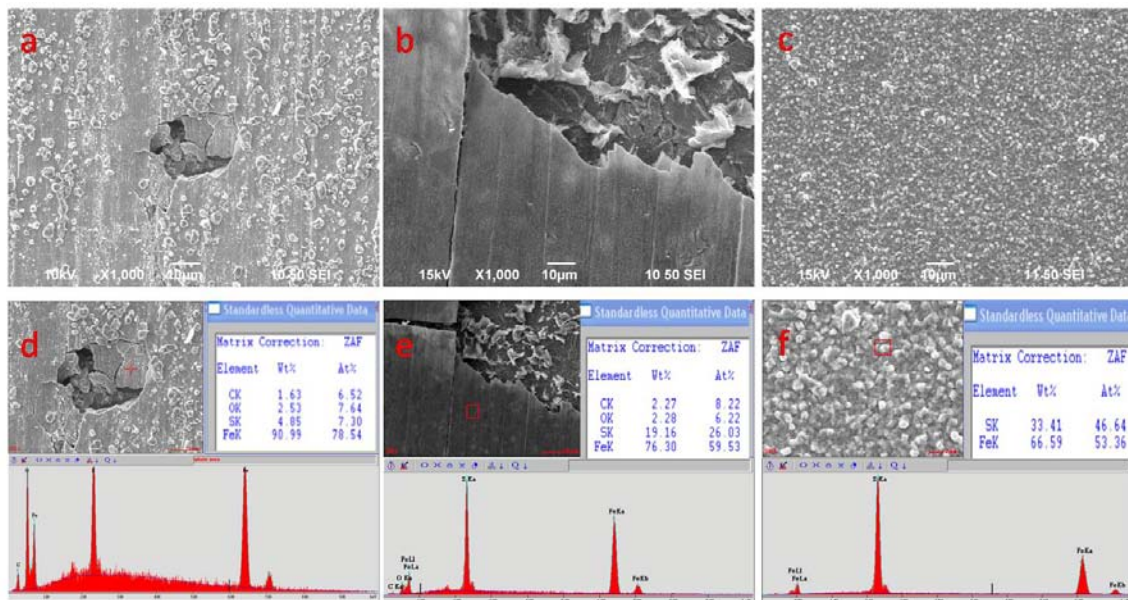
Figure 30. SEM images of CS specimens pretreated at 316°C with (a) the "NAP only" solution, (b) the "DDS only" solution, and (c) the "DDS + NAP" solution followed by the challenge with the naphthenic acid solution (TAN 3.5) at 343°C. Images (d), (e), and (f) show corresponding EDS analysis on the surface. For corrosion rates see Figure 24. SEM and EDS analysis of the cross section is given in Figure 31.

Cross-section images (Figure 31) reveal data consistent with the surface SEM analysis. A detached iron sulfide layer was found in Figure 31 (a) and (d), which was quite similar to the layer formed after the pure TAN 3.5 experiment. This might indicate that pretreating CS specimens in the "NAP only" solution could not affect the challenge corrosion rate or layer morphology. The detached iron sulfide layer seen in Figure 31 (e) clearly explains the corresponding high challenge corrosion rate (6.8 mm/y, Figure 24). With an attached layer fully covered on the surface (Figure 31 (c) and (f)), the challenge corrosion rate for the specimen pretreated in the "DDS + NAP" solution is only about one fourth of that for the pure TAN 3.5 experiment.
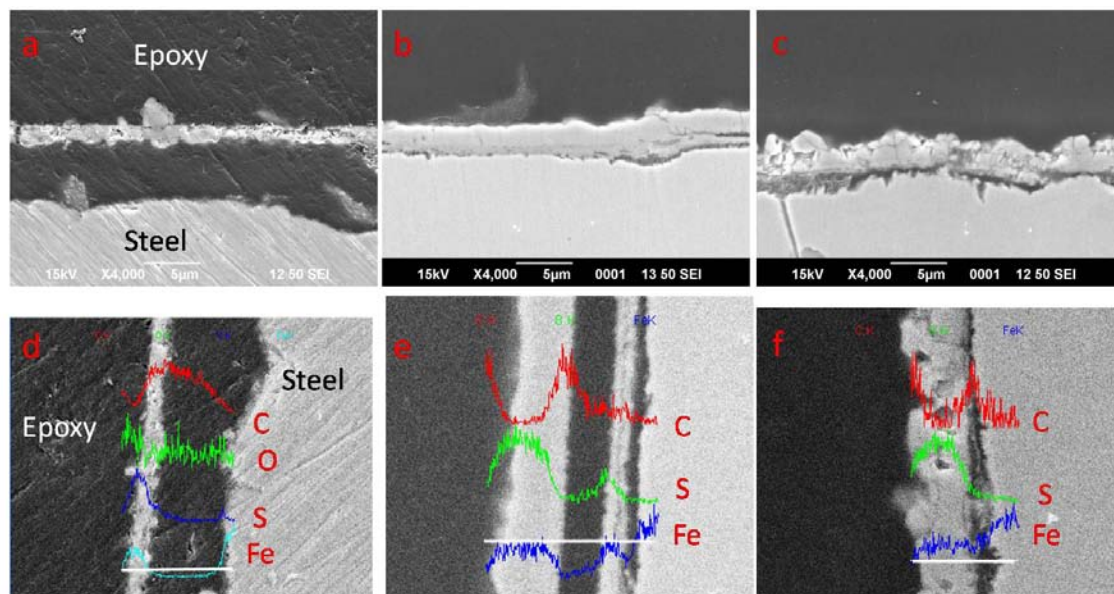
Figure 31. Cross-section SEM images of carbon CS specimens pretreated with (a) the "NAP only" solution, (b) the "DDS only" solution, and (c) the "DDS + NAP" solution followed by the challenge with naphthenic acid solution (TAN 3.5) at 343°C. Images (d), (e), and (f) show corresponding EDS analysis along the white line. For corrosion rates see Figure 24. SEM and EDS analysis of the surface is given in Figure 30.

The 5Cr steel specimen surface after the challenge is shown in Figure 32. The 5Cr steel specimen pretreated with the "NAP only" solution gives a zero challenge corrosion rate (Figure 25), but no obvious layer was found through SEM analysis (Figure 28). After the challenge, a continuous layer was still not visible; only some isolated crystals were observed. However, EDS analysis shows a peak of oxygen in Figure 32 (d) and suggests that there might be a thin oxide layer, but further analysis is necessary for verification. The nonprotective layer formed in the "DDS only" solution (challenge corrosion rate = 1.6 mm/y, Figure 25) is characterized by delaminated layers and flakes of iron sulfide as shown in Figure 32 (b) and (e). For the layer formed in the "DDS + NAP" solution, the integrity of layer was preserved after challenge compared with Figure 27 and the

challenge corrosion rate is only 0.3 mm/y or one fourth of pure TAN 3.5 corrosion rate
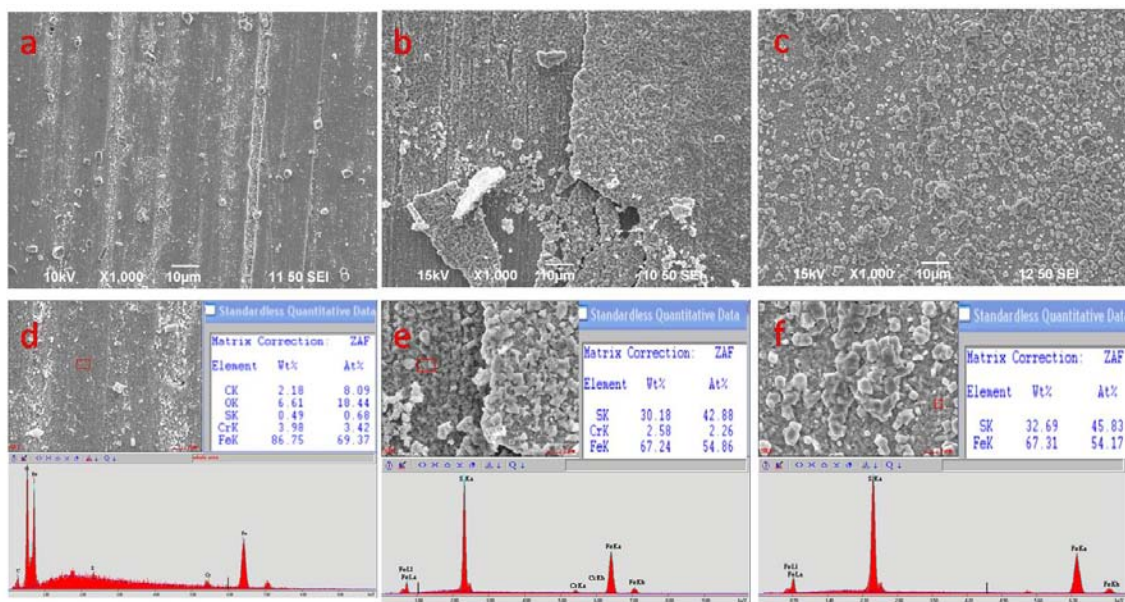
for 5Cr steel.

Figure 32. SEM images of 5Cr steel specimens pretreated with (a) the "NAP only" solution, (b) the "DDS only" solution, and (c) the "DDS + NAP" solution followed by the challenge with naphthenic acid solution (TAN 3.5) at 343°C. Images (d), (e), and (f) show corresponding EDS analysis on the surface. For corrosion rates see Figure 25. SEM and EDS analysis of the cross section is given in Figure 33.

The cross-section SEM/EDS analysis of the same specimen reveals more

information on the layer (Figure 33 (a)). The magnification on is 8,000x and a very thin

layer is visible but blurry. EDS analysis shows the outer iron sulfide layer corresponding

to the observation of crystals in the surface SEM image. The peak of oxygen in Figure 33

(d) is quite interesting and deserves further investigation with a more precise instrument

of higher resolution; given it coincides with a high chromium intensity, this could be

consistent with formation of a chromium oxide or chromite. Again, the delaminated layer

was observed in Figure 33 (b) and (e) and the layer totally failed in the HVR challenge.

Adherent and compact layers formed in the "DDS + NAP" solution survived after

challenge and decreased the corrosion rate (Figure 33 (c) and (f)). It is noteworthy that a

peak of oxygen appears in EDS analysis which might relate to the protective properties of

the layer.
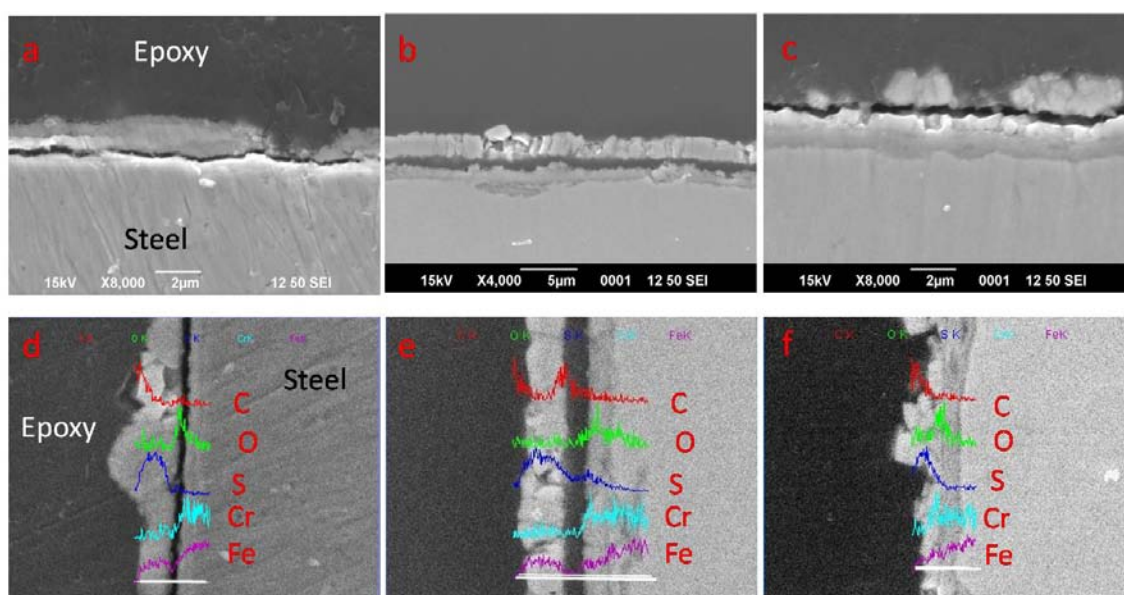
Figure 33. Cross-section SEM images of 5Cr steel specimens pretreated with (a) the "NAP only" solution, (b) "DDS only" solution, and (c) the "DDS + NAP" solution followed by the challenge with naphthenic acid solution (TAN 3.5) at 343°C. Images (d), (e), and (f) show corresponding EDS analysis along the white line on the bottom. For corrosion rates see Figure 25. SEM and EDS analysis of the surface is given in Figure 32.

7.2.2.2 Specimens Pretreated at 343°C

Figure 34 shows the surface of specimens pretreated in the "DDS only" solution

and the "DDS + NAP" solution at 343°C. For the "DDS only" solution, the successive

layers are visible due to layer exfoliation; EDS analysis is consistent with iron sulfide.

For the "DDS + NAP" solution, the layer covers the metal surface uniformly and multiple

layers were formed.
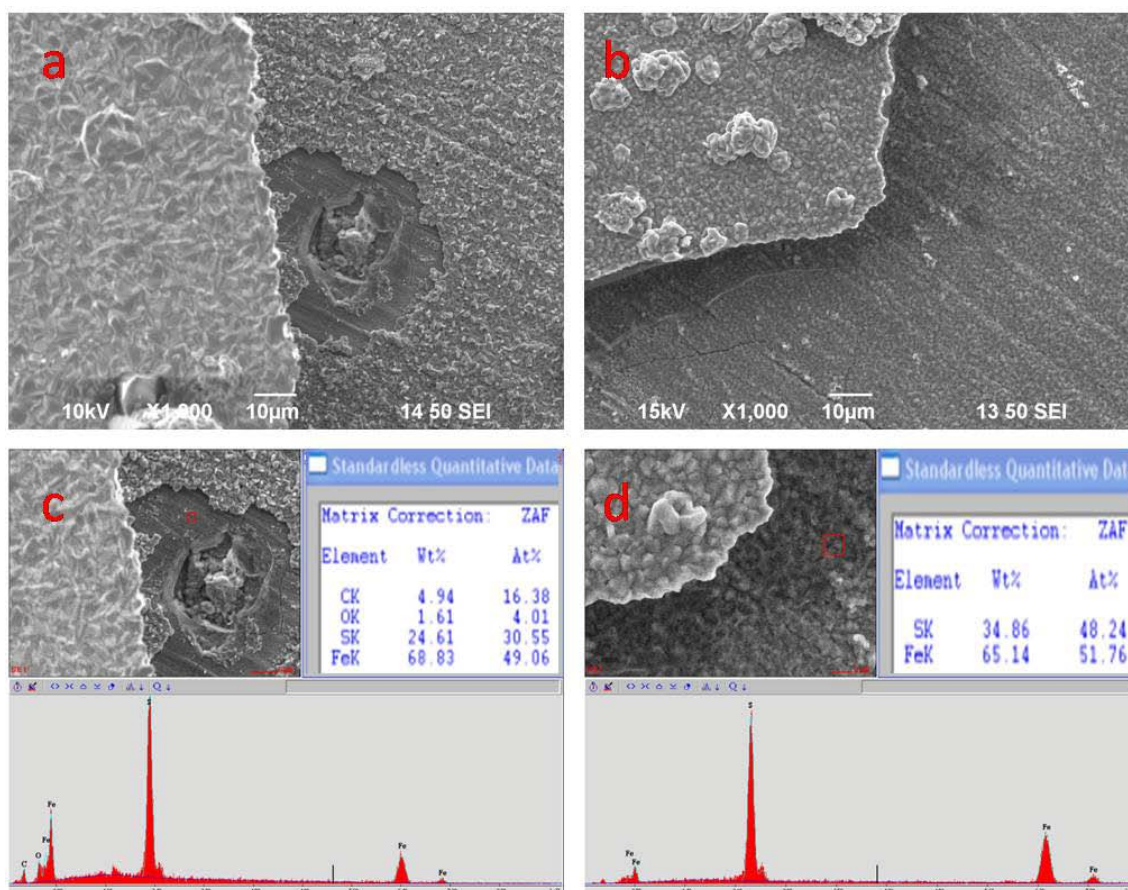
Figure 34. SEM images of CS specimens pretreated with (a) "DDS only" solution and (b) the "DDS + NAP" solution at 343°C. Images (c) and (d) show corresponding EDS analysis on the surface. For corrosion rates see Figure 22. SEM and EDS analysis of the cross section is given in Figure 35.

SEM images of layer cross-section (Figure 35) shows that the layer formed at

higher temperature (343°C) is thicker than the layer formed at lower temperature (316°C)

for both solutions as compared with Figure 27. For the "DDS only" solution, the

delaminating flakes are immobilized in epoxy as shown in Figure 35 (a). Such a layer is

not very protective (HVR corrosion rate is 3.7 mm/y or half of pure TAN 3.5 corrosion

rate). The delaminated layer formed in the "DDS + NAP" solution is much thicker than

its counterpart formed in the "DDS only" solution (20 µm vs. 10 µm), but it is totally

nonprotective with the challenge corrosion rate even greater than for the pure TAN 3.5

corrosion rate. It is noticeable that a peak of oxygen showed up in the inner layer

compared with the results of EDS analysis for the layer formed in the "DDS only"
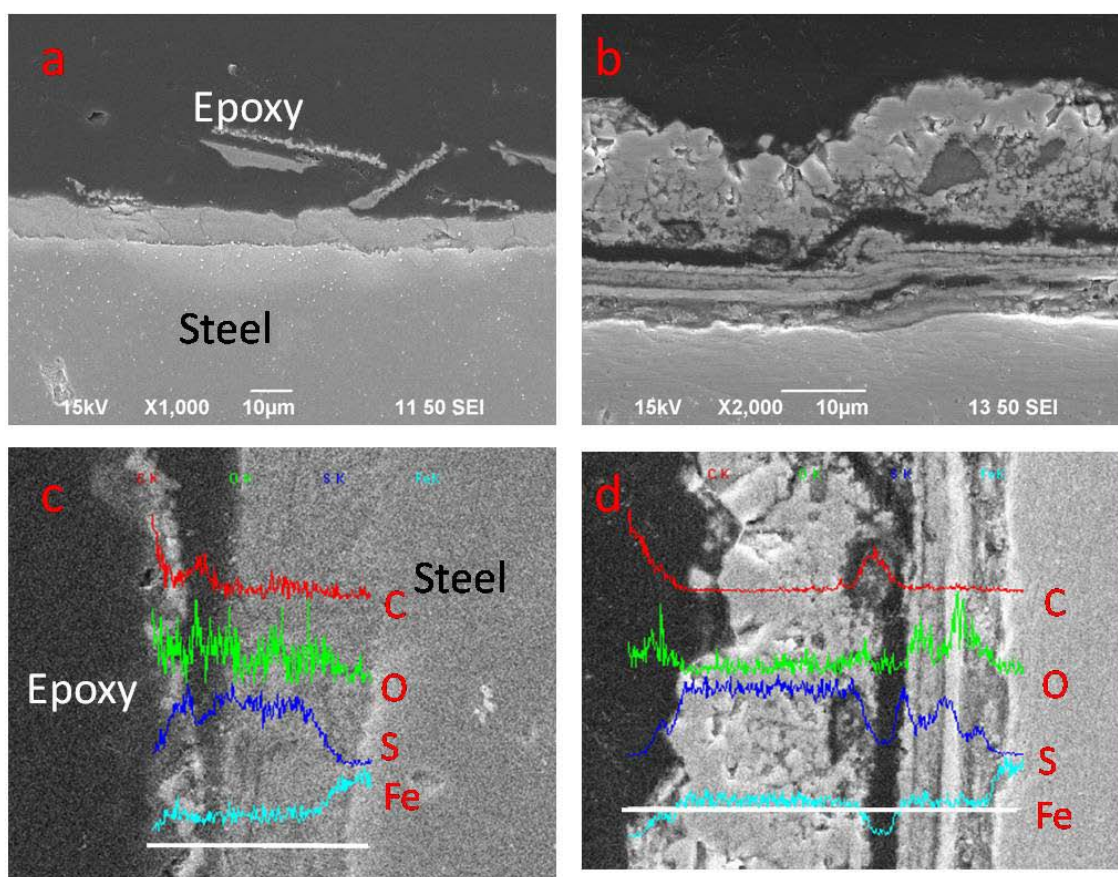
solution.

Figure 35. Cross-section SEM images of CS specimens pretreated with (a) "DDS only" solution and (b) the "DDS + NAP" solution at 343°C. Images (c) and (d) show corresponding EDS analysis along the white line on the bottom. For corrosion rates see Figure 22. SEM and EDS analysis of the surface is given in Figure 34.

The surface of 5Cr steel specimens pretreated in both solutions looks similar to that of CS (Figure 36). For the "DDS only" solution, multiple layers were formed and chromium was found in the inner layer. It should be noted that the layer is not protective. However, the layer became protective when naphthenic acids were dissolved in the pretreatment solution (for the "DDS + NAP" solution, challenge corrosion rate = 0.4 mm/y or one third of pure TAN 3.5 corrosion rate, Figure 25). Figure 36 (b) shows that the surface is fully covered by iron sulfide. Note, too, the presence of oxygen on the metal surface in Figure 36 (d).
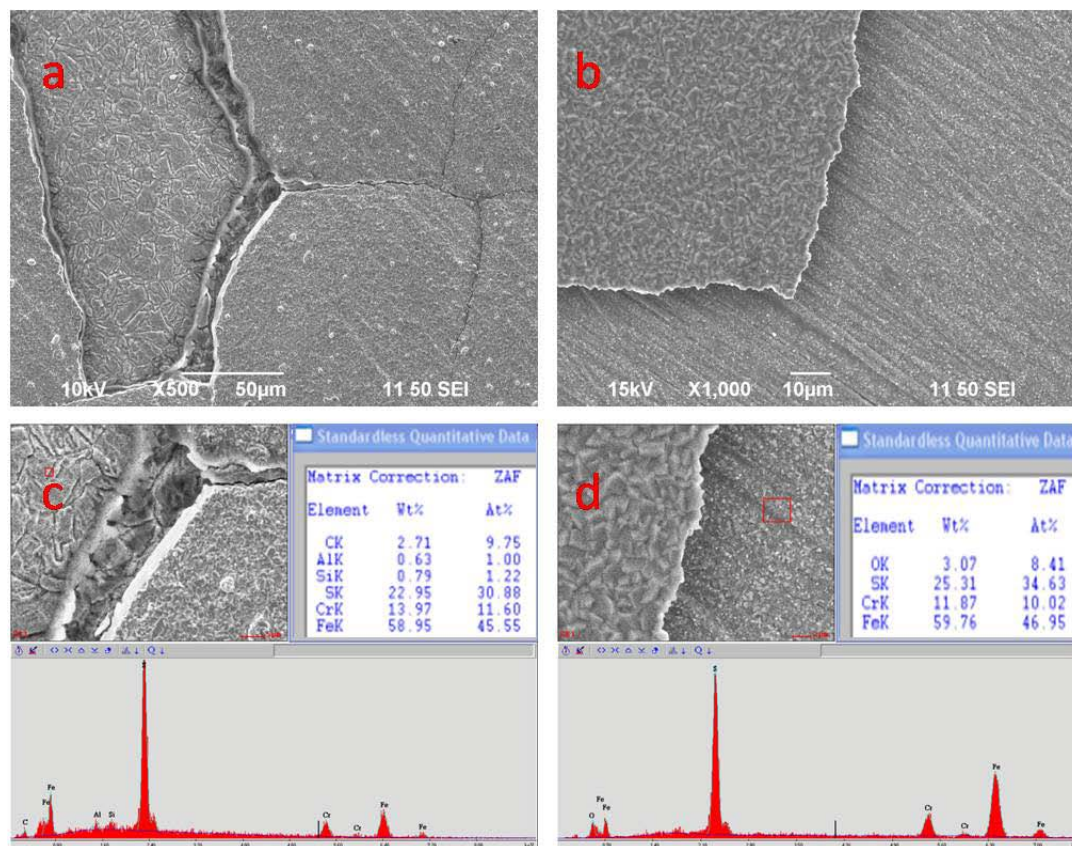
Figure 36. SEM images of 5Cr steel specimen pretreated with (a) "DDS only" solution and (b) the "DDS + NAP" solution at 343°C. Images (c) and (d) show corresponding EDS analysis on the surface. For corrosion rates see Figure 22. SEM and EDS analysis of the cross section is given in Figure 37.

Layer cross-section images are shown in Figure 37. Similarly to CS, an increase of pretreatment temperature lead to the growth of the layer compared with Figure 28. However, layer thickness is not related to layer protectiveness. The thick layer in Figure 37 (a) is as nonprotective as the layer formed at 316°C. However, a delaminated yet protective layer was formed in the "DDS + NAP" solution (Figure 37 (b) and (d)). The layer is as protective as the layer formed at 316°C and EDS analysis also indicates the presence of oxygen and chromium in the inner layer.
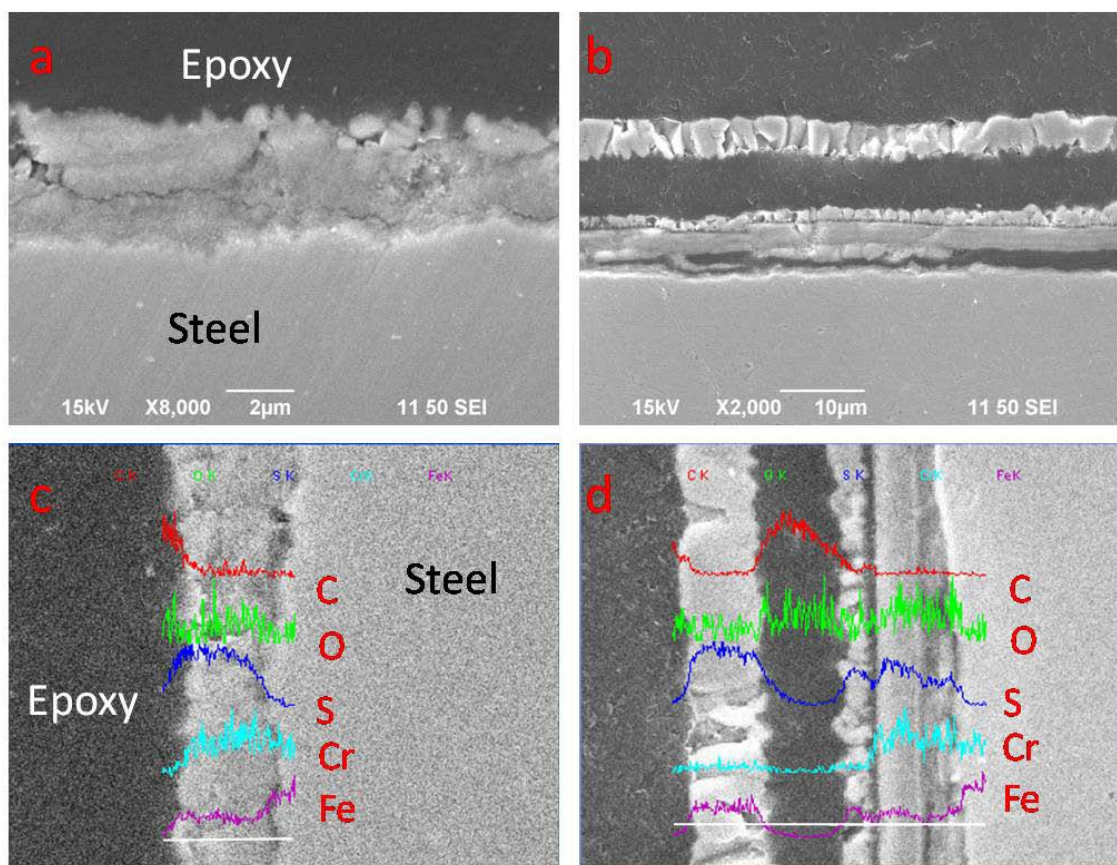
Figure 37. Cross-section SEM images of 5Cr steel specimens pretreated with (a) "DDS only" solution and (b) the "DDS + NAP" solution at 343°C. Images (c) and (d) show corresponding EDS analysis along the white line on the bottom. For corrosion rates see Figure 22. SEM and EDS analysis of the surface is given in Figure 36.

7.3 Summary

Experiments with model compounds improved our understanding of the effect of important parameters in corrosion. Along with the adjustment of the pretreatment temperature, the effect of naphthenic acids and organosulfur compounds on mechanism of corrosion was more clearly demonstrated.

At both pretreatment temperatures, experiments showed that adding naphthenic acids into the fluid did not increase the pretreatment corrosion rate. SEM/EDS analysis revealed that the presence of naphthenic acids improved the layer integrity and promoted the formation of an oxide layer, particularly for 5Cr steel.

More importantly, the presence of naphthenic acids could enhance the layer protectiveness. For CS, both naphthenic acids and the organosulfur compound were indispensable to make the layer more resistant against corrosion. For 5Cr steel, the presence of naphthenic acid only was enough to form a protective layer on which only a trace amount of sulfur was observed (according to EDS analysis). A peak of oxygen, repeatedly appearing in both surface and cross-section SEM/EDS analysis, stimulated much interest and warranted further study.

Observations relating to the corrosion of CS and 5Cr steel defied the traditional theory claiming that the presence of organosulfur compounds was the key factor relating to layer properties with iron sulfide constituting the protective surface layer, while naphthenic acids were aggressive and left no trace on the metal surface. It was, however, possible that the effect observed in this study was related to the choice of the model compound, i.e., a dialkyl sulfide rather than more reactive thiols. Current experimental

data and results of surface analysis strongly suggested that the naphthenic acid was an important player and formation of an oxide layer was related to the protective property of layer.

SEM and EDS analysis provided revealing information on the layer morphology and chemical composition. However, SEM was not sufficiently precise to view the structure of the thin layer, although it suggested that layer delamination in the micrometer range was not a significant factor.

CHAPTER 8: CORROSION BY REAL CRUDE FRACTIONS – EFFECT OF ASPHALTENES

8.1 Introduction

Experimental data involving model compounds in the preceding chapter clearly indicated the important role of naphthenic acids in the formation of protective layers. However, it was not clear that whether similar phenomenon could be observed for real crude fractions.

Additionally, it was suspected that other components of real crude fractions, such as asphaltenes, might affect the corrosive behavior and change the properties of the surface layer. Asphaltenes refer to large-molecule compounds in the crude that are not soluble in heptane but can dissolve in toluene.[47] Asphaltenes are a mixture of complicated molecules; some model structures are shown in Figure 38.[48]

$C_{48}H_{63}N$ $C_{54}H_{59}N$ $C_{44}H_{55}N$

$C_{46}H_{57}N$ $C_{52}H_{63}N$ $C_{44}H_{53}NS$
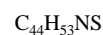
Figure 38. Typical structures of asphaltene (based on Alshareef, A. H.; Scherer, A.; Stryker; J. M.; Tykwinski, R. R.; Gray, M. R.; Thermal Cracking of Substituted Cholestane-Benzoquinoline Asphaltene Model Compounds. *Energy & Fuels*, **2012**, *26* (6), 3592-3603.).

It was well known that asphaltenes can affect corrosion of steel in the presence of water.[49] However, the possible effect of asphaltenes on high-temperature corrosion by crude oil is not well understood. Initially, it was assumed that asphaltenes might lower the corrosivity of crude oil or promote formation of a more protective layer. In order to examine this assumption, several real crude oil fractions with various asphaltene

concentrations were selected for experimentation. The natural TAN, total sulfur content,

and asphaltene content are presented in Table 9.

Table 9.

Selected Real Crude Fractions for Effect of Asphaltenes Evaluation

Crude Oil Fraction	TAN (mg KOH / g oil)	Total Sulfur Content (wt%)	Asphaltene Content (wt%)	Description
L (650+)	1.06	4.29	14.9	Same
K (VGO)	1.42	3.29	0	Source
N (650+)	1.4	1.05	0.49	Same
M (VGO)	1.4	1.02	0.02	Source
H (650+)	2.23	4.53	1.3	Same
G (650+)	3	5.19	10.3	Source
F (VGO)	4.6	3.65	0	
J (650+)	2.62	4.65	7	Same
I (VGO)	3.73	3.34	0	Source
P (650+)	4.3	0	0	Same
O (VGO)	4.9	0.11	0.05	Source

As shown in Table 9, there were eleven fractions used in this series of

experiments, which were divided into four pairs and one set of three according to the oil

sources. In each set, there was at least one fraction labeled "650+" and the other as

"VGO". As described in the Chapter 6, the 650+ fraction was the product from

distillation at 650°F (343°C) while VGO was generated from vacuum distillation of the

650+ fraction.

These crude oil fractions were listed in the sequence of TAN. Generally, the

fraction of VGO was more acidic than its 650+ counterpart, but its total sulfur content

was lower. This might indicate that naphthenic acids were more volatile than

organosulfur compounds. Given that asphaltenes were high-boiling-point molecules,

VGO fractions were depleted of asphaltenes which were concentrated in 650+ fractions.

In particular, Fraction H was distilled in a way to remove most asphaltenes compared

with the ordinary distillation product of Fraction G.

8.2 Results and Discussion

8.2.1 Corrosion Rates and Discussion

Following the same experimentation procedures, steel specimens were pretreated

with each crude fraction in the stirred autoclave at 316°C for 24 hours. Figure 39 shows

the pretreatment corrosion rates of CS specimens. Generally, there is no obvious trend

relating crude corrosivity with its TAN or sulfur content. For instance, Fraction L and

Fraction G, despite different TAN, have similar corrosion rates.

	L	K	N	M	H	G	F	J	I	P	O
TAN:	1.06	1.42	1.4	1.4	2.23	3	4.6	2.62	3.73	4.3	4.9
S%:	4.29	3.29	1.05	1.02	4.53	5.19	3.65	4.65	3.34	0	0.11
A%:	14.9	0	0.49	0.02	1.3	10.3	0	7	0	0	0.05
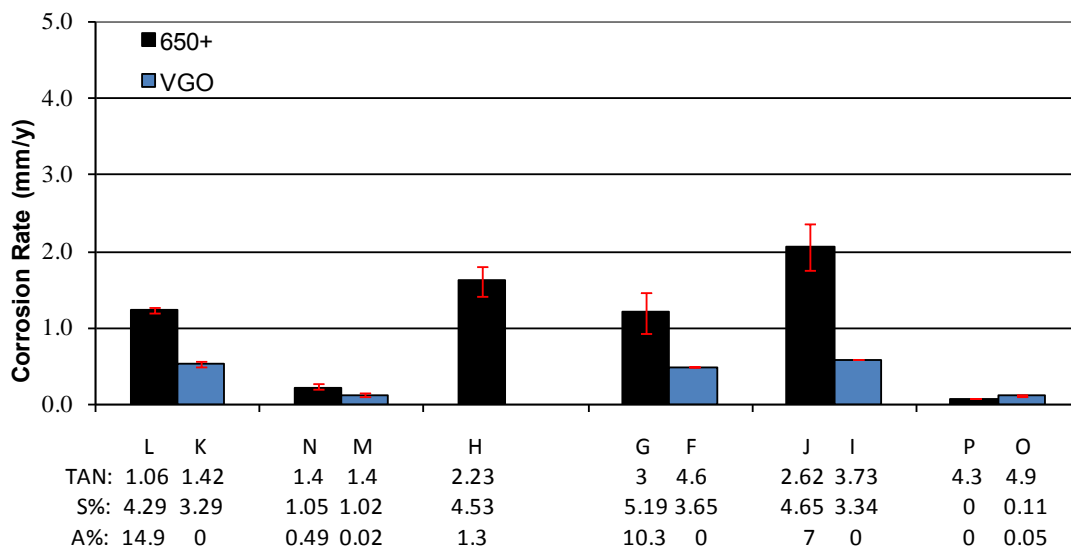
Figure 39. Pretreatment corrosion rates for CS specimens pretreated with different real crude fractions in the stirred autoclave. The pretreatment duration was 24 hours and the temperature was 316°C.

Determining possible effects of asphaltenes was the focus of this series of experiments. Fractions G & H, distilled from the same crude, show similar corrosion rates despite possessing close to an order of magnitude difference in asphaltene content. Pretreatment results of CS clearly reject the assumption relating to the protective effect of asphaltenes.

Figure 40 illustrates the corrosion rates for 5Cr steel specimens which were pretreated in the same stirred autoclave as the CS specimens. Comparison between these two figures shows that CS and 5Cr specimens have similar corrosion rates for each crude oil fraction.
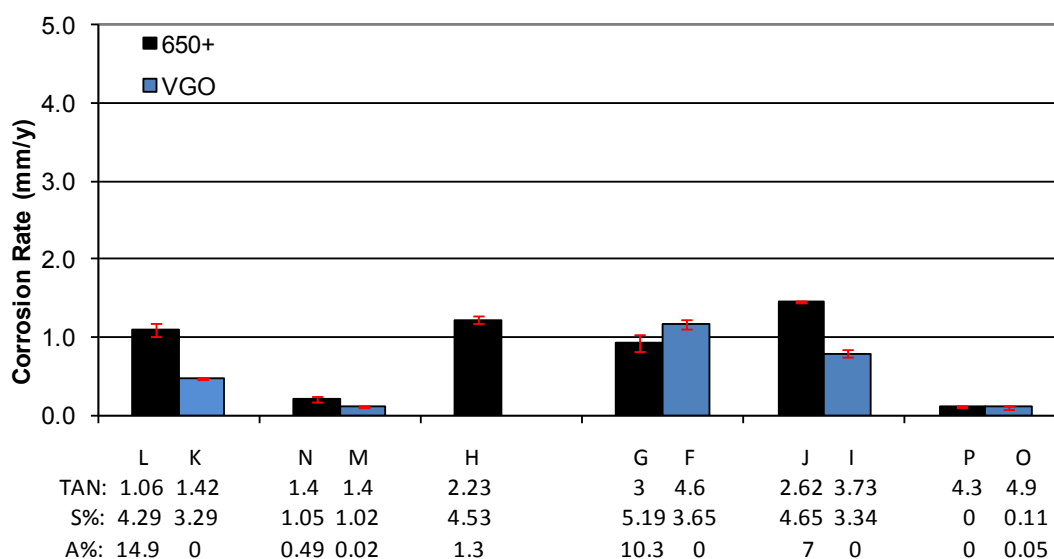
Figure 40. Pretreatment corrosion rates for 5Cr steel pretreated with different real crude fractions in the stirred autoclave. The pretreatment duration was 24 hours and the temperature was 316°C.

These pretreatment experiments show that asphaltene could not decrease the corrosivity of crude oil fractions at 316°C. The next step was to investigate whether

asphaltenes might affect the layer properties, i.e., the layer protectiveness against naphthenic acid attack, which would be revealed by experimentation in the HVR.

According to the experimentation procedures, steel specimens were pretreated in the stirred autoclave followed by the challenge with the naphthenic acid solution (TAN 3.5) in the HVR. The net challenge corrosion rates are shown in Figure 41. Generally, it is difficult to form a protective layer on the surface of CS specimens and all of the challenge corrosion rates are higher than 1 mm/y. Interestingly the natural TAN of Fractions P & O is even higher than the TAN of challenge solution, but the challenge corrosion rates are much higher than for the pretreatment solution. This suggests that properties of naphthenic acids from different sources could be quite different.
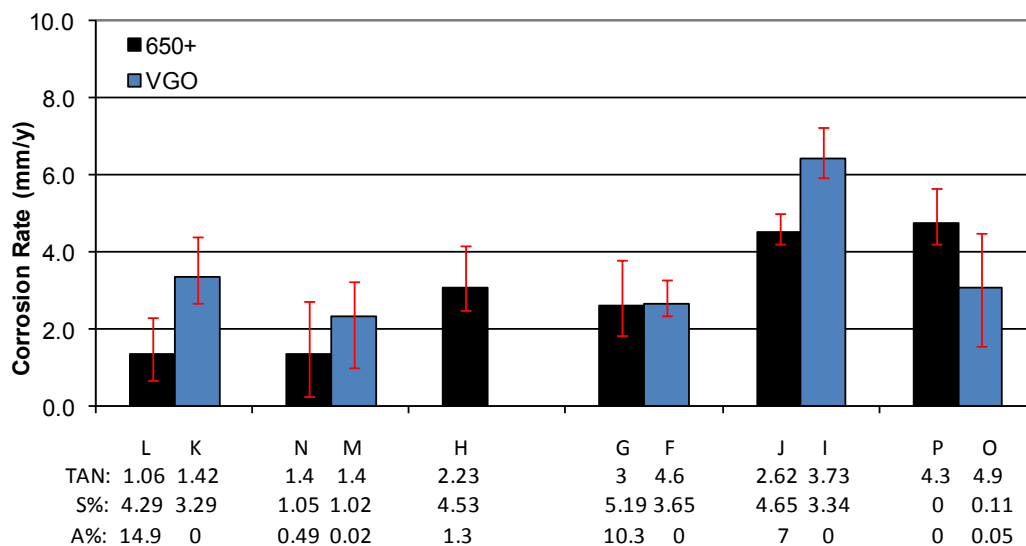
Figure 41. Challenge corrosion rates for CS pretreated with different real crude fractions. For the pretreatment in the stirred autoclave, the pretreatment duration was 24 hours and the temperature was 316°C. For the challenge in the HVR, the time of exposure was 24 hours, the temperature was 343°C, and the peripheral velocity was 8.56 m/s.

The effect of asphaltenes on the layer protectiveness is the focus of Figure 41. For pairs of Fractions L & K, Fractions N & M, and Fractions J & I, 650+ fractions with a high content of asphaltenes seems to generate more protective layers than VGO. However, the difference of challenge corrosion rates is not significant when the error is taken into account. Moreover, challenge corrosion rates for Fractions H & G are similar suggesting that content of asphaltenes is not a major factor determining the properties of layer.

Figure 42 depicts the challenge corrosion rates for 5Cr steel specimens. Although 5 percent of chromium in the steel is not high enough to resist corrosion by crude fractions, it seems that the layer formed on the 5Cr steel surface is more protective than the layer on CS surface when comparing Figure 41 with Figure 42. Layers formed in Fractions P & O are quite protective for 5Cr steel. There is little sulfur in Fractions P & O and the iron sulfide layer was not expected to be formed on the metal surface. The reason behind such layer protectiveness requires further investigation. It is consistent with the protective layer formed in the "NAP only" solution shown in Figure 25.
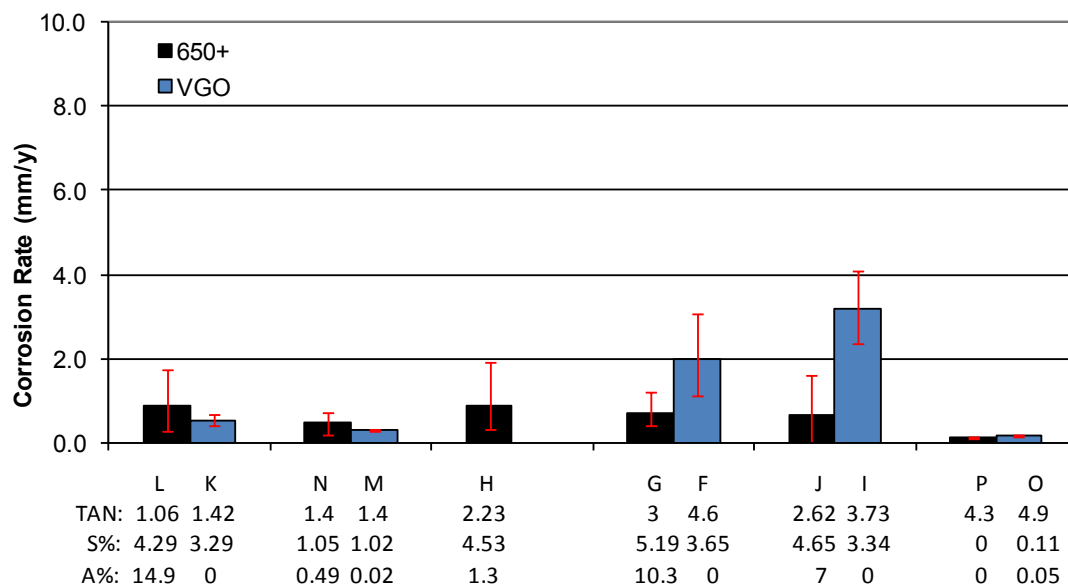
Figure 42. Challenge corrosion rates for 5Cr steel specimens pretreated with different real crude fractions. For the pretreatment in the stirred autoclave, the pretreatment duration was 24 hours and the temperature was 316°C. For the challenge in the HVR, the time of exposure was 24 hours, the temperature was 343°C, and the peripheral velocity was 8.56 m/s.

The asphaltene content of Fraction L is the highest among all fractions while there is no asphaltene in its counterpart Fraction K. However, their challenge corrosion rates are similar. As 650+ fractions from the same source, Fraction G and Fraction H show similar layer protectiveness in spite of the difference of asphaltene content. Again, asphaltene is proven to be unrelated to the layer protectiveness.

8.2.2 Surface Analytical Results and Discussion

For the comparison with layers formed in model compounds, SEM/EDS analysis was implemented to examine specimens pretreated in real crude fractions. Given the large amount of data generated, only representative results will be presented and discussed in this section. The complete set of SEM images can be found in Appendix A.

Figure 43 shows the surface SEM analysis on the specimen pretreated with

Fraction O (TAN = 4.9, S% = 0.11%, and asphaltene% = 0.03%). Image (a) reveals that

there is little corrosion product on the metal surface, for scratching from polishing done

during sample preparation is still visible. It is similar to the surface of specimen

pretreated in the "NAP only" solution (Figure 26). This phenomenon is consistent with

classical theory of corrosion which claims that the product of naphthenic acid corrosion is

oil-soluble.[2] EDS analysis indicates a minor amount of sulfur, which might be due to

natural sulfur compounds in the crude or contamination of the stirred autoclave.

However, the presence of oxygen on the metal surface deserves further investigation. It

could result from oxidation after experimentation, but this does not preclude other

possibilities.
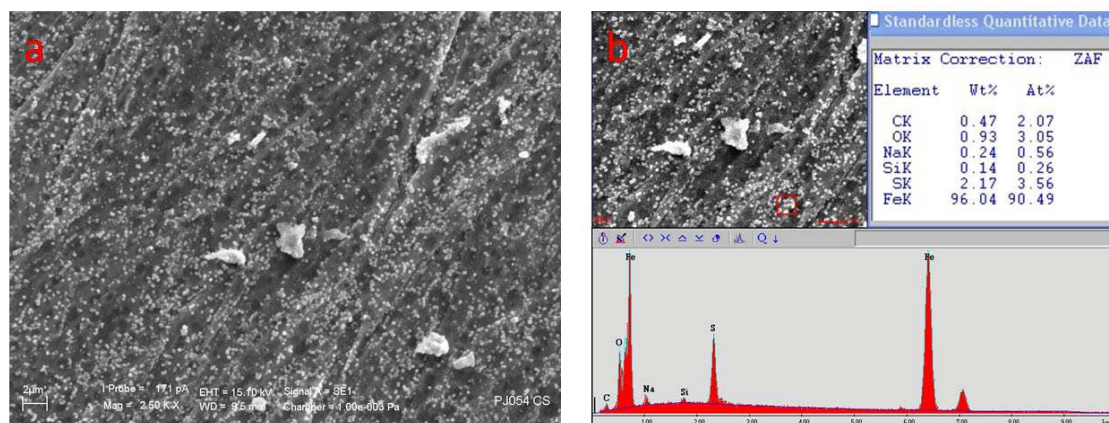
Figure 43. Surface of CS specimen pretreated with Fraction O. (a) Surface SEM image; (b) EDS analysis on the surface. For corrosion rates see Figure 39. SEM and EDS analysis of the cross section is given in Figure 44.

Figure 44 shows the cross-section image of the CS specimen pretreated with

Fraction O. Other than the gap probably generated during polishing, the layer is hardly

visible with a magnification of 5000x, which is consistent with the surface SEM analysis.

Cross-section EDS results shows a peak of sulfur consistent with the surface EDS results.

Moreover, oxygen was again observed.
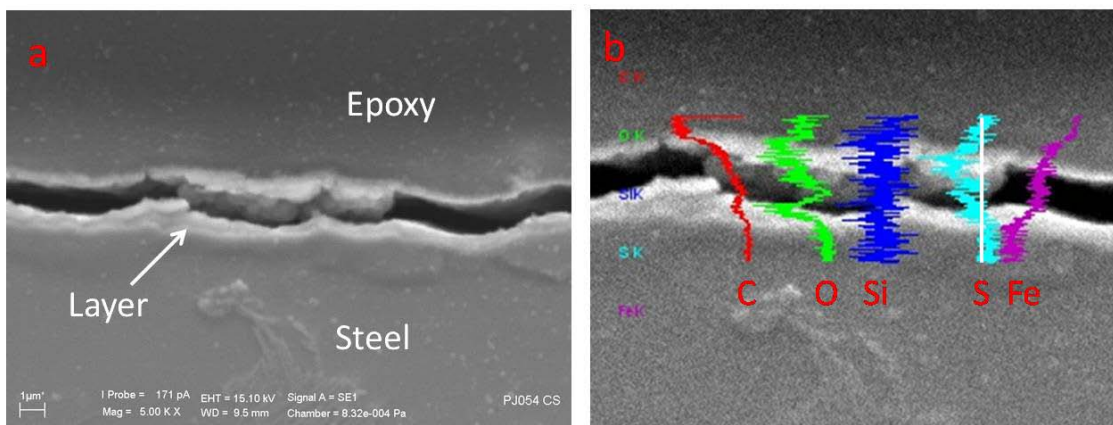
Figure 44. Cross-section analysis of CS specimen pretreated with Fraction O. (a) Cross-section SEM image; (b) Corresponding EDS analysis along the while line on the right. For corrosion rates see Figure 39. SEM and EDS analysis of the surface is given in Figure 43.

The surface of 5Cr steel is similar as that of CS (Figure 45). The polishing marks

are still visible given the low corrosion rate. EDS analysis indicates the presence of

chromium, which is consistent with the elemental composition of 5Cr steel. Moreover,

the oxygen peak was again observed. Cross-section analysis also confirms the finding for

CS – a hardly visible layer with a peak for oxygen (Figure 46).
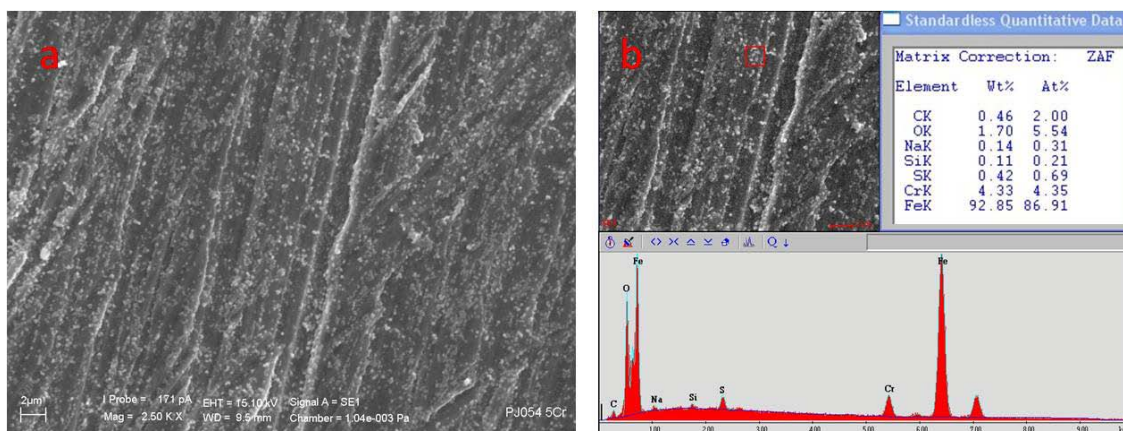
Figure 45. Surface of 5Cr steel specimen pretreated with Fraction O. (a) Surface SEM image; (b) EDS analysis on the surface. For corrosion rates see Figure 40. SEM and EDS analysis of the cross section is given in Figure 46.
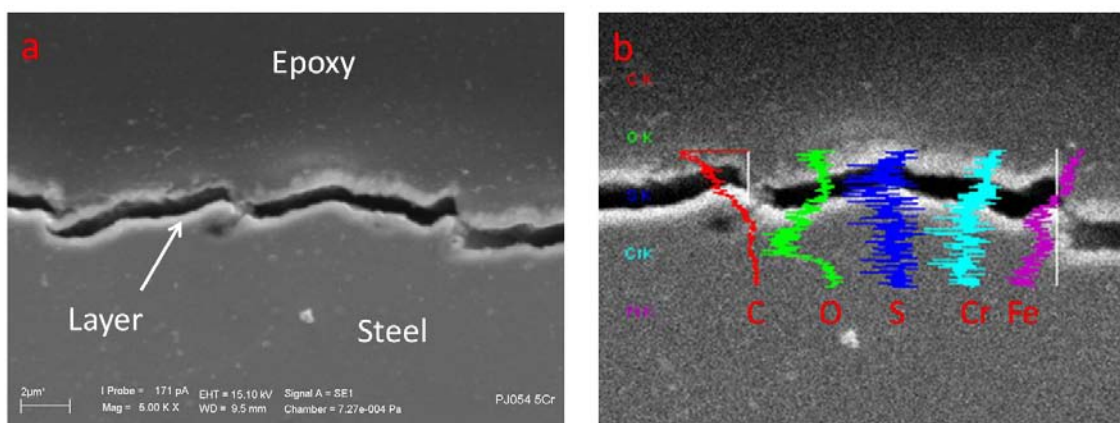
Figure 46. Cross-section analysis of 5Cr steel specimen pretreated with Fraction O. (a) Cross-section SEM image; (b) Corresponding EDS analysis along the while line on the right. For corrosion rates see Figure 40. SEM and EDS analysis of the surface is given in Figure 45.

However, the SEM and EDS analysis cannot provide an explanation of the behavior of steel relating to Fraction O. For instance, the layers formed on both CS and 5Cr steel are quite thin. However, 5Cr steel is somewhat protected while CS is not. Higher resolution analytical techniques are necessary to decipher the reason for the difference in the layer formed on the two types of steel.

8.3 Summary

The asphaltene concentration had no relationship to the corrosivity of crude under the pretreatment conditions. A comparison among corrosion rates for asphaltene-depleted VGO fractions and asphaltene-rich 650+ fractions revealed that the asphaltene in 650+ fractions could not help mitigate the corrosion by the crude oil.

Asphaltene could not be linked to the protectiveness of layer formed in oil fractions in the challenge experiment. Challenge corrosion rates for Fractions H and G undoubtedly negated the assumption relating to the protectiveness granted by asphaltene.

For the high-TAN Fraction O, SEM and EDS analysis showed consistent results with these for the "NAP only" solution. However, it was found again that classical SEM/EDS analysis was not sufficiently powerful to fully reveal the structure of the surface layer due to its innate constraints. It could not reveal the fine layer structure on a nanometers level. Furthermore, the method to prepare cross-sections of steel specimens for SEM/EDS analysis was imperfect. Liquid epoxy was used to fix the layer on the steel specimens before they were cut and polished to expose cross-sections of layers. The morphology of layers could be changed due to the contraction/expansion during solidification of epoxy and to mechanical damage during polishing. A more advanced technique for the in situ layer sampling and microscopy at larger magnification was desirable. Fortunately, the FIB – TEM technique made it possible to investigate the layer at the nanometer level whilst preserving its structure.

CHAPTER 9: FIB - TEM ANALYSIS OF SURFACE LAYER

9.1 Introduction to FIB – TEM Analysis

The Focused Ion Beam (FIB) was developed in the 1970s for microfabrication.[50] The ions in the FIB are generated from a Liquid Metal Ion Source, or LMIS.[51] Usually, the metal is gallium since its melting point is only 29.8°C and it can be easily liquefied. The scheme of the FIB instrument is shown in Figure 47.[52] There is a tungsten needle wetted by liquid gallium in the LMIS. In an applied electrical field, a beam of gallium ions accelerates and converges after field extraction and passing through a series of electric lenses and apertures. The energy of the ion beam is determined by the acceleration voltage and its spot size relates to the current. The common acceleration voltage is 5 keV to 30 keV and the current from 1 pA to 20 nA corresponds to spot sizes from 10 nm to 500 nm.[52] When the high-energy ion beam collides with the solid sample, it can "bombard" the sample surface and sputter away materials in the impacted area. The secondary ions and electrons can be detected for high-resolution surface imaging, which is important to locate the area of interest.
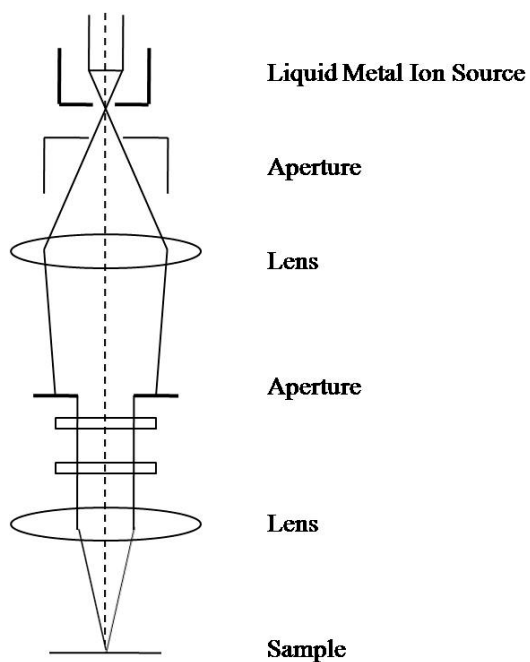
Figure 47. Scheme of a FIB column (based on Langford, R.M.; Petford-Long, A.K.; Preparation of Transmission Electron Microscopy Cross-section Specimens Using Focused Ion Beam Milling. *J. Vac. Sci. Technol., A,* **2001***, 19*(5), 2186-2193.).

In addition to "trenching" on the customized area of sample surface, metals or insulators can be deposited on sample surface by FIB.[52] In this process, the organic metallic compound is fed below the ion beam and decomposes into metal and volatile organic compounds. The most common metals deposited are platinum and tungsten.

The FIB is a versatile method used to prepare foils for TEM analysis which requires a thin sample in the order of nanometers. In this project, the FIB process was conducted in an FEI Helios 600 equipped with a dual beam (positive gallium ion beam and SEM). SEM images of the sample surface were taken in each step of the FIB process which is exemplified in Figure 48.
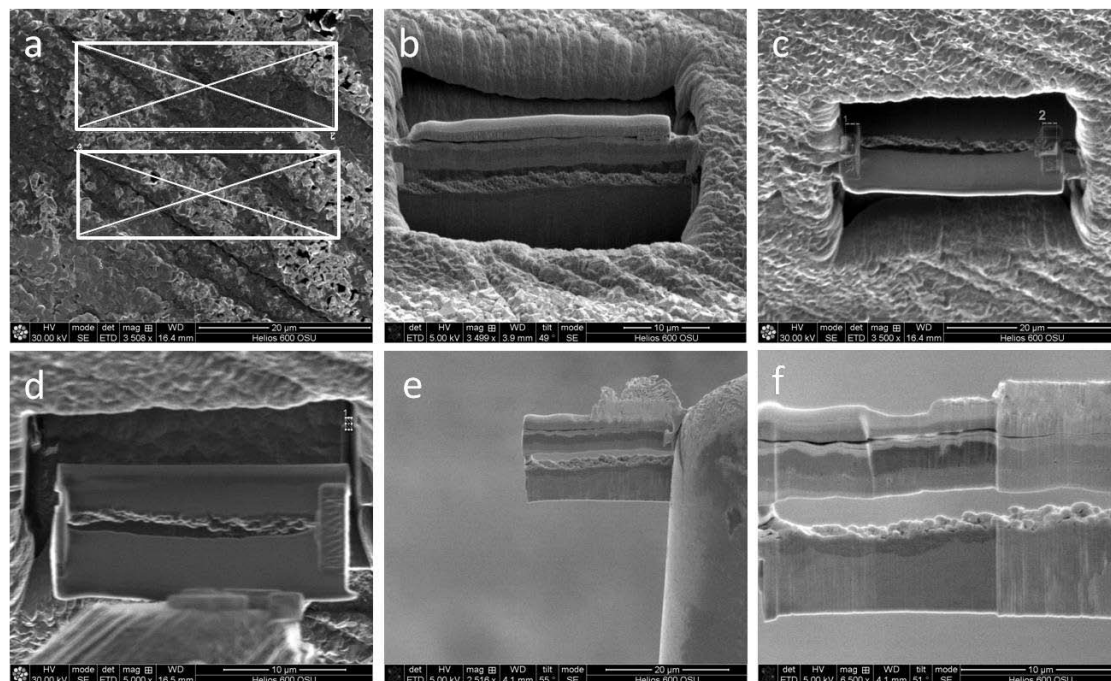
Figure 48. SEM images to illustrate each step of the FIB process. (a) The surface before the deposition of the Pt (platinum) strip and the trenching. (b) Layers after the platinum deposition and the gallium beam trenching. (c) Delaminated layers wielded by Pt strips. (d) The foil connected to the Omniprobe after a U cut. (e) The foil mounted a Cu grid. (f) The foil for TEM analysis.

In Figure 48 an example of steps of FIB foil preparation is shown (actually it is a

5Cr steel specimen covered by a surface layer). The area in the middle of Figure 48 (a)

will be covered by a platinum strip. The two outlined rectangles adjacent to the strip mark

the areas which will be bombarded with an intense gallium beam. Figure 48 (b) shows the

layer after platinum deposition and gallium beam trenching. The white strip on the top is

a protective platinum layer attached to the layer below. It can be clearly seen that

multiple layers are formed and there is a wide gap in between. In addition to revealing in-

situ structure of layer, Figure 48 (b) shows another advantage of the FIB process, which

is generating a foil with straight and parallel sides. This feature is quite important for

accurate elemental analysis in the TEM and EDS analysis. Confronted with the delaminated layer, it is necessary to connect multiple layers; otherwise only the top layer would be lifted out of the specimen. Figure 48 (c) shows the solution of this problem. The specimen is tilted so that platinum strips could be deposited along both edges of the foil and to "weld" the separated layers. These platinum strips can also serve to enhance the mechanical strength of foil. Figure 48 (d) shows the lift-out step. The Omniprobe is inserted until it makes contact with the platinum strip. More platinum strips are deposited in the contact area to connect the probe and the foil. A U-shape cut releases the foil from the substrate sample which could be then lifted out. It is noteworthy that the integrity of layer cross section is preserved due to the deposited platinum as shown in Figure 48 (c). Following the lift-out step, the foil is mounted on the copper grid and the Omniprobe is cut off by a gallium beam shown in Figure 48 (e). On the top is the platinum coating and the steel is on the bottom. The delaminated layer with a wide gap is located in the middle. However, the foil was still too thick for the electron beam in TEM analysis to penetrate. The last step is to thin the foil with a fine gallium beam until a thickness of ~50 nm is achieved. A thick foil might result in a blurred TEM image since it is not penetrable by electrons. On the other hand, a thin foil might be vulnerable to mechanical damage during sample handling and transferring. In order to preserve mechanical strength while making a qualified TEM image possible, only part of the foil is thinned and the finished foil for TEM analysis is shown in Figure 48 (f).

In this project, the foil prepared by the FIB was transferred to Tecnai F20 system to be analyzed in the Scanning Transmission Electron Microscopy (STEM) mode. A

typical setup of the TEM instrument is shown in Figure 49.[53] An electron beam passes

through successive lenses, converges, and penetrates the sample, and is then collected by

different detectors for imaging. The STEM mode combines characteristics of

conventional transmission electron microscopy and scanning electron microscopy. It

relies on scanning the scattered electrons detected by HAADF. Usually, the interested

area is located in the Bright-Field mode and imaged in STEM mode (dark field). The

resolution can be as high as 0.18 nm, which is quite suitable to analyze thin layers. Other

than giving high-resolution images of the layer, Tecnai F20 system is equipped with an

EDS detector which can conduct elemental analysis on a customized area as the

SEM/EDS.
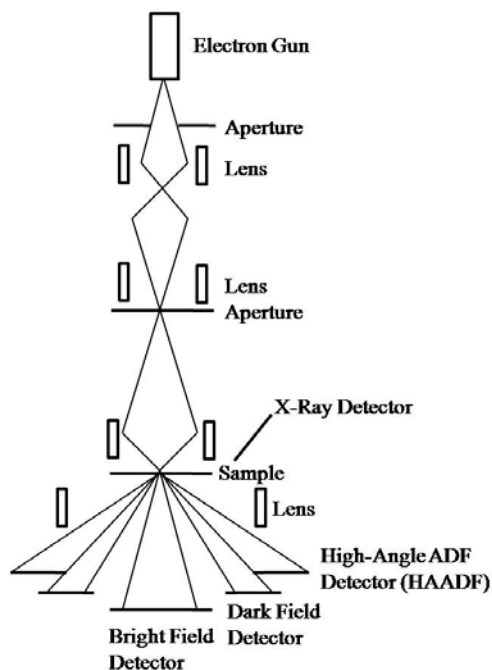
Figure 49. Scheme of TEM (based on Stroppa, D.G.; Zagonel, L.F.; Montoro, L.A.; Leite, E.R.; Ramirez, A.J.; High-Resolution Scanning Transmission Electron Microscopy (HRSTEM) Techniques: High-Resolution Imaging and Spectroscopy Side by Side. *Chemphyschem*, **2012**, *13*(2), 437-443.).

9.2 Criteria for Specimen Selection for FIB – TEM Analysis

As shown in the previous section, FIB and TEM techniques were composed of complicated and tedious procedures. Failure in any step may risk the whole process and lead to a restart. Even for a dedicated and professional operator, it is not unusual to take more than six hours to prepare one qualified FIB foil for TEM analysis, not to mention the expense relating to equipment and labor hours.

Comparing with SEM analysis, the time-consuming and expensive FIB – TEM analysis can only be conducted for selected specimens. To extract maximum information, careful selection of specimen is possible according to following guidelines.

1) Specimens, pretreated in real crude fractions and in model compounds, should be analyzed to compare the layer formed in different fluids;

2) Both CS and 5Cr steel should be included on the list to examine the effect of chromium;

3) Specimens pretreated at 316°C and 343°C should be utilized to explore the influence of temperature on layer formation;

4) Layers, formed after the pretreatment and after the challenge, respectively, should be compared to figure out the transformation of the layer during the challenge;

5) Preferably, protective and unprotective layers should be compared to facilitate the understanding of layer formation and properties.

9.3 FIB – TEM Analysis on Specimens Pretreated in Model Compounds

Due to the advantages associated with using of model compounds, FIB – TEM analysis was conducted first on specimens pretreated in mineral model oil containing DDS and/or NAP. Table 10 shows the selected specimens for FIB – TEM analysis according to guidelines listed in the preceding section. The analytical results will be shown in the following sections regarding each pretreatment fluid.

Table 10.

Experimental Matrix to Select Specimens for the FIB-TEM Analysis – Model Compounds

Pretreatment Fluid	Metallurgy	Pretreatment				Challenge		
		TAN (mg KOH / g oil)	Sulfur Content (wt%)	Temperature (°C)	FIB-TEM	TAN (mg KOH / g oil)	Temperature (°C)	FIB-TEM
DDS	5Cr	0	0.25	316	YES	3.5	343	
DDS	CS	0	0.25	316	YES	3.5	343	
DDS	5Cr	0	0.25	343	YES	3.5	343	YES
DDS + NAP	5Cr	1.75	0.25	316	YES	3.5	343	
DDS + NAP	CS	1.75	0.25	316	YES	3.5	343	
DDS + NAP	5Cr	1.75	0.25	343	YES	3.5	343	YES
NAP	5Cr	1.75	0	316	YES	3.5	343	YES

9.3.1 Specimens Pretreated in the "DDS only" Solution (TAN = 0, S% = 0.25%)

The experimental results involving the "DDS only" solution are summarized in Figure 50. During the pretreatment, an elevated temperature leads to higher corrosion rates for both CS and 5Cr steel. For the challenge, the layer formed on CS specimen at 343°C seems to offer an average protection against the NAP acid challenge. Neither pretreatment temperature works for 5Cr steel, though the absolute challenge corrosion rates are lower than those of CS.
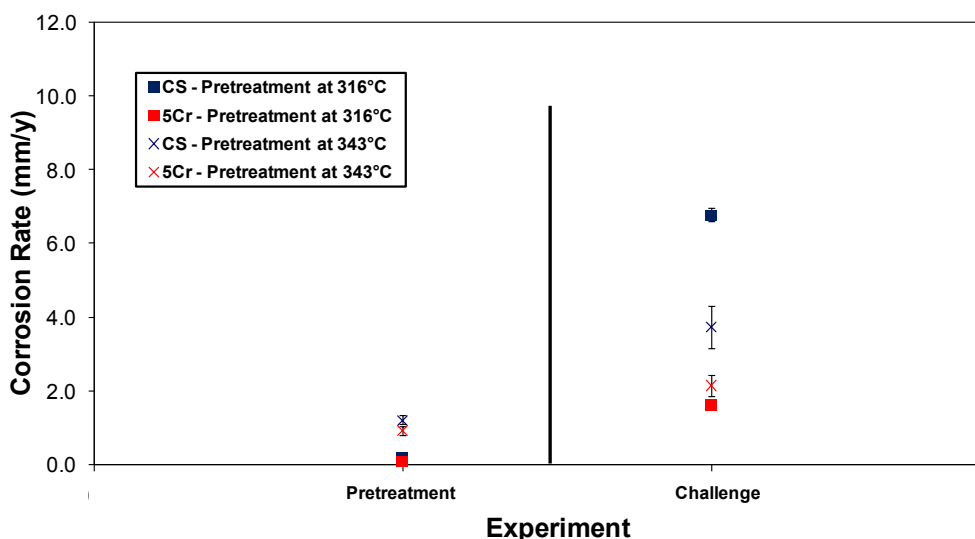
Figure 50. Summary of pretreatment and challenge corrosion rates for CS and 5Cr steel specimens pretreated in the "DDS only" solution. For the pretreatment in the stirred autoclave, the pretreatment duration was 24 hours and the temperature was 316°C or 343°C. For the challenge in the HVR, the time of exposure was 24 hours, the temperature was 343°C, and the peripheral velocity was 8.56 m/s.

The TEM image of the CS specimen pretreated in DDS solution is shown in Figure 51. Comparing with the cross-section SEM image in Figure 27, the high-resolution TEM image gives detailed structure of the layer. The delaminated layer is

located between the protective platinum coating and the steel substrate. The total layer

thickness is about 1.5 µm including the gap.

Figure 51. TEM image of CS specimen pretreated with the "DDS only" solution at 316°C for 24 hours. For corrosion rates see Figure 50.

Figure 52 shows the elemental composition of the top layer given by EDS

analysis. Obviously, iron sulfide is formed after pretreatment with the "DDS only"

solution, which is consistent with the results of EDS analysis in SEM (Figure 27).

<div align="center">(a)   (b)</div>
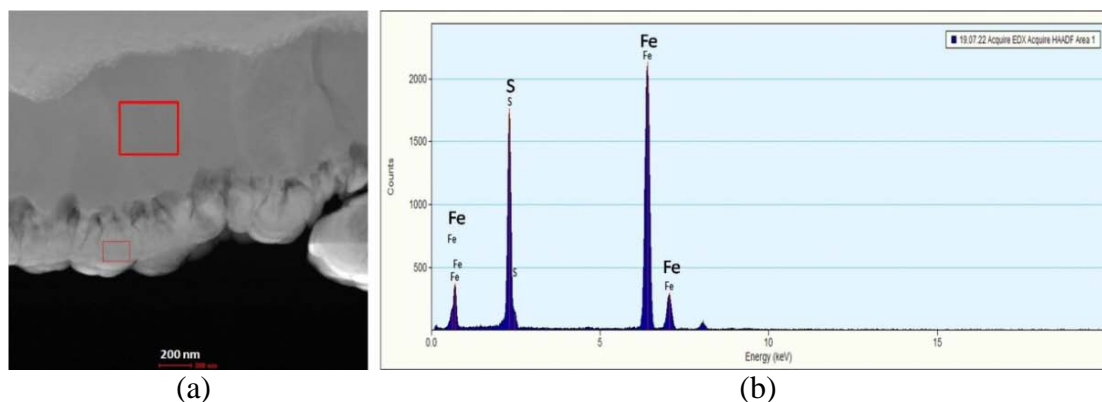
Figure 52. EDS analysis on the top layer shown in Figure 51. (a) Enlarged image of the top layer with the square showing the area of EDS analysis; (b) Results of EDS analysis.

Different shades of gray shown in Figure 53 suggest a varied chemical composition of this layer. To gain a comprehensive profile of elements, an EDS analysis is conducted along the line drawn in Figure 53. In the first 100 nm from the starting point, the major element is iron, which is consistent with it being steel. The 5% of oxygen may be due to contamination or oxidation of the foil. In the following EDS scanning, the content of iron decreases and sulfur appears to be present in almost an equal stoichiometric amount as iron. This suggests that the inner layer is also composed of iron sulfide, though there is a minor amount of oxygen.

(a)   (b)

Figure 53. Elemental profile of the layer presented in the square of Figure 51. (a) Image of layer with the line of EDS scanning; (b) Results of EDS analysis.

The layer morphology for 5Cr steel is similar as that of CS (Figure 54). The layer thickness is 1.2 µm with a gap dividing it into two layers. EDS analysis confirms that the outer layer is iron sulfide (Figure 55).
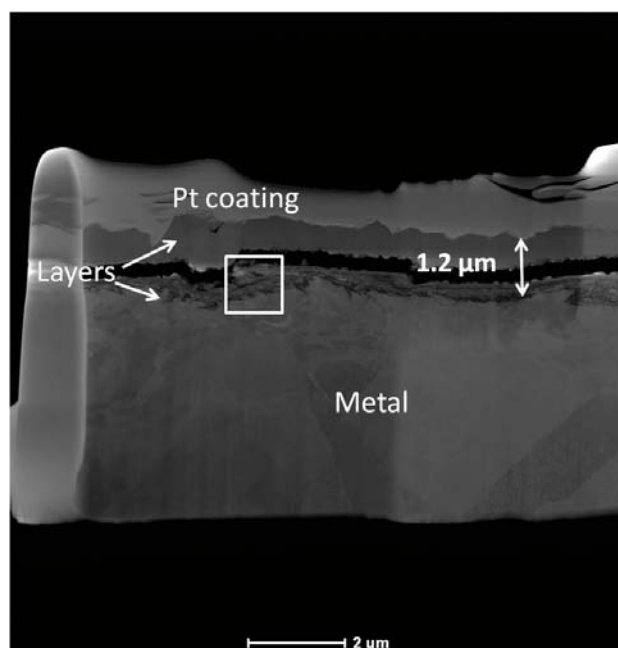
Figure 54. TEM image of 5Cr steel specimen pretreated with the "DDS only" solution at 316°C for 24 hours. For corrosion rates see Figure 50.
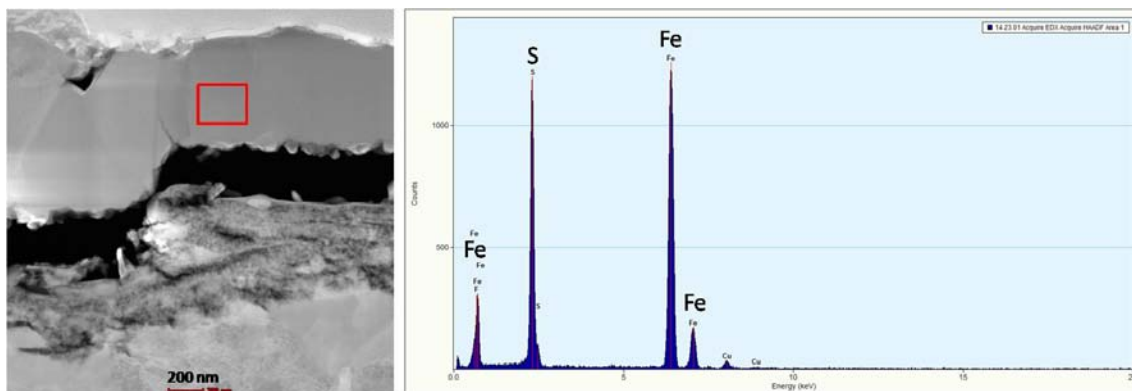
Figure 55. EDS analysis on the top layer shown in Figure 54. The elemental data was collected in the square.

The inner layer elemental profile is shown in Figure 56. The atomic distribution profiles suggest that the inner layer consist mainly of iron sulfide with fragments of oxide inserted in the layer structure.

(a)   (b)
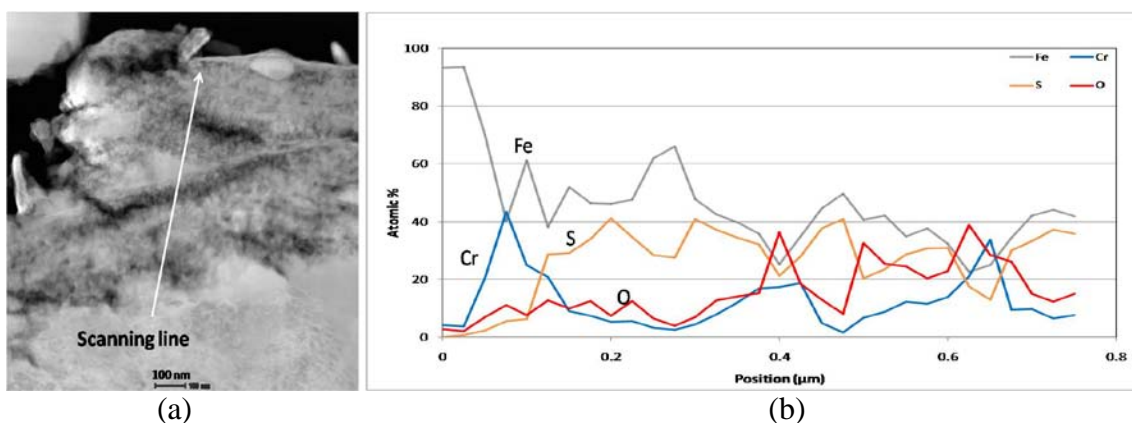
Figure 56. Elemental profile of the layer from the image presented in the square of Figure 54. (a) Image of the layer with the EDS scanning line; (b) Results of EDS analysis.

The morphology of layers before and after the challenge is shown in Figure 57. The layer formed at 343°C is thicker than the layer formed at 316°C for 5Cr steel (Figure 54). A thick layer is formed below the outer iron sulfide layer. After the challenge, the

thickness of inner layer does not change significantly as shown in image b. However, a

new continuous layer appears between the old inner layer and the metal substrate.

Figure 57. TEM images of 5Cr steel specimen: (a) after the pretreatment with the "DDS only" solution at 343°C for 24 hours; (b) after the challenge with naphthenic acid solution (TAN 3.5) at 343°C for 24 hours. For corrosion rates see Figure 50.

The EDS analysis on the layer formed in the DDS solution for 5Cr steel is shown

in Figure 58. The double layer structure of is observed again. It should be noted that

chromium shows up only in the inner layer.

Figure 58. Elemental profile of the layer presented in Figure 57 (a). (a) Image of layer with the line of EDS scanning; (b) Results of EDS analysis.

The EDS analysis of the layer formed after the pretreatment-challenge is helpful to reveal its chemical composition (Figure 59). The newly formed thin layer is of most interest. Its thickness is about 0.5 µm and the sulfur content is almost zero. This distinguishes itself from the layer formed after pretreatment. Interestingly, the oxygen content can account for as much as 40 atomic percent in this layer. It seems that this layer is composed of iron/chromium oxides.

(a) (b)

Figure 59. Elemental profile of the layer presented in Figure 57 (b). (a) Image of layer with the line of EDS scanning; (b) Results of EDS analysis.

9.3.2 Specimens Pretreated in the "DDS + NAP" Solution (TAN = 1.75, S% = 0.25%)

The pretreatment and challenge corrosion rates for the "DDS + NAP" solution are summarized in Figure 60. Generally, the challenge corrosion rates become lower with the presence of naphthenic acids in the pretreatment solution compared with the corrosion rate for the "DDS only" solution. In other words, the layers are more protective. TEM analysis of these protective layers will help us understand why this happened.
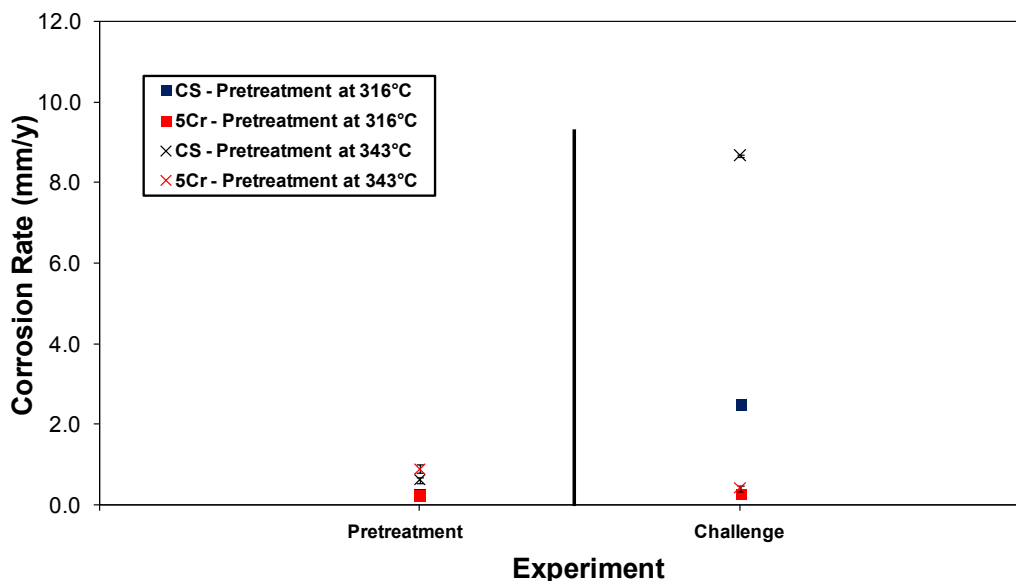
Figure 60. Summary of pretreatment and challenge corrosion rates for CS and 5Cr steel specimens pretreated in the "DDS + NAP" solution. For the pretreatment in the stirred autoclave, the pretreatment duration was 24 hours and the temperature was 316°C or 343°C. For the challenge in the HVR, the time of exposure was 24 hours, the temperature was 343°C, and the peripheral velocity was 8.56 m/s.

TEM image of CS specimen pretreated with the "DDS + NAP" solution at 316°C is shown in Figure 61. Surprisingly, no outer layer is found on this specimen and the inner layer is not continuous, which is not consistent with its SEM images (Figure 27). It is postulated that the area for the FIB sampling is not covered by an outer layer which is delaminated from the substrate.
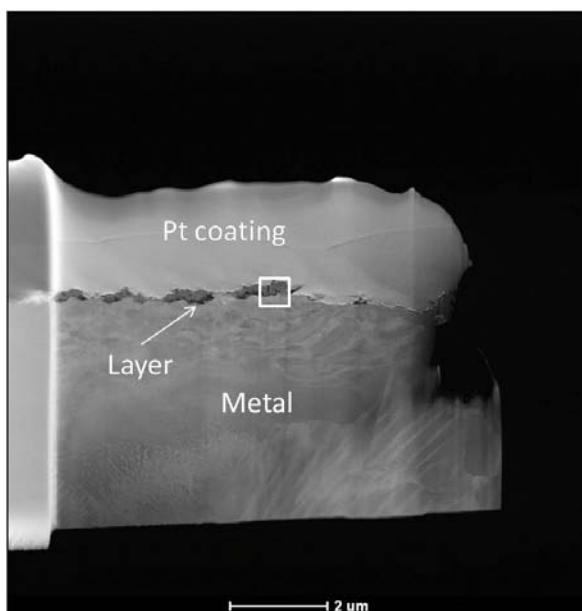
Figure 61. TEM image of CS specimen pretreated with the "DDS + NAP" solution at 316°C for 24 hours. For corrosion rates see Figure 60.

The EDS analysis is shown in Figure 62. A significant amount of oxygen in the layer indicates a presence of an oxide layer which might have been formed by the oxygen produced from naphthenic acid decomposition. However, further evidence is necessary to verify this finding.

(a)   (b)
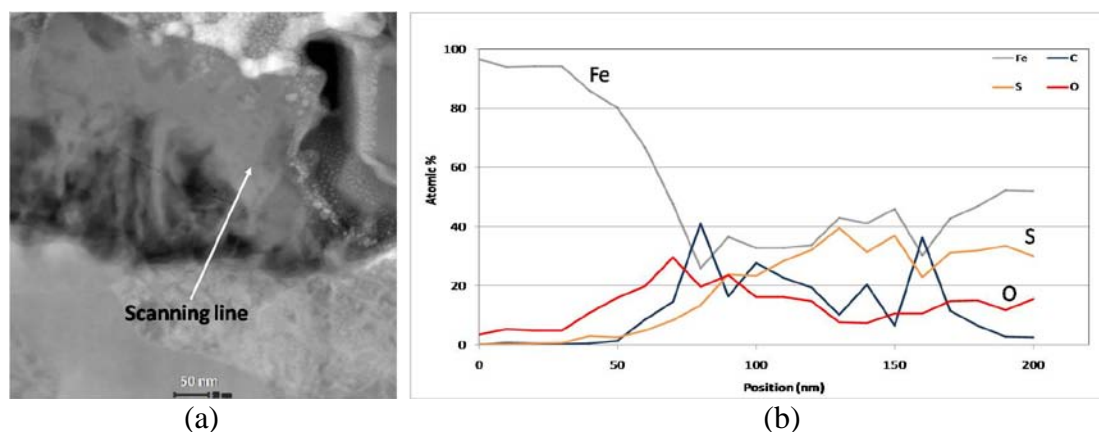
Figure 62. Elemental profile of layer shown in the square of Figure 61. (a) Image of layer with the line of EDS scanning; (b) Results of EDS analysis.

The 5Cr specimen pretreated in the same condition has a much lower challenge corrosion rate as shown in Figure 60 and exhibits a more distinct layer morphology in the TEM image (Figure 63). Compared with the layer pretreated in the "DDS only" solution shown in Figure 54, the outer layer is intimately attached to the inner layer. The total layer thickness is about 1 µm while the inner layer only accounts for less than half of that.
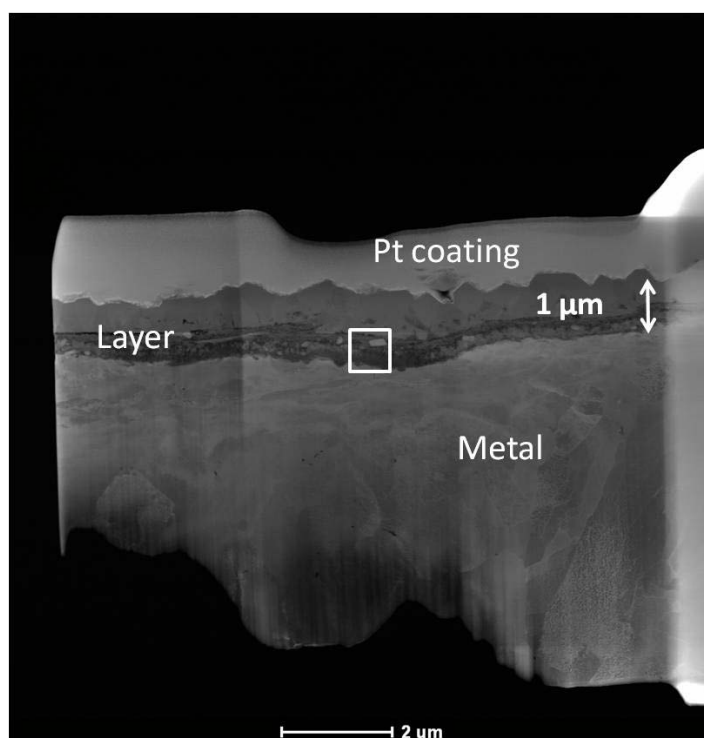
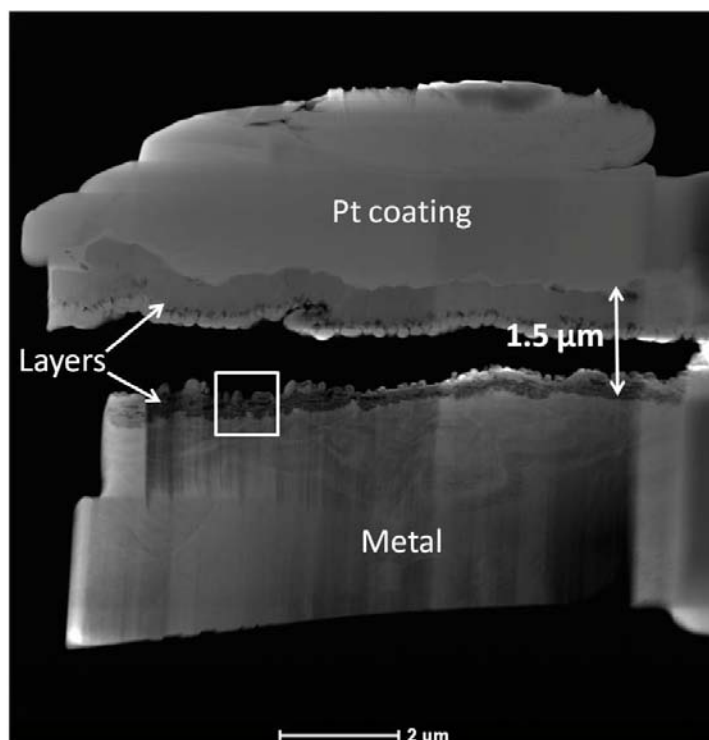Figure 63. TEM image of 5Cr steel specimen pretreated with the "DDS + NAP" solution at 316°C for 24 hours. For corrosion rates see Figure 60.

The EDS analysis on the line across the layer is shown in Figure 64. In the inner layer, the oxygen content is as high as 40% while the sulfur accounts for less than 5%. Moreover, the chromium concentration increases from 5 percent in the steel substrate to

about 10 percent on average in the inner layer. Given that the outer layer is iron sulfide,

just like in the case of other experiments which have shown much higher corrosion rate,

the protective properties of this layer should be attributed to the inner oxide layer.

(a)　　　　　　　　　　　　　(b)
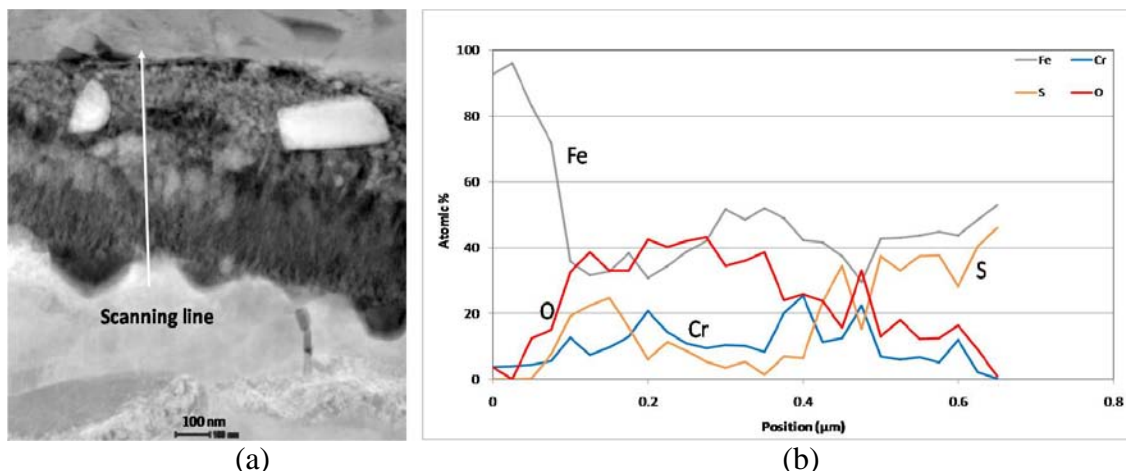
Figure 64. Elemental profile of layer shown in the square of Figure 63. (a) Image of the layer with the line of EDS scanning; (b) Results of EDS analysis.

Comparison of TEM images between 5Cr specimens before and after the

challenge is shown in Figure 65 (The pretreatment temperature is 343°C). At a higher

pretreatment temperature, the inner layer is approximately 3 µm. The black area between

the inner layer and the steel substrate are an artifact obtained during FIB processing when

part of layer was thinned so much that materials began to fall away. The image for the

layer after challenge suffers from similar problems. However, it is still clearly shown that

the inner layer thickness is about the same.
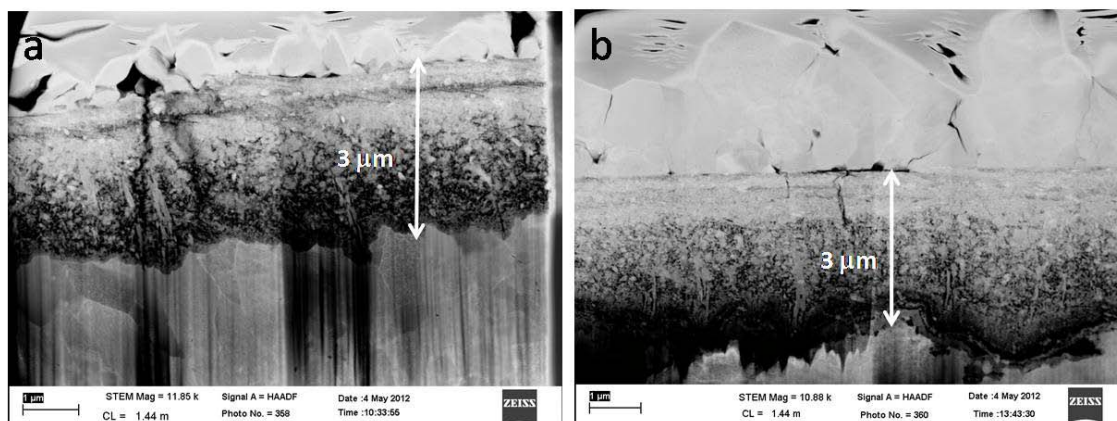
Figure 65. TEM images of 5Cr steel specimen: (a) after the pretreatment with the "DDS + NAP" solution at 343°C for 24 hours; (b) after the challenge with the naphthenic acid solution (TAN 3.5) at 343°C for 24 hours. For corrosion rates see Figure 60.

An EDS analysis across the layer formed in the "DDS + NAP" solution is shown in Figure 66. Again, the presence of oxygen is observed in the inner layer. It is noteworthy that the concentration of chromium in the inner layer is larger than that in the steel substrate.

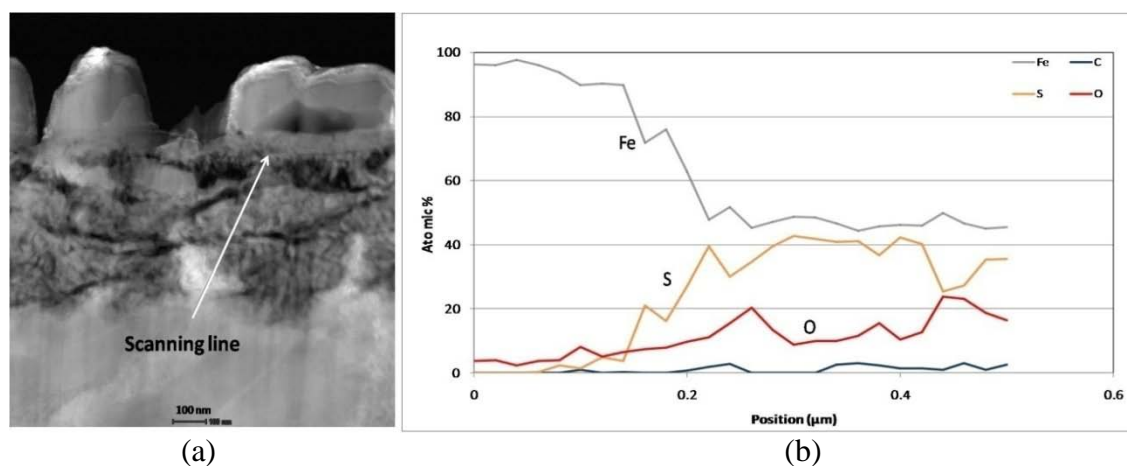(a)   (b)
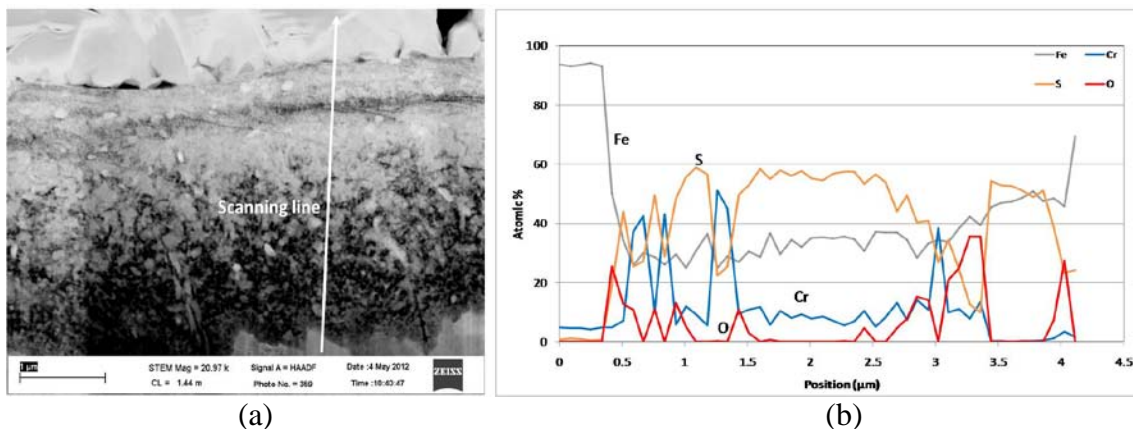
Figure 66. Elemental profile of layer in Figure 65 (a). (a) Image of layer with the line of EDS scanning; (b) Results of EDS analysis.

After the challenge, the inner layer becomes richer in oxygen but sulfur is scarce (Figure 67). Similarly in Figure 59, peaks of oxygen are found near the interface between the steel substrate and the inner layer. This suggests that iron oxide was formed during the challenge with the naphthenic acid solution.

(a)   (b)
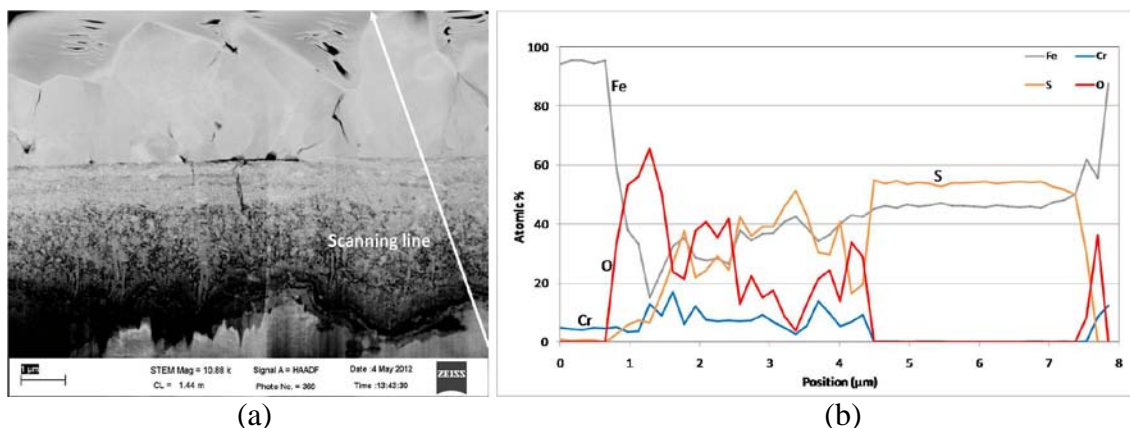
Figure 67. Elemental profile of the layer shown in Figure 65 (b). (a) Image of layer with the line of EDS scanning; (b) Results of EDS analysis.

9.3.3 Specimens Pretreated in the "NAP only" Solution (TAN = 1.75, S% = 0)

The summary of corrosion rates involving the "NAP only" solution is shown in Figure 68. The pretreatment temperature is 316°C. The presence of chromium in the steel slightly decreases the pretreatment corrosion rate for 5Cr steel. However, the challenge corrosion rate of 5Cr steel is almost zero while CS shows comparably high corrosion rate as in the pure TAN 3.5 experiment. SEM/EDS analysis on metal surface cannot provide a clear explanation of this behavior and TEM analysis is the best option.

Figure 68. Summary of pretreatment and challenge corrosion rates for CS and 5Cr steel specimens pretreated in the "NAP only" solution. For the pretreatment in the stirred autoclave, the pretreatment duration was 24 hours and the temperature was 316°C. For the challenge in the HVR, the time of exposure was 24 hours, the temperature was 343°C, and the peripheral velocity was 8.56 m/s.

Images collected from TEM analysis are shown in Figure 69. After pretreatment in the "NAP only" solution, a thin layer with a thickness of 165 nm was formed and it survived the challenge. Comparing with the layer formed in the solution with the organosulfur compounds (Figure 63), it seems that the layer in Figure 69 is composed of only one compact layer.
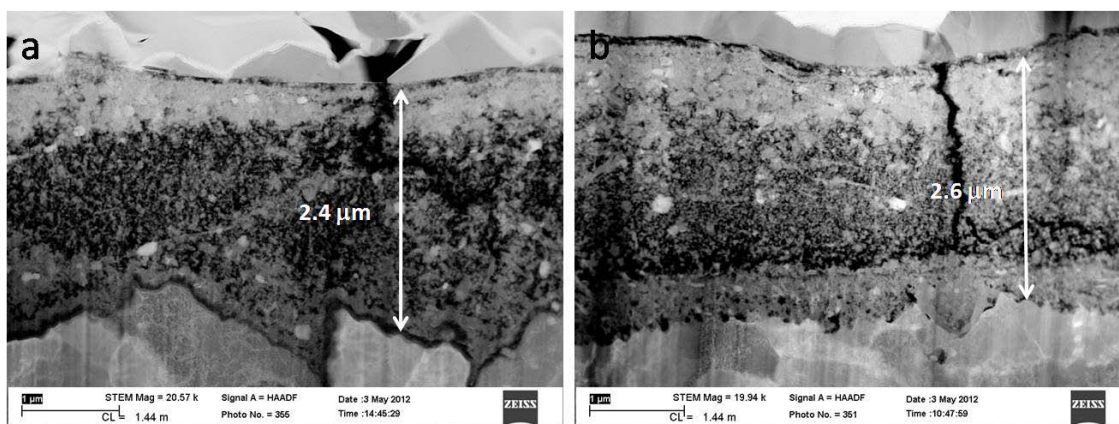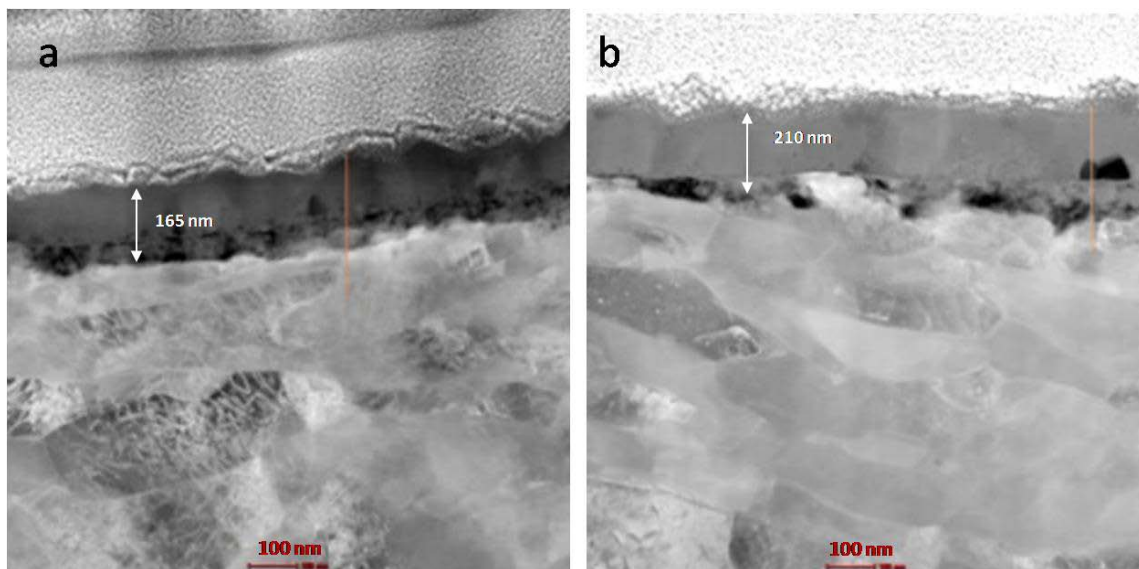
Figure 69. TEM images of 5Cr steel specimen: (a) after the pretreatment with the "NAP only" solution at 316°C for 24 hours; (b) after the challenge with naphthenic acid solution (TAN = 3.5) at 343°C for 24 hours. For corrosion rates see Figure 68.

The EDS analysis of the layer formed in the "NAP only" solution is shown in Figure 70. The EDS scanning along the line across the steel substrate and the layer reveals that there is only one homogenous layer. It is composed of iron and oxygen, though trace amounts of chromium and sulfur are found. The chromium can be traced back to the 5Cr steel and sulfur may be from the contamination in the stirred autoclave or from the small amount contained in the NAP source solution. It can be concluded that iron/chromium oxide formed in the solution of the "NAP only" is protecting the steel from corrosion.
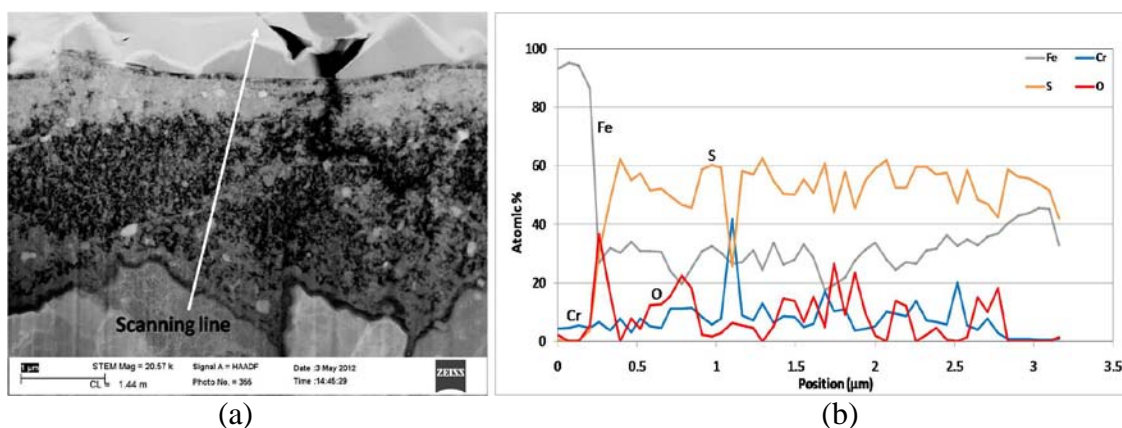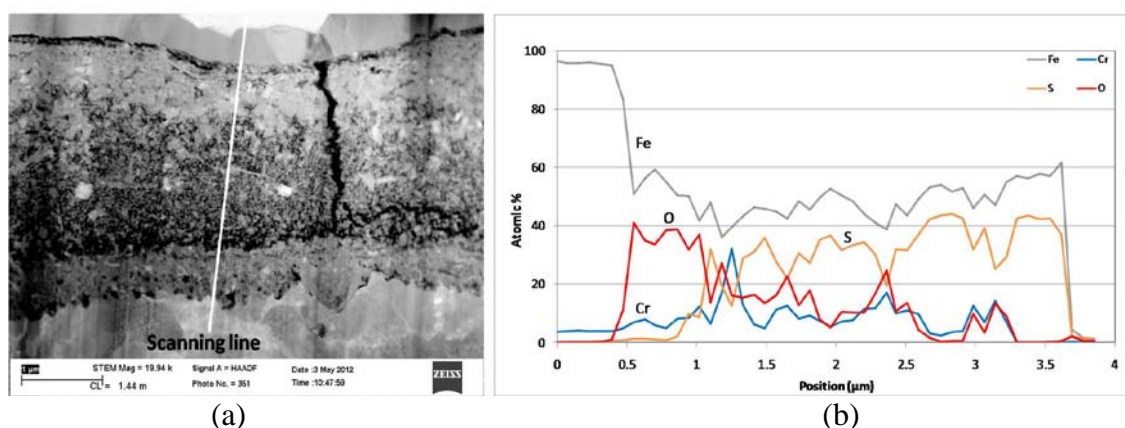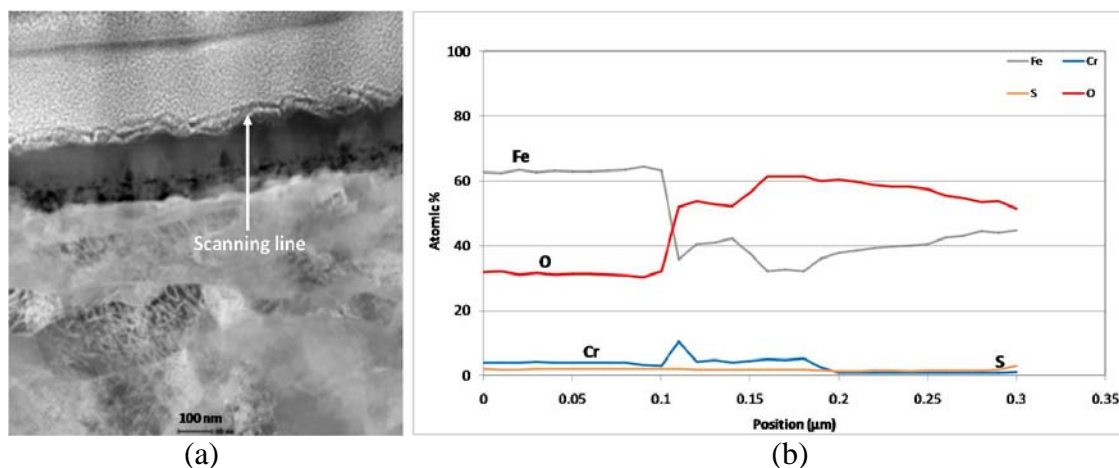
Figure 70. Elemental profile of layer shown in the Figure 69 (a). (a) Image of layer with the line of EDS scanning; (b) Results of EDS analysis.

After challenge, the chemical composition of layer does not change significantly (Figure 71). The high content of oxygen in the steel substrate may be due to the sample contamination/oxidation or the inaccurate measurement by EDS. Nevertheless, oxygen is still the major element in the layer and there is trace amount of chromium and sulfur. It seems that the layer survived the attack by the naphthenic acids in which it was formed.

Figure 71. Elemental profile of layer presented in Figure 69 (b). (a) Image of layer with the line of EDS scanning; (b) Results of EDS analysis.

9.3.4 Summary of TEM Analysis on Specimens Pretreated in Model Compounds

As a powerful analytical technique, TEM analysis provided high resolution images of the layer cross section. Furthermore, the EDS analysis, coupled with the layer morphology, shed light on layer chemistry and the corrosion protection mechanism.

From the TEM/EDS analysis, common features of the surface layer could be summarized.

1) The uppermost layer of iron sulfide always covered the specimen surface as long as sulfur compound existed in the pretreatment solution;

2) For the solution with the organosulfur compound only, the iron sulfide layer tended to be delaminated;

3) If both the organosulfur compound and naphthenic acids existed in the pretreatment solution, an inner oxide layer appeared on the steel surface;

4) The presence of naphthenic acids in the pretreatment solution promoted the integrity of the layer – the iron sulfide layer attached to the oxide layer which adhered to the steel substrate;

5) For the solution with naphthenic acids only, an oxide layer formed without any iron sulfide layer on the top;

6) After the challenge with naphthenic acids, the oxide layer morphology was preserved.

Experimental data showed that the presence of naphthenic acids in the pretreatment solution could promote more protective layers compared with the solution with the organosulfur compound only. Given that the iron sulfide was always found in

the outer layer in cases when the corrosion rate was high as well as low, the protectiveness of layer should be related to the inner oxide layer which formed due to the presence of naphthenic acids.

This conclusion was strongly supported by the fact that the most protective layer formed in the solution of naphthenic acids and was composed of an iron/chromium oxide layer exclusively. Moreover, the increase of oxygen content in the layer, after being challenged with naphthenic acids, indicated that the formation of oxide layer was directly related to naphthenic acids. However, whether similar phenomena may be observed for real crude fractions needs to be verified.

9.4 FIB – TEM Analysis on Specimens Pretreated in Real Crude Fractions

The experiment matrix involving real crude fractions is shown in Table 11. The corresponding results of TEM analysis are shown in following sections.

Table 11.

Experiment Matrix - Specimens Selection for the FIB-TEM Analysis – Real Crude Fractions

| Pretreatment Fluid | Metallurgy | Pretreatment | | | | Challenge | | |
		TAN (mg KOH / g oil)	Sulfur Content (wt%)	Temperature (°C)	FIB-TEM	TAN (mg KOH / g oil)	Temperature (°C)	FIB-TEM
B (VGO)	5Cr	< 0.1	1.92	302	YES	3.5	343	
B (VGO)	CS	< 0.1	1.92	343	YES	3.5	343	
B (VGO)	5Cr	< 0.1	1.92	343	YES	3.5	343	YES
L (650+)	CS	1.06	4.29	316	YES	3.5	343	
A (VGO)	5Cr	1.75	0.53	343	YES	3.5	343	YES
A (VGO)	CS	1.75	0.53	343	YES	3.5	343	
O (VGO)	5Cr	4.9	0.11	316	YES	3.5	343	
O (VGO)	CS	4.9	0.11	316	YES	3.5	343	

9.4.1 Specimens Pretreated in Fraction B (TAN < 0.1, S% = 1.92%)

Fraction B is a VGO fraction with a high amount of sulfur content and a trace amount of naphthenic acids, as shown in Table 11. According to Figure 72, layers on CS surface, formed at 302 or 343C, cannot resist the corrosion by naphthenic acids (challenge corrosion rate about 5.5 mm/y which is almost as high as the pure TAN attack on bare steel). For the pretreatment at 343°C, the challenge corrosion rate of 5Cr steel is around 1.3 mm/y, which is likewise almost the same as the pure attack with no protective layer. The layer is more protective when the pretreatment temperature is 302°C for 5Cr steel. The TEM analysis starts from the most protective layer formed in pretreatment.
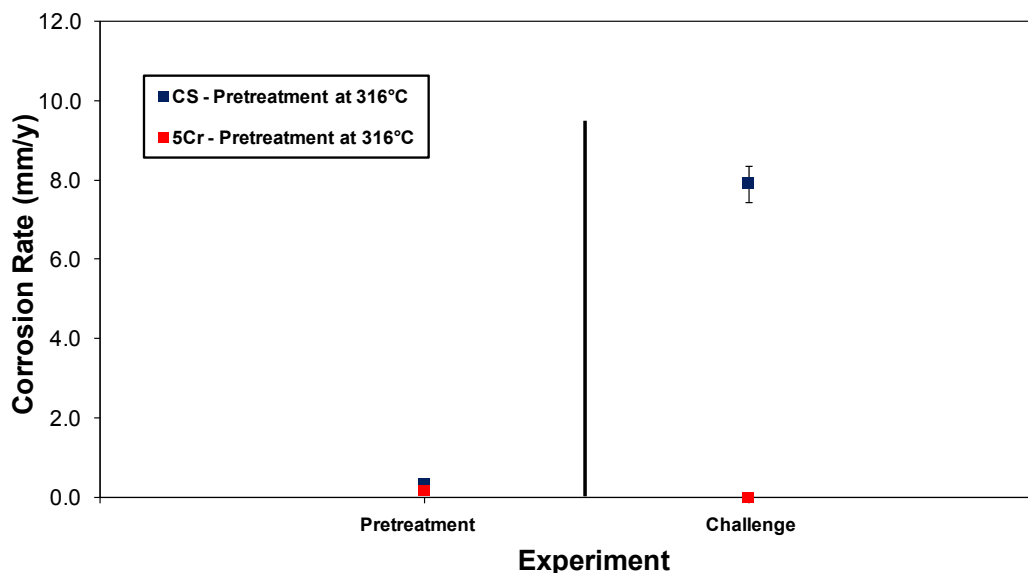

Figure 72. Summary of the pretreatment and challenge corrosion rates for CS and 5Cr steel specimens pretreated in Fraction B. For the pretreatment in the stirred autoclave, the pretreatment duration was 24 hours and the temperature was 302°C or 343°C. For the challenge in the HVR, the time of exposure was 24 hours, the temperature was 343°C, and the peripheral velocity was 8.56 m/s.

Figure 73 shows the TEM image of the layer (pretreatment at 302°C, 5Cr). The total layer thickness is as high as 6.5 µm, with a gap of 2 µm making it appear delaminated. More interestingly, the outer part of the layer seems to be composed of different layers and the EDS analysis should shed light on the composition.

Figure 73. TEM images of 5Cr steel specimen pretreated with Fraction B (TAN < 0.1, S% = 1.92%) at 302°C for 24 hours. For corrosion rates see Figure 72.

The EDS analysis on the outer layer is shown in Figure 74 and Figure 75. Iron sulfide is indicated. However, the elemental profile of material below the iron sulfide layer indicates that a different layer is present - possibly iron carbide.

(a) (b)
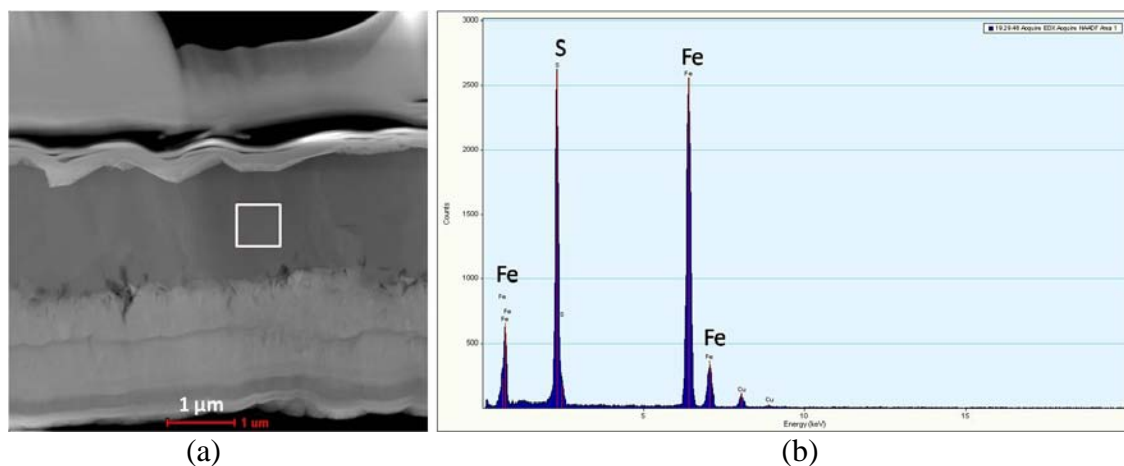
Figure 74. EDS analysis of the top layer shown in the top square of Figure 73. (a) Enlarged image of the top layer with the square showing the area of EDS analysis; (b) Results of EDS analysis.

(a) (b)

Figure 75. Elemental profile of the top layer of the layer shown in the top square of Figure 73. (a) Image of the layer with the line of EDS scanning; (b) Results of EDS analysis.

The elemental profile of the inner layer is shown in Figure 76 (b). Even with a minor concentration of naphthenic acids in the solution, the oxygen still appears in the inner layer, though sulfur is the major non-metallic element. Again, the chromium concentration is higher in the inner layer. It seems that the layer protectiveness is attributed to the mixture of iron sulfide and iron/chromium oxide in the inner layer.
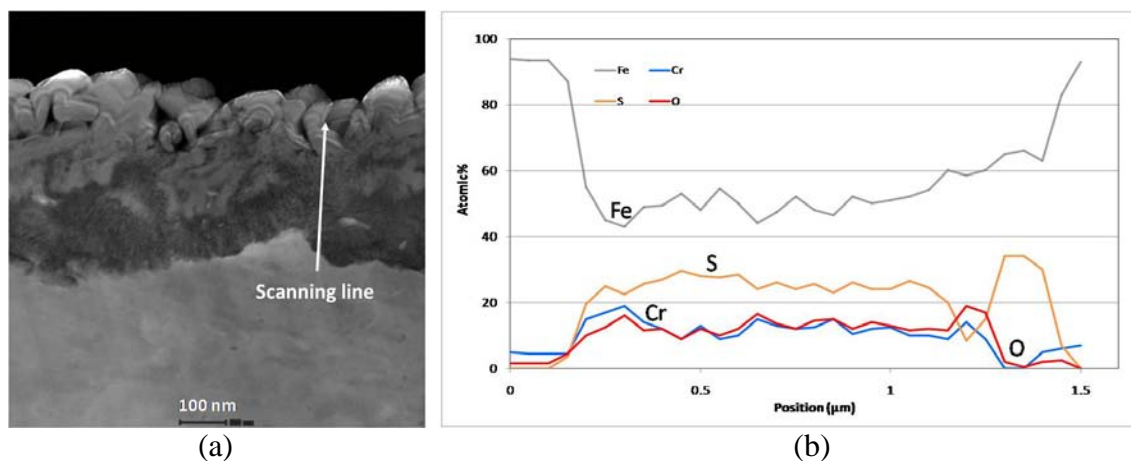
Figure 76. Elemental profile of the inner layer of the layer shown in the bottom square of Figure 73. (a) Enlarged image of inner layer with the line of EDS scanning; (b) Results of EDS analysis.

Figure 77 (a) shows that the non-protective layer formed at 343°C has a thicker inner layer. However, there is a detachment/gap between the inner layer and the steel substrate, which is expected to be the reason for the lack of protectiveness of the layer. After the challenge with the naphthenic acid solution, the outer layer survived while the inner layer became thinner (Figure 77 (b)). It seems that naphthenic acids diffused through the inner layer and corroded the steel underneath.
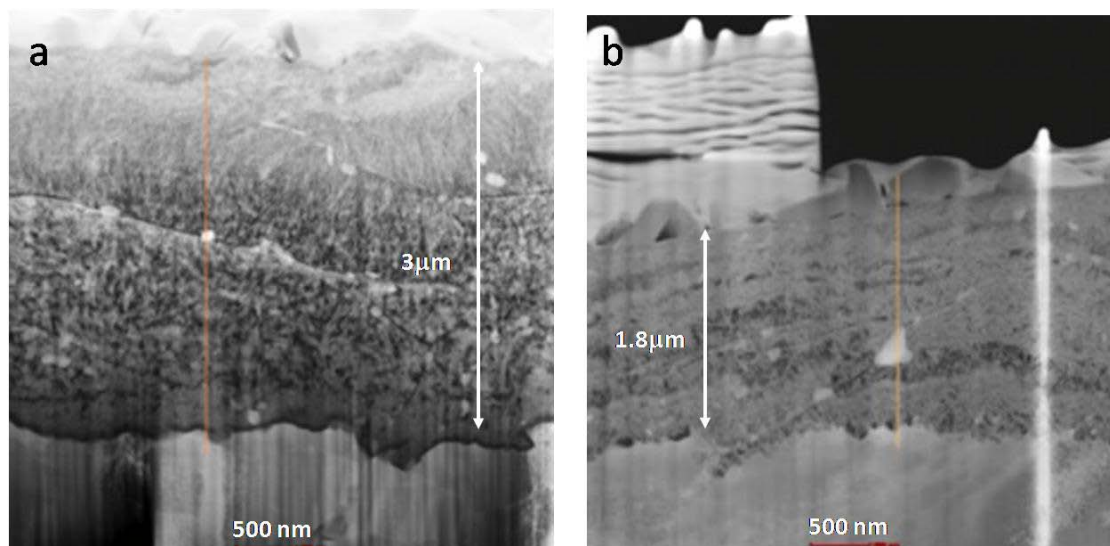
Figure 77. TEM images of 5Cr steel specimen: (a) after the pretreatment with Fraction B at 343°C for 24 hours; (b) after the challenge with naphthenic acid solution (TAN 3.5) at 343°C for 24 hours. For corrosion rates see Figure 72.

The EDS analysis on the layer formed in the pretreatment is shown in Figure 78. Although the oxygen content in the inner layer is as high as 40%, the 30% of oxygen found in the signal coming from the steel substrate indicates that the measurement of oxygen is exaggerated and its actual concentration in the layer is likely to be around 10% or less. Comparing with Figure 76, the chromium content is only slightly higher than in the steel substrate.
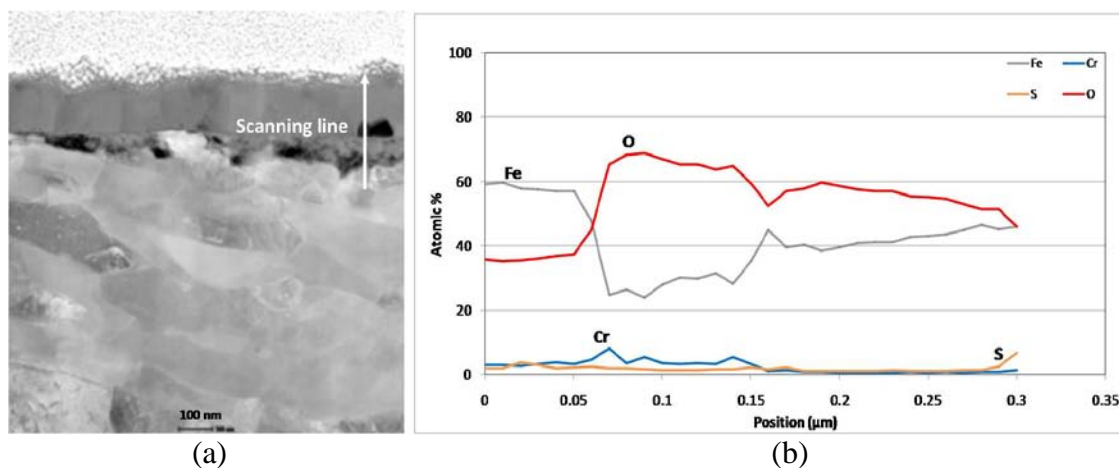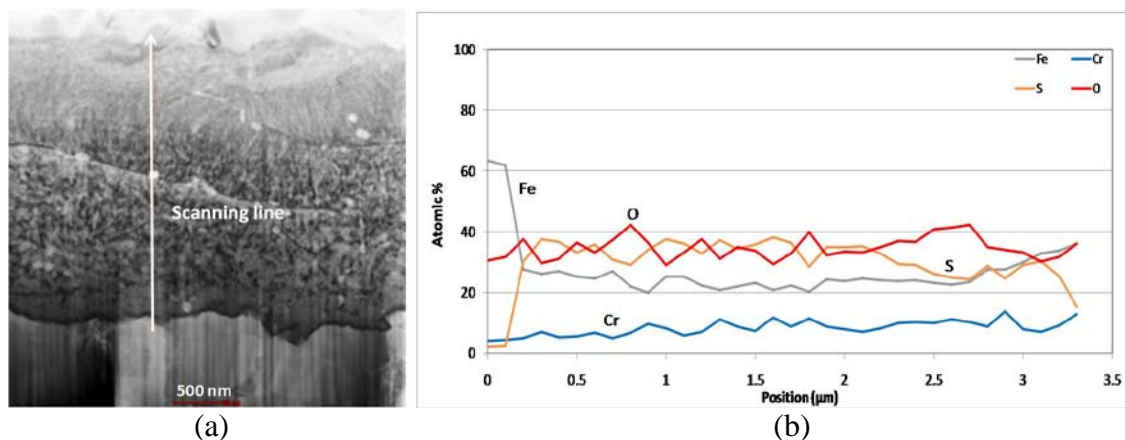
Figure 78. Elemental profile of the layer presented in Figure 77 (a). (a) Image of layer with the line of EDS scanning; (b) Results of EDS analysis.

The chemical composition of the layer after the challenge with naphthenic acids is shown in Figure 79. When the oxygen content measured in the layer is compared with that detected in steel substrate, the overall oxygen content in the inner layer is probably around 30%. This increase of oxygen concentration after the challenge is consistent with the behavior discovered in experiments with model compounds. The chromium content does not change significantly when compared with Figure 78.

Figure 79. Elemental profile of the layer shown Figure 77 (b). (a) Image of layer with the line of EDS scanning; (b) Results of EDS analysis.

Figure 80 shows the TEM image for the layer formed on the CS specimen after pretreatment at 343°C. Consistent with the layer on 5Cr steel, there is a thick inner layer (3.7 µm), but the outer layer is delaminated. When challenged this layer was not protective against naphthenic acid corrosion, which could be explained by cracks found in the inner layer.
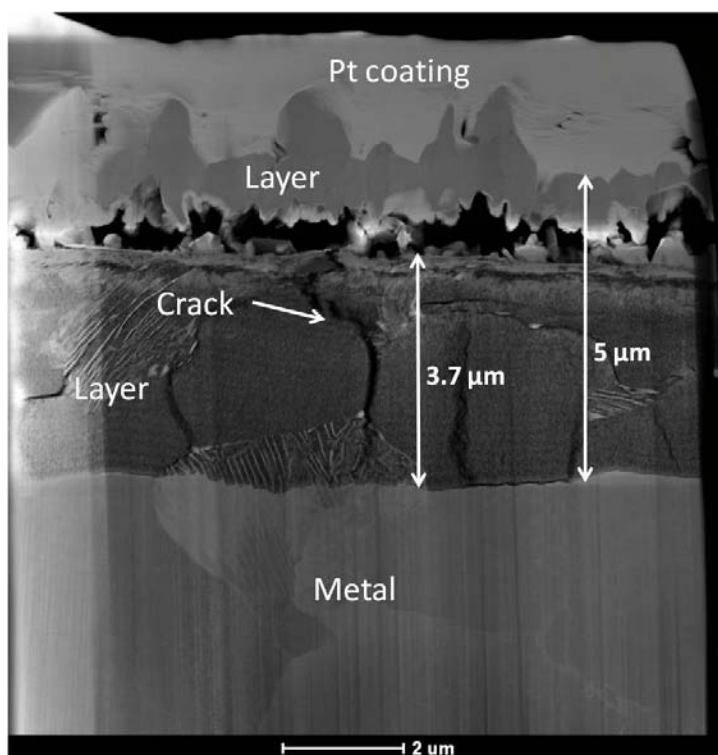
Figure 80. TEM images of CS specimen pretreated with Fraction B (TAN < 0.1, S% = 1.92%) at 343°C for 24 hours. For corrosion rates see Figure 72.

Results of EDS analysis of selected areas are shown in Figure 81. As seen before, the outer layer is composed of iron sulfide. In the inner layer, there is a stoichiometric amount of iron and sulfur while oxygen is a minor component of less than 10%. This is

consistent with the elemental profile of inner layer on 5Cr steel surface shown in Figure 77.

A	
Element	Atomic%
S	43.08
Fe	56.91

B	
Element	Atomic%
O	10.85
S	43.13
Fe	46.01
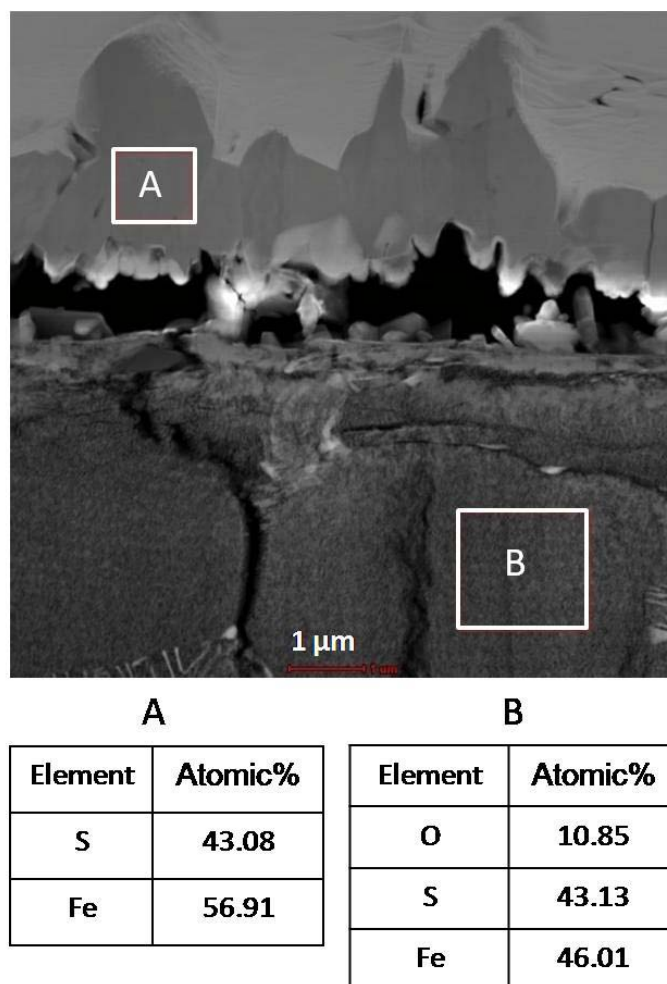
Figure 81. EDS analysis of the selected areas of the layer formed in Fraction B at 343°C for 24 hours.

9.4.2 Specimens Pretreated in Fraction L (TAN = 1.06, S% = 4.29%)

Fraction L is the only 650+ fraction in the list for FIB – TEM analysis. As a medium-TAN and high-sulfur crude fraction, it is one of the few fractions that formed

protective layers on the surface of CS (Figure 82). TEM analysis of the layer should provide information on the characteristics of the protective layer.
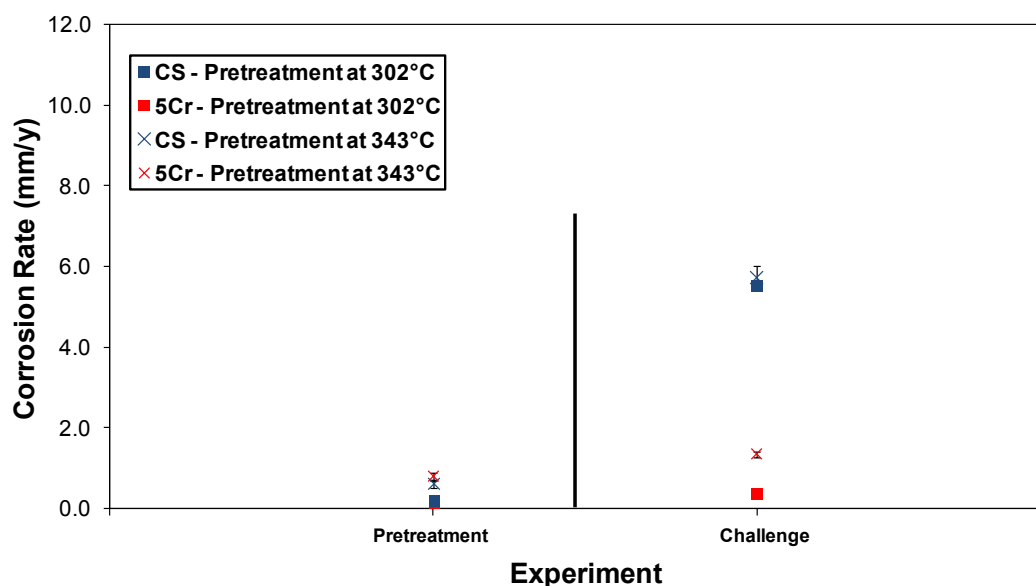

Figure 82. Summary of the pretreatment and challenge corrosion rates for CS and 5Cr steel specimens pretreated in Fraction L. For the pretreatment in the stirred autoclave, the pretreatment duration was 24 hours and the temperature was 316°C. For the challenge in the HVR, the time of exposure was 24 hours, the temperature was 343°C, and the peripheral velocity was 8.56 m/s.

TEM image of layer in Figure 83 shows delaminated layers. The homogeneous outer layer is iron sulfide (see the Appendix A for EDS results). The inner layer is more interesting given that the boundary between this layer and the steel substrate is not clear.
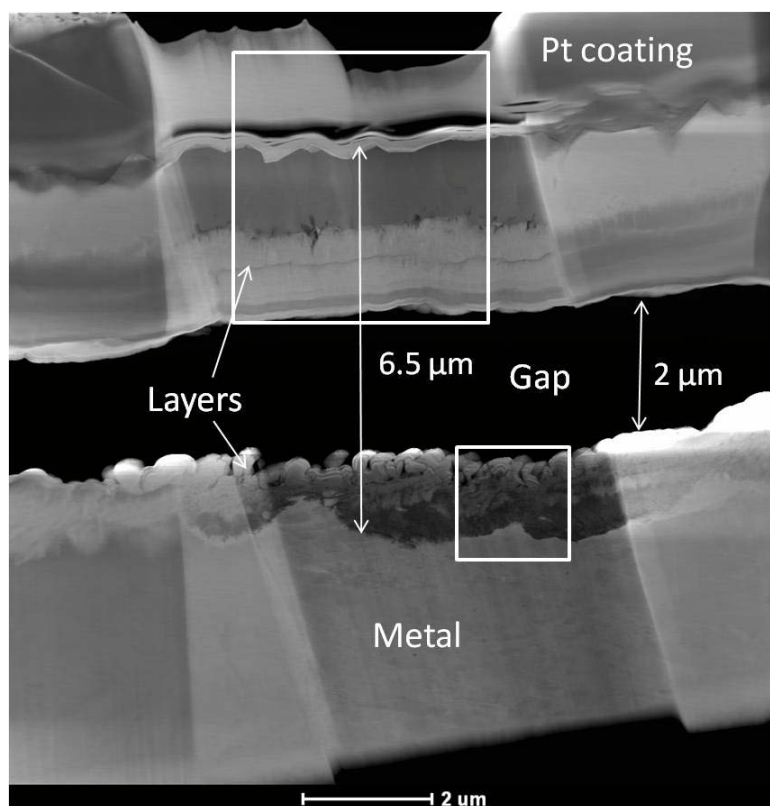
Figure 83. TEM images of CS specimen pretreated with Fraction L (TAN = 1.06, S% = 4.29%) at 316°C for 24 hours. For corrosion rates see Figure 82.

EDS analysis on the inner layer is shown in Figure 84. Compared with the steel substrate, both sulfur and oxygen contents increase from 0 to 20%. It should be noted that the oxygen content increases gradually while the sulfur seems to have been present in the bands. Also, the oxygen content for Fraction L with TAN 1.06 is almost double when compared to that seen when using Fraction B with TAN < 0.1.

(a)   (b)
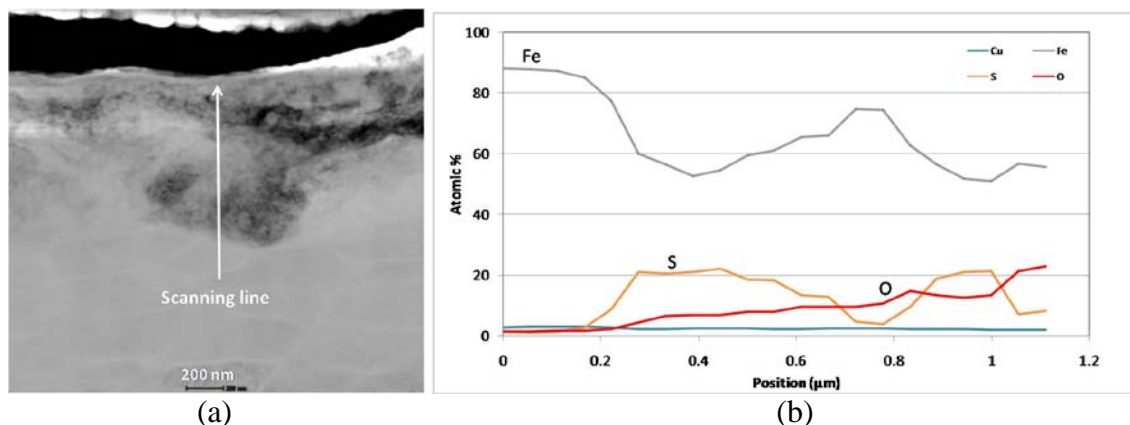
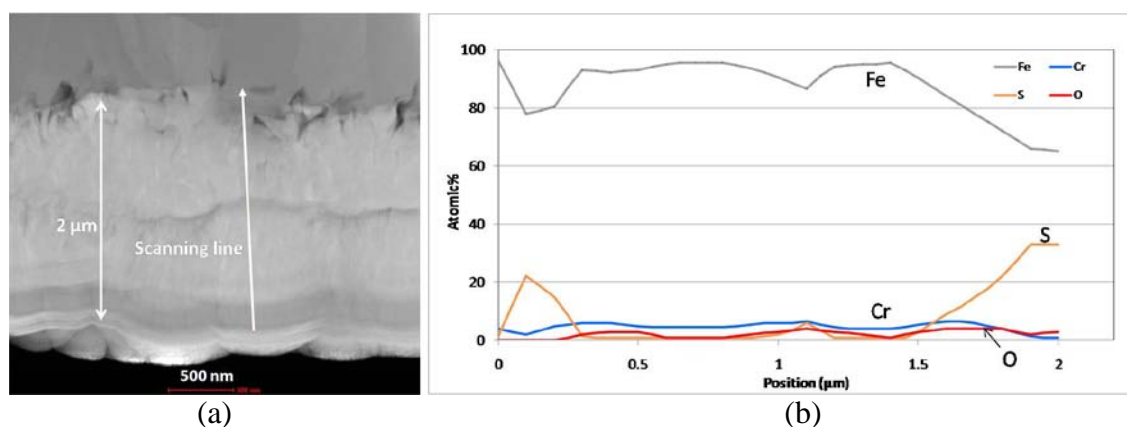Figure 84. Elemental profile of the inner layer of the layer shown in the square of Figure 83. (a) Enlarged image of inner layer with the line of EDS scanning; (b) Results of EDS analysis.

9.4.3 Specimens Pretreated in Fraction A (TAN = 1.75, S% = 0.53%)

Fraction A is another fraction with a medium content of naphthenic acids and organosulfur compounds. More importantly, it is one of the few fractions forming a protective layer on the surface of CS specimens, as shown in Figure 85. Additionally, the challenge corrosion rate for 5Cr steel is even lower than the pretreatment corrosion rate. TEM analysis of the layers formed on both of the CS and 5Cr specimens should provide valuable information on the properties of layer.
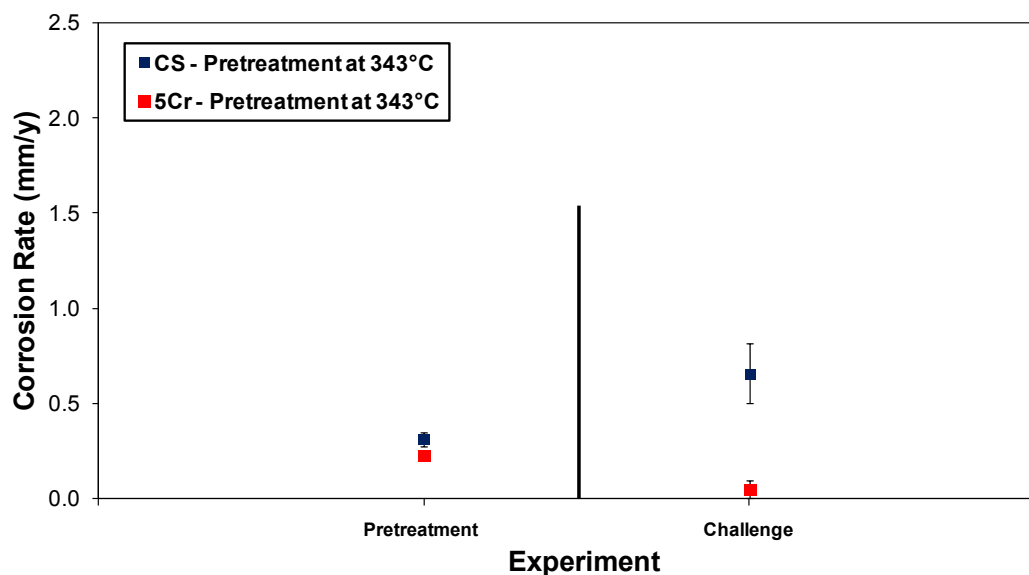
Figure 85. Summary of pretreatment and challenge corrosion rates for CS and 5Cr steel specimens pretreated in Fraction A. For the pretreatment in the stirred autoclave, the pretreatment duration was 24 hours and the temperature was 343°C. For the challenge in the HVR, the time of exposure was 24 hours, the temperature was 343°C, and the peripheral velocity was 8.56 m/s.

Firstly, the layer on the CS specimen was analyzed by TEM (Figure 86). The layer is thinner than that formed in fractions with higher amount of organosulfur compounds (Fraction B, for instance). Moreover, three delaminated layers appear.

Figure 86. TEM images of CS specimen pretreated with Fraction A (TAN = 1.75, S% = 0.53%) at 343°C for 24 hours. For corrosion rates see Figure 85.

The results of the EDS analysis of selected layer areas are shown in Figure 87. The iron sulfide layer is present in the two layers (A and B). The intermediate layer B, even if it is delaminated from the inner layer, was composed of 21% oxygen. For the inner layer, the oxygen content is over 40% and sulfur decreases to a minimum level. This clearly suggests that the protectiveness against naphthenic acid corrosion was attributed to the inner oxide layer.
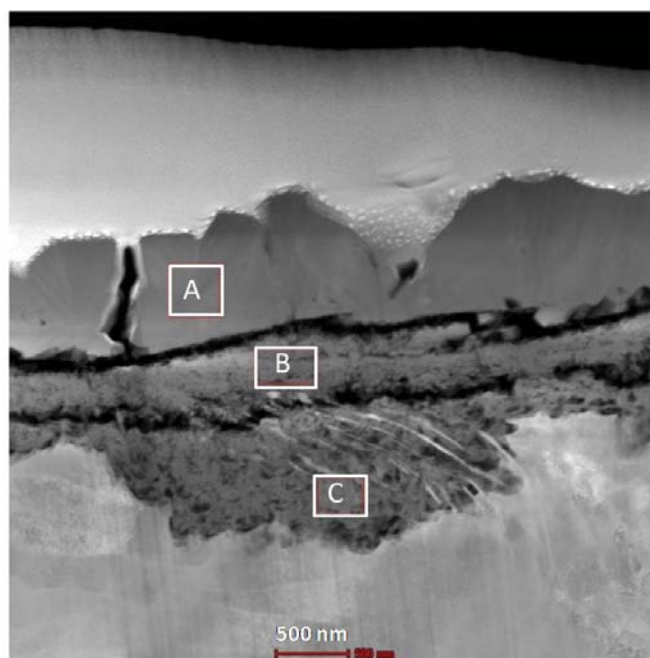
A			B			C		
Element	Atomic%		Element	Atomic%		Element	Atomic%	
S	48.11		O	21.34		O	43.54	
Fe	51.88		S	23.56		S	8.39	
			Fe	39.70		Fe	41.45	

Figure 87. EDS analysis on selected areas of the layer formed in Fraction A at 343°C for 24 hours shown in the square of Figure 86.

For 5Cr steel, the comparison of the layer morphology before and after the challenge is shown in Figure 88. In both cases, the layer is without delaminations, but the protective layer is thinner following the challenge under the combined effect of the naphthenic acid attack and high velocity.
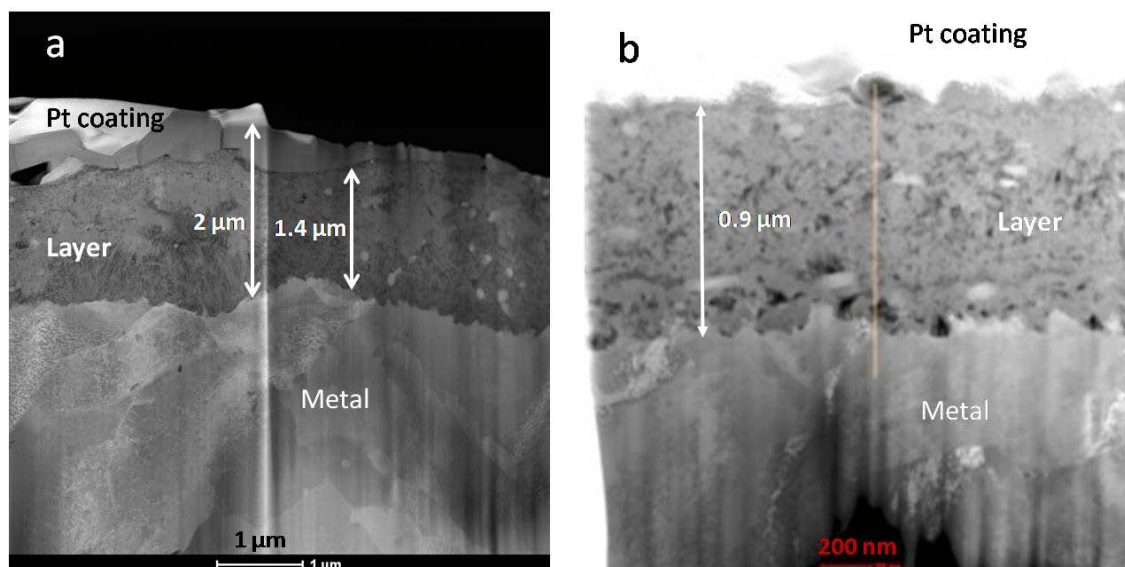
Figure 88. TEM images of 5Cr steel specimen: (a) after the pretreatment with Fraction A at 343°C for 24 hours; (b) after the challenge with the naphthenic acid solution (TAN 3.5) at 343°C for 24 hours. For corrosion rates see Figure 85.

The elemental profile of the layer formed after pretreatment is shown in Figure 89. The outer iron sulfide layer covers the inner oxide layer. Contrary to the elemental profile of the inner layer on the CS specimen shown in Figure 87, the oxygen content in the area contiguous to the iron sulfide layer is the highest. This area is depleted of sulfur. It seems that the oxide layer is composed of two areas – one of iron oxide and one of iron oxide/iron sulfide mixture.

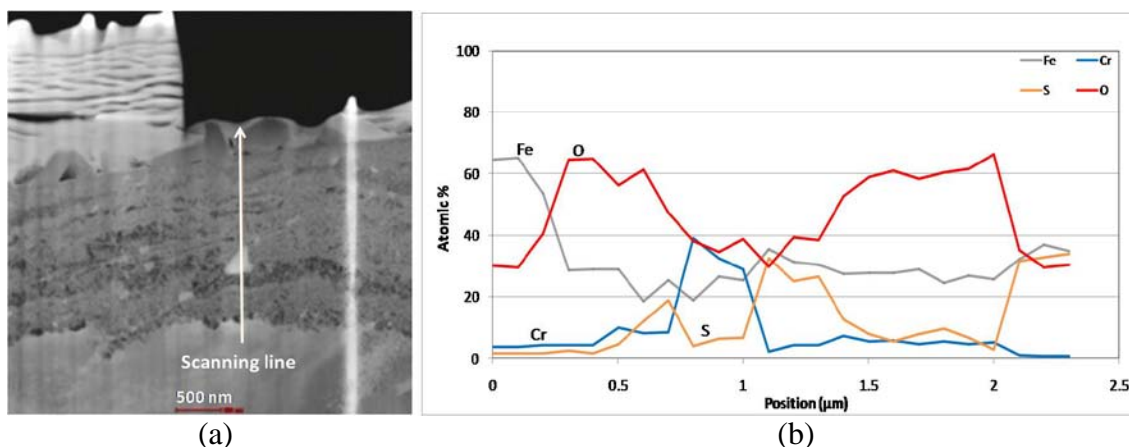(a)   (b)
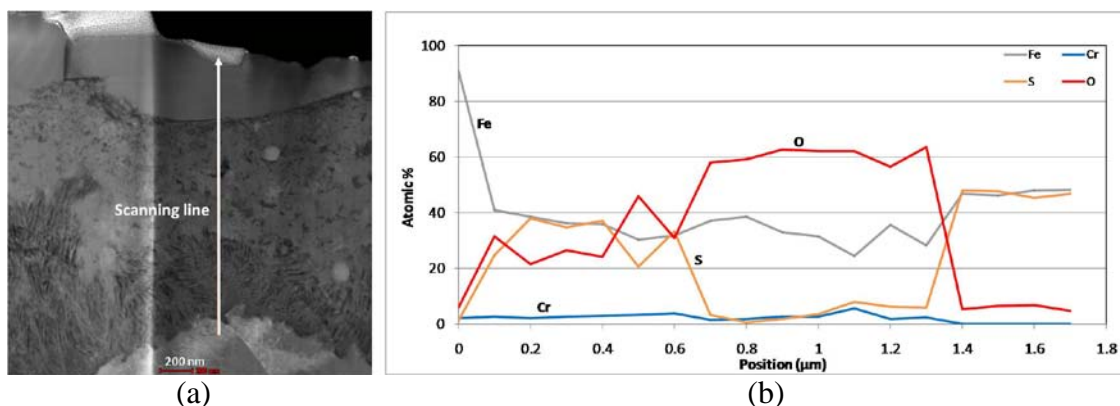
Figure 89. Elemental profile of the layer presented in Figure 88 (a). (a) Image of layer with the line of EDS scanning; (b) Results of EDS analysis.

After the challenge with naphthenic acids, the chemical composition of the inner layer changed significantly (Figure 90). The oxygen content is highest in the region adjacent to the steel-layer boundary and the sulfur and chromium are depleted in the same region. In the region below the diminished outer iron sulfide layer, the oxygen content decreases and the sulfur content increases. The oxygen and sulfur profiles are quite similar to the elemental profile of the inner layer formed after the pretreatment with the "DDS only" solution and the challenge with naphthenic acids (Figure 59). This reinforces the postulation that naphthenic acids were involved in the formation of the protective oxide layer.
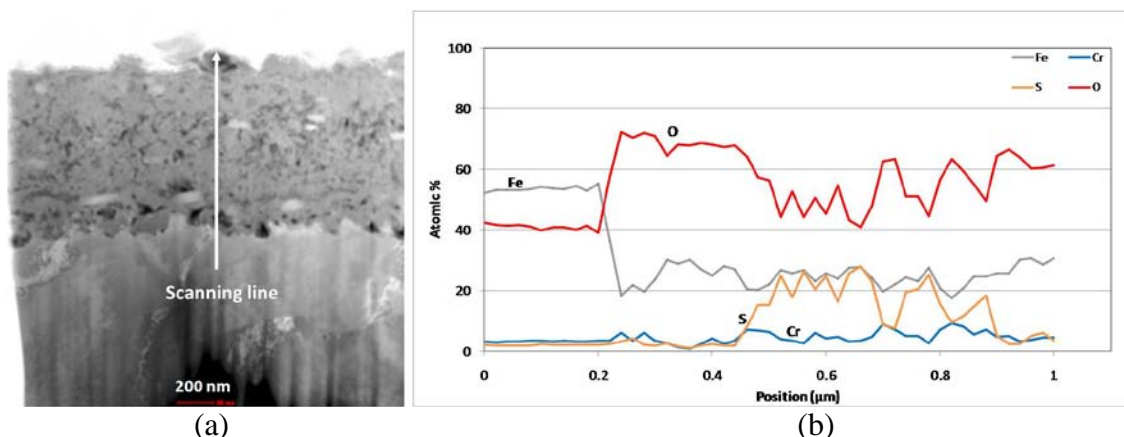
Figure 90. Elemental profile of the layer presented in Figure 88 (b). (a) Image of layer with the line of EDS scanning; (b) Results of EDS analysis.

9.4.4 Specimens Pretreated in Fraction O (TAN = 4.9, S% = 0.11%)

As a high-TAN and low-sulfur crude fraction, Fraction O shows low pretreatment corrosion rates for both the CS and 5Cr steel (Figure 91). However, properties of layers formed on different types of steel were differentiated during the challenge. Although the challenge solution (TAN 3.5) is less acidic than Fraction O, the challenge corrosion rate for CS is much higher than its pretreatment corrosion rate. On the contrary, the layer formed on 5Cr steel specimen is quite protective in both the pretreatment and the challenge. TEM analysis of both layers was conducted.
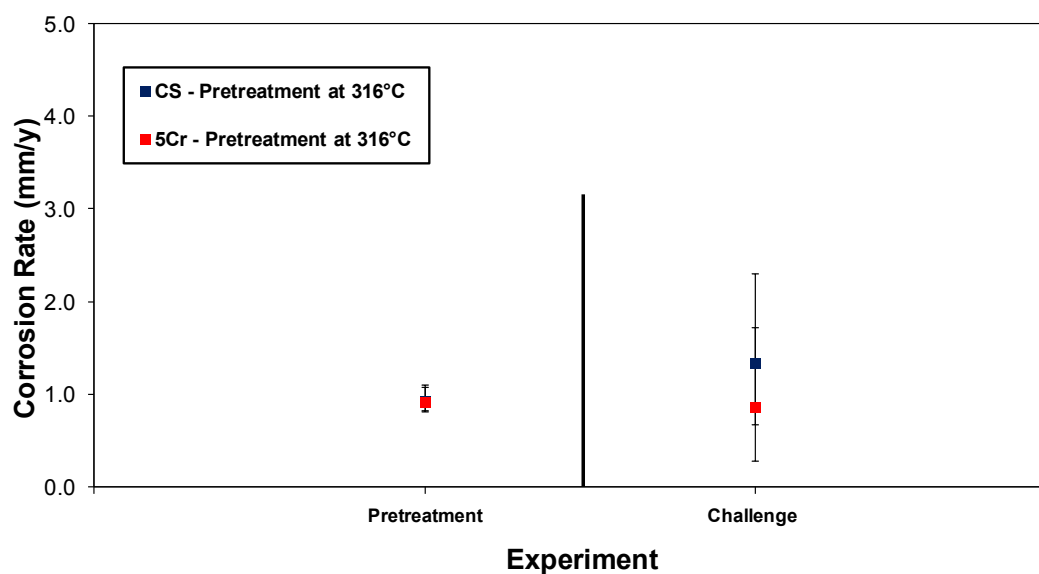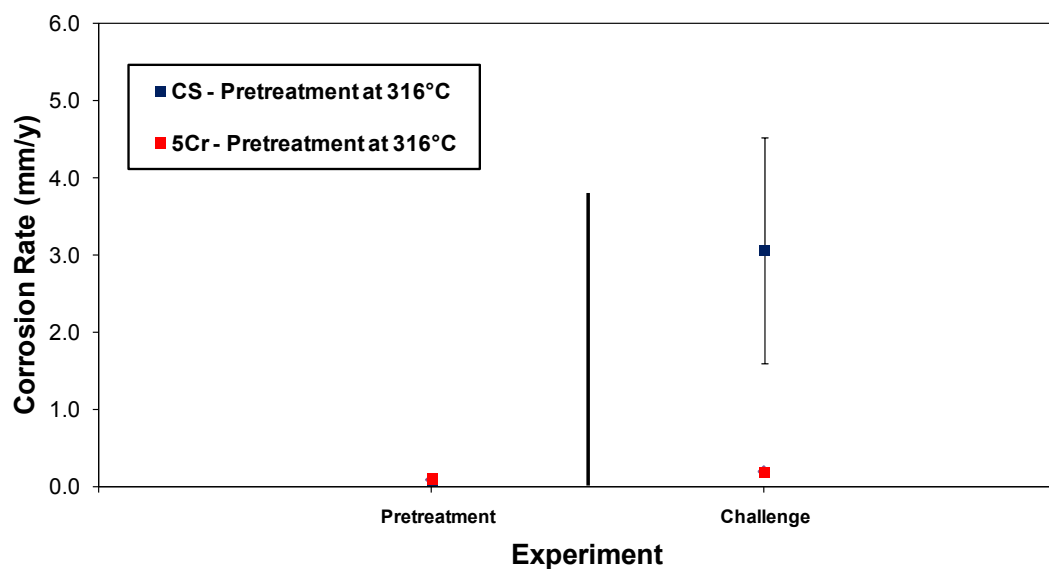
Figure 91. Summary of pretreatment and challenge corrosion rates for CS and 5Cr steel specimens pretreated in Fraction O. For the pretreatment in the stirred autoclave, the pretreatment duration was 24 hours and the temperature was 316°C. For the challenge in the HVR, the time of exposure was 24 hours, the temperature was 343°C, and the peripheral velocity was 8.56 m/s.

After pretreatment with Fraction O, a thin layer formed on the CS specimen

(Figure 92). It seems that a blurred boundary divides the unprotective layer into two
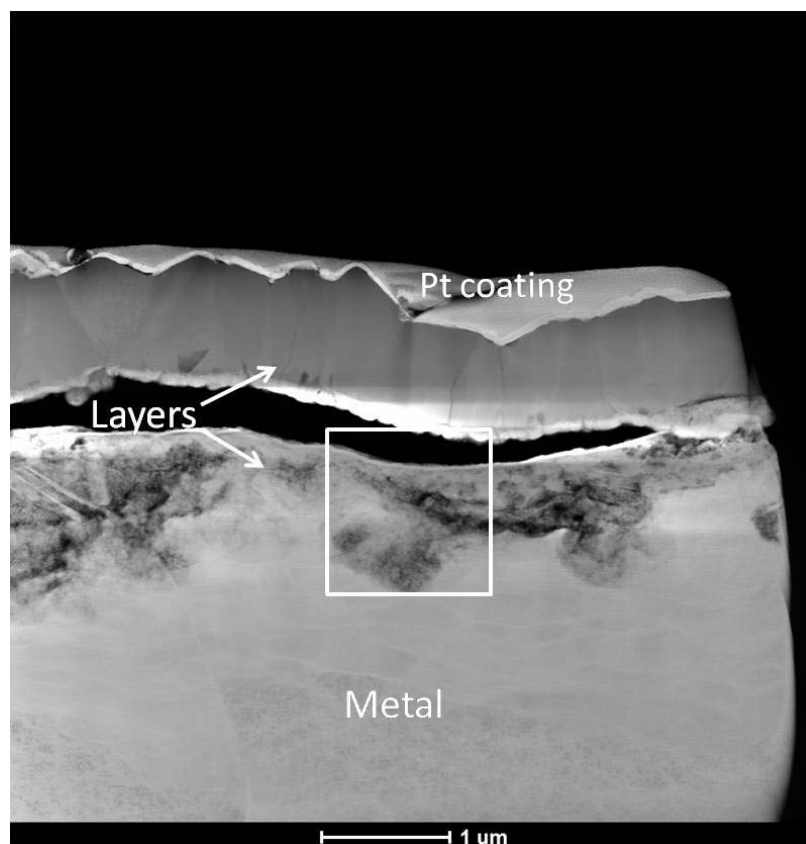
layers and the total layer thickness is around 0.35 µm.
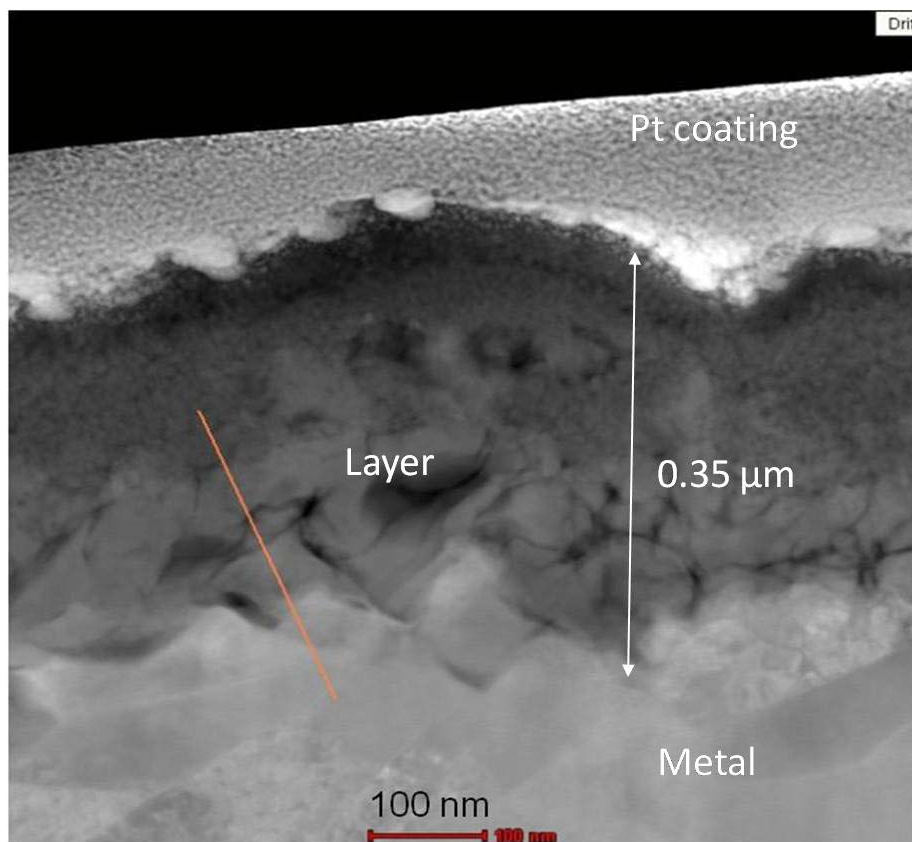
Figure 92. TEM images of CS specimen pretreated with Fraction O (TAN = 4.9, S% = 0.11%) at 316°C for 24 hours. For corrosion rates see Figure 91.

The EDS analysis of the layer clearly suggests that there are two layers with different chemical compositions (Figure 93). The inner layer is composed of iron oxide without sulfur. In the outer layer, the oxygen content decreases to the level in the steel substrate and the sulfur content rises to be of nearly equal moles with iron. The appearance of zinc in the outer layer is interesting and it may be attributed to the zinc compounds in the crude. It is clearly shown that the iron sulfide layer covers the iron oxide layer despite the low sulfur content in the crude.

(a)   (b)
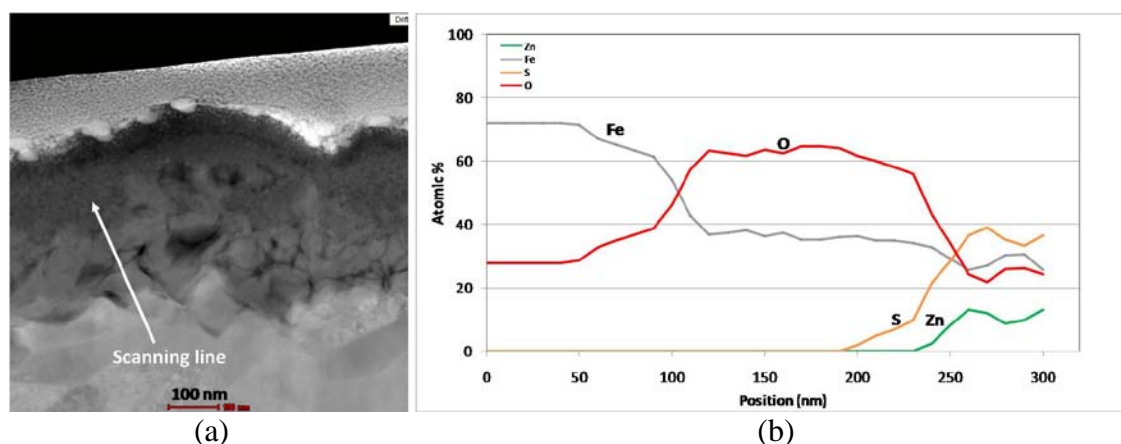
Figure 93. Elemental profile of the layer presented in Figure 92. (a) Image of layer with the line of EDS scanning; (b) Results of EDS analysis.

The layer formed on 5Cr steel, which is more protective against naphthenic acid corrosion, looks quite different from the layer formed on CS (Figure 94). Two distinct layers form boundaries: (1) between the steel substrate and the inner layer and (2) between the inner and outer layer. The inner layer thickness is around 250 nm which is close to the thickness of the layer formed in the "NAP only" solution shown in Figure 69.
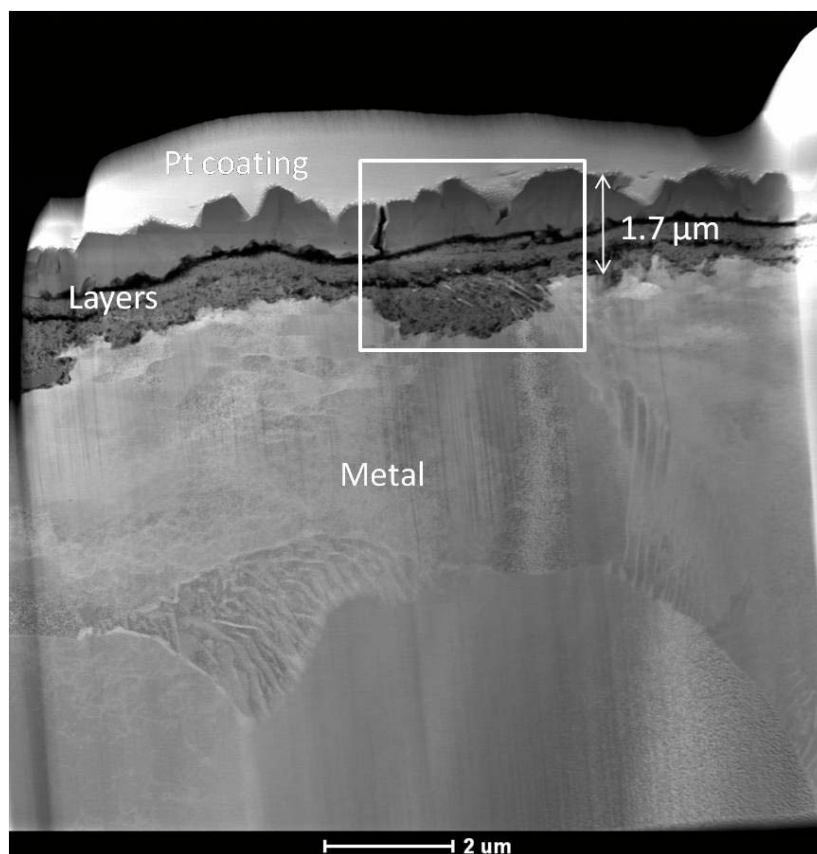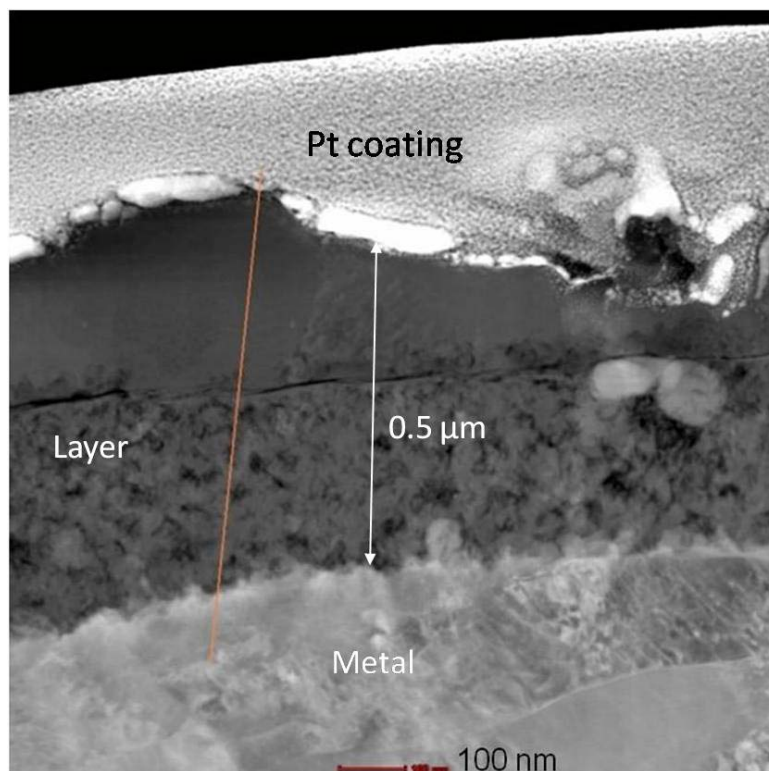
Figure 94. TEM images of 5Cr steel specimen pretreated with Fraction O (TAN = 4.9, S% = 0.11%) at 316°C for 24 hours. For corrosion rates see Figure 91.

The results of the EDS analysis shown in Figure 95 are consistent with the layer morphology shown in Figure 94. The outer iron sulfide layer covers the inner oxide layer. The chemical composition of inner layer of the 5Cr steel is similar to that of the CS. The only major difference is in the chromium content. Chromium may determine the layer protectiveness, although its concentration is only 5 percent in the inner layer.

(a)   (b)
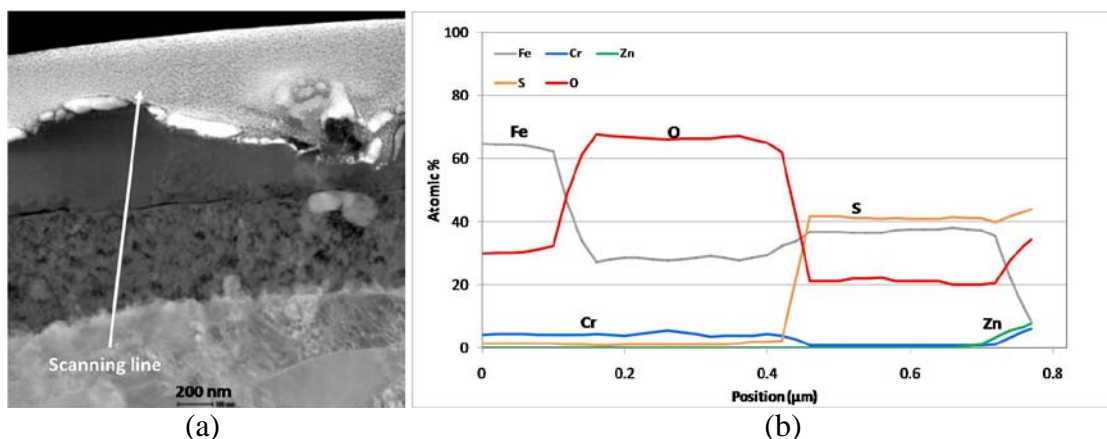
Figure 95. Elemental profile of the layer presented in Figure 94. (a) Image of the layer with the line of EDS scanning; (b) Results of EDS analysis.

9.4.5 Summary of the TEM Analysis on Specimens Pretreated in Real Crude Fractions

Generally, there were both naphthenic acids and organosulfur compounds in real crude fractions. Experiments with real crude fractions offered a unique opportunity to examine the layer formed in various fractions with different concentrations of naphthenic acids and organosulfur compounds. Similarities could be found among layers formed in these systems.

1) The layer was always composed of an outer iron sulfide layer and an inner oxide layer(s);

2) Generally, the sulfur content in the inner layer increased with the sulfur content in the crude;

3) After the challenge with naphthenic acid, the oxygen content in the inner layer increased.

4) Generally, layer formed on 5Cr steel was more protective and chromium

concentrated in the inner layer.

9.5 Summary of FIB-TEM Analysis Results

The difference among the protective properties of layers should correlate with its

chemical composition. Given the amount of data generated in the EDS analysis, it would

be tempting to compare the challenge corrosion rates against the elemental concentrations

in the layer.

Figure 96 compares the challenge corrosion rate for each layer against its oxygen

content of the inner layer regardless of the source of pretreatment fluid and pretreatment

temperature. For CS, there is a clear trend that the higher oxygen content of the inner

layer promotes a more protective layer. For 5Cr steel, a similar trend was found. For both

types of steel, the challenge corrosion rates are close to their pure TAN 3.5 corrosion

rates when the oxygen content is the lowest. With a higher amount of oxygen, the

challenge corrosion rates become lower indicating more protective layers. When the

oxygen content is higher than 30%, challenge corrosion rates for both types of steel

decrease to less than 1 mm/y.
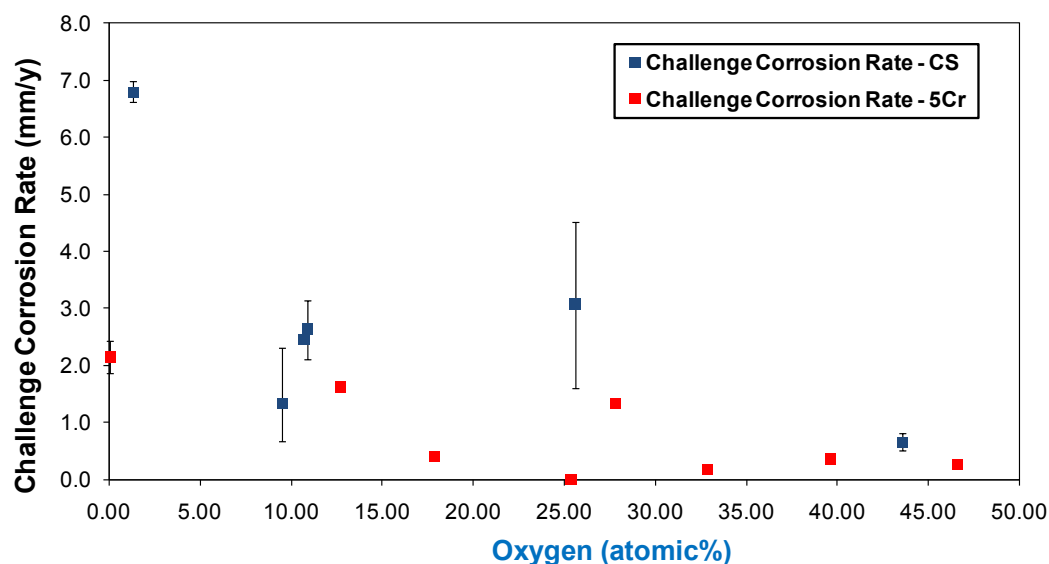
Figure 96. Comparison of layer protectiveness (challenge corrosion rates) against its oxygen content of the inner layer. Layers formed in model compounds and real crude fractions are not differentiated.

The (lack of a) relationship between layer protectiveness and sulfur content of the inner layer is shown in Figure 97. Contrary to the conventional theory of layer protection, which claims that iron sulfide is the protective component in the layer, Figure 97 suggests that sulfur concentration correlates to challenge corrosion rates negatively. There is a trend indicating that higher sulfur content results in a less protective layer, especially for 5Cr steel. When the sulfur content is over 35%, the layer formed on either CS or 5Cr steel cannot resist corrosion by naphthenic acids.
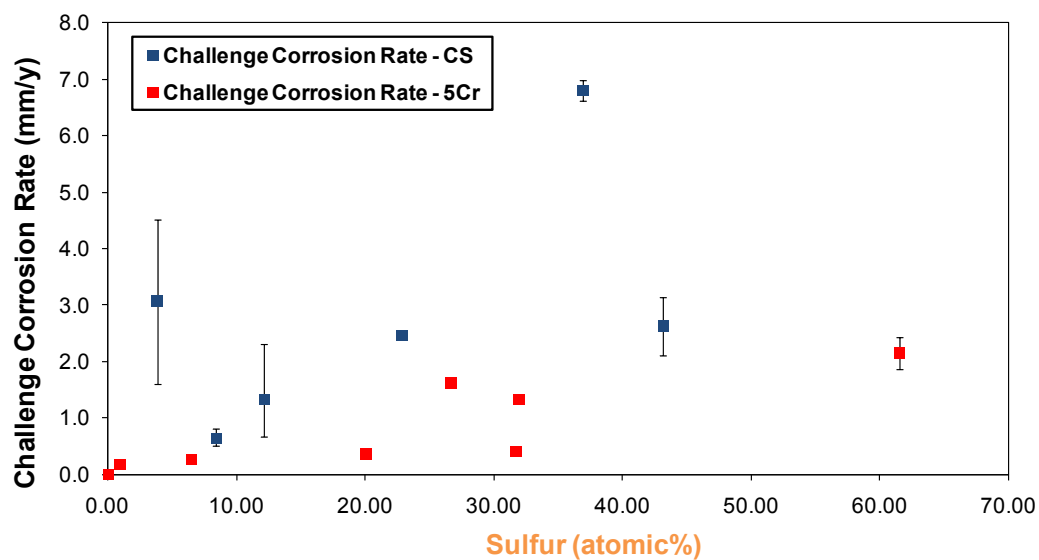
Figure 97. Comparison of layer protectiveness (challenge corrosion rates) against its sulfur content of the inner layer. Layers formed in model compounds and real crude fractions are not differentiated.

CHAPTER 10: MECHANISM OF IRON OXIDE LAYER FORMATION

10.1 Composition of Iron Oxide Layer

The positive correlation between the formation of an iron oxide layer and the layer protectiveness against naphthenic acid corrosion was well established in previous chapters. The next challenge will be to find the chemical composition of the oxide layer and the formation mechanism.

Electron diffraction, including CBED (Convergent Beam Electron Diffraction) and SAD (Selected Area Diffraction), and XRD could provide valuable information on crystal structure. Combining with results of EDS analysis, the chemical component of oxide layer could be revealed.

For example, the results of CBED analysis are shown in Figure 98 for the layer formed in the "NAP only" solution (see Figure 69 (a) for the TEM image). The diffraction pattern clearly indicates that the oxide layer is composed of magnetite. Given that XRD analysis shows consistent results with the electron diffraction analysis, only the results of XRD analysis are summarized in Table 12 (see Appendix A for XRD, CBED, and SAD patterns). The presence of magnetite was confirmed in the layer formed in both model compounds and real crude fractions.
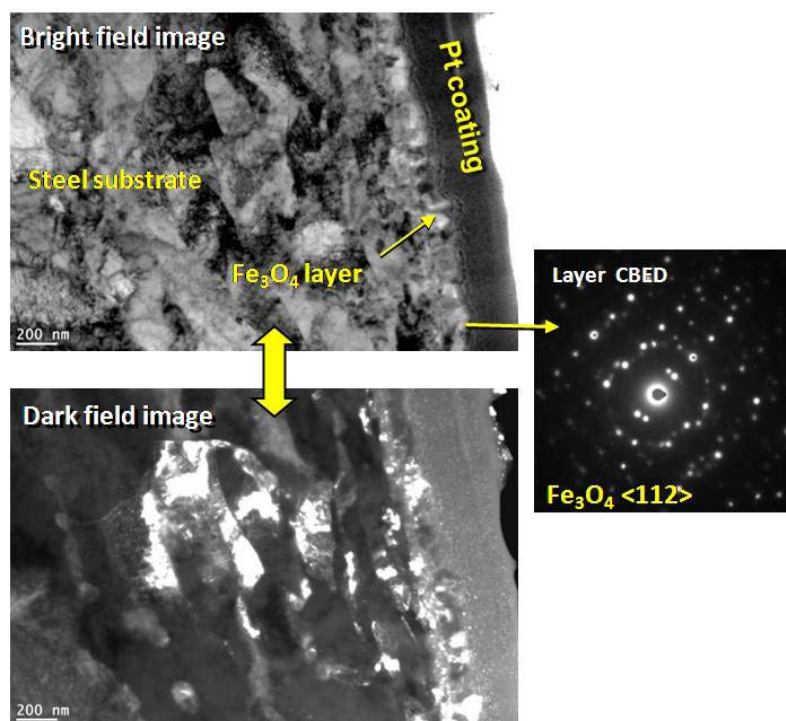
Figure 98. TEM images and CBED pattern of layer formed in the "NAP only" solution at 316°C for 5Cr steel specimen (images taken and analyzed by Fang Cao, ExxonMobil Research and Engineering Company). For corrosion rates see Figure 68.

Table 12.

Results of XRD Analysis on Layers Formed in Various Fluids

Steel	Feed	TAN	S%	Temp °C	Time hr	Bulk XRD	TAN	Temp °C	Time hr	Bulk XRD
				Pretreatment				**Challenge**		
CS	Fraction L	1.06	4.29	316	24	Fe, FeS(T), Fe$_3$O$_4$	3.5	343	24	
CS	Fraction O	4.9	0.11	316	24	Fe, Fe$_3$O$_4$	3.5	343	24	
5Cr	Fraction O	4.9	0.11	316	24	Fe, Fe$_3$O$_4$, FeS(T)	3.5	343	24	
5Cr	DDS only Solution	0	0.25	343	24	FeS(T), Fe	3.5	343	24	FeS(T), Fe, Fe$_3$O$_4$
5Cr	DDS + NAP Solution	1.75	0.25	343	24	FeS(T), Fe	3.5	343	24	FeS(T), Fe, Fe$_3$O$_4$
5Cr	Fraction A	1.75	0.53	343	24	Fe, FeS(T), Fe$_3$O$_4$	3.5	343	24	Fe, Fe$_3$O$_4$, FeS(T)
5Cr	NAP only Solution	1.75	0	316	24	Fe, Fe$_3$O$_4$	3.5	343	24	Fe, Fe$_3$O$_4$
5Cr	Fraction B	<0.1	1.92	343	24	FeS(T), Fe, Fe$_3$O$_4$	3.5	343	24	Fe, FeS(T), Fe$_3$O$_4$

Notes: FeS(T): troilite; Fe$_3$O$_4$: magnetite. Results compiled by Fang Cao, ExxonMobil Research and Engineering Company.

10.2 Mechanism of Iron Naphthenate Decomposition

The next target will be to investigate the mechanism of forming magnetite. The formation of magnetite during naphthenic acid corrosion was reported in the literature. Kamel, *et al*., noted that magnetite was revealed by XRD analysis on steel samples corroded by crude fractions in the stirred autoclave.[54] However, it was postulated that the oxide layer existed in the outermost layer and resulted from sample oxidation after the experiment. Smart, *et al*., found the existence of magnetite and minor amounts of hematite and pyrrhotite on the carbon steel surface after experimentation with a high-TAN crude.[55] The layer of magnetite was suspected to be protective, but the role of naphthenic acids in the formation of iron oxide layer was not indicated. Magnetite was also found after experimentation with a model sulfur compound (dimethyl disulfide) and naphthenic acids.[56] Again, the appearance of magnetite was considered as the result of contamination and oxidation.

However, analytical results shown in previous chapters clearly indicated that naphthenic acids were closely related to the formation of oxide layer. It was widely accepted that oil-soluble iron naphthenate was formed during naphthenic acid corrosion ($Fe + 2RCOOH \rightarrow Fe(RCOO)_2 + H_2$), but magnetite was not considered as a product of corrosion. However, the decomposition of iron naphthenate at 200 to 800°C was reported in 1976 and magnetite was one of products.[57] With a similar structure as iron naphthenate, ferric carboxylate dissolved in aliphatic hydrocarbons decomposed at 245°C and magnetite could be the only product.[58] Moreover, decomposition of ferrous acetate was widely used in the preparation of nano-scale magnetite.[59] Investigation on the

reaction mechanism suggested that wüstite (FeO) was the initial product and would disproportionate to magnetite.[62] It is postulated that the following reactions explain the formation of the oxide layer during the process of NAP corrosion.

$$(RCOO)_2Fe \rightarrow FeO + CO_2 + RCOR \qquad\qquad Reaction\ 5$$

$$4FeO \rightarrow Fe_3O_4 + \alpha\text{-}Fe \qquad\qquad Reaction\ 6$$

To verify the hypothesis relating to the role iron naphthenates, the pretreatment-challenge experimentation involving the "NAP only" solution was repeated in two ways. In the first experiment, the pretreatment was repeated exactly with six ring specimens (three made of CS and three made of 5Cr steel) and six square specimens (three made of CS and three made of 5Cr steel) in the stirred autoclave. Ring specimens were challenged in the HVR while square specimens were saved for surface analysis. The second experiment followed the same procedure except that only two ring specimens and two square specimens, all of which were made of 5Cr steel, were pretreated in the stirred autoclave. According to the hypothesis, a less amount of iron oxide should be observed on specimens in the second experiment due to the lower concentration of iron naphthenates generated in the pretreatment.

Figure 99 summarizes the pretreatment and challenge corrosion rates for the repeating experiments. Given that the fluid in the stirred autoclave was not replenished, a fewer number of specimens lead to a higher pretreatment corrosion rate. However, layers formed in both pretreatments are protective, as shown by the challenge corrosion rates.

Note that the pretreatment corrosion rate in the second repeating experiment is even

higher than the challenge corrosion rate.
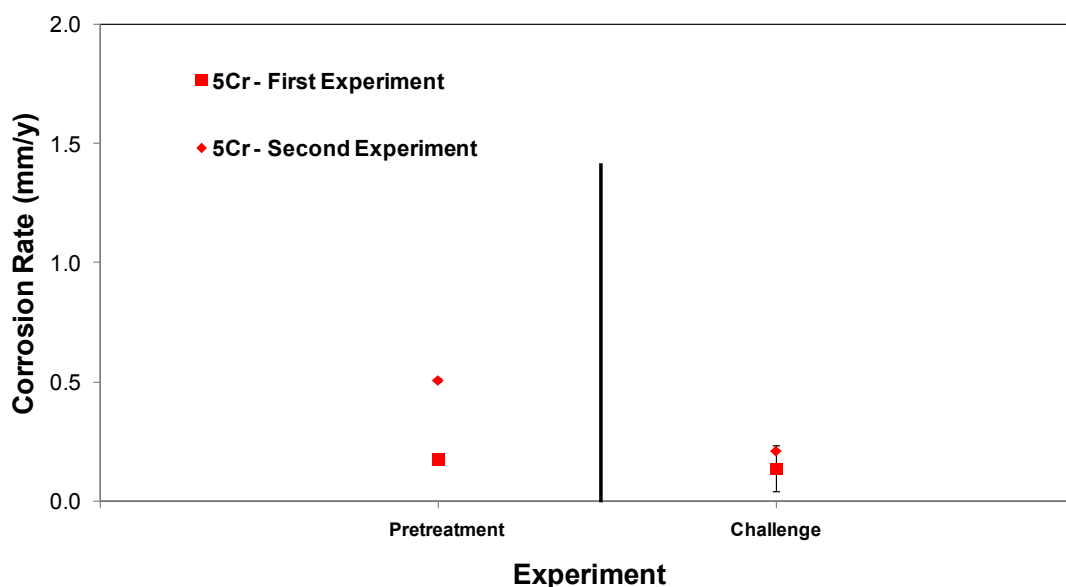
Figure 99. Summary of pretreatment and challenge corrosion rates for 5Cr steel specimens pretreated in the "NAP only" solution. For the pretreatment in the stirred autoclave, the pretreatment duration was 24 hours and the temperature was 316°C. For the challenge in the HVR, the time of exposure was 24 hours, the temperature was 343°C, and the peripheral velocity was 8.56 m/s.

The TEM image for the 5Cr specimen in the first experiment reveals the total

layer thickness of 0.5 μm (Figure 100). Interestingly, an attached inner layer of ~50 nm is

observed to follow the profile of the metal surface with compact crystal particles above it.

EDS analysis indicates that both the continuous layer and crystal particles are

composed of iron oxide (Figure 101), which is consistent with results shown in Figure 70.

Moreover, the oxygen is not evenly distributed. The oxygen content in the inner layer

could be as high as ~70% while it decreases to ~50% in the outer layer. Trace amount of

chromium and sulfur is observed only in the corrosion product above the inner layer which is composed of iron and oxygen exclusively. However, CBED analysis suggests that both the continuous layer and the crystal particles are composed of magnetite (Figure 102). It is the magnetite layer which is protecting the 5Cr steel.
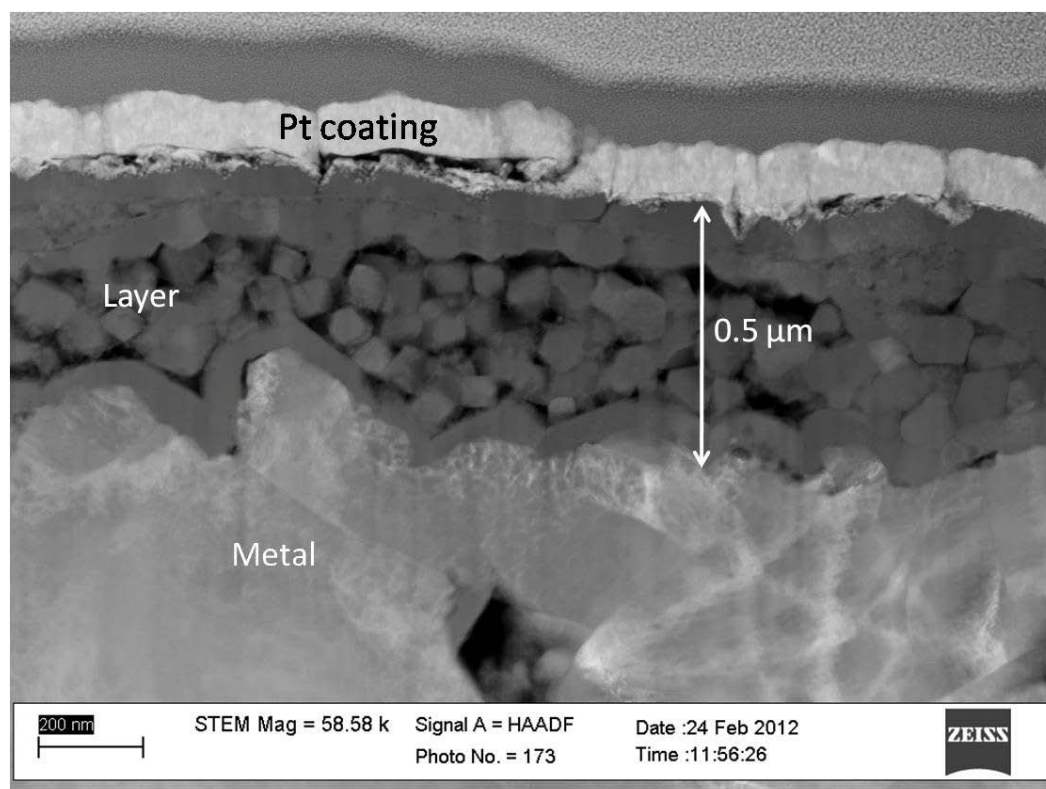
Figure 100. TEM images of 5Cr steel specimen pretreated with the "NAP only" solution at 316°C for 24 hours in the first repeating experiment. For corrosion rates see Figure 99.
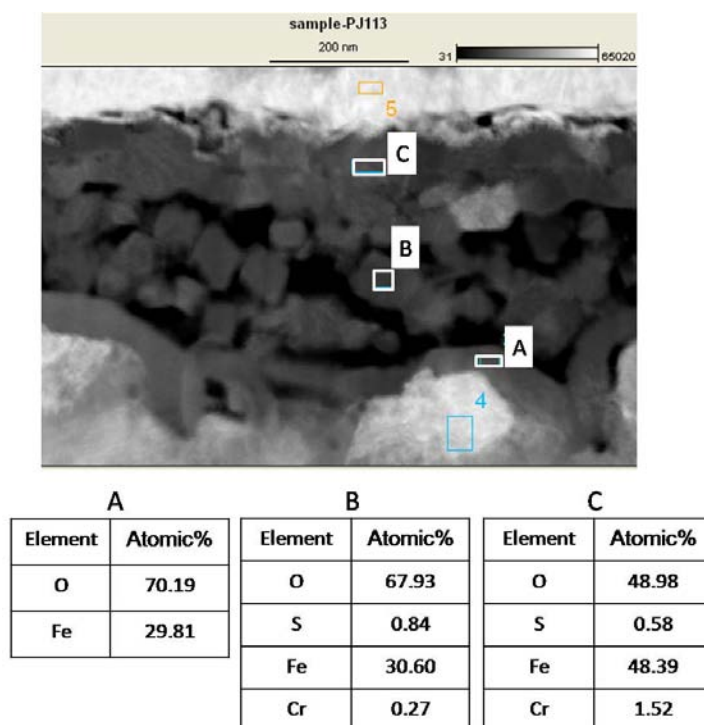
Figure 101. EDS analysis on selected areas of the layer shown in Figure 100.

A			B			C	
Element	Atomic%		Element	Atomic%		Element	Atomic%
O	70.19		O	67.93		O	48.98
Fe	29.81		S	0.84		S	0.58
			Fe	30.60		Fe	48.39
			Cr	0.27		Cr	1.52
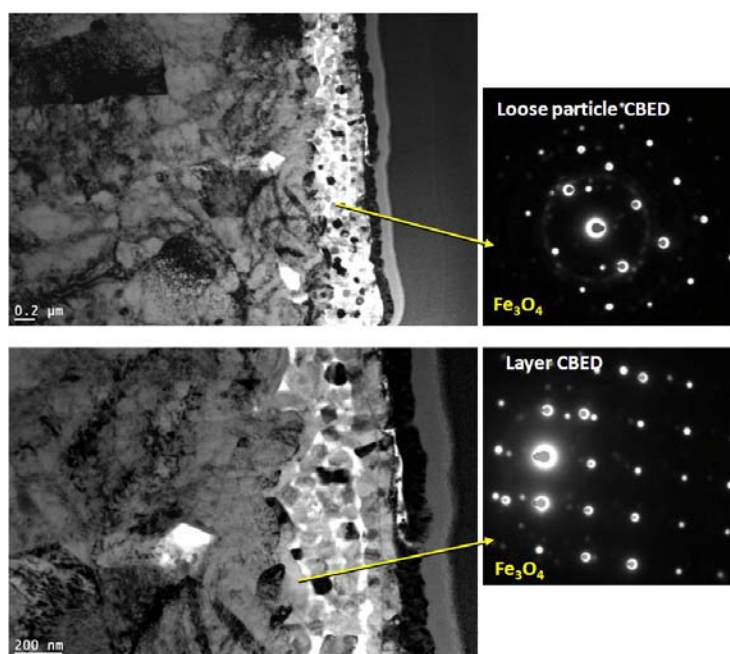
Figure 102. TEM images and CBED pattern of the continuous layer and the crystal particle shown in Figure 100 (images taken and analyzed by Fang Cao, ExxonMobil Research and Engineering Company).

In the second experiment, the zigzag profile of the metal surface suggests the initiation of pitting corrosion (Figure 103). Less amount of the corrosion product formed when there was less amount of metal in the stirred autoclave. This phenomenon may be due to the fact that less amount of iron naphthenate was released when there was less amount of metal available for corrosion by naphthenic acids. Nevertheless, a continuous layer (~50 nm) is observed again and it was also protective (and probably stopped the growth of pits), which is consistent with the finding in Figure 100.
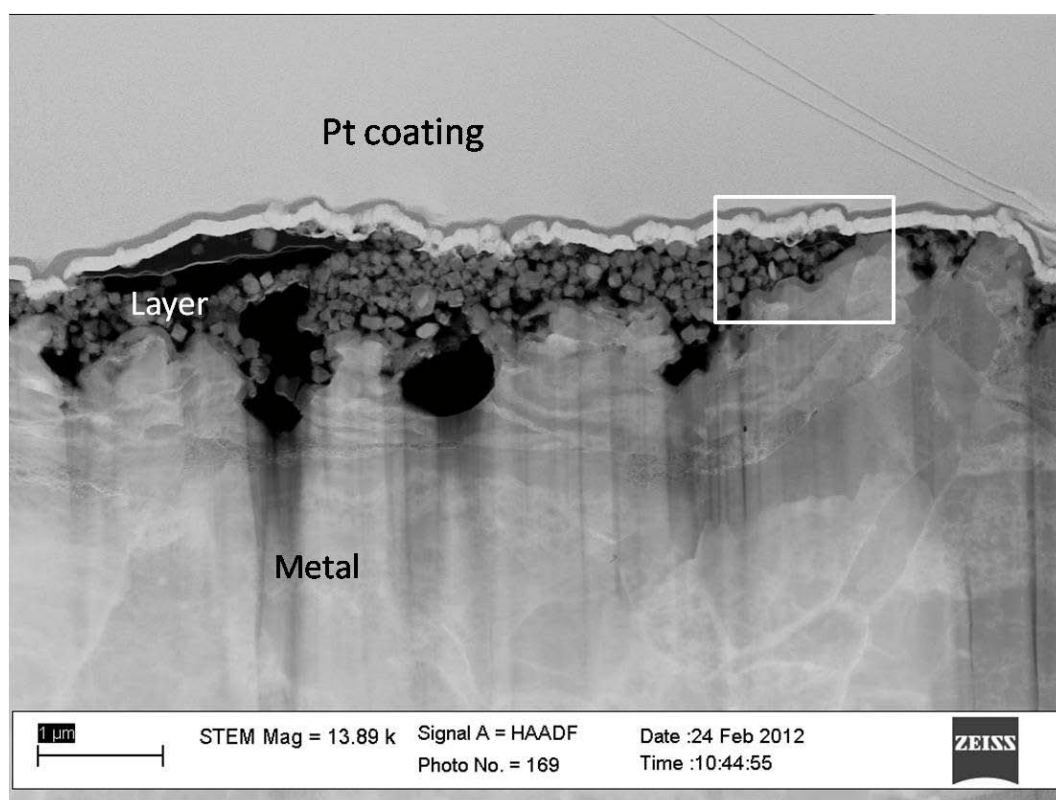
Figure 103. TEM images of 5Cr steel specimen pretreated with the "NAP only" solution at 316°C for 24 hours in the second repeating experiment. For corrosion rates see Figure 99.

Figure 104 reveals a consistent elemental profile as in Figure 101. The oxygen content in the inner layer is higher than that of crystal particles. Chromium is found only in the crystal particles rather than in the inner layer. Obviously, the low challenge corrosion rate should be attributed to the inner layer rather than the crystal particles. Again, it is implied that the protective properties of the surface layers are determined by the inner layer of iron oxide rather than the corrosion product above. CBED reveals the presence of magnetite in the corrosion product (Figure 105).

A	
Element	Atomic%
O	60.54
S	0.70
Fe	38.77

B	
Element	Atomic%
O	47.58
S	3.80
Fe	47.77
Cr	0.84
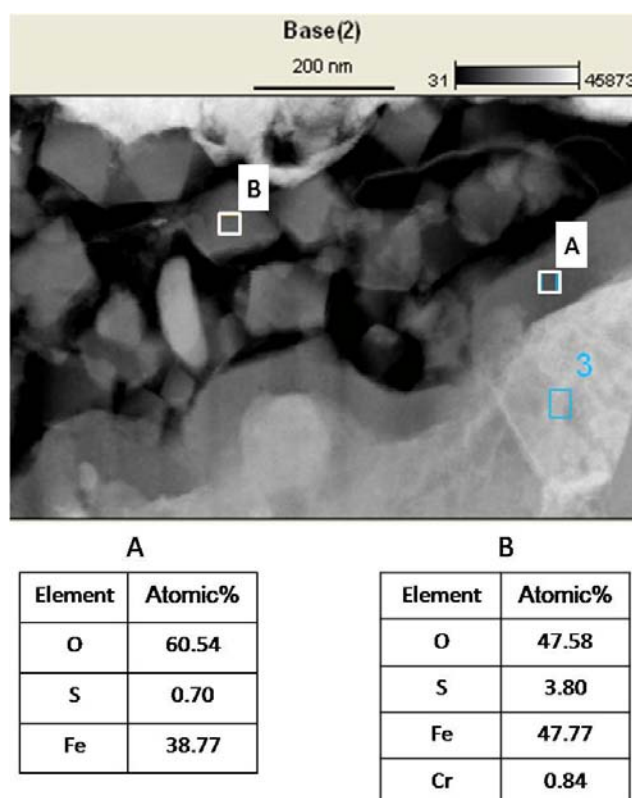
Figure 104. EDS analysis on selected areas of the layer shown in the rectangle of Figure 103.
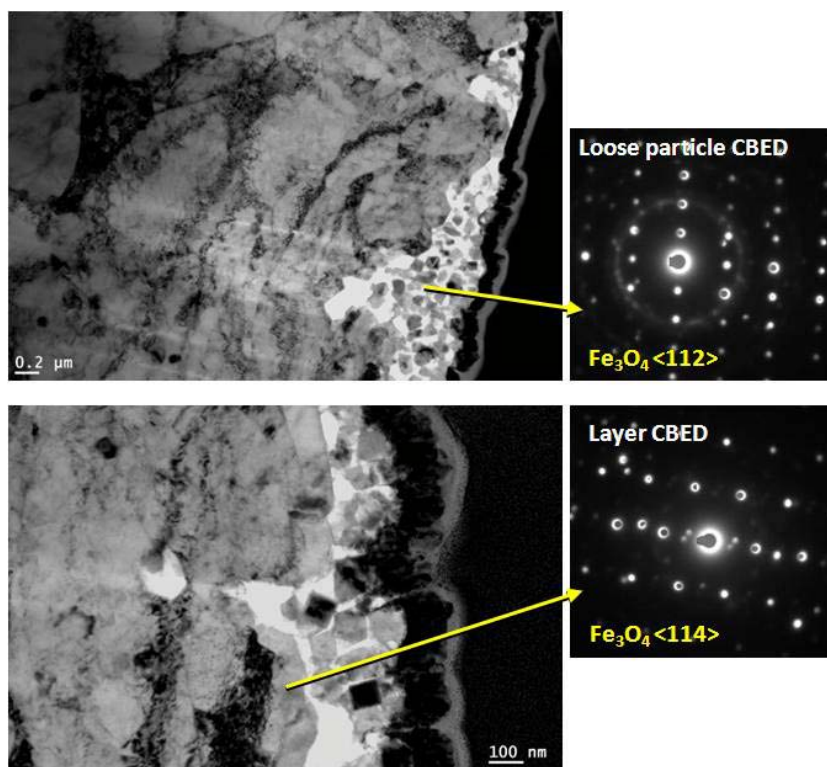
Figure 105. TEM images and CBED pattern of the continuous layer and the crystal particle shown in Figure 103 (images taken and analyzed by Fang Cao, ExxonMobil Research and Engineering Company).

Figure 104 and Figure 105 show that crystal particles of magnetite accumulate in cavities while they seem to be uniformly distributed on the metal surface illustrated in Figure 100. This phenomenon could be explained by the difference in concentrations of iron naphthenates which would decompose to form iron oxide. With a high concentration of iron naphthenates in the first experiment, the inner oxide layer was formed quickly and crystal particles of iron oxide deposited on the uniformly corroded metal surface. On the other hand, when the concentration of iron naphthenates was as low as in the second experiment, iron oxide could only crystallize in cavities where the concentration of iron

naphthenates was higher than the bulk fluid. These experiments reinforced the hypothesis that the iron oxide was formed due to the decomposition of iron naphthenates.

However, the role of chromium on the layer protectiveness is not very clear. Although layers formed on 5Cr steel specimens are more protective than those on CS specimens generally, the major component of inner layers is magnetite for both steels. It implies that the chromium, despite its low content, is the crucial factor to enhance the layer protectiveness. It may act as a "catalyst" to promote the formation of magnetite. By replacing some iron atoms in the magnetite, chromium may make the layer more chemically stable. These postulations are also supported by the pure TAN 3.5 corrosion rate of 5Cr steel (Figure 7) and the high contents of oxygen and chromium in the inner layer (Figure 11). But the mechanism is still ambiguous and deserves further investigation.

CHAPTER 11: CONCLUSION FOR EXPERIMENTAL WORK

The pretreatment-challenge experimentation procedure provided valuable information on the corrosivity of various model oil and real crude fractions and the protectiveness of surface layers which formed. By varying pretreatment and/or challenge conditions, factors affecting corrosion by naphthenic acid and sulfur compound could be investigated extensively. The following conclusions were reached:

1. Asphaltene was found to have a negligible effect on the high-temperature corrosion by crude oil. Pretreatment at different temperatures (316°C and 343°C) indicated that asphaltene could not influence the corrosivity of the crude. Furthermore, challenge with naphthenic acid solution showed that asphaltene was irrelevant to the protectiveness of layer.

2. An oxide layer was found beneath the iron sulfide layer via the FIB-TEM analysis on the surface layer. Electron diffraction and XRD analysis showed that the inner oxide layer was composed of magnetite.

3. Experimental results indicated that the inner oxide layer, rather than the outer iron sulfide layer, was closely related to the layer protectiveness against naphthenic acid corrosion. Higher content of oxygen in inner oxide layer promoted a more protective layer while the outer layer was always composed of iron sulfide and seemed to be irrelevant when it comes to protection. The most protective layer was formed in a model solution containing only naphthenic acids and no organosulfur compounds, which was consistent with formation of a protective iron/chromium oxide layer.

4. Experimental data suggest that the oxide layer was formed due to naphthenic acid corrosion. Iron naphthenate as the corrosion product was suspected to decompose and form the oxide layer.

CHAPTER 12: MODELING OF CORROSION BY NAPHTHENIC ACIDS AND ORGANOSULFUR COMPOUNDS

12.1 Introduction

Several years ago, a physicochemical model that simulated the corrosion by naphthenic acids and organosulfur compounds was built for the industrial project initiated by the Institute for Corrosion and Multiphase Technology.[60] The model assumes that chemical reactions between steel and naphthenic acids and/or organosulfur compounds takes place on the boundary between the steel and the surface layer. Moreover, the rate of reaction is supposed to be so fast that all the corrosive components are consumed immediately after its arrival on the steel surface.

Therefore, the corrosion rate is determined by the steady diffusion of corrosive components from bulk fluid to the steel surface. The model further assumes that there is a thin inner iron sulfide layer adjacent to the steel surface and that the diffusion through the inner layer is the rate-determining step.

However, FIB-TEM analysis shown in preceding chapters revealed that the inner layer is composed of iron sulfide and/or iron oxide rather than only iron sulfide. The proposed modeling incorporates the new finding. Thus, the accuracy of corrosion prediction should be improved.

Figure 106 illustrates the diffusion-controlled process of corrosion. Both naphthenic acids and organosulfur compounds have to diffuse through the bulk fluid, the porous outer iron sulfide layer, and the intact inner iron oxide and/or iron sulfide layer.

The mathematic expressions for each stage of diffusion are as follows (refer to Appendix

B for values of parameters).[60]
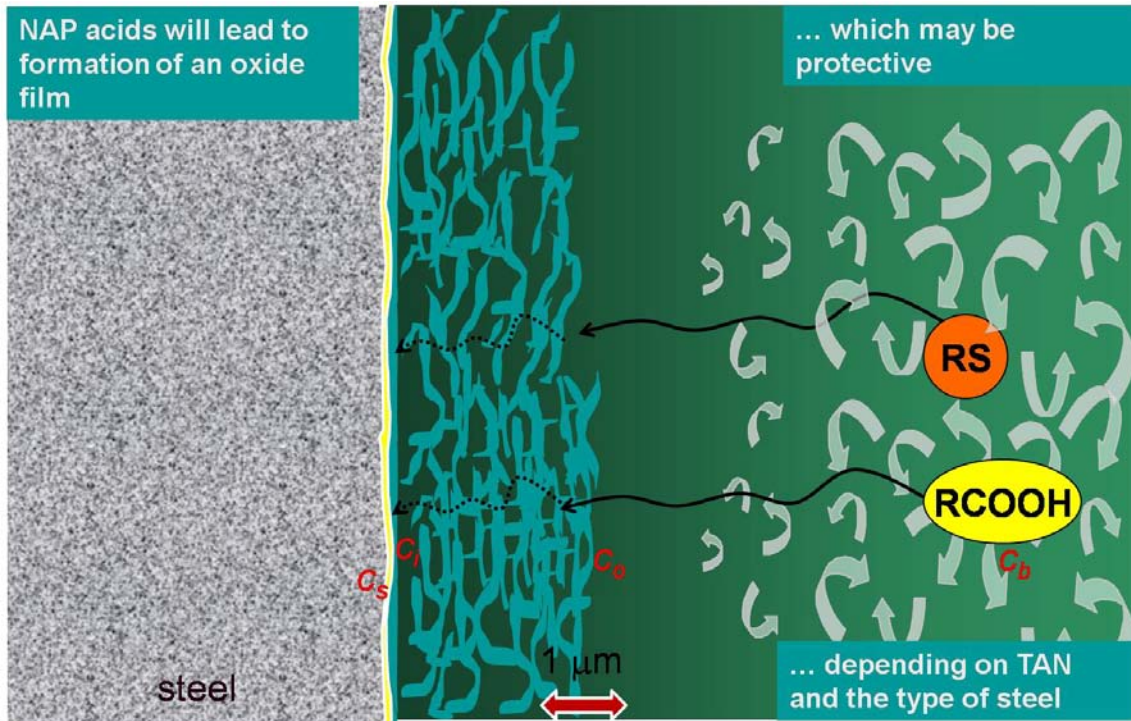
Figure 106. Diffusion of naphthenic acids and organosulfur compounds from the bulk fluid to the steel surface (reproduced from ICMT image library).

For the convective diffusion from the bulk fluid to the outer layer surface, Fick's

law could be applied (Equation 3).

$$Flux_{RS \text{ or } RCOOH} = k_{m,RS \text{ or } RCOOH} \times (c_{b,RS \text{ or } RCOOH} - c_{o,RS \text{ or } RCOOH}) \qquad (3)$$

where

$Flux_{RS \text{ or } RCOOH}$ – Flux of sulfur compounds or naphthenic acids, [mol/(m^2·s)]

$k_{m, RS \text{ or } RCOOH}$ – Mass transfer coefficient for sulfur compounds or naphthenic

acids in the boundary layer, [m/s]

$c_{b,\ RS\ or\ RCOOH}$ – Bulk concentration of sulfur compounds or naphthenic acids in the fluid, [mol/m^3]

$c_{o,\ RS\ or\ RCOOH}$ – Concentration of sulfur compounds or naphthenic acids on the outer iron sulfide layer surface, [mol/m^3]

The diffusion through the porous outer iron sulfide layer can be illustrated by Equation 4.

$$Flux_{RS\ or\ RCOOH} = \frac{D_{RS\ or\ RCOOH} \times \varepsilon \times \Psi}{\delta_{OS}} \times (c_{b,RS\ or\ RCOOH} - c_{i,RS\ or\ RCOOH}) \quad (4)$$

where

$D_{RS\ or\ RCOOH}$ – Diffusion coefficient of sulfur compounds or naphthenic acids in the fluid, [m^2/s]

ε – Porosity of outer iron sulfide layer

Ψ – Tortuosity of outer iron sulfide layer

δ_{OS} – Thickness of outer iron sulfide layer, [m]

$c_{i,\ RS\ or\ RCOOH}$ – Concentration of sulfur compounds or naphthenic acids on the interface between the outer iron sulfide layer and the inner layer,[mol/m^3]

The diffusion through the inner layer does not follow the Fick's law. It is found that a log-type diffusion equation should be feasible (Equation 5).

$$Flux_{RS\ or\ RCOOH} = A_{RS\ or\ RCOOH} \times e^{-\frac{E_{RS\ or\ RCOOH}}{RT}} \times In\frac{c_{i,RS\ or\ RCOOH}}{c_{s,RS\ or\ RCOOH}} \quad (5)$$

where

$A_{RS\ or\ RCOOH}$ – Kinetic constant for diffusion of sulfur compounds or naphthenic acids through the inner layer, [mol/(m^2·s)]

$E_{RS\,or\,RCOOH}$ – Activation energy for diffusion of sulfur compounds or naphthenic

acids through the inner layer, [J/mol]

R – Ideal gas constant, [J/(mol·K)]

T – Temperature, [K]

$c_{s,\,RS\,or\,RCOOH}$ – Concentration of sulfur compounds or naphthenic acids on the

interface between the inner layer and the steel surface, [mol/m^3]

By solving Equation 3 through 5, the sulfidation rate (SR) and naphthenic acid

corrosion rate (NAP) can be found in following expressions.

$$SR = A_{RS} \times e^{-\frac{E_{RS}}{RT}} \times In\frac{c_{b,RS} - SR \times [\frac{\delta_{OS}}{D_{RS} \times \varepsilon \times \Psi} + \frac{1}{k_{m,RS}}]}{c_{s,RS}} \tag{6}$$

$$NAP = A_{RCOOH} \times e^{-\frac{E_{RCOOH}}{RT}} \times In\frac{c_{b,RCOOH} - NAP \times [\frac{\delta_{OS}}{D_{RCOOH} \times \varepsilon \times \Psi} + \frac{1}{k_{m,RCOOH}}]}{c_{s,RCOOH}} \tag{7}$$

The total corrosion rate (CR) is the sum of SR and NAP.

$$CR = SR + NAP \tag{8}$$

12.2 Discussion of Diffusion through Inner Layer

In previous modeling, the inner layer is assumed to be iron sulfide and kinetic

constants for diffusion (A_{RS} and A_{RCOOH}) do not change for different fluids.[60] Given the

finding of the inner iron oxide/iron sulfide layer, it is plausible that the chemical

composition of the inner layer determines the diffusive properties.

In this proposed modeling, the respective effects of naphthenic acids and

organosulfur compounds on the protective properties of layers are taken into account

(Figure 107). The presence of organosulfur compounds promotes the formation of the

iron sulfide layer. The corrosion by naphthenic acids leads to the formation of the iron oxide layer. Two effects are incorporated in the proposed modeling. On the one hand, protective effect is observed when iron sulfide and iron oxide deter the diffusion of organosulfur compounds and naphthenic acids through the layer and mitigated corrosion. On the other hand, there is also a cross-effect of these two components that should not be overlooked. Organosulfur compounds and naphthenic acids could affect the properties of iron oxide and iron sulfide, respectively.
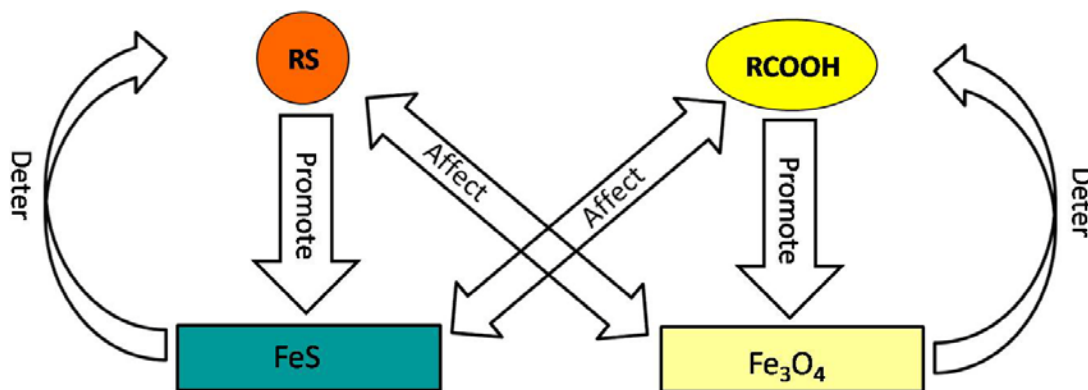
Figure 107. Interaction among naphthenic acid/organosulfur compound and layers.

It seems that presence of naphthenic acids and organosulfur compounds result in two opposite effects. To account for such effects, kinetic constants for diffusion (A_{RS} and A_{RCOOH}) are modified as follows.

$$A_{RS} = a + b \times [TAN - c \times S\%]^2 \tag{9}$$

$$A_{RCOOH} = d + e \times [TAN - f \times S\%]^2 \tag{10}$$

where

TAN – Total acidic number, [mg KOH / g oil]

S% – Weight percentage of sulfur element in the oil

a, b…f – Constants

12.3 Model Validation with the Model Compounds

To evaluate the effectiveness of the proposed modeling, corrosion rates predicted by the model are compared with real experimental data. Figure 108 and Figure 109 compare predicted corrosion rates with experimental results for model compounds investigated in the stirred autoclave at 343°C. For both CS and 5Cr steel, the model works well although it underestimates the corrosion of CS by the "DDS only" solution and the corrosion of 5Cr steel by the "NAP only" solution.

Figure 108. Model validation with pretreatment corrosion rates for CS specimens pretreated with model compounds in the stirred autoclave at 343°C for 24 hours.

Figure 109. Model validation with pretreatment corrosion rates for 5Cr steel specimens pretreated with model compounds in the stirred autoclave at 343°C for 24 hours.

Generally, the model over estimates the corrosion rates at 316°C both for CS and for 5Cr steel (Figure 110 and Figure 111). However, the trend of corrosion is predicted correctly.
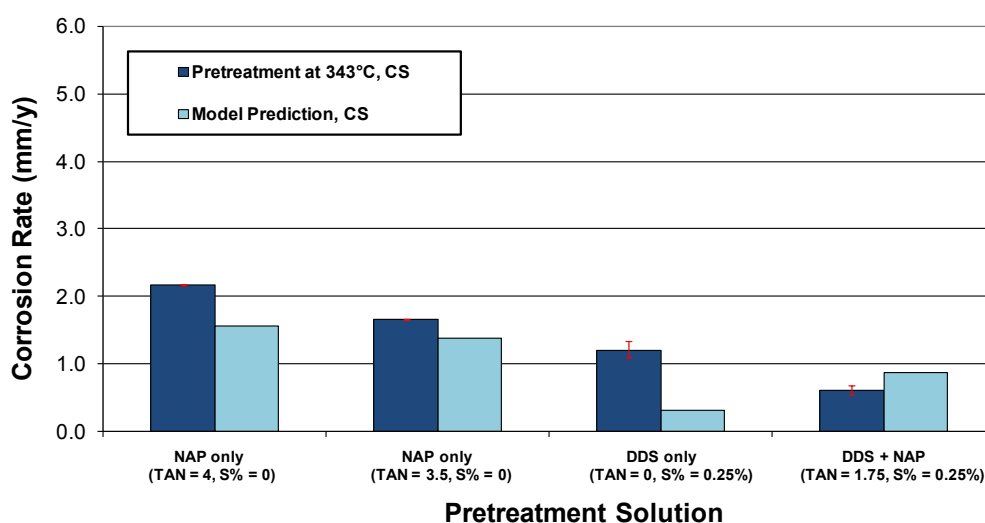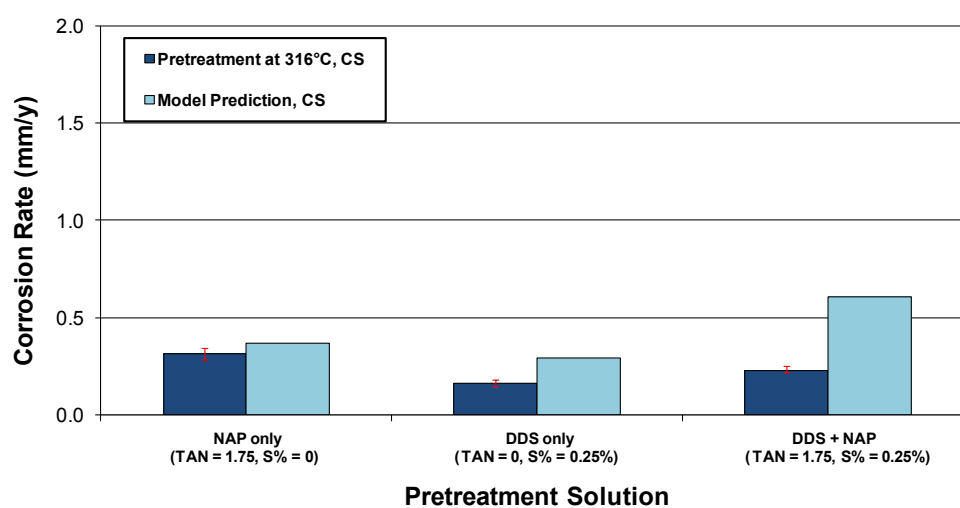

Figure 110. Model validation with pretreatment corrosion rates for CS specimens pretreated with model compounds in the stirred autoclave at 316°C for 24 hours.
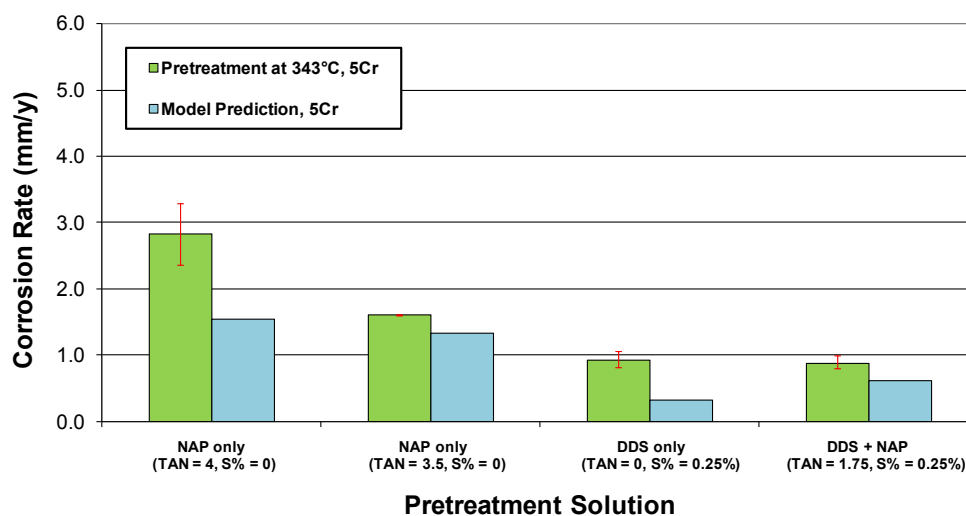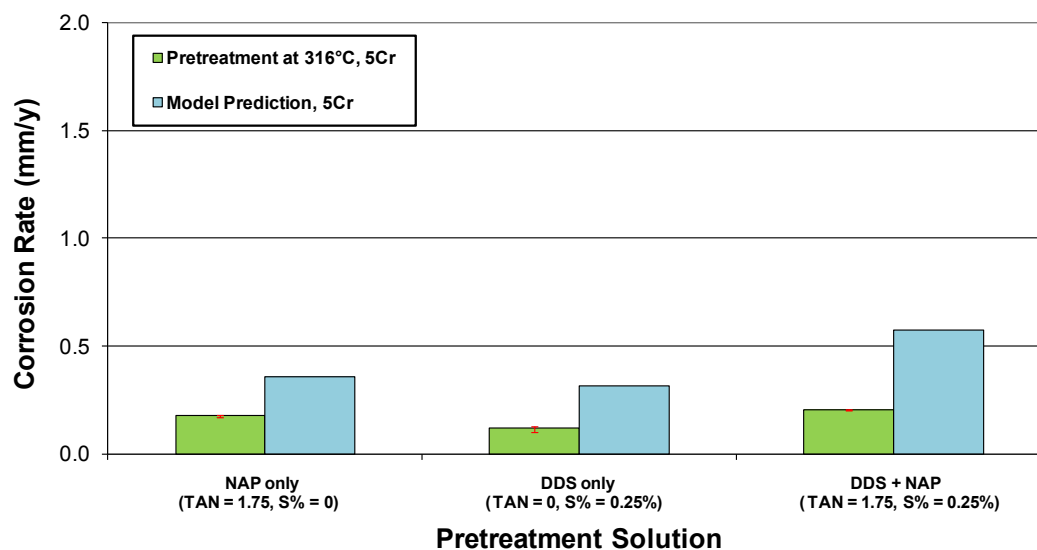
Figure 111. Model validation with pretreatment corrosion rates for 5Cr steel specimens pretreated with model compounds in the stirred autoclave at 316°C for 24 hours

The model can be applied to predict the corrosion under flow conditions. Flow enhances the mass diffusion in the fluid and increases the corrosion rate. Figure 112 and Figure 113 compare the results of pure TAN experimentation in HVR with model prediction.[60] For CS, predicted results are consistent with experimental data. Prediction for 5Cr steel is accurate for the TAN less than 5. However, the model cannot reproduce the steep increase of corrosion rates from TAN 5 to 6.5.

Figure 112. Model validation with pure TAN experimentation in HVR at 343°C for 24 hours (CS). Experimental data are based on Bota, G. M.; Corrosion of Steel at High Temperature in Naphthenic Acid and Sulfur Containing Crude Oil Fractions. PhD dissertation, Ohio University, **2010**.

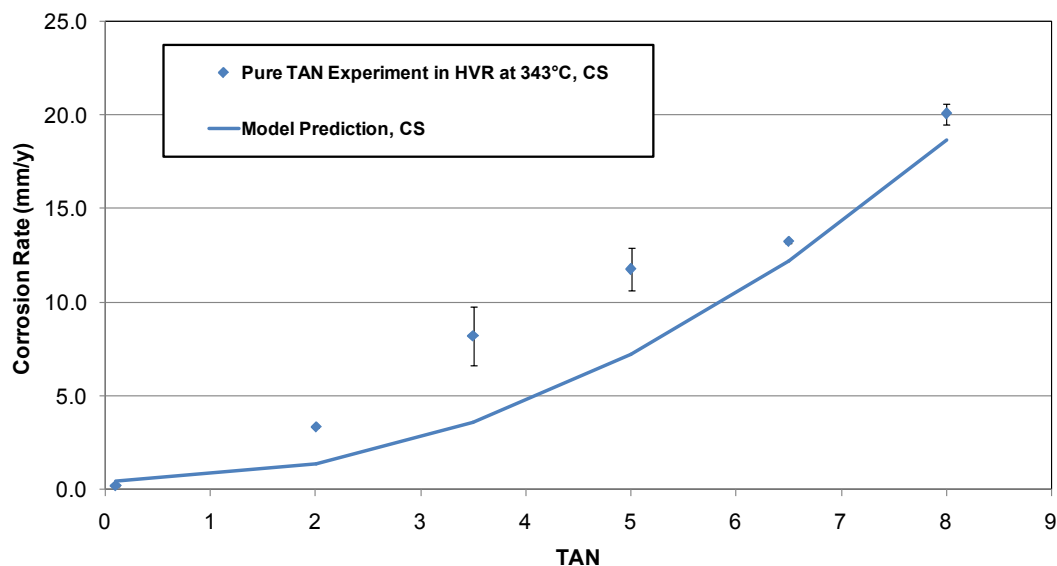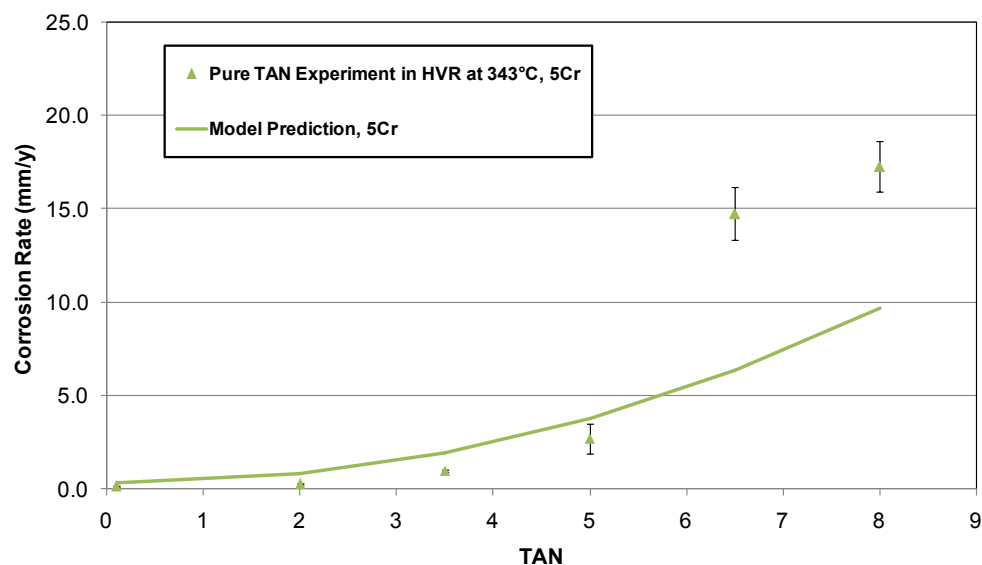Figure 113. Model validation with pure TAN experimentation in HVR at 343°C for 24 hours (5Cr steel). Experimental data are based on Bota, G. M.; Corrosion of Steel at High Temperature in Naphthenic Acid and Sulfur Containing Crude Oil Fractions. PhD dissertation, Ohio University, **2010**.

12.4 Model Validation with Real Crude Factions

Contrary to model compounds, real crude fractions have complicated chemical compositions which makes corrosion prediction more difficult, but still possible. Figure 114 and Figure 115 compare the simulated results with corrosion rates CS and 5Cr steel pretreated in the stirred autoclave at 343°C for 24 hours.[60] Generally, predicted corrosion rates are close to experimental ones, except the overestimating for some high-sulfur-content crude fractions.

Figure 114. Model validation with pretreatment corrosion rates for CS specimens pretreated with real crude fractions in the stirred autoclave at 343°C for 24 hours. Experimental data are based on Bota, G. M.; Corrosion of Steel at High Temperature in Naphthenic Acid and Sulfur Containing Crude Oil Fractions. PhD dissertation, Ohio University, **2010**.

Figure 115. Model validation with pretreatment corrosion rates for 5Cr steel specimens pretreated with real crude fractions in the stirred autoclave at 343°C for 24 hours. Experimental data are based on Bota, G. M.; Corrosion of Steel at High Temperature in Naphthenic Acid and Sulfur Containing Crude Oil Fractions. PhD dissertation, Ohio University, **2010**.

The prediction for specimens pretreated at 316°C is shown in Figure 116 and Figure 117. Similarly as the prediction for model compounds, predicted corrosion rates of crude fractions are higher than the experimental data. Moreover, some crude factions of high TAN and high sulfur content are not as corrosive as the model prediction. It suggests that other components of crudes may affect the corrosive effect.
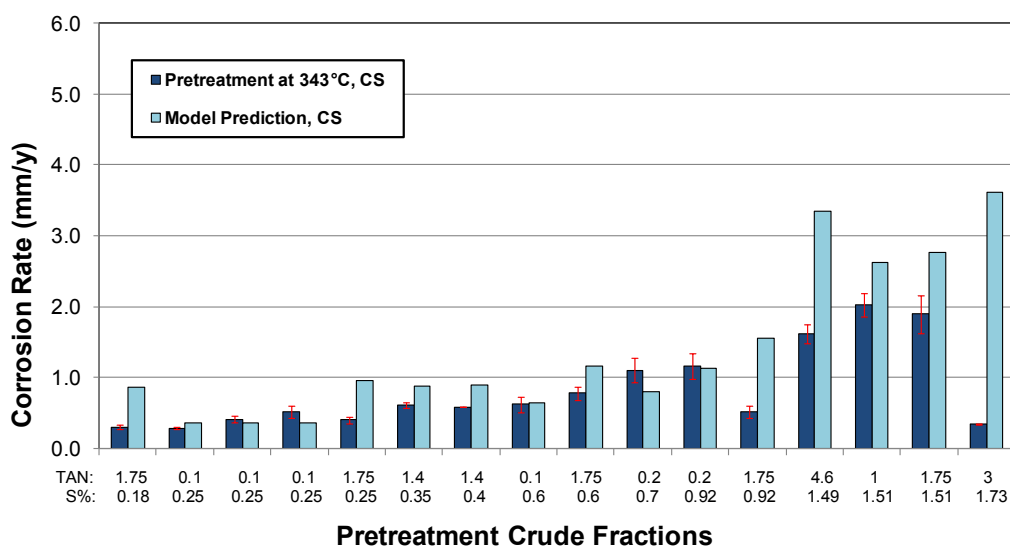
Figure 116. Model validation with pretreatment corrosion rates for CS specimens pretreated with real crude fractions in the stirred autoclave at 316°C for 24 hours.
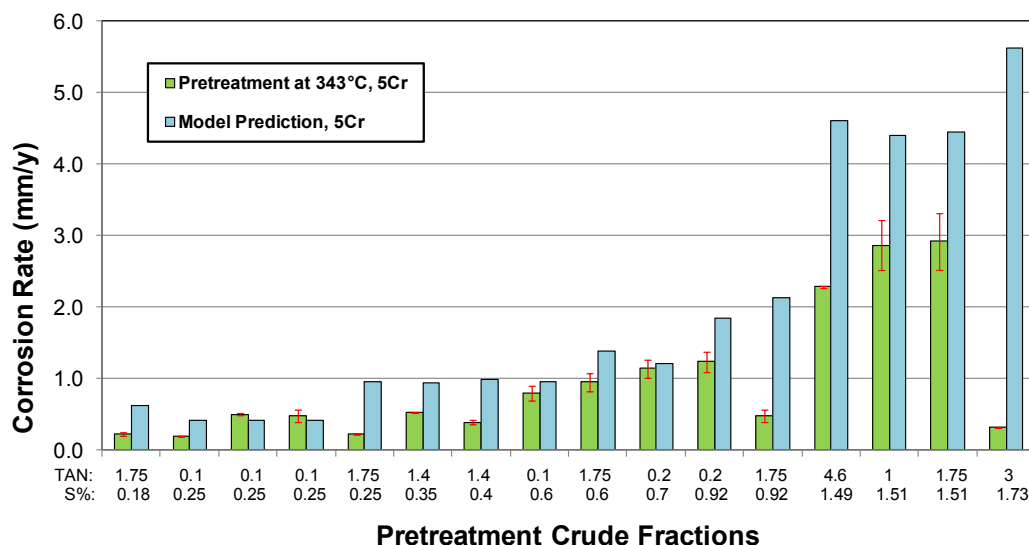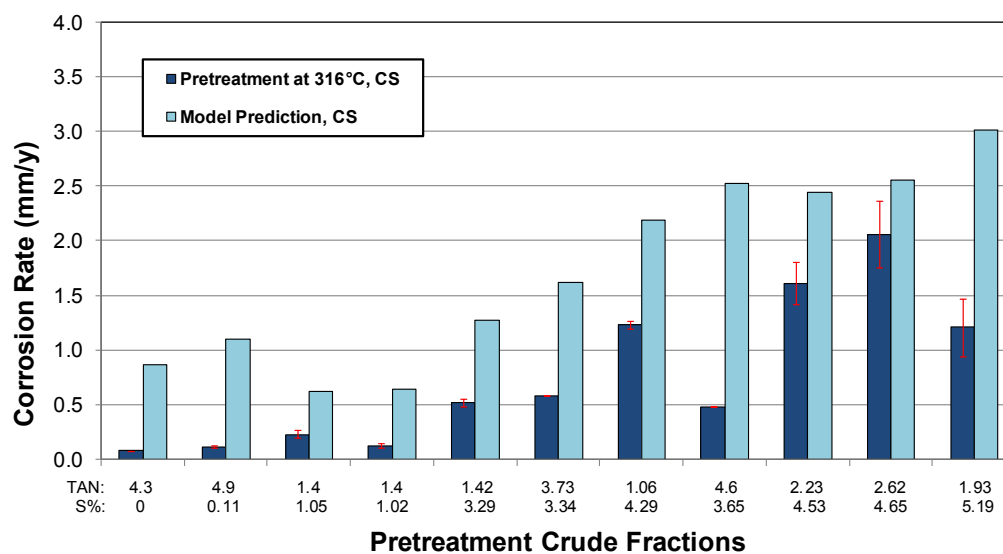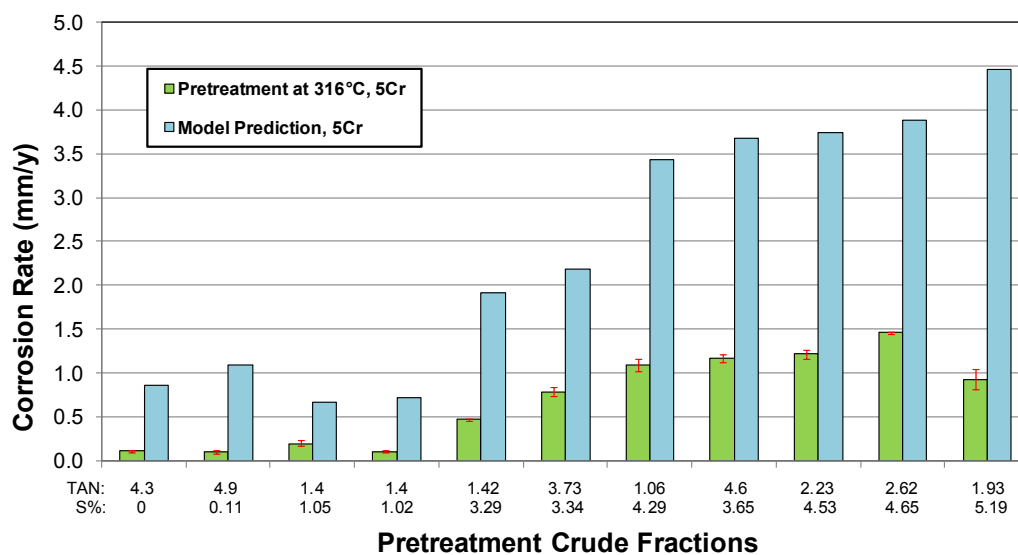

Figure 117. Model validation with pretreatment corrosion rates for 5Cr steel specimens pretreated with real crude fractions in the stirred autoclave at 316°C for 24 hours.

12.5 Model Validation with Pretreatment-Challenge Experimentation

In the preceding section, the model was validated with the corrosion rates in the pretreatment, which was intended to simulate the corrosion of fresh steel pipe exposed to a crude fraction. In the refinery different types of crude fractions are processed using the same installations; therefore the model takes into account the case of the same pipe exposed to crudes with different corrosivities. Thus in such cases the conditions in the pipe are different in terms of TAN, S%, temperature, flow, velocity, and they will influence the corrosion processes. The model takes into consideration the variations in the crude corrosivity and the surface of the pipe exposed to the crudes fractions. When the pipe surface is brand new and exposed to corrosive components (TAN and S%) the model considers the process "pretreatment" and calculates the corresponding corrosion rate. If the pipe is further exposed to acidic crudes (TAN and S%) after "pretreatment", the model will predict the corrosion rate for the new surface condition calling this new prediction "challenge".

In the current model, kinetic constants for diffusion (A_{RS} and A_{RCOOH}) in the inner oxide layer are determined by TAN and S% of the crude fraction according to Equations 8 and 9. These kinetic constants for diffusion are specific for each type of predictions ("pretreatment" or "challenge") and they are calculated by the model. In other words, A_{RS} and A_{RCOOH} should gradually change to new values when the pipe is used to process another crude fraction because the pipe surface quality is changed by the previously processed crude. However, it is reasoned that the new values cannot be achieved

immediately. It is assumed that A_{RS} and A_{RCOOH} will change linearly to new values in 24 hours.

In this project, steel specimens are pretreated in the stirred autoclave with various real crude fractions at 343°C followed by the challenge in the HVR with the TAN 3.5 solution at 343°C (Figure 118 and Figure 119).[60] Within the range of error of experimental results, predicted corrosion rates are close to the real data except the prediction for some crude fractions. It seems that the model overestimates the challenge corrosion rates for medium-sulfur-content crude fractions. It implies that some inner oxide layers are more protective than expectation.

Figure 118. Model validation with challenge corrosion rates for CS specimens pretreated with real crude fractions in the stirred autoclave at 343°C for 24 hours and challenged in the HVR with TAN 3.5 solution at 343°C for 24 hours. Experimental data are based on Bota, G. M.; Corrosion of Steel at High Temperature in Naphthenic Acid and Sulfur Containing Crude Oil Fractions. PhD dissertation, Ohio University, **2010**.
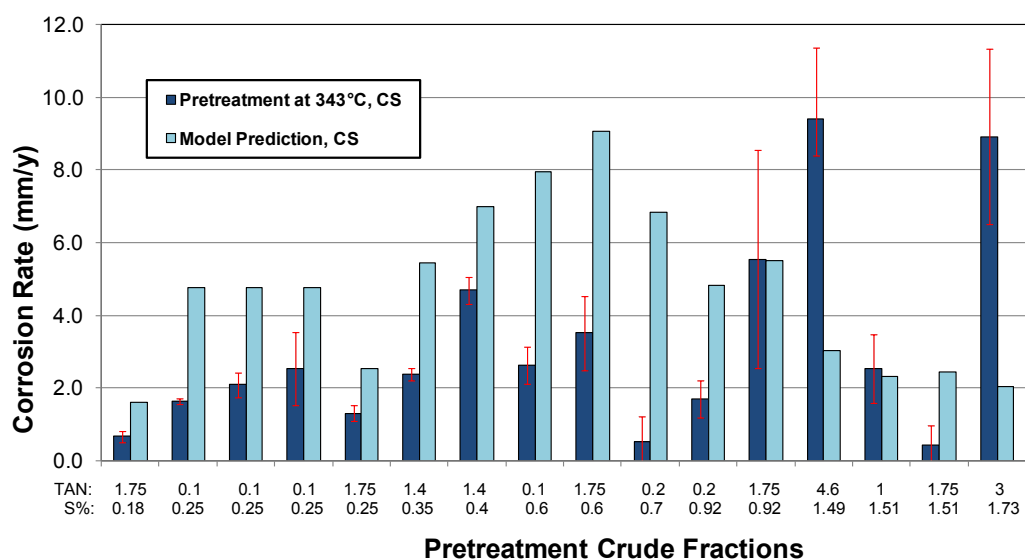
Figure 119. Model validation with challenge corrosion rates for 5Cr steel specimens pretreated with real crude fractions in the stirred autoclave at 343°C for 24 hours and challenged in the HVR with TAN 3.5 solution at 343°C for 24 hours. Experimental data are based on Bota, G. M.; Corrosion of Steel at High Temperature in Naphthenic Acid and Sulfur Containing Crude Oil Fractions. PhD dissertation, Ohio University, **2010**.

Challenge corrosion rates for specimens pretreated at 316°C are shown in Figure 120 and Figure 121. For CS, the model performs well generally, but overestimates the corrosion for some medium-sulfur-content crude fractions. However, challenge corrosion rates of 5Cr steel exhibit an opposite trend compared with that of CS – layers formed in low-sulfur-content crude fractions are more protective than the prediction. It seems that the inner oxide layer for 5Cr steel may be preserved for a longer time and protect the steel in the HVR challenge.

Figure 120. Model validation with challenge corrosion rates for CS specimens pretreated with real crude fractions in the stirred autoclave at 316°C for 24 hours and challenged in the HVR with TAN 3.5 solution at 343°C for 24 hours.
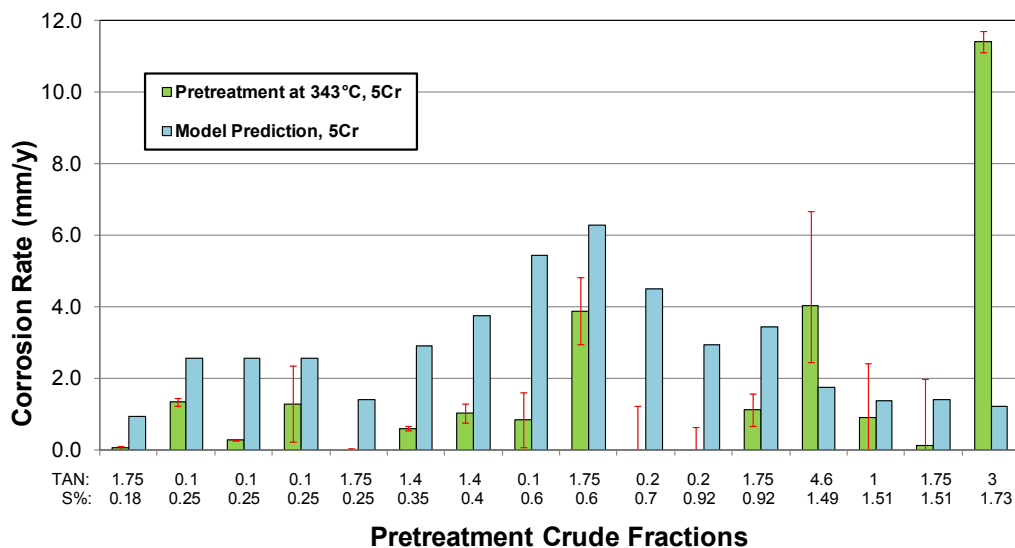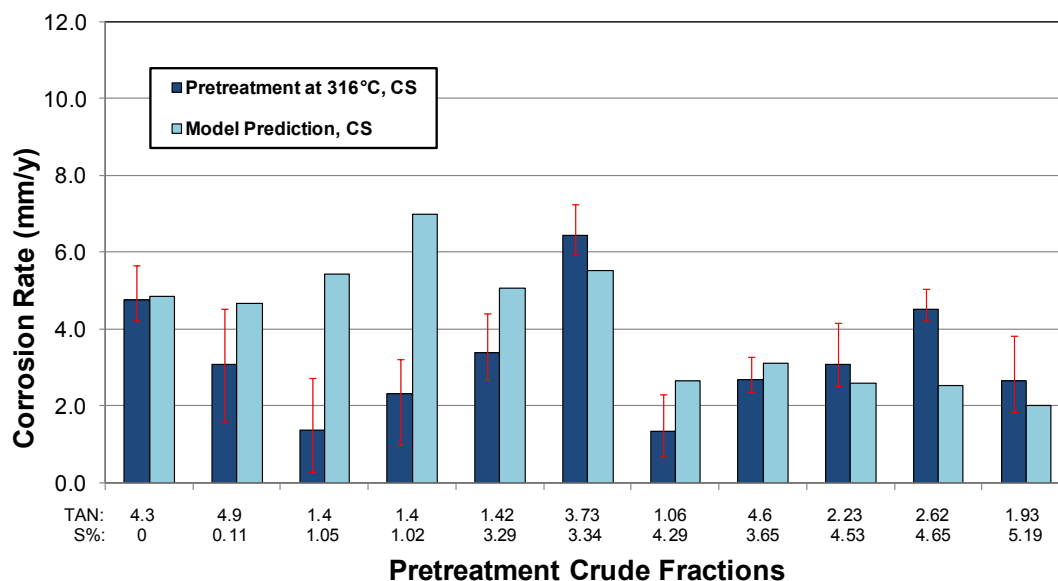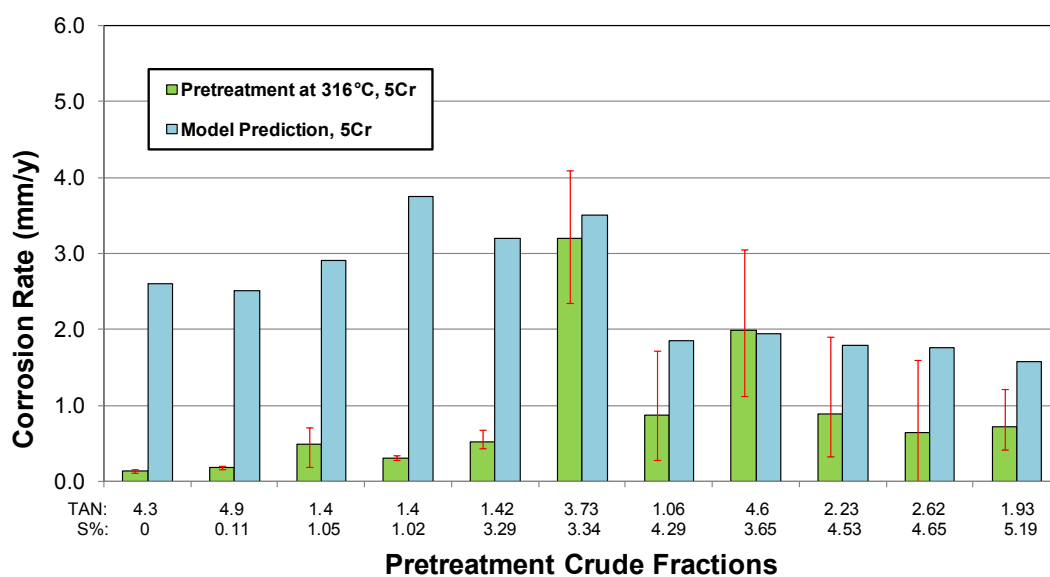

Figure 121. Model validation with challenge corrosion rates for 5Cr steel specimens pretreated with real crude fractions in the stirred autoclave at 316°C for 24 hours and challenged in the HVR with TAN 3.5 solution at 343°C for 24 hours.

12.6 Summary of Modeling

The physicochemical model was improved to reconcile with the finding of the inner oxide layer during FIB-TEM analysis. The kinetic constants for diffusion, A_{RS} and A_{RCOOH}, were found to be functions of the chemical composition of the investigated fluid (TAN and S%). The superiority of 5Cr steel in corrosion resistance was attributed to its lower diffusion kinetic constants while the diffusive properties of outer iron sulfide layer were supposed to be uniform for both metallurgies.

The model was validated with the corrosion by model compounds and real crude fractions. Within the range of error, the predicted pretreatment corrosion rates were consistent with the experimental data. The model also worked well in simulating challenge corrosion rates for most crude fractions.

However, there were some drawbacks in the current model. Firstly, the corrosion rates at a lower temperature (316°C) were overestimated. Secondly, high-sulfur crude fractions were not as corrosive as predicted by the model. Thirdly, when the steel specimen was exposed to a new corrosive condition, the change of kinetic constants for diffusion was not investigated in enough detail.

CHAPTER 13: RECOMMENDATIONS FOR FUTURE WORK

Corrosion by naphthenic acids and organosulfur compounds is a complicated process and the research study shown in previous chapters is far less than enough to explain the corrosive behaviors. Although it was found that presence of naphthenic acids would lead to the formation of a protective iron oxide or magnetite layer, more questions relating to this issue arise and need further investigation.

1. The formation mechanism of iron oxide layer should be investigated in detail. Although the literature review indicated that decomposition of iron naphthenates might result in magnetite, preliminary experimental results suggested that the steel had to be corroded before a protective layer could be formed.

2. Factors determining the protectiveness of iron oxide layer should be examined. Sulfur compounds, naphthenic acid structures, metallurgy, and temperature were expected to be important factors.

3. The layer protectiveness should be explored using a wider range of parameters. Although the iron oxide layer was protective in the challenge with TAN up to 3.5 at 343°C, it was conceivable that the layer would fail if TAN and temperature were high enough. Moreover, the layer protectiveness against sulfidation should be investigated.

4. The corrosion model should be improved. The over estimation relating to challenge corrosion rates should be addressed. Additionally, the further

experimentation may be necessary to find the time when the preformed layer

could adapt to the new condition.

REFERENCES

1. Yergin, D.; The Prize: The Epic Quest for Oil, Money, and Power. Simon & Schuster, New York **1991**.

2. Derungs, W.A.; Naphthenic Acid Corrosion – An Old Enemy of the Petroleum Industry. *Corr.,* **1956**, *12*, 617-622.

3. Bota, G.M.; Qu, D.; Nesic, S.; Wolf, H.A.; Naphthenic Acid Corrosion of Mild Steel in the Presence of Sulfide Scales Formed in Crude Oil Fractions at High Temperature. *Corr. Paper No.10353,* **2010**, 1-16.

4. Rogers, V.V.; Liber, K.; MacKinnon M.D.; Isolation and Characterization of Naphthenic Acids from Athabasca Oil Sands Tailings Pond Water. *Chemosphere* **2002**, *48*(5), 519-527.

5. ASTM D974: Standard Test Method for Acid Number and Base Number by Color-Indicator Titration. (West Conshohocken, PA, Annual Book of ASTM Standards Vol. *05.01*, 1990).

6. ASTM D664: Standard Test Method for Acid Number of Petroleum Products by Potentiometric Titration. (West Conshohocken, PA, Annual Book of ASTM Standards Vol. *05.01*, 1990).

7. Dzidic, I.; Somerville A.C.; Raia J.C.; Hart H.V.; Determination of Naphthenic Acids in California Crudes and Refinery Wastewaters by Fluoride Ion Chemical Ionization Mass Spectrometry. *Anal Chem.,* **1988**, *60*(13), 1318–1323.

8. Qian, K.; Robbins, W.K.; Hughey, C.A.; Cooper, H.J.; Rodgers, R.P.; Marshall, A.G.; Resolution and Identification of Elemental Compositions for more than 3000 Crude acids in Heavy Petroleum by Negative-ion Microelectrospray High-field Fourier Transform Ion Cyclotron Resonance Mass Spectrometry. *Energy Fuels,* **2001**, *15*(6), 1505–1511.

9. Coleman, H.J.; Hopkins, R.L.; Thompson, C.J.; Highlights of Some 50 Man-years of Petroleum Sulfur Studies by the Bureau of Mines. *Int. J. of Sulfur Chem. Part B*, **1971**, *6*, 41-61.

10. Lipshtein, R.S.; Shakhnovish, M.I.; *Transformer Oil*, 2nd Edition, Israel Program for Scientific Translations, Jerusalem, **1970**.

11. ASTM D5623: Standard Test Method for Sulfur Compounds in Light Petroleum Liquids by Gas Chromatography and Sulfur Selective Detection. (West Conshohocken, PA, Annual Book of ASTM Standards Vol. *05.02*, 2012)

12. ASTM D4294: Standard Test Method for Sulfur in Petroleum and Petroleum Products by Energy Dispersive X-ray Fluorescence Spectrometry. (West Conshohocken, PA, Annual Book of ASTM Standards Vol. *05.02*, 2012)

13. Ali, M.F.; Perzanowski, H.; Koreish, S.A.; Sulfur Compounds in High-boiling Fractions of Saudi Arabian Crude Oil, *Fuel Sci. Technol. Int.*, **1991**, *9*, 397-424.

14. ASTM D1275: Standard Test Method for Corrosive Sulfur in Electrical Insulating Oils. (West Conshohocken, PA, Annual Book of ASTM Standards Vol. *10.03*, 2012)

15. Roussis, S.G.; Fedora, J.W.; Cameron, A.S.; Method for Analyzing Total Reactive Sulfur, US Patent 5,744,702, **1998**.

16. Katritzky, A.R.; Murugan, R.; Balasubramanian, M.; Greenhill, J.V.; Siskin, M; Brons, G; Aqueous High-Temperature Chemistry of Carbo- and Heterocycles. 16. Model Sulfur Compounds: A Study of Hydrogen Sulfide Generation. *Energ Fuel.*, **1991**, *5*(6), 823-834.

17. Turnbull, A.; Slavcheva, E; Shone, B.; Factors controlling naphthenic acid corrosion. *Corr.*, **1998**, *54*(11), 922-930.

18. Messer, B.; Tarleton B.; Beaton M.; Phillips, T.; New Theory for Naphthenic Acid Corrosivity of Athabasca Oilsands Crudes. *Corr. Paper No.04634*, **2004**, 1-11.

19. Messer, B.; Tarleton B.; Beaton M.; Compositions, Configurations, and Methods of Reducing Naphtenic Acid Corrosivity, US Patent 8118994, **2012**.

20. Kaputsa, S.D.; Ooms, A.; Smith, A.; Berg, F.; Fort, W.; Safe Processing of High Acid Crudes. *Corr. Paper No. 04637,* **2004**, 1-19.

21. Dettman, H.D.; Li, N.; Wickramasinghe, D.; Luo, J.; The Influence of Naphthenic Acid and Sulphur Compound Structure on Global Crude Corrosivity under Vacuum Distillation Conditions. NACE 2010 Northern Area Western Conference, February 15-18, 2010, Calgary, Alberta, Canada.

22. Gutzeit, J.; Naphthenic Acid Corrosion in Oil Refineries. *Mater. Perform.*, **1977**, *16*, 24-35.

23. Yépez, O.; On the Chemical Reaction between Carboxylic Acids And Iron, Including the Special Case of Naphthenic Acid. *Fuel*, **2007**, *86*, 1162-1168.

24. Kane, R.D.; Cayard, M.S.; Understanding Critical Factors that Influence Refinery Crude Corrosiveness. *Mater. Perform.* **1999**, July, 48-54.

25. Couper, A.S.; High Temperature Mercaptan Corrosion of Steels, *Corr*, **1963**, *19*, 396-401.

26. Jong, J.D.; Saunders-Tack, A.; Sargent, M.; Etheridge, A.M.; Fort, W.C.; Dowling, N.; Effect of Mercaptans and Other Organic Sulfur Species on High Temperature Corrosion in Crude and Condensate Distillation Units. *Corr. Paper No. 07565,* **2007**, 1-7.

27. Kane, R.D.; Cayard, M.S.; A Comprehensive Study on Naphthenic Acid Corrosion. *Corr. Paper No.02555*, **2002**, 1-16.

28. Slavcheva, E.; Shone, B.; Turnbull, A.; Review of Naphthenic Acid Corrosion in Oil Refining. *Br. Corros. J.,* **1999**, *34*, 125–131.

29. Tebbal, S.; Kane, R.D.; Review of Critical Factors Affecting Crude Corrosivity. *Corr. Paper No.607*, **1996**, 1-10.

30. Wang, C.; Wang, Y.; Chen, J.; Sun, X.; Liu, Z.; Wan, Q.; Dai, Y.; Zheng, W.; High Temperature Naphthenic Acid Corrosion of Typical Steels. *Canadian Journal on Mechanical Sciences and Engineering*, **2011**, *2*(2), 23-30.

31. Risk-Based Inspection, Base Resource Document. API 581. Washington, DC: American Petroleum Institute, 2000.

32. Wu, X.; Jing, H.; Zheng, Y.; Yao, Z.; Ke, W.; Erosion-Corrosion of Various Oil-Refining Materials in Naphthenic Acid. *Wear*, **2004**, *256*(1-2), 133-144.

33. Qu, D.R.; Zheng, Y.G.; Jing, H.M.; Jiang, X.; Ke, W.; Erosion-Corrosion of Q235 and 5Cr1/2Mo Steels in Oil with Naphthenic Acid and/or Sulfur Compound at High Temperature. *Mater. Corros.*, **2005**, *56*(8), 533-541.

34. API. RP 939-C Guidelines for avoiding sulfidation (sulfidic) corrosion failures in oil refineries. API Subcommittee on Corrosion &Materials, Version 5.0, February 2008. New Orleans, LA.

35. Petersen, P.R.; Robbins, F.P.; Winston, W.; Naphthenic Corrosion Inhibitors, US Patent 5,182,013; **1993**.

36. Slavcheva, E.; Shone, B., Turnbull, A.; Factors Controlling Naphthenic Acid Corrosion. *Corr. Paper No. 579,* **1998**, 1-19.

37. Piehl, R.L.; Naphthenic Acid Corrosion in Crude Distillation Units. *Mater. Perform*., **1988**, *44*(1*)*, 37-43.

38. Yépez, O.; Influence of Different Sulfur Compounds on Corrosion due to Naphthenic Acid. *Fuel*, **2005**, *84*, 97-104.

39. Qu, D.R.; Zheng, Y.G.; Jing, H.M.; Yao, Z.M.; Ke, W.; High Temperature Naphthenic Acid Corrosion and Sulphidic Corrosion of Q235 and 5Cr0.5Mo Steels in Synthetic Refining Media. *Corros. Sci.*, **2006**, *48*(8), 1960-1985.

40. Huang, B.S.; Yin, W.F.; Sang, D.H.; Jiang, Z.Y.; Synergy Effect of Naphthenic Acid Corrosion and Sulfur Corrosion in Crude Oil Distillation Unit. *Appl. Surf. Sci.,* **2012**, *259*, 664-670.

41. Kanukuntla, V.; Qu, D.; Nesic, S.; Wolf, A.; Experimental Study of Concurrent Naphthenic Acid and Sulfidation Corrosion. *Corr. Paper No. 2764,* **2009**, 1-22.

42. Sartori, G.; Dalrymple, D.C.; Blum, S.C.; Monette, L.M.; Yeganeh, M.S.; Vogel, A.; Method for Inhibiting Corrosion Using certain Aromatic Acidic Species, US Patent 6559104, **2003**.

43. Yeganeh, M.S.; Dougal, S.M.; Sartori, G.; Dalrymple, D.C.; Zhang, C.; Blum, S.C.; Monette, L. M.; Method for Inhibiting Corrosion Using certain Phosphorus and Sulfur-free Compounds, US Patent 6593278, **2003**.

44. Sartori, G.; Dalrymple, D.C.; Blum, S.C.; Monette, L.M.; Yeganeh, M.S.; Vogel, A.; Method for Inhibiting Corrosion Using 4-Sulfophthalic Acid, US Patent 6583091, **2003**.

45. Sartori, G.; Dalrymple, D.C.; Blum, S.C.; Monette, L.M.; Yeganeh, M.S.; Vogel, A.; Method for Inhibiting Corrosion Using Phosphorous Acid, US Patent 6706669, **2004**.

46. Blum, S.C.; Sartori, G.; Savage, D.W.; Gorbaty, M.L.; Ballinger, B.H.; Anderson, M.P.; Ramanarayanan, T.A.; Martella, D.J.; Process for Decreasing the Acid Content and Corrosivity of Crudes, US Patent 6679987, **2004**.

47. Mitchell, D.L.; Speight, J.G.; The Solubility of Asphaltenes in Hydrocarbon Solvents. *Fuel*, **1973**, *52* (4), 149-152.

48. Alshareef, A.H.; Scherer, A.; Stryker; J.M.; Tykwinski, R.R.; Gray, M.R.; Thermal Cracking of Substituted Cholestane-Benzoquinoline Asphaltene Model Compounds. *Energy & Fuels*, **2012**, *26* (6), 3592-3603.

49. Ajmera, P.; Robbins, W.; Richter, S.; Nesic, S.; The Role of Asphaltenes in Inhibiting Corrosion and Altering the Wettability of the Steel Surface. *Corr. Paper No.10329*, 2010, 1-11.

50. Seliger, R.L.; Fleming, W.P.; Focused Ion Beams in Microfabrication. *J. Appl. Phys.,* **1974***, 45*(3), 1416-1422.

51. Czarczynski, W.; Znamirowski, Z.; Liquid Metal Ion Sources. *Vacuum,* **1993**, *44*(11-12), 1095-1099.

52. Langford, R.M.; Petford-Long, A.K.; Preparation of Transmission Electron Microscopy Cross-section Specimens Using Focused Ion Beam Milling. *J. Vac. Sci. Technol., A,* **2001***, 19*(5), 2186-2193.

53. Stroppa, D.G.; Zagonel, L.F.; Montoro, L.A.; Leite, E.R.; Ramirez, A.J.; High-Resolution Scanning Transmission Electron Microscopy (HRSTEM) Techniques: High-Resolution Imaging and Spectroscopy Side by Side. *Chemphyschem*, **2012**, *13*(2), 437-443.

54. El Kamel, M.; Galtayries, A.; Vermaut, P.; Albinet, B.; Foulonneau, G.; Roumeau, X., Roncin, B; Marcus, P.; Sulfidation Kinetics of Industrial Steels in a Refinery Crude Oil at 300 °C: Reactivity at the Nanometer Layer. *Surf. Interface Anal.,* **2010**, *42*(6-7), 605-609.

55. Smart, N.R.; Rance, A.P.; Pritchard, A.M.; Laboratory Investigation of Naphthenic Acid Corrosion Under Flowing Conditions. *Corr. Paper 02484*, **2002**, 1-23.

56. Huang, B.S.; Yin, W.F.; Sang, D.H.; Jiang, Z.Y.; Synergy Effect of Naphthenic Acid Corrosion and Sulfur Corrosion in Crude Oil Distillation Unit. *Appl. Surf. Sci.,* **2012***, 259*, 664-670.

57. Fukushima, J.; Kodaira, K.; Matsushita, T.; Preparation and Formation Process of Various Iron Oxide Films by Thermal Decomposition of Iron Naphthenate. *J. Ceram. Soc. Jpn.*, **1976**, *84*(11), 529-533.

58. Konishi, Y.; Kawamura, T.; Asai, S.; Preparation and Characterization of Fine Magnetite Particles from Iron (III) Carboxylate Dissolved in Organic Solvent. *Ind. Eng. Chem. Res.,* **1993***, 32*(11), 2888-2891.

59. Redl, F.X.; Black, C.T.; Papaefthymiou, G.C.; Sandstrom, R.L.; Yin, M.; Zeng, H.; Murray, C.B.; O'Brien, S.P.; Magnetic, Electronic, and Structural Characterization of Nonstoichiometric Iron Oxides at the Nanolayer. *JACS,* **2004***, 126*(44), 14583-14599.

60. Bota, G.M.; Corrosion of Steel at High Temperature in Naphthenic Acid and Sulfur Containing Crude Oil Fractions. PhD dissertation, Ohio University, **2010**.

61. Kaimal, T.; Matsunaga, A.; Determination of Sulfur Compounds in High-Boiling Petroleum Distillates by Ligand-Exchange Thin-Layer Chromatography. *Anal. Chem.*, **1978**, *50*(2), 268-270.

62. Stolen, S.; Gloeckner, R.; Gronvold, F.; Nearly Stoichiometric Iron Monoxide Formed as a Metastable Intermediate in a Two-Stage Disproportionation of Quenched Wüstite. Thermodynamic and Kinetic Aspects. *Thermochim. Acta*, **1995**, 256, 91-106.

APPENDIX A: SUPPLEMENTAL RESULTS OF ANALYSIS OF LAYERS

FORMED IN REAL CRUDE FRACTIONS AND MODEL COMPOUNDS
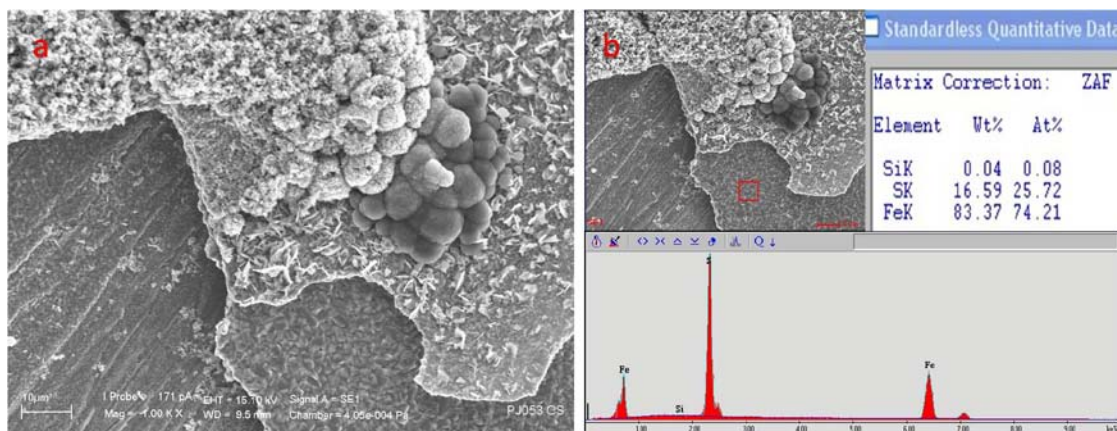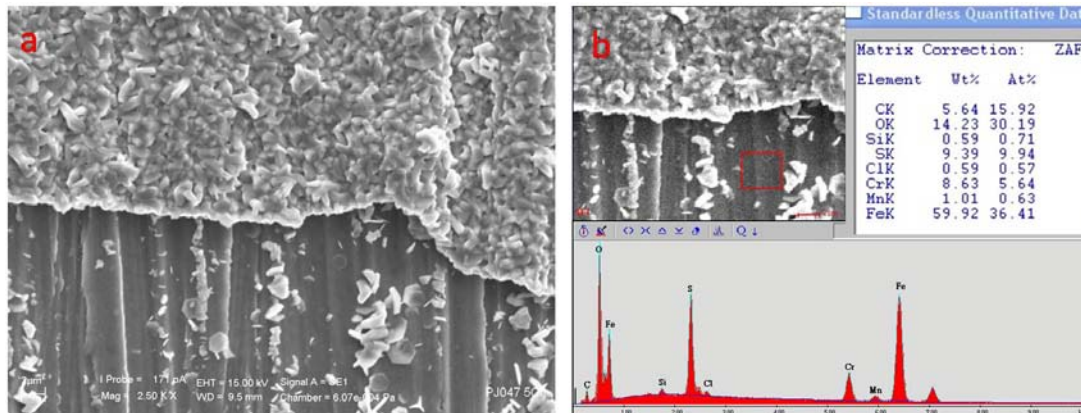

Figure A-1. Surface of CS specimen pretreated with Fraction L at 316°C. (a) Surface SEM image; (b) EDS analysis on the surface. SEM and EDS analysis of the cross section is given in Figure A-2. Refer to Figure 39 in the main text for the corrosion rate.
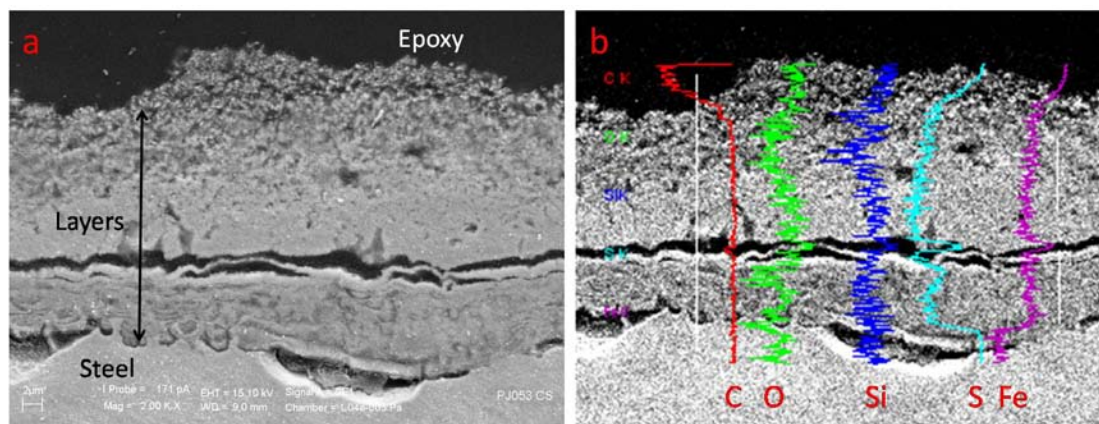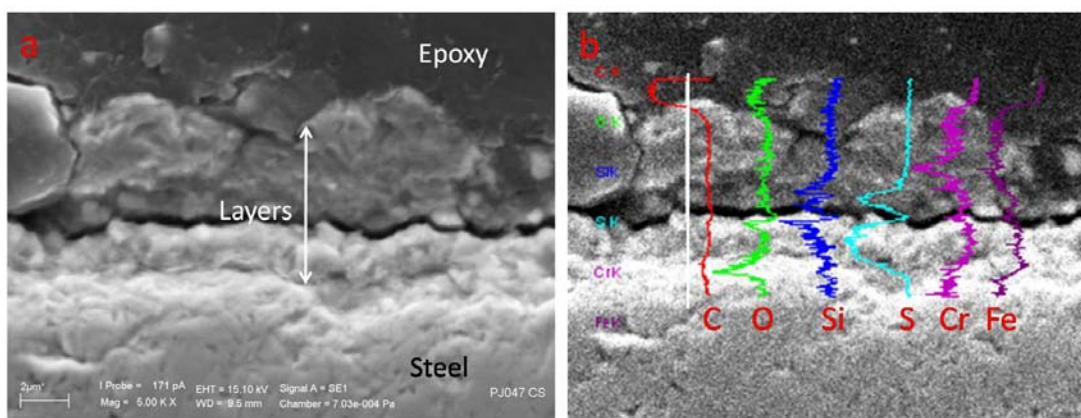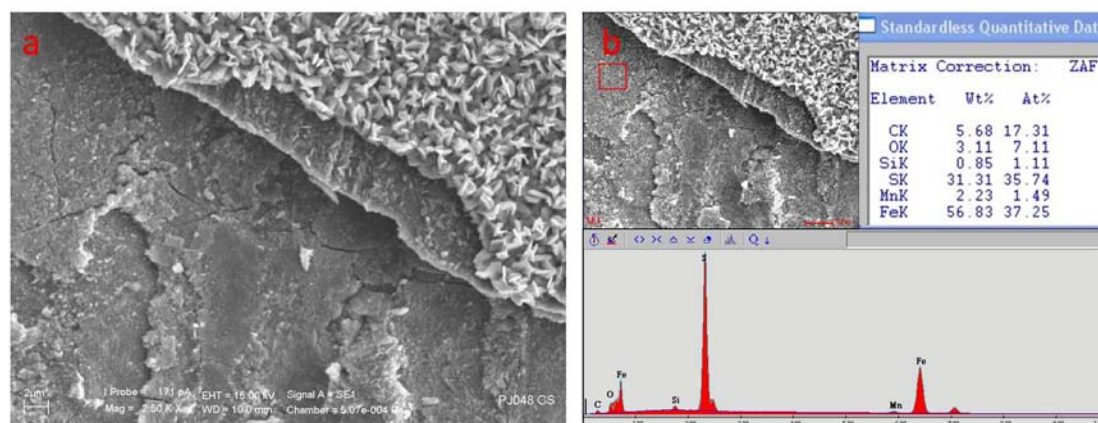

Figure A-2. Cross-section analysis of CS specimen pretreated with Fraction L at 316°C. (a) Cross-section SEM image; (b) Corresponding EDS analysis along the white line on the left. SEM and EDS analysis of the surface is given in Figure A-1. Refer to Figure 39 in the main text for the corrosion rate.
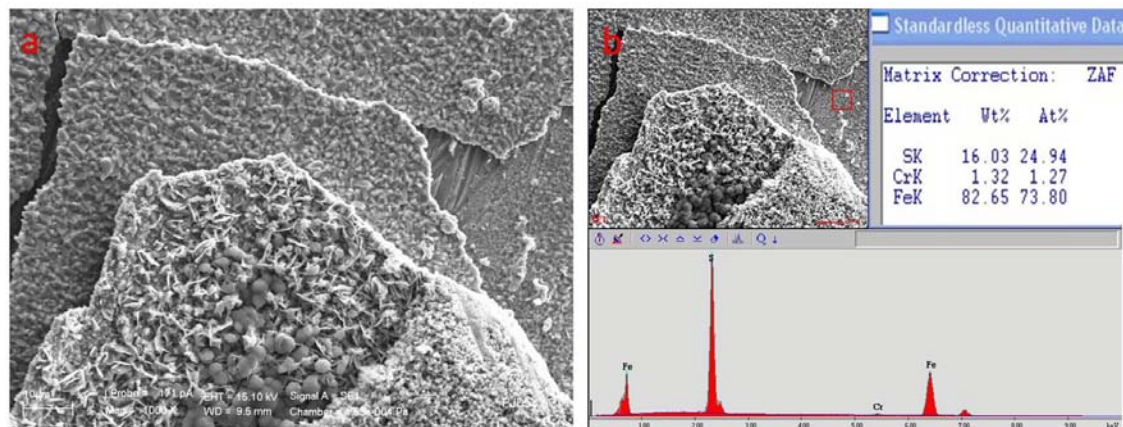
Figure A-3. Surface of 5Cr steel specimen pretreated with Fraction L at 316°C. (a) Surface SEM image; (b) EDS analysis on the surface. SEM and EDS analysis of the cross section is given in Figure A-4. Refer to Figure 40 in the main text for the corrosion rate.
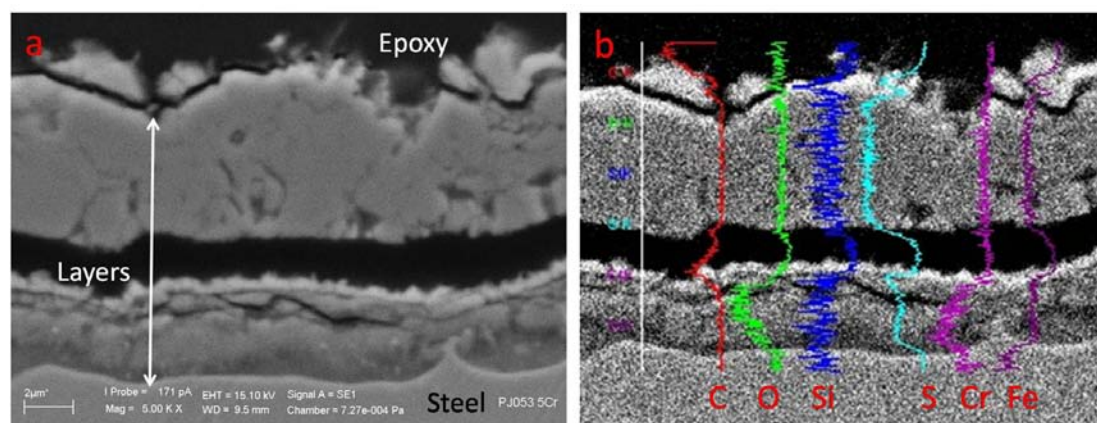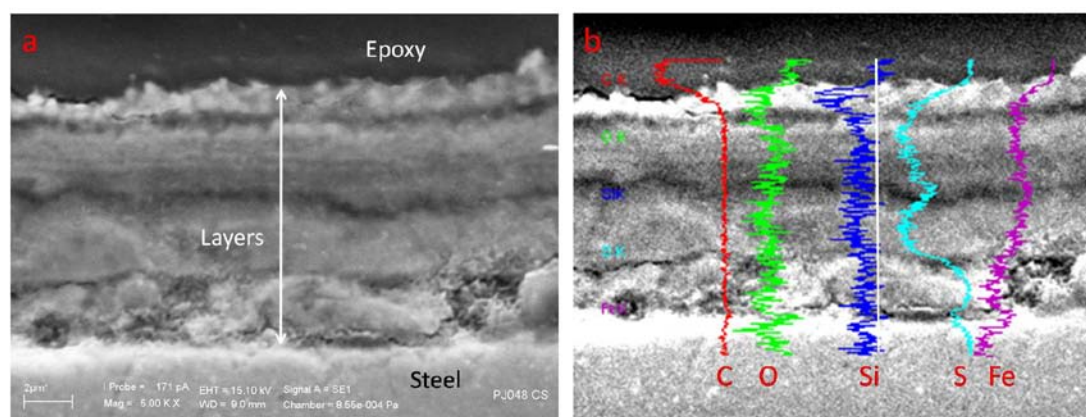

Figure A-4. Cross-section analysis of 5Cr steel specimen pretreated with Fraction L at 316°C. (a) Cross-section SEM image; (b) Corresponding EDS analysis along the white line on the left. SEM and EDS analysis of the surface is given in Figure A-3. Refer to Figure 40 in the main text for the corrosion rate.
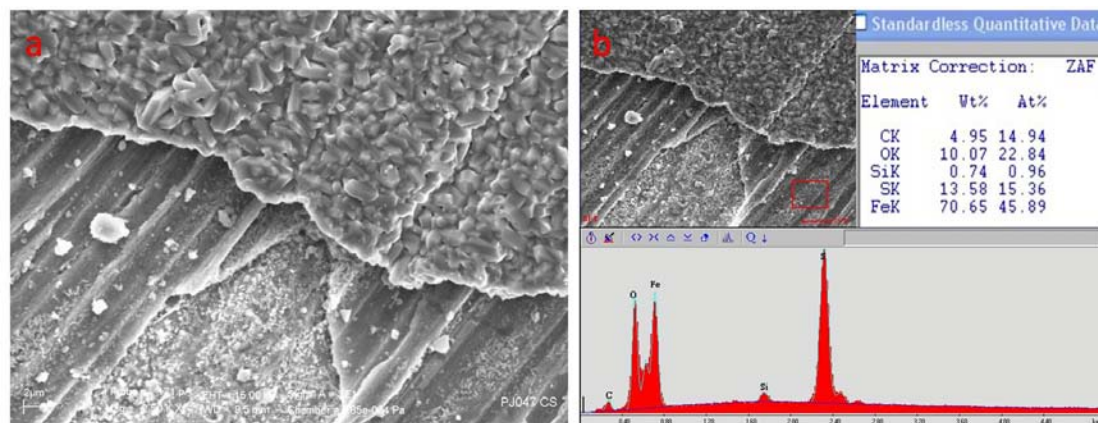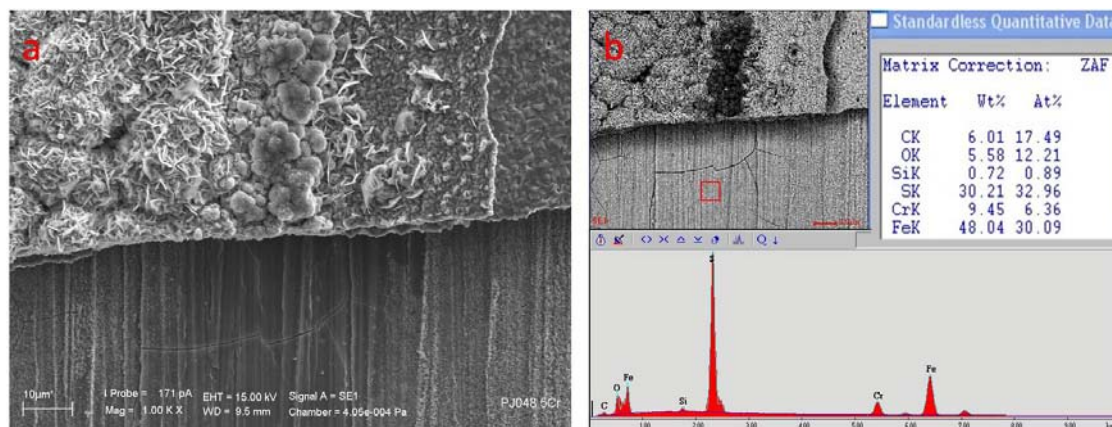
Figure A-5. Surface of CS specimen pretreated with Fraction K at 316°C. (a) Surface SEM image; (b) EDS analysis on the surface. SEM and EDS analysis of the cross section is given in Figure A-6. Refer to Figure 39 in the main text for the corrosion rate.
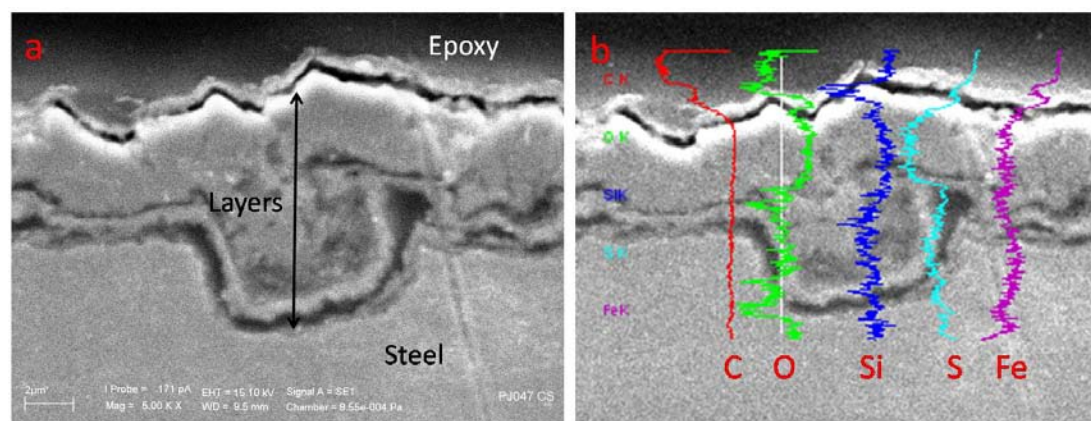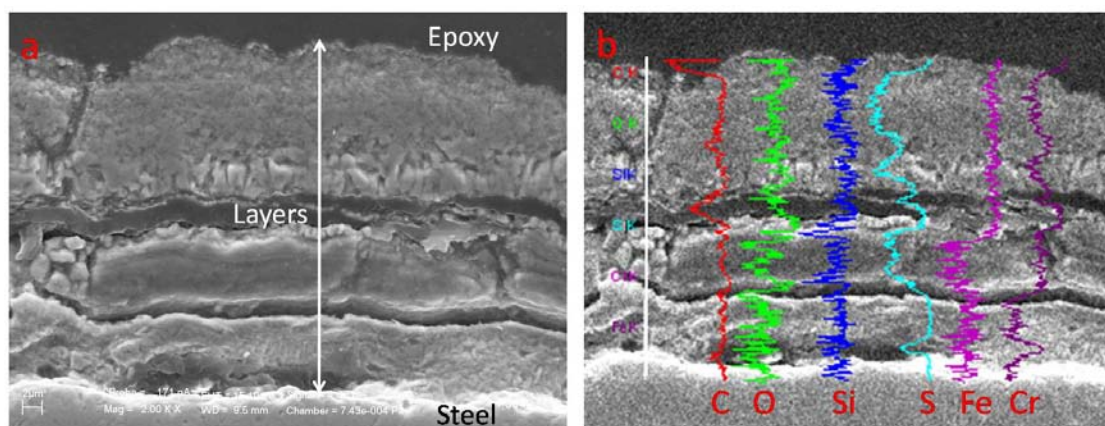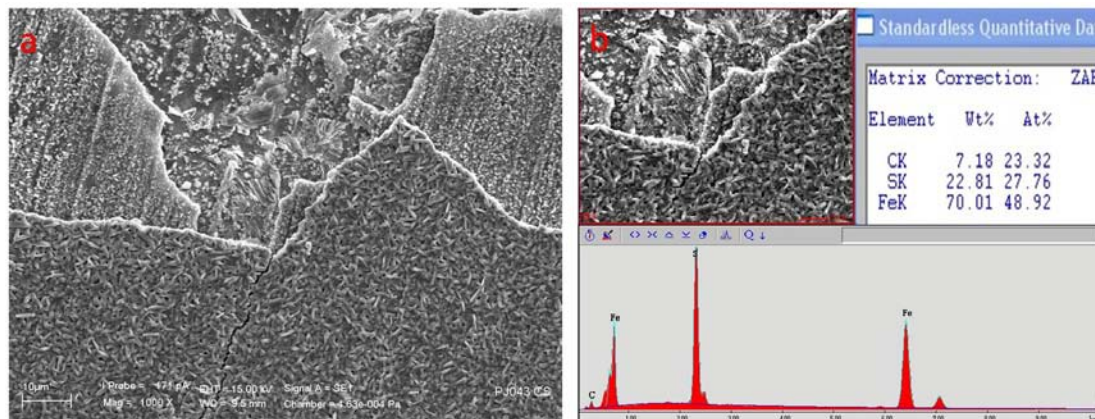

Figure A-6. Cross-section analysis of CS specimen pretreated with Fraction K at 316°C. (a) Cross-section SEM image; (b) Corresponding EDS analysis along the white line in the middle. SEM and EDS analysis of the surface is given in Figure A-5. Refer to Figure 39 in the main text for the corrosion rate.

Figure A-7. Surface of 5Cr steel specimen pretreated with Fraction K at 316°C. (a) Surface SEM image; (b) EDS analysis on the surface. SEM and EDS analysis of the cross section is given in Figure A-8. Refer to Figure 40 in the main text for the corrosion rate.

Figure A-8. Cross-section analysis of 5Cr steel specimen pretreated with Fraction K at 316°C. (a) Cross-section SEM image; (b) Corresponding EDS analysis along the white line on the left. SEM and EDS analysis of the surface is given in Figure A-7. Refer to Figure 40 in the main text for the corrosion rate.

Figure A-9. Surface of CS specimen pretreated with Fraction G at 316°C. (a) Surface SEM image; (b) EDS analysis on the surface. SEM and EDS analysis of the cross section is given in Figure A-10. Refer to Figure 39 in the main text for the corrosion rate.
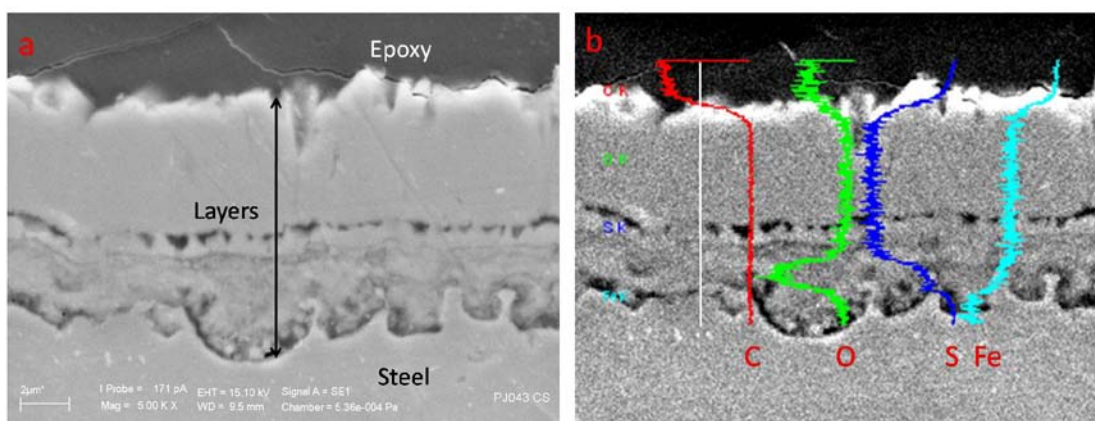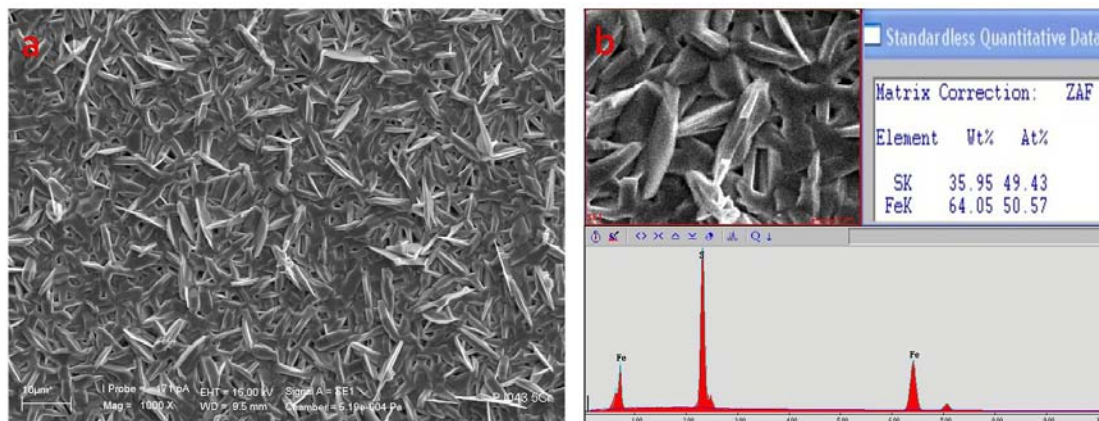

Figure A-10. Cross-section analysis of CS specimen pretreated with Fraction G at 316°C. (a) Cross-section SEM image; (b) Corresponding EDS analysis along the white line in the middle. SEM and EDS analysis of the surface is given in Figure A-9. Refer to Figure 39 in the main text for the corrosion rate.

Figure A-11. Surface of 5Cr steel specimen pretreated with Fraction G at 316°C. (a) Surface SEM image; (b) EDS analysis on the surface. SEM and EDS analysis of the cross section is given in Figure A-12. Refer to Figure 40 in the main text for the corrosion rate.
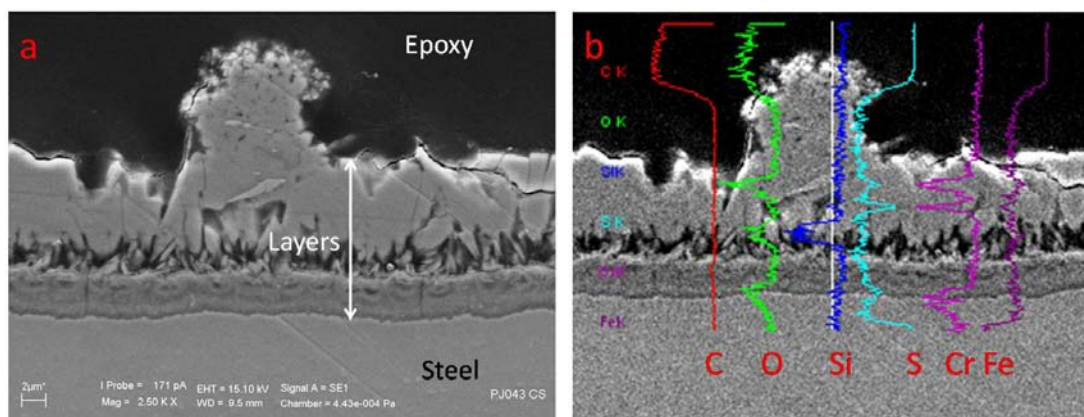

Figure A-12. Cross-section analysis of 5Cr steel specimen pretreated with Fraction G at 316°C. (a) Cross-section SEM image; (b) Corresponding EDS analysis along the white line on the left. SEM and EDS analysis of the surface is given in Figure A-11. Refer to Figure 40 in the main text for the corrosion rate.
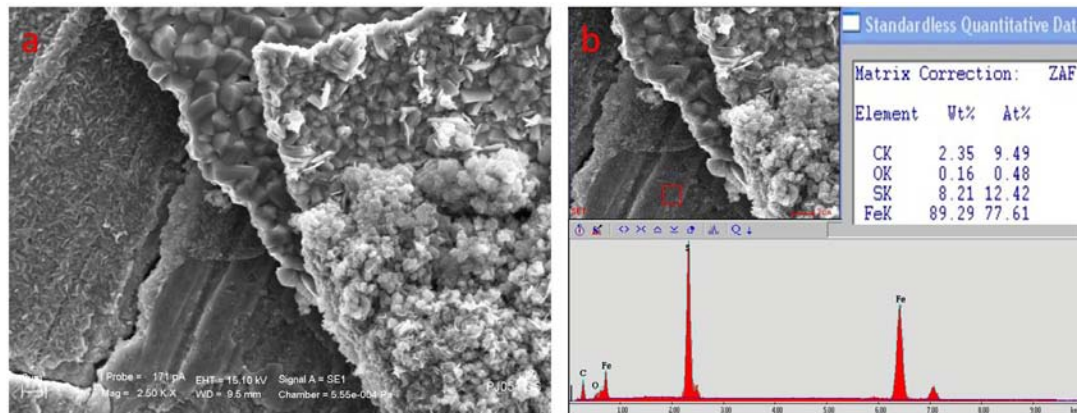
Figure A-13. Surface of CS specimen pretreated with Fraction F at 316°C. (a) Surface SEM image; (b) EDS analysis on the surface. SEM and EDS analysis of the cross section is given in Figure A-14. Refer to Figure 39 in the main text for the corrosion rate.
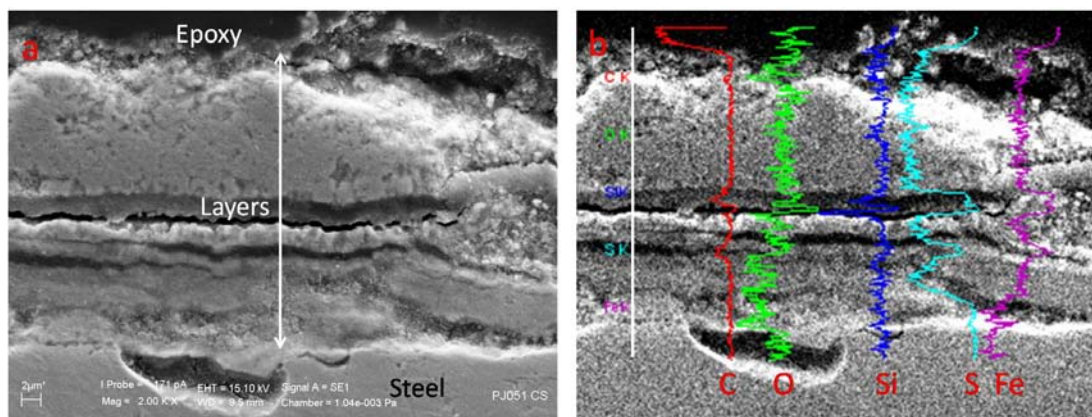

Figure A-14. Cross-section analysis of CS specimen pretreated with Fraction F at 316°C. (a) Cross-section SEM image; (b) Corresponding EDS analysis along the white line on the left. SEM and EDS analysis of the surface is given in Figure A-13. Refer to Figure 39 in the main text for the corrosion rate.
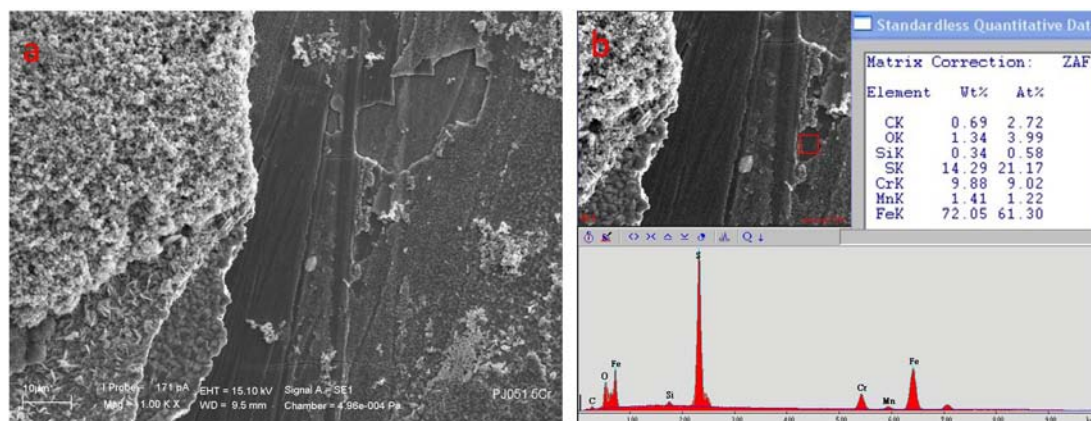
Figure A-15. Surface of 5Cr steel specimen pretreated with Fraction F at 316°C. (a) Surface SEM image; (b) EDS analysis on the surface. SEM and EDS analysis of the cross section is given in Figure A-16. Refer to Figure 40 in the main text for the corrosion rate.
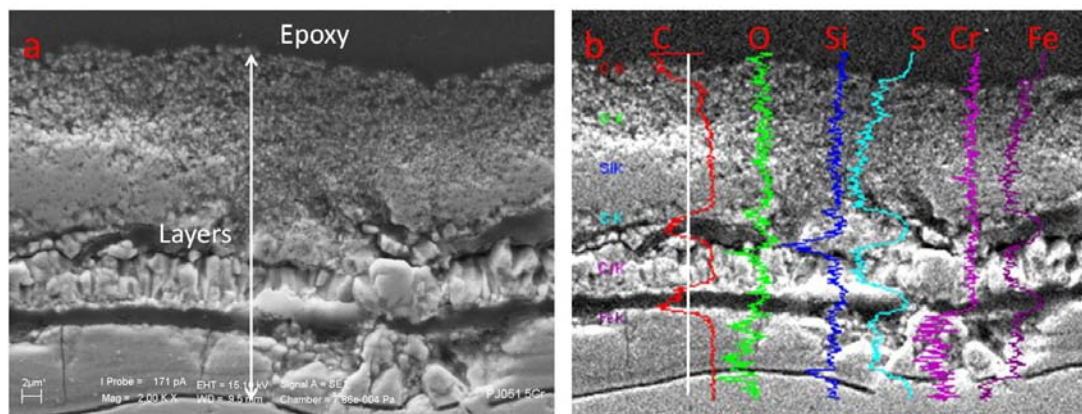

Figure A-16. Cross-section analysis of 5Cr steel specimen pretreated with Fraction F at 316°C. (a) Cross-section SEM image; (b) Corresponding EDS analysis along the white line in the middle. SEM and EDS analysis of the surface is given in Figure A-15. Refer to Figure 40 in the main text for the corrosion rate.
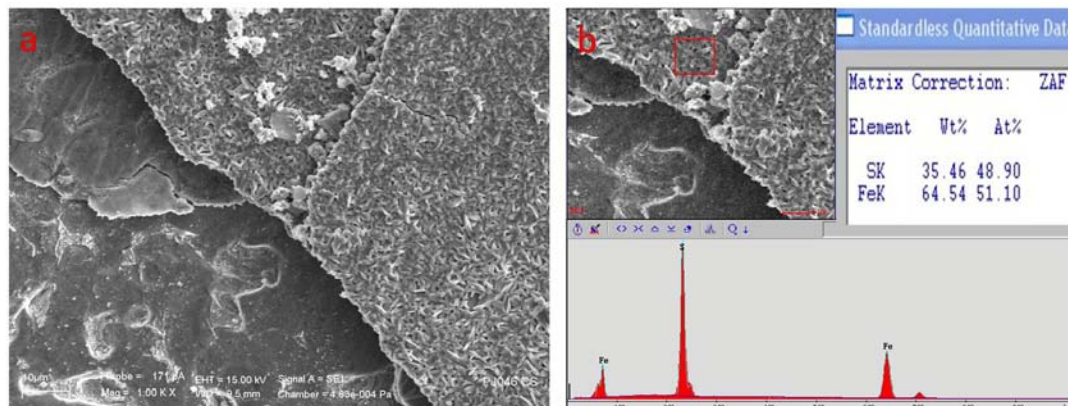
Figure A-17. Surface of CS specimen pretreated with Fraction J at 316°C. (a) Surface SEM image; (b) EDS analysis on the surface. SEM and EDS analysis of the cross section is given in Figure A-18. Refer to Figure 39 in the main text for the corrosion rate.
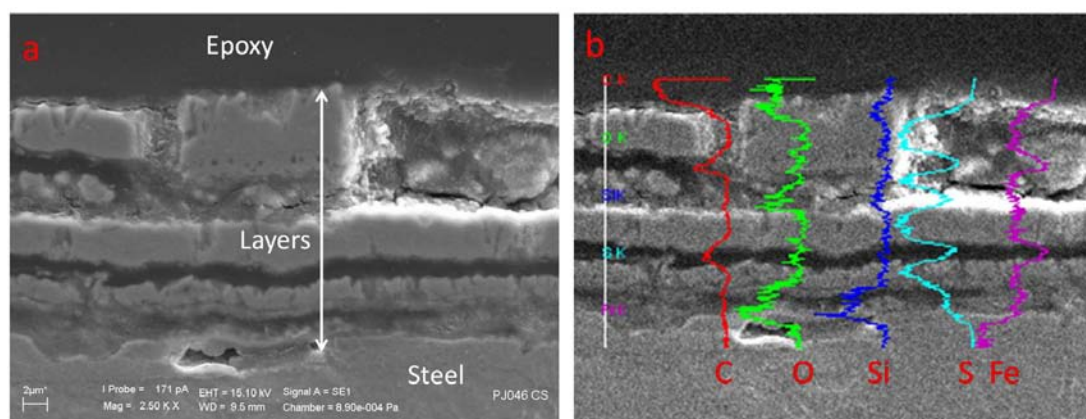

Figure A-18. Cross-section analysis of CS specimen pretreated with Fraction J at 316°C. (a) Cross-section SEM image; (b) Corresponding EDS analysis along the white line on the left. SEM and EDS analysis of the surface is given in Figure A-17. Refer to Figure 39 in the main text for the corrosion rate.
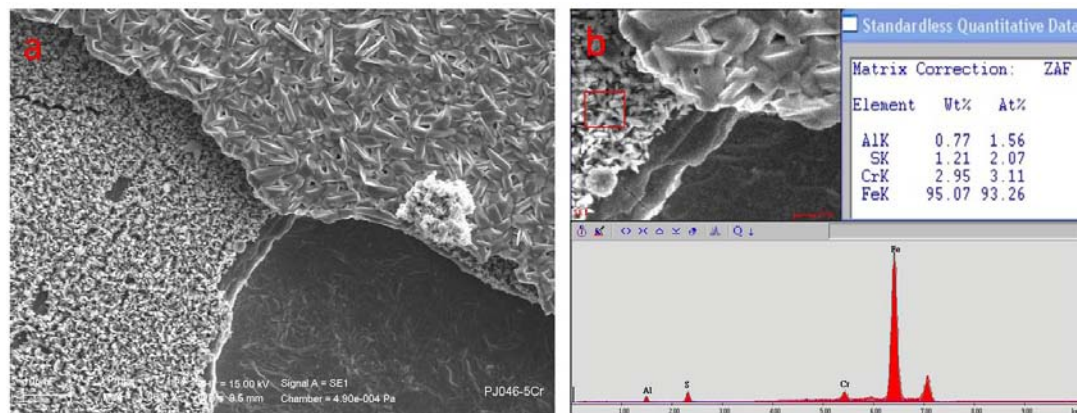
Figure A-19. Surface of 5Cr steel specimen pretreated with Fraction J at 316°C. (a) Surface SEM image; (b) EDS analysis on the surface. SEM and EDS analysis of the cross section is given in Figure A-20. Refer to Figure 40 in the main text for the corrosion rate.
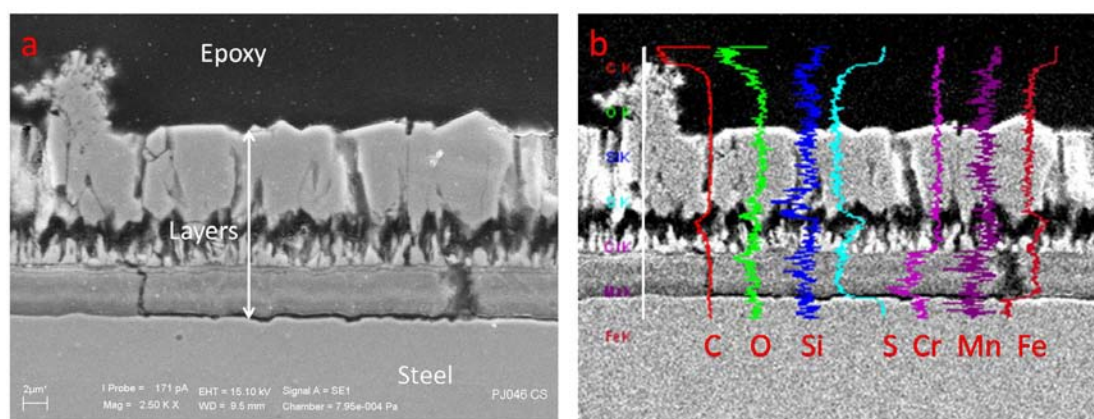

Figure A-20. Cross-section analysis of 5Cr steel specimen pretreated with Fraction J at 316°C. (a) Cross-section SEM image; (b) Corresponding EDS analysis along the white line on the left. SEM and EDS analysis of the surface is given in Figure A-19. Refer to Figure 40 in the main text for the corrosion rate.
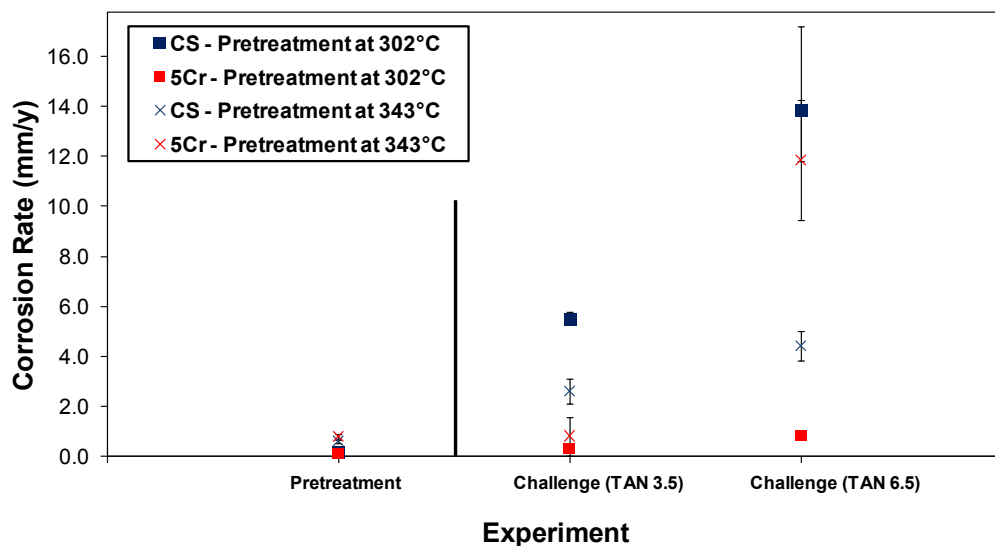
Figure A-21. Surface of CS specimen pretreated with Fraction I at 316°C. (a) Surface SEM image; (b) EDS analysis on the surface. SEM and EDS analysis of the cross section is given in Figure A-22. Refer to Figure 39 in the main text for the corrosion rate.

Figure A-22. Cross-section analysis of CS specimen pretreated with Fraction I at 316°C. (a) Cross-section SEM image; (b) Corresponding EDS analysis along the white line on the left. SEM and EDS analysis of the surface is given in Figure A-21. Refer to Figure 39 in the main text for the corrosion rate.
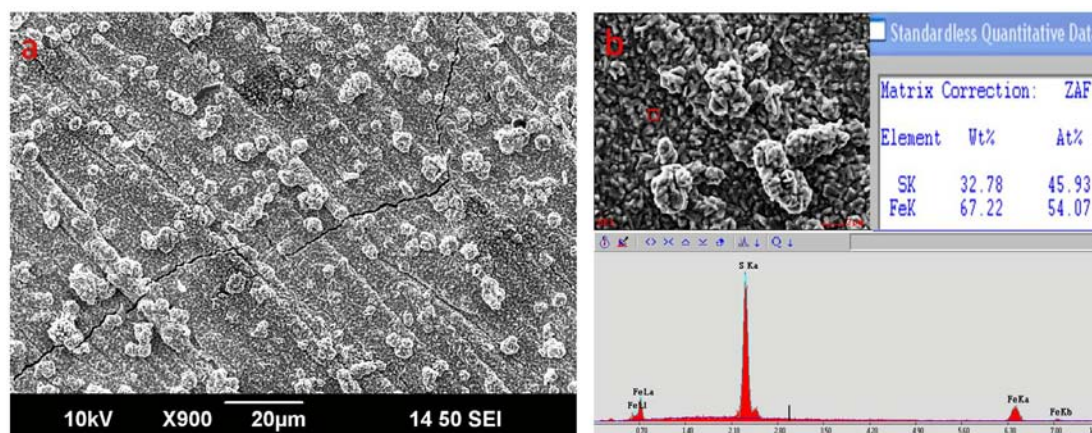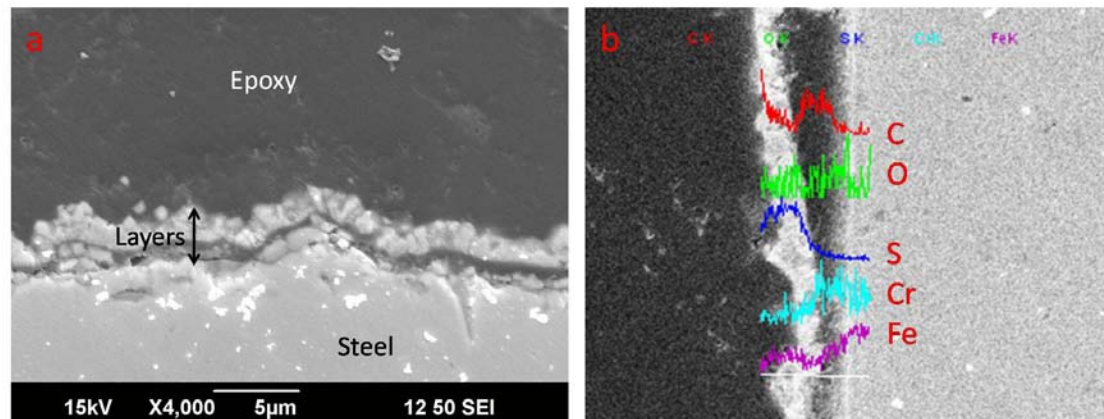
Figure A-23. Surface of 5Cr steel specimen pretreated with Fraction I at 316°C. (a) Surface SEM image; (b) EDS analysis on the surface. SEM and EDS analysis of the cross section is given in Figure A-24. Refer to Figure 40 in the main text for the corrosion rate.

Figure A-24. Cross-section analysis of 5Cr steel specimen pretreated with Fraction I at 316°C. (a) Cross-section SEM image; (b) Corresponding EDS analysis along the white line on the left. SEM and EDS analysis of the surface is given in Figure A-23. Refer to Figure 40 in the main text for the corrosion rate.

Figure A-25. Summary of pretreatment and challenge corrosion rates for CS and 5Cr steel specimens pretreated in Fraction B. For the pretreatment in the stirred autoclave, the pretreatment duration was 24 hours and the temperature was 302°C or 343°C. For the challenge in the HVR, the time of exposure was 24 hours, the temperature was 343°C, and the peripheral velocity was 8.56 m/s.

Figure A-26. Surface of CS specimen pretreated with Fraction B at 302°C. (a) Surface SEM image; (b) EDS analysis on the surface. For corrosion rates see Figure A-25. SEM and EDS analysis of the cross section is given in Figure A-27.

Figure A-27. Cross-section analysis of CS specimen pretreated with Fraction B at 302°C. (a) Cross-section SEM image; (b) Corresponding EDS analysis along the white line on the bottom. For corrosion rates see Figure A-25. SEM and EDS analysis of the surface is given in Figure A-26.
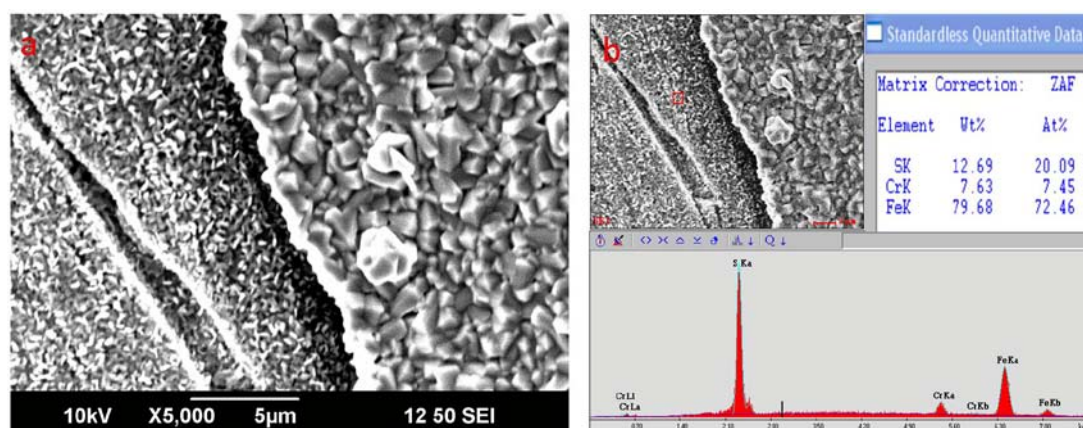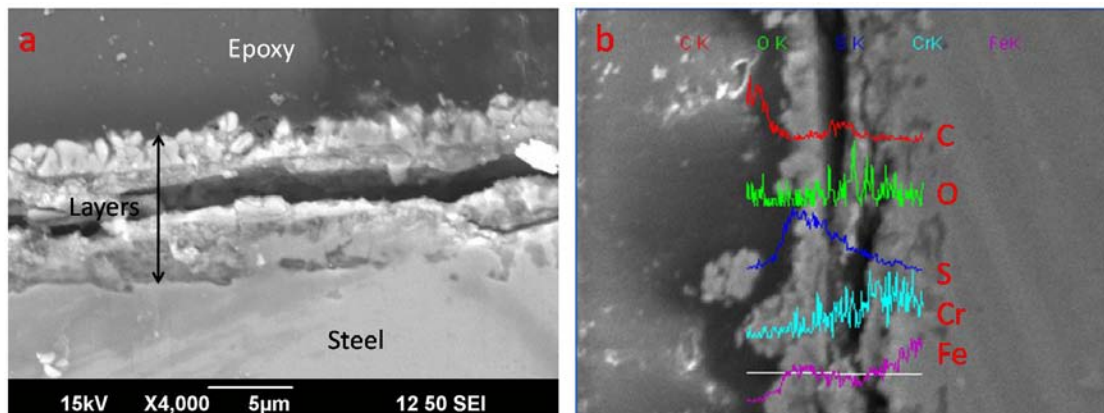

Figure A-28. Surface of 5Cr steel specimen pretreated with Fraction B at 302°C. (a) Surface SEM image; (b) EDS analysis on the surface. For corrosion rates see Figure A-25. SEM and EDS analysis of the cross section is given in Figure A-29.

Figure A-29. Cross-section analysis of 5Cr steel specimen pretreated with Fraction B at 302°C. (a) Cross-section SEM image; (b) Corresponding EDS analysis along the white line on the bottom. For corrosion rates see Figure A-25. SEM and EDS analysis of the surface is given in Figure A-28.
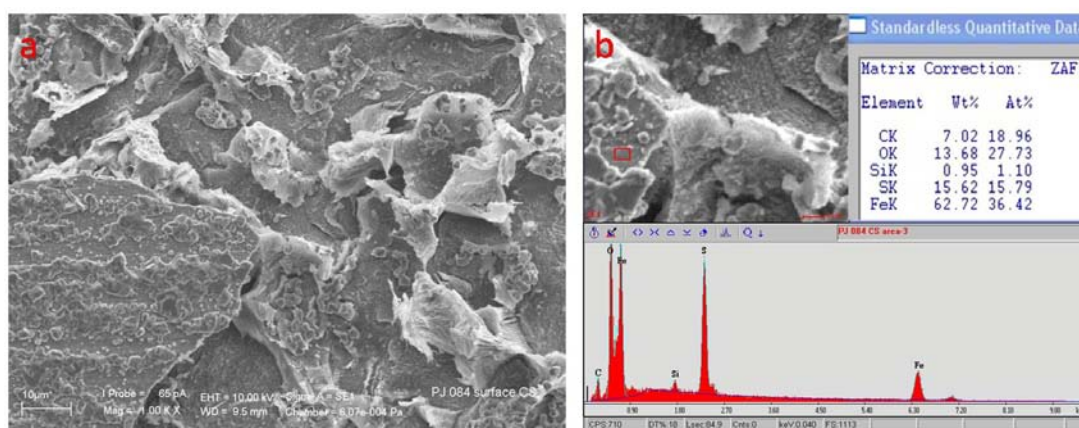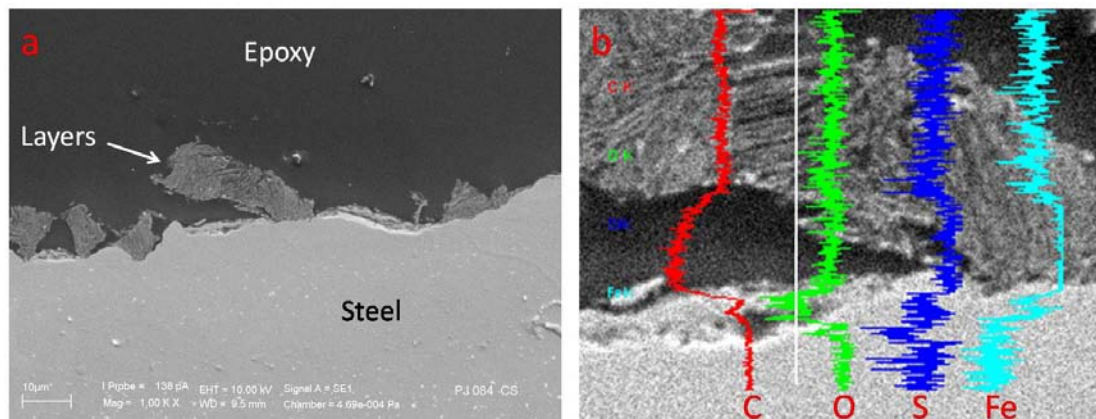

Figure A-30. Surface of CS specimen pretreated with Fraction B at 302°C and challenged with the naphthenic acid solution (TAN 6.5) at 343°C. (a) Surface SEM image; (b) EDS analysis on the surface. For corrosion rates see Figure A-25. SEM and EDS analysis of the cross section is given in Figure A-31.

Figure A-31. Cross-section analysis of CS specimen pretreated with Fraction B at 302°C and challenged with the naphthenic acid solution (TAN 6.5) at 343°C. (a) Cross-section SEM image; (b) Corresponding EDS analysis along the white line in the middle. For corrosion rates see Figure A-25. SEM and EDS analysis of the surface is given in Figure A-30.
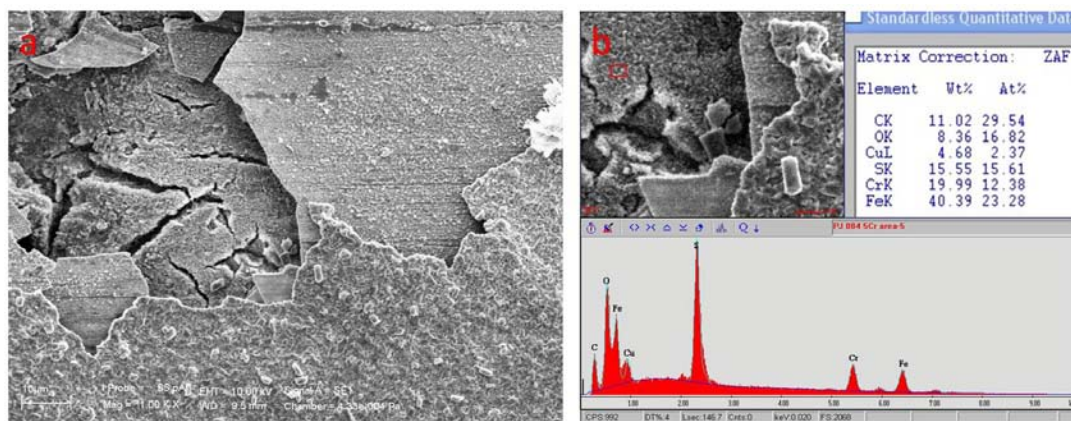

Figure A-32. Surface of 5Cr steel specimen pretreated with Fraction B at 302°C and challenged with the naphthenic acid solution (TAN 6.5) at 343°C. (a) Surface SEM image; (b) EDS analysis on the surface. For corrosion rates see Figure A-25. SEM and EDS analysis of the cross section is given in Figure A-33.
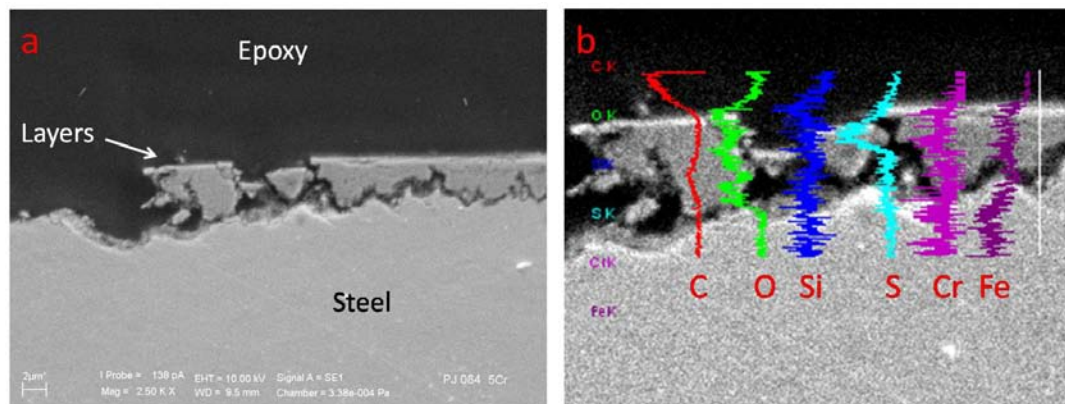
Figure A-33. Cross-section analysis of 5Cr steel specimen pretreated with Fraction B at 302°C and challenged with the naphthenic acid solution (TAN 6.5) at 343°C. (a) Cross-section SEM image; (b) Corresponding EDS analysis along the white line on the right. For corrosion rates see Figure A-25. SEM and EDS analysis of the surface is given in Figure A-32.
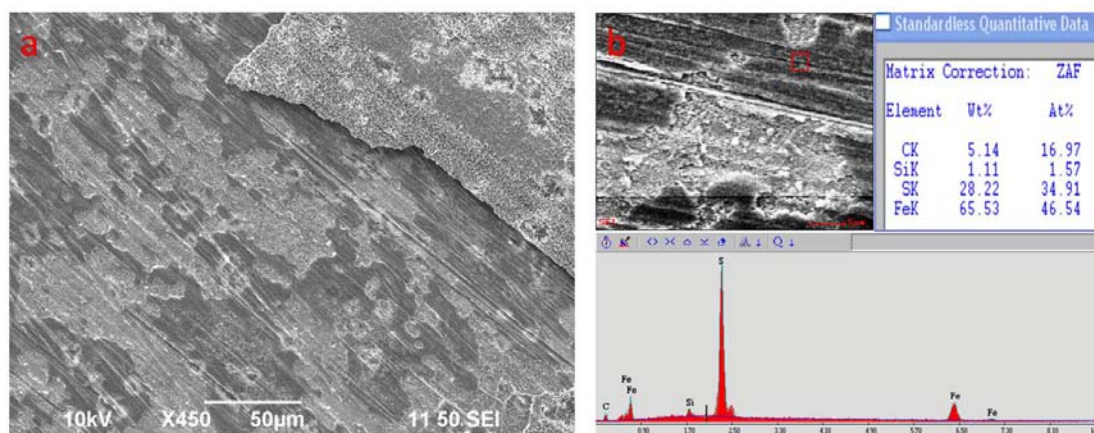

Figure A-34. Surface of CS specimen pretreated with Fraction B at 343°C. (a) Surface SEM image; (b) EDS analysis on the surface. For corrosion rates see Figure A-25. SEM and EDS analysis of the cross section is given in Figure A-35.
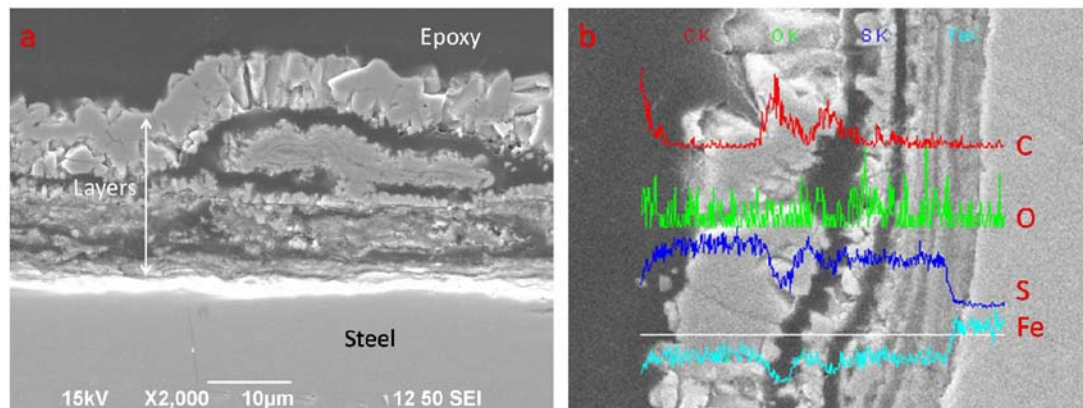
Figure A-35. Cross-section analysis of CS specimen pretreated with Fraction B at 343°C. (a) Cross-section SEM image; (b) Corresponding EDS analysis along the white line on the bottom. For corrosion rates see Figure A-25. SEM and EDS analysis of the surface is given in Figure A-34.
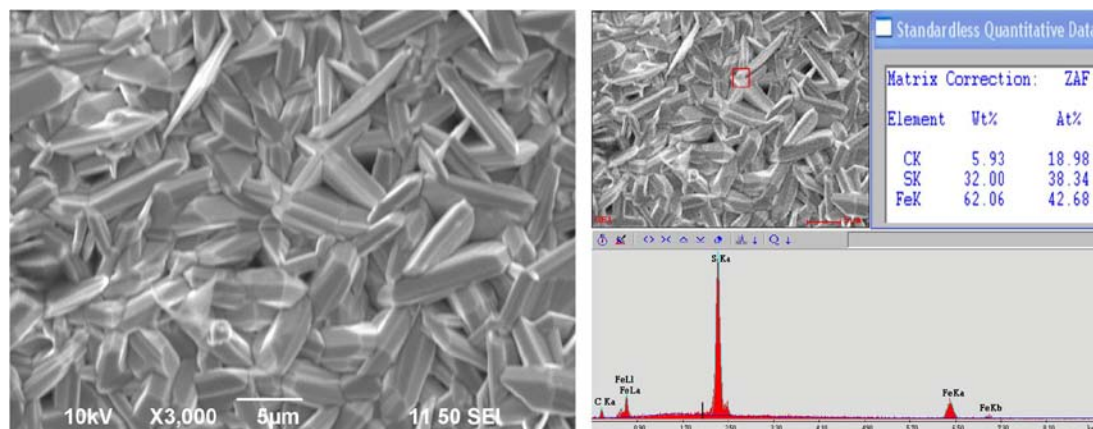

Figure A-36. Surface of 5Cr steel specimen pretreated with Fraction B at 343°C. (a) Surface SEM image; (b) EDS analysis on the surface. For corrosion rates see Figure A-25. SEM and EDS analysis of the cross section is given in Figure A-37.
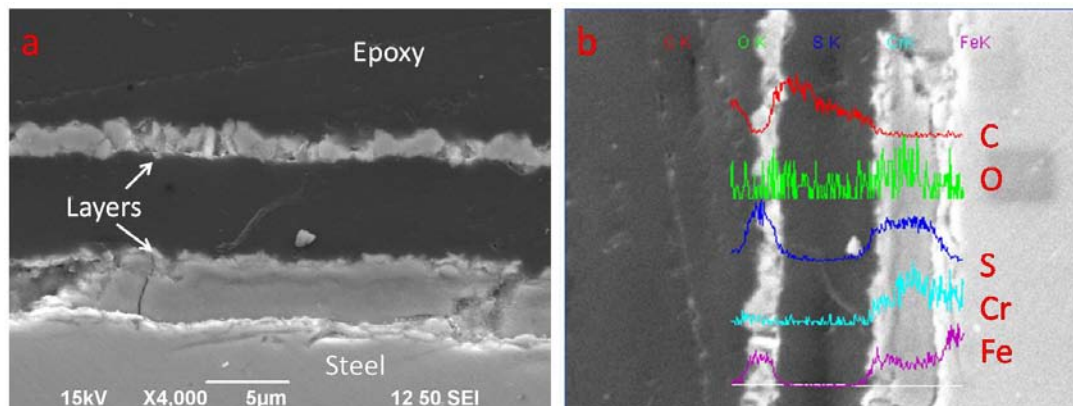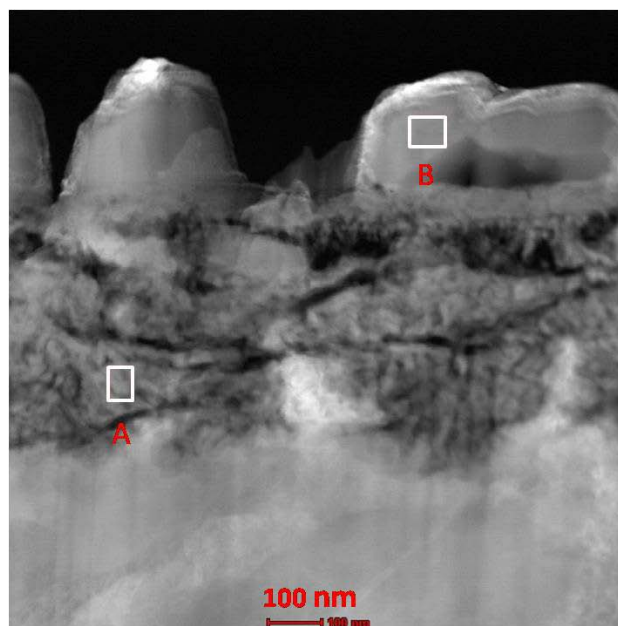
Figure A-37. Cross-section analysis of 5Cr steel specimen pretreated with Fraction B at 343°C. (a) Cross-section SEM image; (b) Corresponding EDS analysis along the white line on the bottom. For corrosion rates see Figure A-25. SEM and EDS analysis of the surface is given in Figure A-36.

A	
Element	Atomic%
O	11.73
S	38.48
Fe	46.56

B	
Element	Atomic%
O	4.95
S	44.42
Fe	50.61

Figure A-38. EDS analysis of selected areas on the layer formed in the "DDS only" solution at 316°C for 24 hours (CS specimen). Refer to Figure 50 in the main text for the corrosion rate.
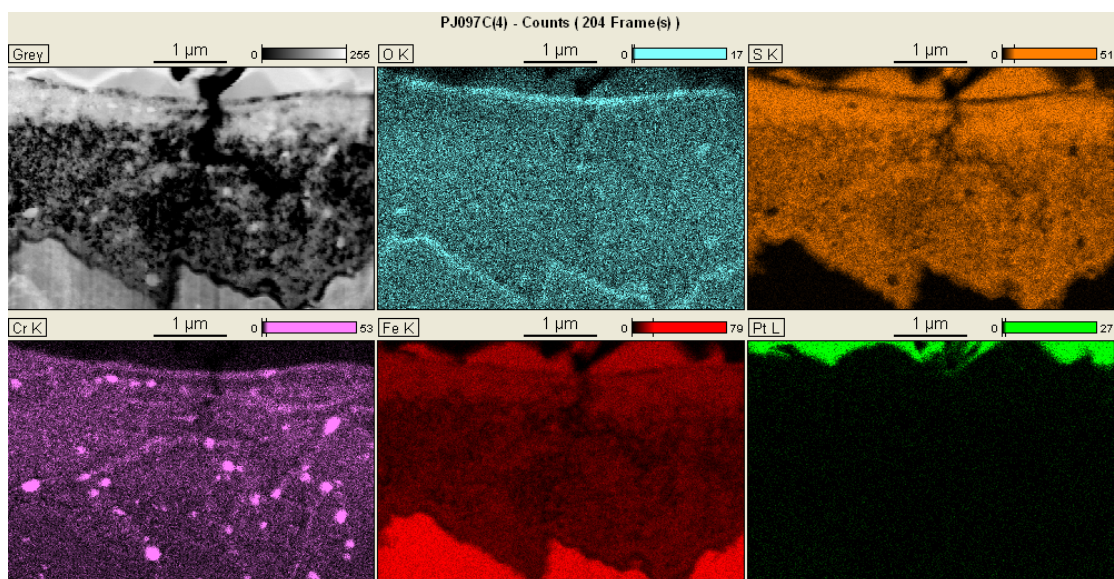
Figure A-39. Mapping of elements for 5Cr steel specimen pretreated in the "DDS only" solution at 343°C for 24 hours. Refer to Figure 50 in the main text for the corrosion rate.
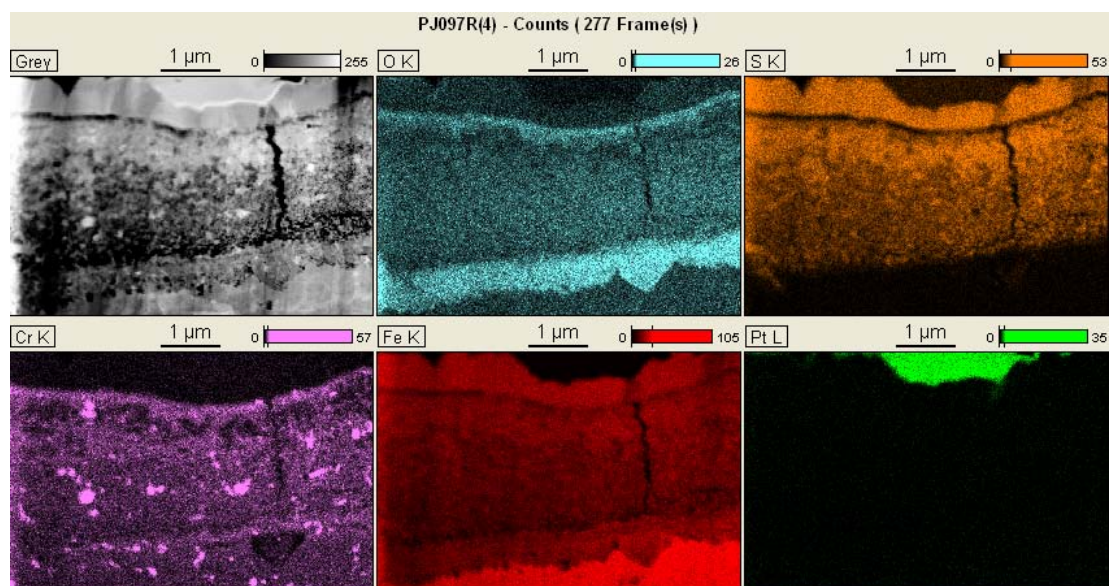

Figure A-40. Mapping of elements for 5Cr steel specimen pretreated in the "DDS only" solution at 343°C for 24 hours and challenged with the naphthenic acid solution (TAN 3.5) at 343°C. Refer to Figure 50 in the main text for the corrosion rate.
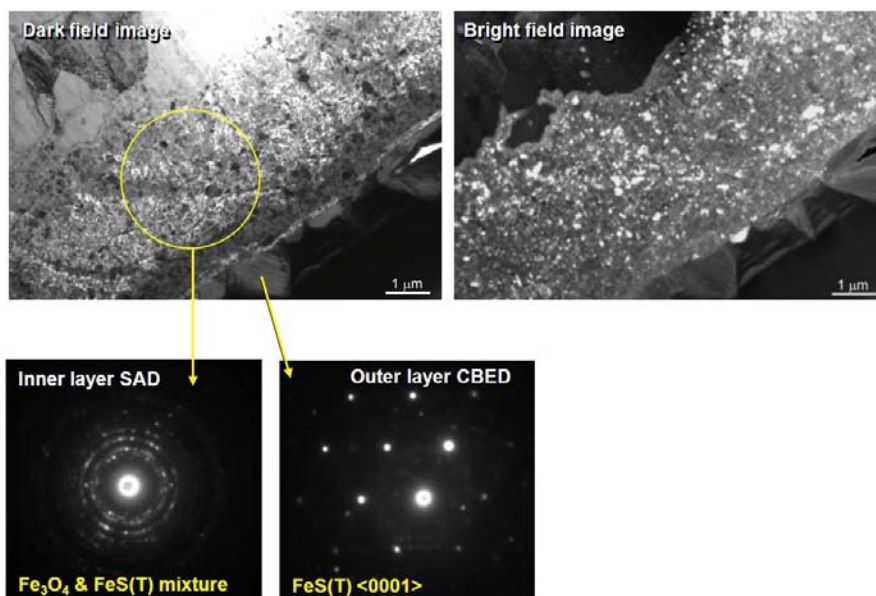
Figure A-41. TEM images and SAD and CBED patterns of layers formed in the "DDS only" solution at 343°C (5Cr steel specimen; images taken and analyzed by Fang Cao, ExxonMobil Research and Engineering Company). Refer to Figure 50 in the main text for the corrosion rate.
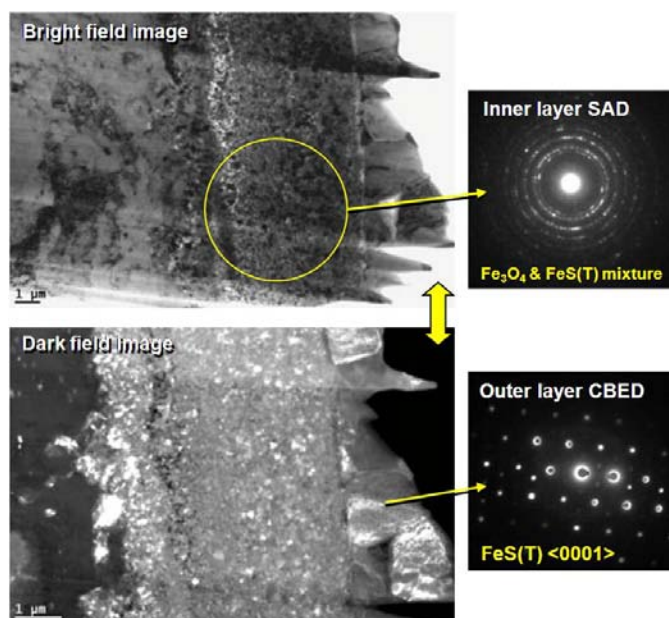

Figure A-42. TEM images and SAD and CBED patterns of layers formed after the pretreatment in the "DDS only" solution at 343°C and the challenge with the naphthenic acid solution (TAN 3.5) at 343°C (5Cr steel specimen; images taken and analyzed by Fang Cao, ExxonMobil Research and Engineering Company). Refer to Figure 50 in the main text for the corrosion rate.
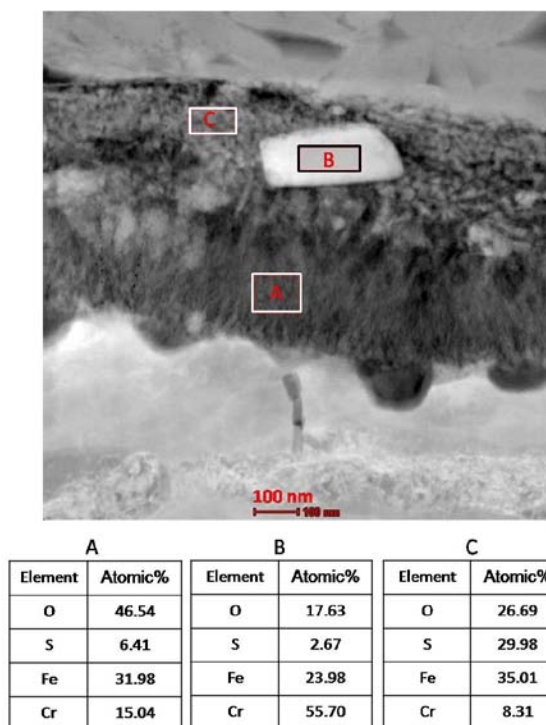
A			B			C	
Element	Atomic%		Element	Atomic%		Element	Atomic%
O	46.54		O	17.63		O	26.69
S	6.41		S	2.67		S	29.98
Fe	31.98		Fe	23.98		Fe	35.01
Cr	15.04		Cr	55.70		Cr	8.31

Figure A-43. EDS analysis of selected areas on the layer formed after the pretreatment in the "DDS + NAP" solution at 316°C for 24 hours (5Cr steel specimen). Refer to Figure 60 in the main text for the corrosion rate.
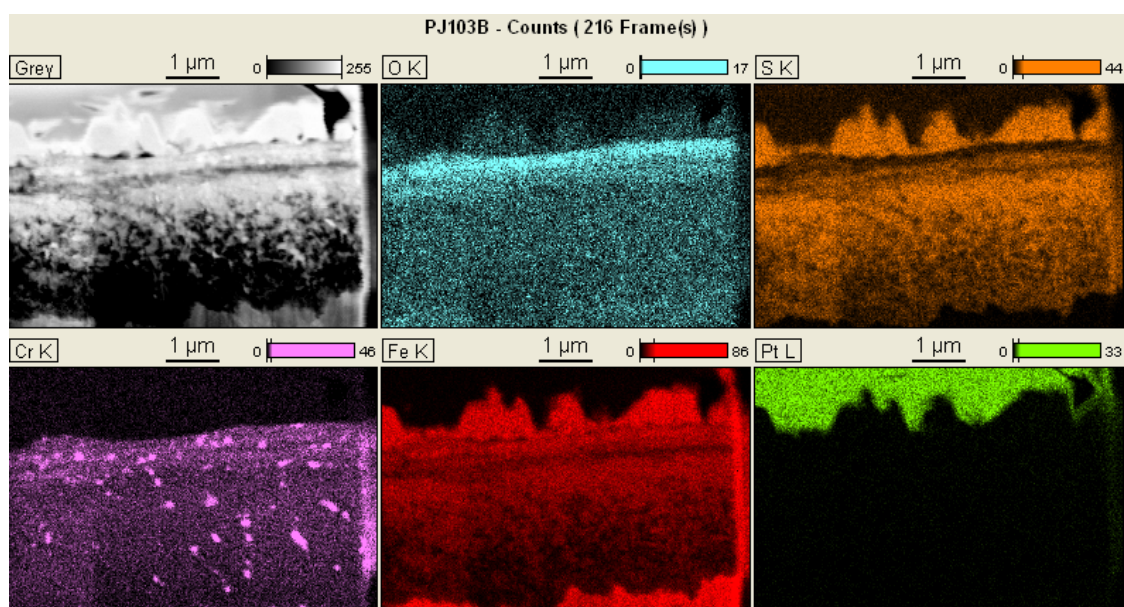

Figure A-44. Mapping of elements for 5Cr steel specimen pretreated in the "DDS + NAP" solution at 343°C for 24 hours. Refer to Figure 60 in the main text for the corrosion rate.
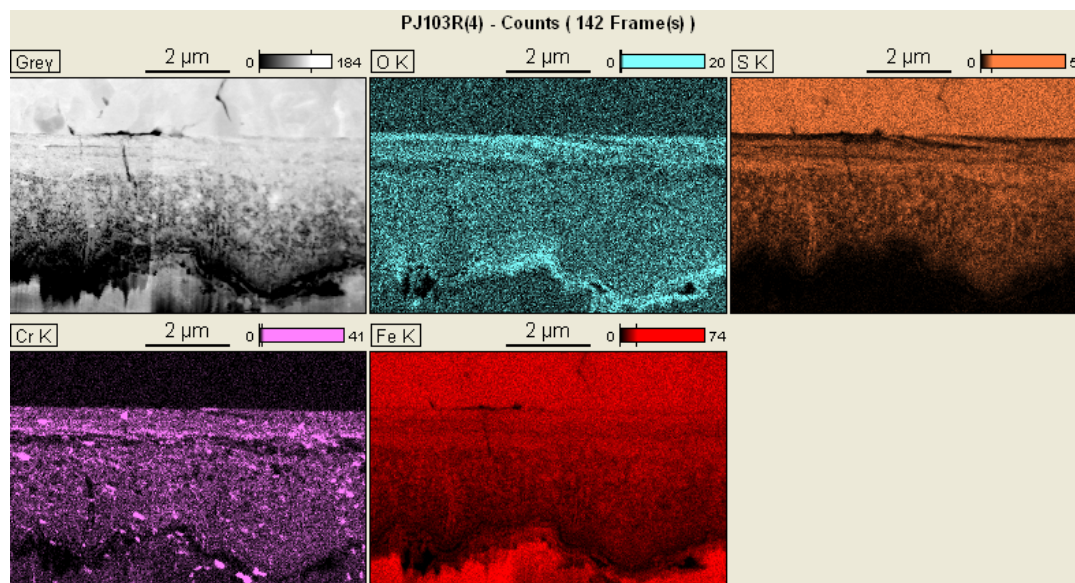
Figure A-45. Mapping of elements for 5Cr steel specimen pretreated in the "DDS + NAP" solution at 343°C for 24 hours and challenged with the naphthenic acid solution (TAN 3.5) at 343°C for 24 hours. Refer to Figure 60 in the main text for the corrosion rate.
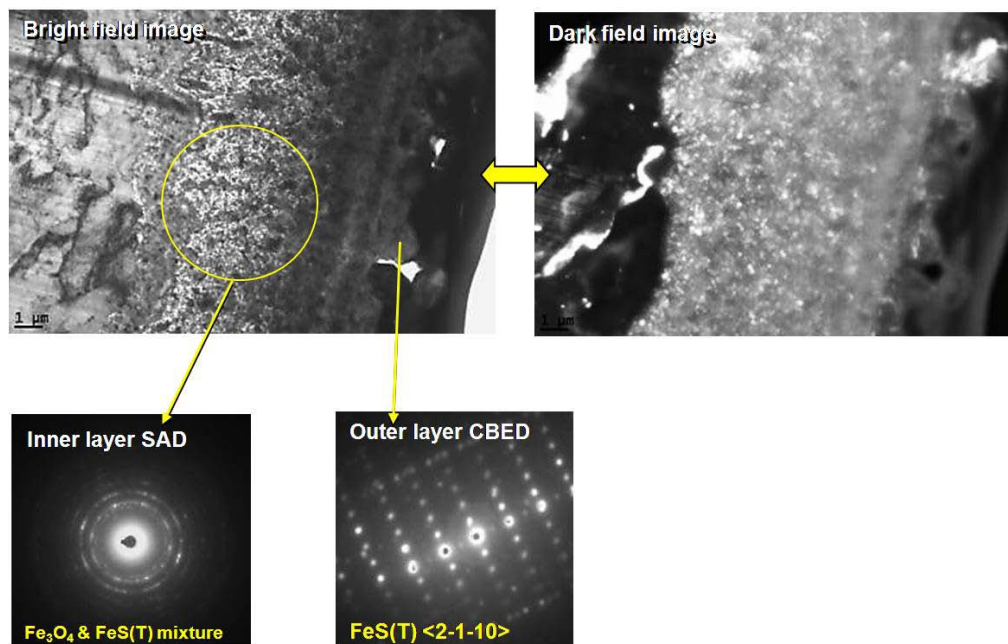

Figure A-46. TEM images and SAD and CBED patterns of layers formed after the pretreatment in the "DDS + NAP" solution at 343°C and the challenge with the naphthenic acid solution (TAN 3.5) at 343°C (5Cr steel specimen; images taken and analyzed by Fang Cao, ExxonMobil Research and Engineering Company). Refer to Figure 60 in the main text for the corrosion rate.
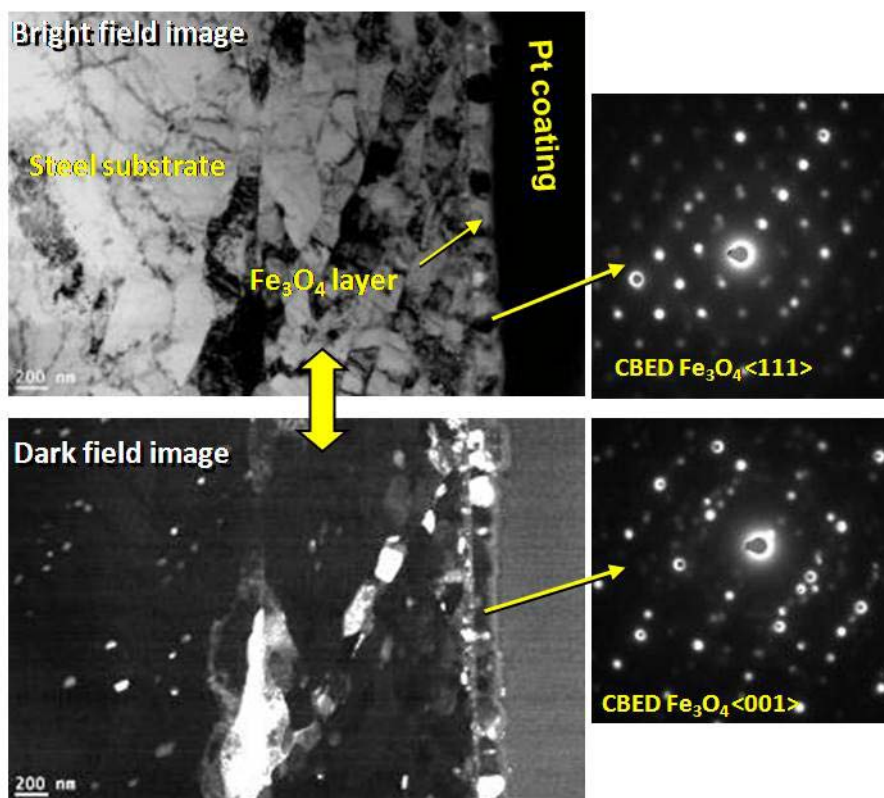
Figure A-47. TEM images and SAD and CBED patterns of layers formed after the pretreatment in the "NAP only" solution at 316°C and the challenge with the naphthenic acid solution (TAN 3.5) at 343°C (5Cr steel specimen; images taken and analyzed by Fang Cao, ExxonMobil Research and Engineering Company). Refer to Figure 60 in the main text for the corrosion rate.
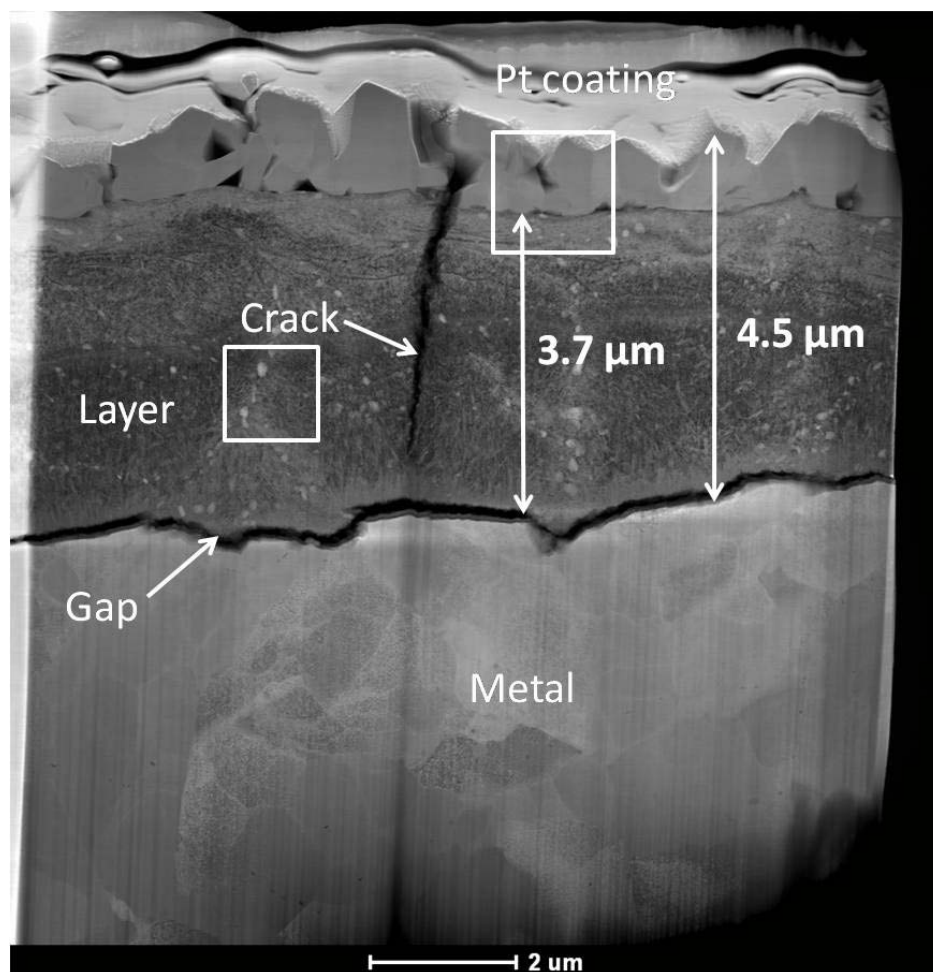
Figure A-48. TEM images of 5Cr steel specimen pretreated with Fraction B at 343°C for 24 hours. Refer to Figure 72 in the main text for the corrosion rate.
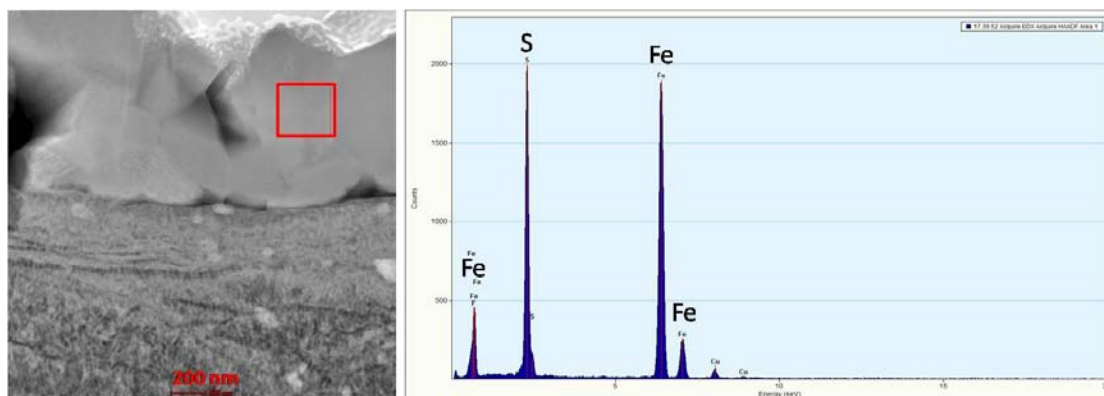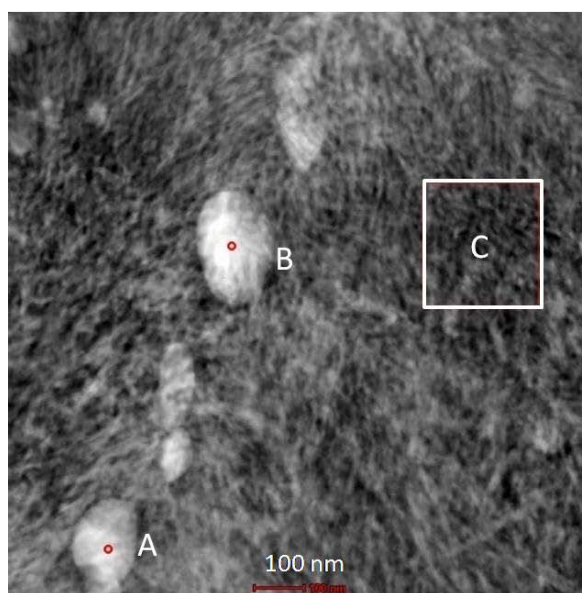

Figure A-49. EDS analysis of the layer presented in the top square of Figure A-48. The elemental data were collected in the square. Refer to Figure 72 in the main text for the corrosion rate.

A			B			C	
Element	Atomic%		Element	Atomic%		Element	Atomic%
O	17.73		O	20.17		O	27.74
S	11.83		S	8.08		S	31.96
Fe	28.41		Fe	23.85		Fe	27.64
Cr	42.01		Cr	47.88		Cr	12.63

Figure A-50. EDS analysis of the layer presented in the middle square of Figure A-48. The elemental data were collected in selected areas A, B, and C. Refer to Figure 72 in the main text for the corrosion rate.
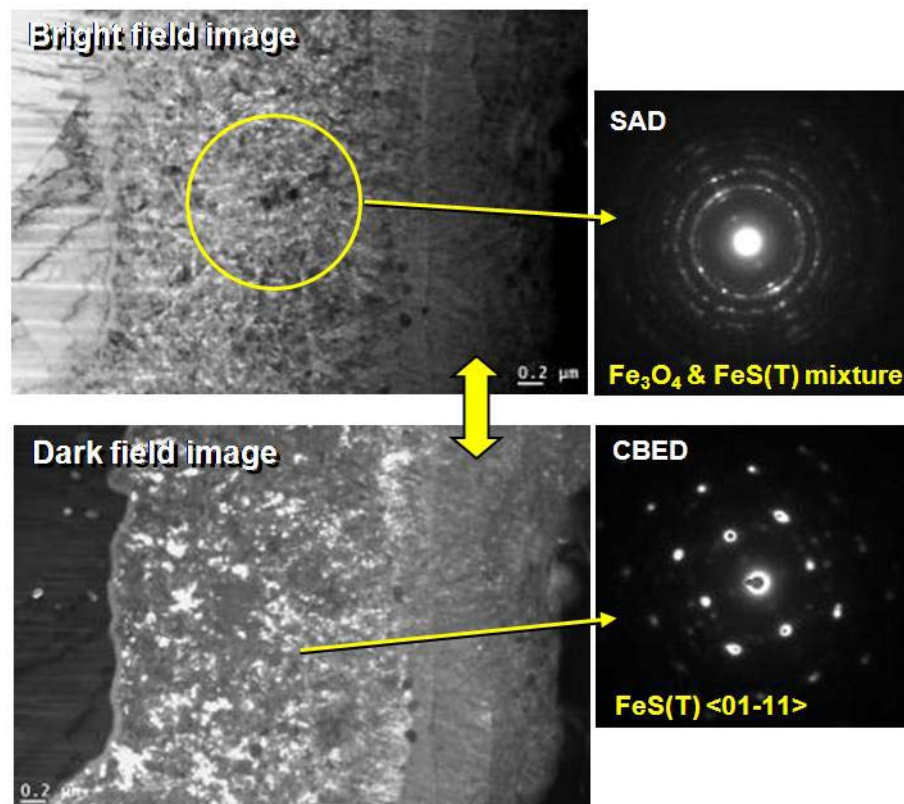
Figure A-51. TEM images and SAD and CBED patterns of layers formed after the pretreatment in Fraction B at 343°C (5Cr steel specimen; images taken and analyzed by Fang Cao, ExxonMobil Research and Engineering Company). TEM image is given in Figure A-48. Refer to Figure 72 in the main text for the corrosion rate.
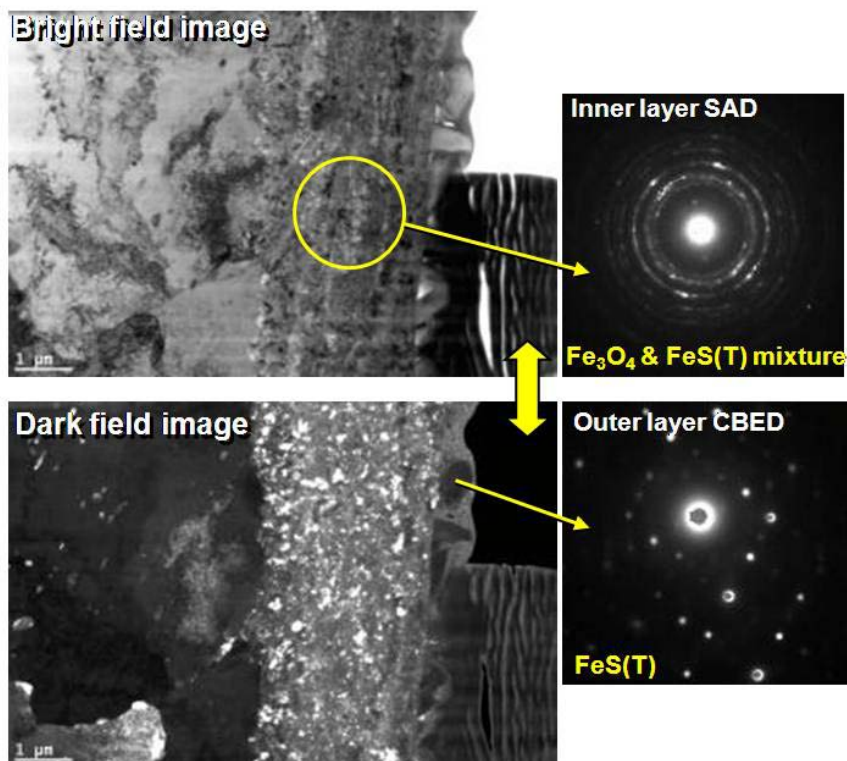
Figure A-52. TEM images and SAD and CBED patterns of layers formed after the pretreatment in Fraction B at 343°C and the challenge with naphthenic acid solution (TAN 3.5) at 343°C (5Cr steel specimen, images taken and analyzed by Fang Cao; ExxonMobil Research and Engineering Company). Refer to Figure 72 and Figure 77 in the main text for the corrosion rate and the TEM image, respectively.

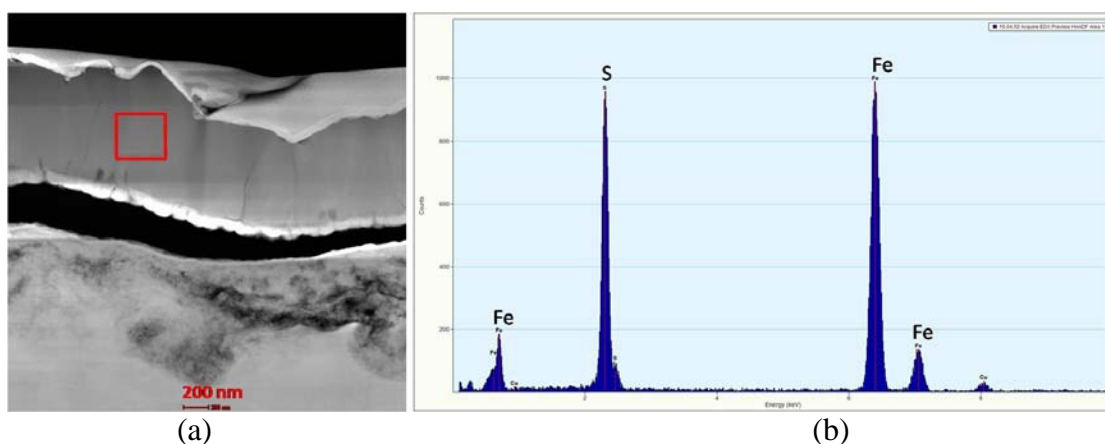(a)   (b)

Figure A-53. EDS analysis on the top layer for CS specimen pretreated in Fraction L at 316°C for 24 hours. (a) Enlarged image of top layer with the square showing the area of EDS analysis; (b) Results of EDS analysis. Refer to Figure 82 and Figure 83 in the main text for the corrosion rate and the TEM image, respectively.
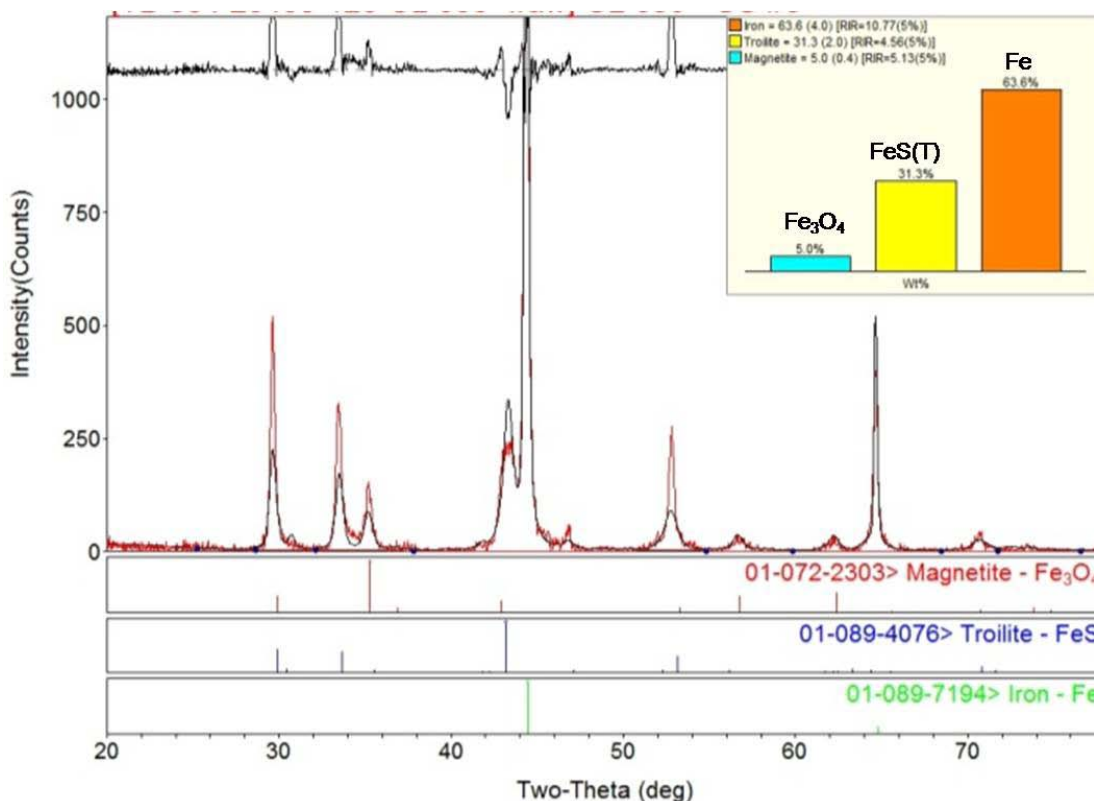
Figure A-54. XRD analysis on layers formed after the pretreatment in Fraction L at 316°C (CS specimen; images taken and analyzed by Fang Cao; ExxonMobil Research and Engineering Company). Refer to Figure 82 and Figure 83 in the main text for the corrosion rate and the TEM image, respectively.
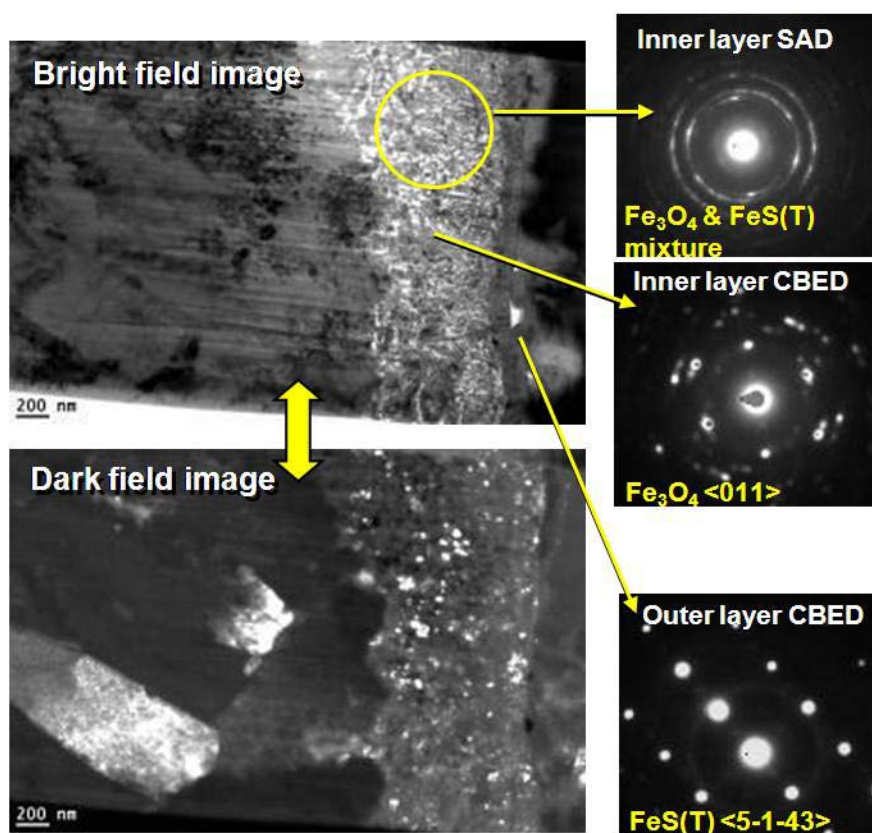
Figure A-55. TEM images and SAD and CBED patterns of layers formed after the pretreatment in Fraction A at 343°C (5Cr steel specimen; images taken and analyzed by Fang Cao, ExxonMobil Research and Engineering Company). Refer to Figure 85 and Figure 88 in the main text for the corrosion rate and the TEM image, respectively.
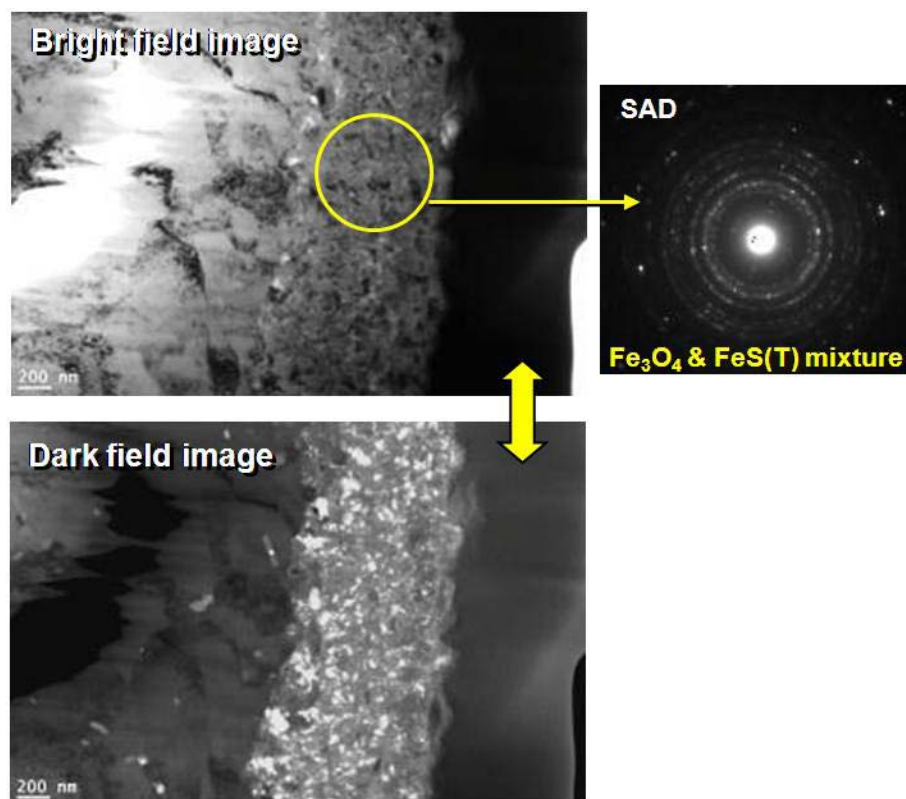
Figure A-56. TEM images and SAD pattern of layers formed after the pretreatment in Fraction A at 343°C and the challenge with naphthenic acid solution (TAN 3.5) at 343°C (5Cr steel specimen, images taken and analyzed by Fang Cao; ExxonMobil Research and Engineering Company). Refer to Figure 85 and Figure 88 in the main text for the corrosion rate and the TEM image, respectively.
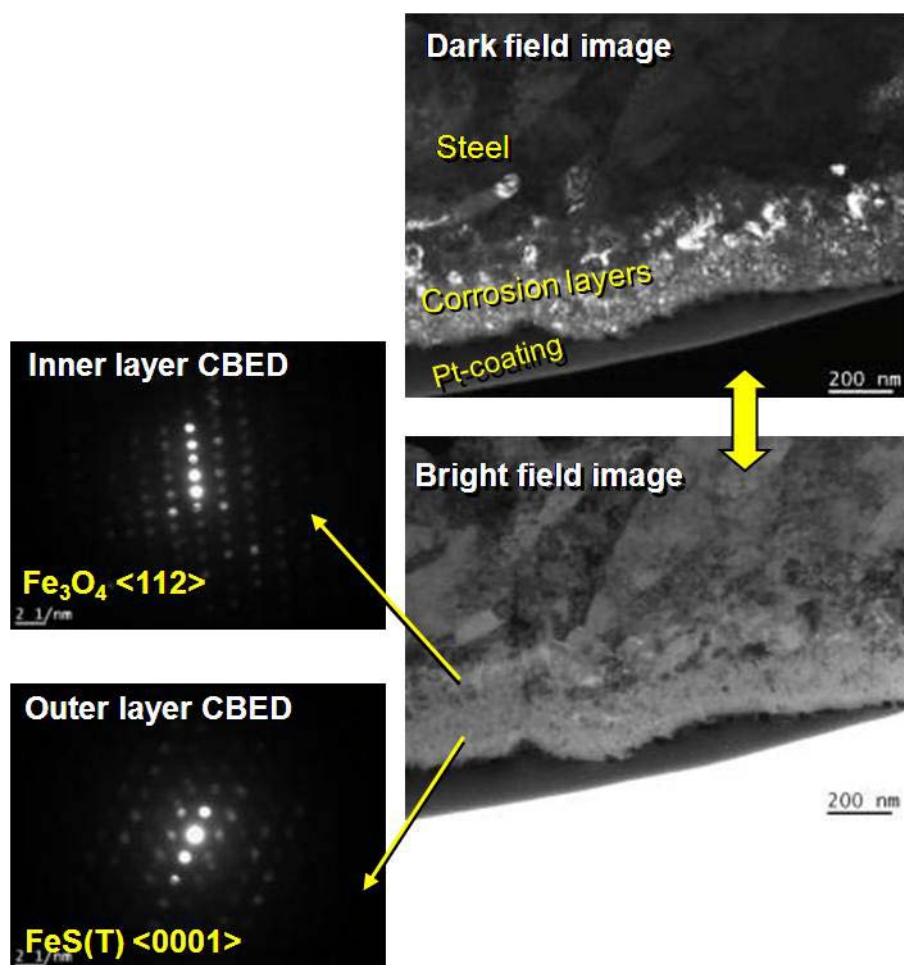
Figure A-57. TEM images and CBED patterns of layers formed after the pretreatment in Fraction O at 316°C (CS specimen; images taken and analyzed by Fang Cao, ExxonMobil Research and Engineering Company). Refer to Figure 91 and Figure 92 in the main text for the corrosion rate and the TEM image, respectively.
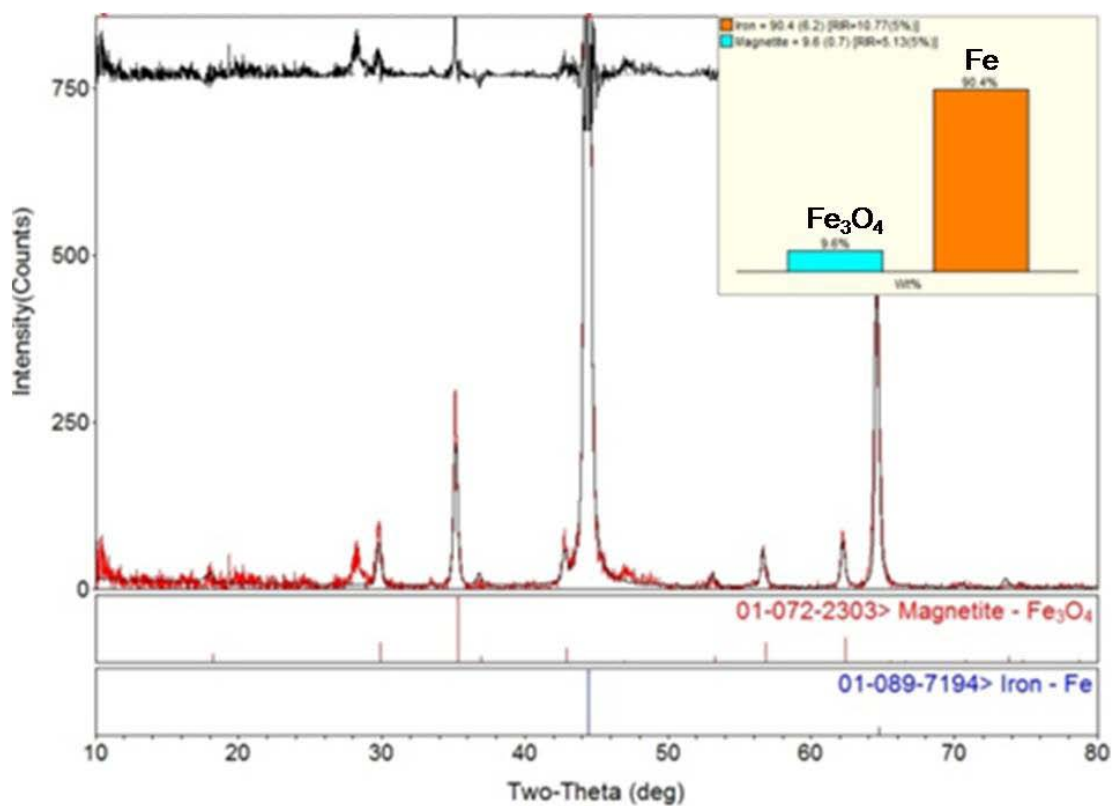
Figure A-58. XRD analysis on layers formed after the pretreatment in Fraction O at 316°C (CS specimen; images taken and analyzed by Fang Cao, ExxonMobil Research and Engineering Company). Refer to Figure 91 and Figure 92 in the main text for the corrosion rate and the TEM image, respectively.
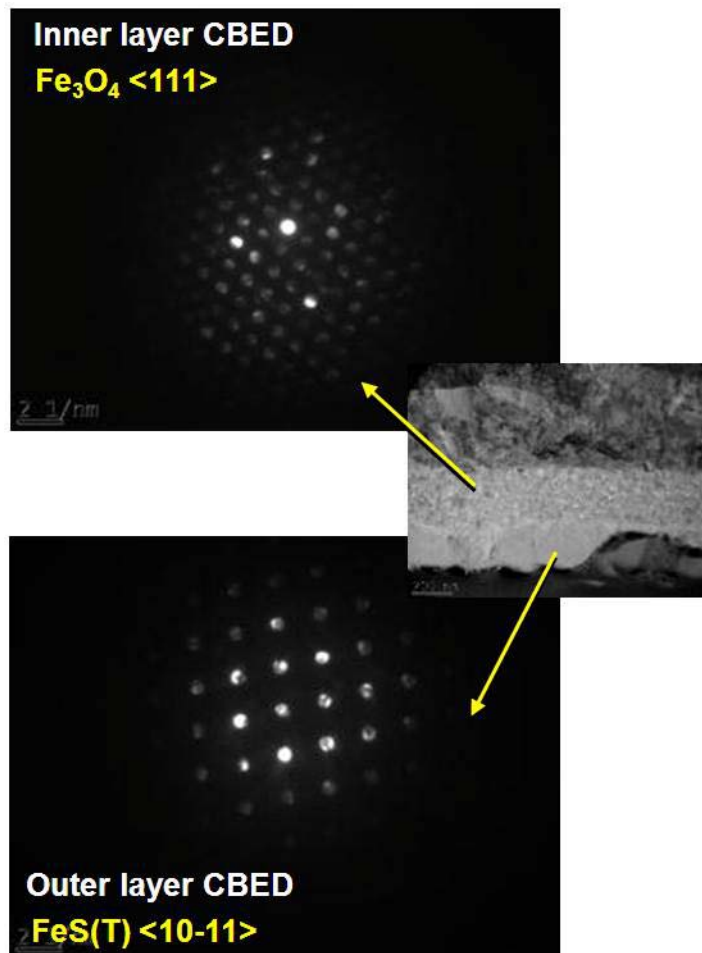
Figure A-59. TEM images and CBED patterns of layers formed after the pretreatment in Fraction O at 316°C (5Cr steel specimen; images taken and analyzed by Fang Cao, ExxonMobil Research and Engineering Company). Refer to Figure 91 and Figure 94 in the main text for the corrosion rate and the TEM image, respectively.
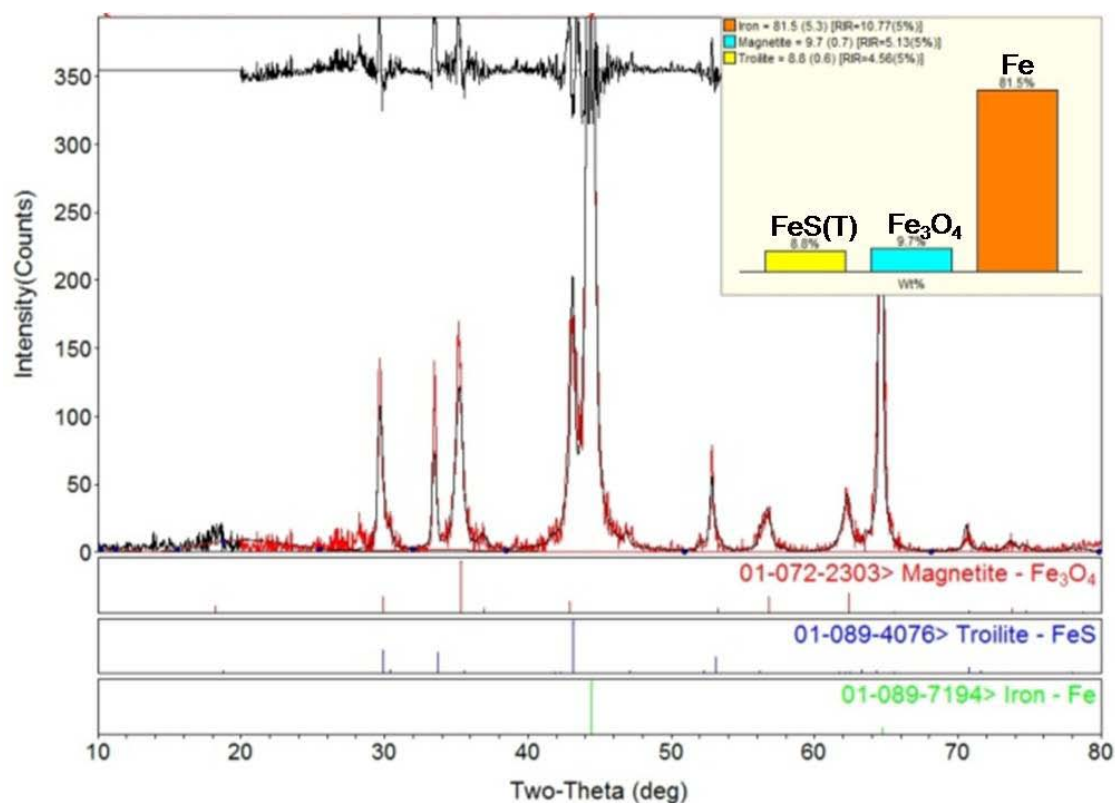
Figure A-60. XRD analysis on layers formed after the pretreatment in Fraction O at 316°C (5Cr steel specimen; images taken and analyzed by Fang Cao, ExxonMobil Research and Engineering Company). Refer to Figure 91 and Figure 94 in the main text for the corrosion rate and the TEM image, respectively.

APPENDIX B: VALUES OF PARAMETERS IN MODELING OF CORROSION BY NAPHTHENIC ACIDS AND ORGANOSULFUR COMPOUNDS

Common Parameters

T – Temperature, 550 to 650 K

R – Ideal gas constant, 8.314 J/(mol·K)

M_{Fe} – Molecular weight of iron, 55.845 kg/kmol

M_{FeS} – Molecular weight of iron sulfide, 87.911 kg/kmol

ρ_{Fe} – Iron density, 7874 kg/m^3

ρ_{FeS} – Iron sulfide density, 4700 kg/m^3

t – Corrosion duration, > 0.01 s

$c_{s,\,RS}$ – Concentration of sulfur compounds on the interface between the inner layer and the steel surface, 0.0000001 mol/m^3

$c_{s,\,RCOOH}$ – Concentration of naphthenic acids on the interface between the inner layer and the steel surface, 0.0000001 mol/m^3

Oil Characteristics

TAN – Total acidic number, 0.1 to 10 mg KOH / g oil

$S\%$ – Weight percent of sulfur in the fluid, 0.01 to 2

ρ_{oil} – Oil density, 800 kg/m^3

Hydraulic Parameters

D – Pipe diameter, > 0.01 m

v – Flow velocity, > 0.01 m/s

Layer Parameters

ε – Porosity of outer iron sulfide layer, 0.6

Ψ – Tortuosity of outer iron sulfide layer, 0.05

Diffusion Parameters

v_{oil} – Oil viscosity, $5 \times 10^6 \times 10^{10 \times (253.16 - T) - \frac{0.001053 \times (253.16 - T)^2}{T - 168.16}}$, m^2/s

$k_{m, RS}$ – Mass transfer coefficient for sulfur compounds in the boundary layer,

$\frac{0.365}{D} \times (\frac{v \times D \times \rho_{oil}}{v_{oil}})^{0.86} \times (\frac{v_{oil}}{\rho_{oil} \times D_{RS}})^{0.28} \times D_{RS}$, m/s

D_{RS} – Diffusion coefficient of sulfur compounds in the fluid, $2 \times 10^{-9} \times \frac{0.007 \times T}{298.16 \times v_{oil}}$, m^2/s

A_{RS} – Kinetic constant for diffusion of sulfur compounds through the inner layer,

$10^{-10} + 10^{-12} \times (TAN - 17 \times S\%)^2$ for CS, $10^{-10} + 2 \times 10^{-12} \times (TAN -$

$17 \times S\%)2$ for 5Cr steel, mol/(m^2·s)

E_{RS} – Activation energy for diffusion of sulfur compounds through the inner layer, 150

J/mol

$k_{m, RCOOH}$ – Mass transfer coefficient for naphthenic acids in the boundary layer,

$\frac{0.365}{D} \times (\frac{v \times D \times \rho_{oil}}{v_{oil}})^{0.86} \times (\frac{v_{oil}}{\rho_{oil} \times D_{RCOOH}})^{0.28} \times D_{RCOOH}$, m/s

D_{RCOOH} – Diffusion coefficient of naphthenic acids in the fluid, $6.6 \times 10^{-9} \times \frac{0.007 \times T}{298.16 \times v_{oil}}$,

m^2/s

A_{RCOOH} – Kinetic constant for diffusion of naphthenic acids through the inner layer,

$2 \times 10^{-10} + 2 \times 10^{-10} \times (TAN - 17 \times S\%)^2$ for CS, $10^{-10} + 10^{-10} \times (TAN -$

$17 \times S\%)2$ for 5Cr steel, mol/(m^2·s)

E_{RCOOH} – Activation energy for diffusion of naphthenic acids through the inner layer, 255

J/mol